5-1992

Solid State ^{13}C NMR and Thermal Analysis of Conformational Motion and Disorder in Small and Large Molecules

Jinlong Cheng

University of Tennessee - Knoxville

To the Graduate Council:

I am submitting herewith a dissertation written by Jinlong Cheng entitled "Solid State ^{13}C NMR and Thermal Analysis of Conformational Motion and Disorder in Small and Large Molecules." I have examined the final electronic copy of this dissertation for form and content and recommend that it be accepted in partial fulfillment of the requirements for the degree of Doctor of Philosophy, with a major in Chemistry.

B. Wunderluch, Major Professor

We have read this dissertation and recommend its acceptance:

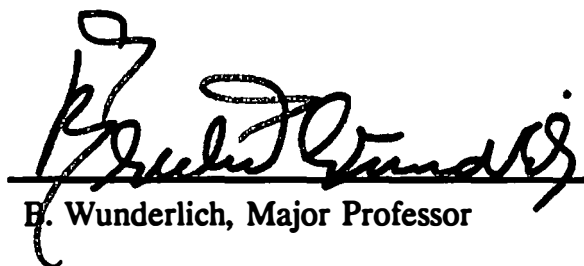Paul Phillips, Craig Barnes, Alexander Van Hook

Accepted for the Council:
Dixie L. Thompson

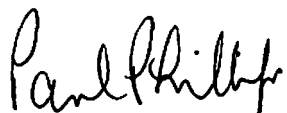Vice Provost and Dean of the Graduate School

(Original signatures are on file with official student records.)
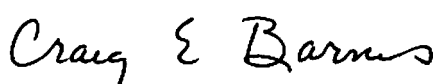
To the Graduate Council:
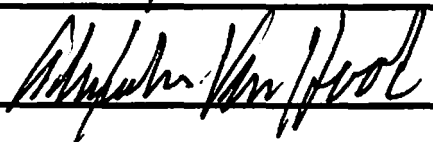
I am submitting herewith a dissertation written by Jinlong Cheng entitled "Solid State ^{13}C NMR and Thermal Analysis of Conformational Motion and Disorder in Small and Large Molecules." I have examined the final copy of this dissertation for form and content and recommend that it be accepted in partial fulfillment of the requirements for the degree of Doctor of Philosophy, with a major in Chemistry.

B. Wunderlich, Major Professor

We have read this dissertation
and recommend its acceptance:

Accepted for the Council:

Associate Vice Chancellor

and Dean of The Graduate School

SOLID STATE ^{13}C NMR AND THERMAL ANALYSIS OF CONFORMATIONAL MOTION AND DISORDER IN SMALL AND LARGE MOLECULES

A Dissertation Presented for

the Degree of Doctor of Philosophy

The University of Tennessee, Knoxville

Jinlong Cheng

May 1992

DEDICATION

This dissertation is dedicated to my parents

Mr. Lizhi Cheng and Mrs. Shouwu Pi-Cheng

who have given me invaluable educational opportunities.

此博士论文谨献给我的父母

程立志，皮守武

ACKNOWLEDGMENTS

TABLE OF CONTENTS

LIST OF TABLES

LIST OF FIGURES

ABSTRACT

In this work it is attempted to explore the conformational motion and disorder through a large number of examples of molecular systems differing in shape, rigidity, and molecular weight: a series of tetra-*n*-alkylammonium bromides and iodides, a liquid-crystal-forming molecule, N,N'-*bis*(4-*n*-octyloxybenzal)-1,4-phenylenediamine (OOBPD), and polymers, poly[oxy-1,4-(3-methylphenylene)ethylene-1,4-phenyleneoxy-nonamethylene] (MBPE-9) and poly[oxy-1,4-(3-methylphenylene)ethylene-1,4-phenyleneoxypentamethylene] (MBPE-5). The techniques used to study the conformational motion and disorder are mainly solid state ^{13}C nuclear magnetic resonance (NMR) spectroscopy and thermal analysis.

The results of this work show that *conf*ormational *dis*ordered states (condis crystals) exist indeed in these molecules containing flexible chemical bonds (single bonds) or more than one accessible conformer. The unique characteristics of the condis crystal and the phase transitions to a condis crystal and to isotropic state have been studied in detail. It could be shown that motifs in condis crystals show only conformational disorder but maintaining orientational and positional order, while liquid and plastic crystals show conformational motion in addition to their characteristic positional and orientational disorder and motion, respectively. The molecular motion in the condis state is slow compared to well-known plastic and liquid crystals. Besides the large-amplitude motion in a first-order transition, it is documented that gradual start of motion is possible increasing the conformational entropy over a broad temperature range.

CHAPTER 1

INTRODUCTION

A survey of thermotropic mesophases of small and large molecules by Wunderlich and Grebowicz (1984) resulted in a division of the mesophases into three major types: 1. The long-known liquid crystals, characterized by elongated, rod-like or flat, disc-like mesogens that permit liquid-like motion while retaining orientational order (Smith, 1975); 2. The well-described plastic crystals, characterized by close-to-spherical mesogens which are able to attain rotational motion in the crystal without losing positional order (Sherwood, 1979), and 3. The newly-proposed condis crystals (short for *con*formationally *dis*ordered crystals) which consist of flexible molecules, able to change between different conformations within the crystals (Wunderlich *et al.*, 1988). For each of the mesophases a corresponding metastable glassy state was also suggested (LC-, PC-, and CD-glass, respectively). These glasses are solid with mesophase disorder frozen on cooling below the glass transition temperature.

To illustrate the discussion of the above mentioned mesophases and their relationships with the three classical condensed phases, namely, glass, crystal and melt, a schematic summary is given in Fig. 1. All glasses and crystals are considered solid, the melt is liquid, and the mesophase crystals are intermediate states. Condis crystal, plastic crystal, and liquid crystal are increasingly less solid (more liquid). The lines between the boxes on the right-hand side of Fig. 1 indicate transitions between
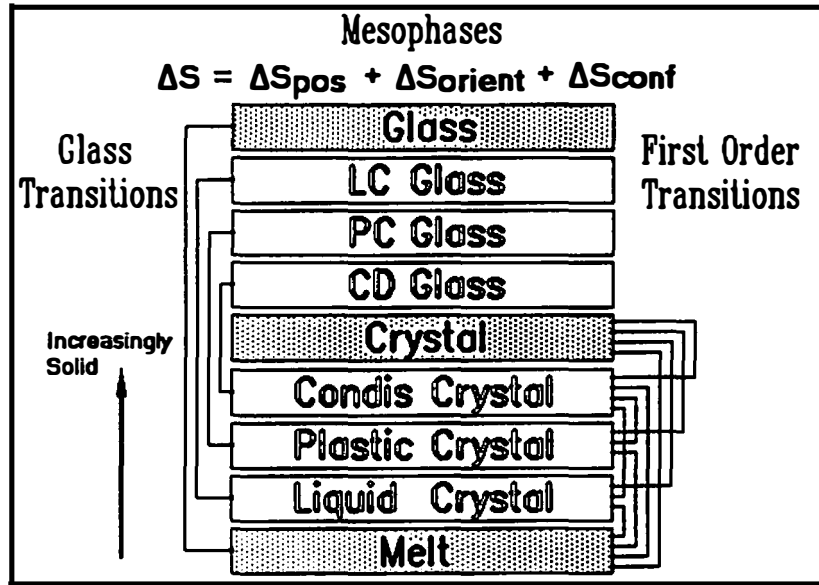
Figure 1   Relationships between the phases

the phases that cause changes in order and lead ultimately to the crystal or the melt, and are often first order transitions (Ehrenfest, 1933), *i.e.*, transitions that involve a discontinuity in the first derivative of the Gibbs energy function, the entropy. When starting with the crystal, the entropy increases on going to successively lower states as drawn in Fig. 1. On the left-hand side, the connections between the indicate changes between states of equal structure (constant entropy), but with changing large-scale motion.

The terminology of condis has proven to be particularly useful and important for the description of crystals of macromolecules with high conformational mobility since it had become increasingly difficult to distinguish between the various mesophases. For example, the special mesophases of polyethylene, polytetrafluoro-

ethylene, polypropylene, *trans*-1,4-polyisoprene, polyoxybenzoate, polyparaxylylene, *etc.*, have often been called smectic liquid crystals (for a discussion see Wunderlich and Grebowicz, 1984). To account for the special behavior of polymers, terms such as viscous liquid crystals (Schneider, *et al.*, 1978), one-dimensional plastic crystals (Economy, *et al.*, 1988), and columnar liquid crystalline phases (Ungar, *et al.*, 1991) have been proposed. Indeed, many similarities exist between the classifications suggested in the various names. One must, however, recognize that the definitions of liquid and plastic crystals were often made before macromolecules were discovered, and were based on translational and orientational disorder and motion of the *whole* molecule.

Macromolecules show on fusion only a negligible amount of translational (positional) and orientational disordering (Wunderlich, 1980). Almost all their entropy of fusion can be linked to conformational disordering. In order to show liquid crystalline behavior in macromolecules, it is necessary to separate rod- or disc-like mesogens with flexible spacers (in the main chain or in the side chains). The conformational motion of the flexible spacer gives the mesogen a possibility of "translation-like" disorder and motion. With a proper mesogen and sufficiently long flexible spacer a macromolecule can then achieve for the mesogens orientational order while being positionally disordered (Wunderlich, and Grebowicz, 1984).

Close-to-spherical mesogens, as required for plastic crystals, seem to be impossible to be incorporated in macromolecules if their motion is to involve rotation

about more than one axis. A globular macromolecule might itself become a mesogen, but its almost macroscopic size would prevent mobility in the mesophase.

One-dimensional plastic crystalline phases and columnar phases, as seem in some liquid crystals for small, rigid molecules are only superficially similar to the macromolecular mesophases. The main difference is that the motion in the small molecules involves rotation or translation of the molecule as a whole, while in a macromolecule the motion is conformational, i.e., in macromolecules rotation is based on segmental motion. Thermodynamically, segmental disorder accounts for considerably larger increases in entropy than disorder of the whole molecule.

In a recent review more than 100 condis crystals of small and large molecular size were analyzed (Wunderlich et al., 1988). About two-thirds of these were small molecules, the rest being macromolecules. It has become clear that liquid crystals and plastic crystals that have conformational isomers show almost as much conformational disorder in the mesophase as is seen in the melt, but that there are many condis crystals in which the mesogens have gained full order, but the flexible parts of the molecules remain fully or partially disordered and mobile. These are then better called condis crystals instead of crystals, since further freezing of large-amplitude motion and ordering is possible at lower temperatures.

Introduction of the term "condis" crystal has solved many problems of classification of mesophases, but many intermediate cases still exist and can, if at all, only be resolved with detailed information on order and motion, as is provided in this thesis on several selected model molecules. Three types of molecules were chosen.

4

(1) Symmetric tetra-*n*-alkylammonium halides (with four linear alkyl chains of equal length): It will be demonstrated for this class of compounds that the plastic crystalline motion, possible for short chain alkyls, can be separated from the conformational mobility. The conformational motion will be shown to begin at a temperature below or equal to that of orientational motion of the molecule as a whole. The longer alkyl chain salts show only conformational disorder and motion before ultimate fusion. (2) N,N'-*bis*-(4-*n*-octyloxybenzal)-1,4-phenylene diamine (OOBPD): It will be shown that for this prior-investigated, liquid-crystal-forming material, some of the low-temperature mesophases (stable at 200−415 K) can be classified as condis crystals. (3) Poly[oxy-1,4-(3-methylphenylene)ethylene-1,4-phenyleneoxynonamethylene], (MBPE-9), and poly[oxy-1,4-(3-methylphenylene)-ethylene-1,4-phenyleneoxypentamethylene], (MBPE-5): It will be shown that the mesophases formed on cooling can be classified as condis crystals. Although the polymers possess a mesogen-like group ($C_6H_3CH_3−CH_2−CH_2−C_6H_4−$), it will be proven that this group remains flexible in the first crystallization step. The conformational disordering in these three types of compounds may occur either gradually, stepwise, or in both ways, depending on the molecular and crystal structures. In this thesis an attempt is made to reveal the details of the disordering processes and, therefore, to delineate the existence of condis states in these small and large molecules.

Distinguishing between the different phases and the different ways (gradual *vs.* stepwise) in which the transitions between the phases take place was possible by

a unique combination of thermal analysis for macroscopic measurement of disorder (through entropy considerations) and solid state NMR (through microscopic motion and conformation considerations). The former technique is well established in the Laboratory of *A*dvanced *TH*ermal *A*nalysi*S*, *ATHAS* (see, for examples, the theses of Roles 1991, Xenopoulos 1990, and Lau 1982). The latter technique is new in our laboratory and has been set up during this thesis work. The basic principles of the applications of these techniques to the problems described above will be given in Chapter 2. The relationships between experimental results and materials properties will be illustrated. In Chapter 3, Results, all the experimental results on the materials analyzed will be presented. It consists of a list of thermal parameters (transition temperatures and entropies), heat capacities, variable-temperature solid state ^{13}C NMR spectra and tables of chemical shifts, and ^{13}C spin-lattice relaxation times (T_1). The results will be discussed in Chapter 4, Discussion, in terms of motion and disorder. Finally, conclusions will be drawn in Chapter 5, Conclusions.

CHAPTER 2

EXPERIMENTAL METHODS

2.1   Introduction

In order to study the mesophases, particularly the condis phase, many techniques have proven to be useful. Among these are, for example, thermal analysis (Wunderlich, 1990), diffraction methods (X-ray, neutron, and electron diffractions) (Sherwood, 1979; Parsonage and Staveley, 1978), solid state nuclear magnetic resonance (NMR) spectroscopy (Slichter, 1969; Boden, 1979; Mehring, 1983; Saitô, 1986; Jelinski, 1987; Tonelli, 1989), infrared and Raman spectroscopy (Dows, 1963; Cabana, 1975; Bailey, 1979), neutron scattering spectroscopy (Egelstaff, 1965), dielectric properties (Smyth, 1955; Pethrick, 1979) and other spectroscopies. In this thesis work, the major techniques used were thermal analysis and solid state ^{13}C NMR. It is the purpose of this chapter to illustrate the kind of information these two techniques may provide for the interpretation of the property and behavior of interesting mesophases. Experimental details of thermal analysis and solid state ^{13}C NMR are provided in Section 2.2.7 and 2.3.6. The discussion of how to combine the two complementary techniques, thermal analysis and solid state NMR, to make a full macroscopic and microscopic characterization of the mesophases will be made in Chapter 4. A description of the analyzed samples is given at the end of this chapter.

2.2   Thermal Analysis

The subject of *Thermal Analysis* (Wunderlich, 1990) is based on the theories of thermodynamics, irreversible thermodynamics, and kinetics. It covers five basic techniques: differential thermal analysis (DTA), calorimetry, thermomechanical analysis (TMA) and dilatometry, and thermogravimetry. The most intensively used techniques in this work are DTA and calorimetry which represents the effort of measuring transition (or reaction) temperatures and heats. In the following, a brief description is given for the applications of DTA and calorimetry to the characterization of phase transitions and measurement of heat capacity. Finally, the computation of the heat capacity, leading to the *A*dvanced *TH*ermal *A*nalysis *System*, *ATHAS*, and comparison between the experimental and calculated heat capacities will be discussed.

2.2.1   Differential Thermal Analysis and Calorimetry

In principle, Differential Thermal Analysis (DTA) is a technique which combines the ease of measurement of the cooling and heating curves with the quantitative features of calorimetry. Temperature is measured continuously and a differential technique is used in an effort to compensate for heat gains and losses. A typical DTA consists of a computerized programme to change the furnace temperature at a preset, linear rate; a control-thermocouple to check the furnace temperature against the program temperature, any difference between the two is used to adjust the power supplied to the heater; two or more sample cells are placed

symmetrically into the furnace so that for the same temperature difference with respect to the furnace the heat flow should be the same.

Calorimetry is the technique that is used to measure the heat produced or absorbed in a process such as a phase transition or chemical reaction. There is, however, no heat meter, *i.e.*, there is no instrument that permits one to find the total heat content of a system directly. The heat content must be deduced by reference to the state without thermal energy at absolute zero of temperature. A common way to measure a change in heat content is conversion of a known amount of electrical energy to produce a known heat flow, and thus measure the difference in heat content by comparison. Most calorimetric data in this work are obtained by the method of *differential scanning calorimetry* (DSC), which is a differential thermal analysis (DTA) used to give calorimetric information. The quantities derived from DSC are *heat capacity* and *heats and temperatures of first-order transitions*. Detailed descriptions of instrumentation of DSC and methods of measurement on these quantities are given in the literature (Wunderlich, 1990).

2.2.2 Transition Parameters

To characterize a phase transition at constant pressure, two parameters need to be known: the equilibrium temperature, T_{tr}, and enthalpy, ΔH_{tr}. The equilibrium temperature, T_{tr}, is often obtained by extrapolating the apparent transition temperature to zero heating rate. The transition ΔH_{tr} is called a latent heat, *i.e.*, heat that does not show up in the total thermal energy of motion expressed by heat

capacity (discussed below). One needs, therefore, to separate the transition enthalpy from the effects caused by the thermal energy of motion. The heat absorbed in a transition is largely in the form of potential energy (change in interaction energy) and counterbalanced by the corresponding change in disorder, the entropy ($\Delta S_{tr} = \Delta H_{tr}/T_{tr}$) which is emphasized below.

2.2.3 Empirical Rules of Transition Entropy

It has been mentioned in the Introduction that when a fully ordered, rigid, crystal is heated, it may undergo one or more transitions into disordered phases (condis crystal, plastic crystal, liquid crystal, and ultimately the melt). Starting with the crystalline state, the entropy increases going successively to lower states illustrated in Fig. 1. The overall melting process (in one or more steps) is characterized by the overall entropy of fusion.

The overall entropy of fusion of a crystal, ΔS_f, can approximately be separated into the three contributions (Wunderlich and Grebowicz, 1984) arising from positional disordering, ΔS_{pos}, orientational disordering, ΔS_{orient}, and conformational disordering, ΔS_{conf}, so that

$$\Delta S_f = \Delta S_{pos} + \Delta S_{orient} + \Delta S_{conf} \tag{1}$$

It is possible to make a first judgment of a phase classification based on the thermal analysis of the first order transitions. Such analysis is facilitated by the empirical "rules" as follows:

10

$$\Delta S_{pos} = 7-14 \text{ JK}^{-1}\text{mol}^{-1} \quad \text{(Richards's rule, Richards, 1897)},$$

$$\Delta S_{pos} + \Delta S_{orient} = 30-60 \text{ JK}^{-1}\text{mol}^{-1} \quad \text{(Walden's rule, Walden, 1908)},$$

$$i.e., \ \Delta S_{orient} = 20-50 \text{ JK}^{-1}\text{mol}^{-1}, \quad \text{and finally:}$$

$$\Delta S_{conf} = 7-12 \text{ JK}^{-1}\text{mol}^{-1} \quad \text{(Wunderlich, 1980)}.$$

The positional and orientational entropies, ΔS_{pos} and ΔS_{orient}, refer always to the whole molecule, *i.e.*, they do not change with size of the molecules, while ΔS_{conf} refers to a single flexible bond (or a rigid bead), *i.e.*, for a molecule, the total ΔS_{conf} is size-dependent. The rather broad ranges of values indicate the approximate nature of this description. For a more precise analysis, the smaller effects of additional disorder, volume change, changes in vibrational frequency, *etc.* must be accounted for. Nevertheless, the empirical rules permit estimations of the entropies for various transitions between the phases indicated in Fig. 1.

Particularly well obeyed is a transition entropy of $7-14 \text{ JK}^{-1}\text{mol}^{-1}$ (Richards' rule) for the melting of crystals of spherical motifs, such as noble gases, metals, as well as for almost spherical motifs, *i.e.*, the plastic crystals (Wunderlich 1990), where only ΔS_{pos} is expected. Simple salts (consisting of two atomic ions of opposite charge, therefore, with two spherical motifs per one formula unit) have been documented (Xenopoulos *et al.*, 1991) to also fall into this category. The plastic crystals of this research observe the same entropy rules on ultimate fusion.

For crystals which separate on melting into small, non-spherical, rigid motifs, the overall entropy of fusion consists of positional and orientational contributions,

being $\Delta S_{pos} + \Delta S_{orient} = 30-60 \, JK^{-1}mol^{-1}$ (Walden's rule). Plastic crystals gain this entropy of fusion in two steps. The first disordering occurs at a temperature T_d lower than the ultimate melting temperature, T_i (isotropization). On heating beyond the low-temperature transition, the molecules become orientationally disordered and rotate more or less freely at their fixed crystal sites. The entropy change of the plastic crystals at the low-temperature disordering transition, T_d, is, thus, related to the gain in orientational disorder having a value of $\Delta S_{orient} = 20-50 \, JK^{-1}mol^{-1}$. The orientational disordering and magnitude of the entropy change for small, almost-spherical molecules have previously been demonstrated using 26 examples from the literature (Wunderlich, 1990). A recently analyzed series of hexa-substituted benzenes also shows an entropy change on disordering within the same range of ΔS_{orient} at temperatures lower than isotropization (Fu *et al.*, 1992). Small tetraalkylammonium halides (with 1, 2, and 3 carbon atoms in each alkyl chain) also show a crystal-to-plastic transition and an overall entropy change predicted by Walden's rule. Details will be given in Chapter 4. The transition from the liquid crystalline phase to the melt, on the other hand, are always much less than expected from the average ΔS_{orient}, indicative of the rather high degree of orientational disorder and mobility in liquid crystals (Wunderlich and Grebowicz, 1984). The smectic phase of liquid-crystal forming molecule, OOBPD, studied in this work, is one such example.

Finally, conformational disordering is expected in flexible molecules having more than one possible conformation. The entropy of fusion for normal *n*-paraffins

increases with increasing chain length, *i.e.,* it is molecular size dependent (Wunderlich and Grebowicz, 1984; Wunderlich 1990). The larger paraffins are not rigid molecules; they are flexible. By rotation about the back-bone bonds, different conformations can be produced. In the crystal the flexible molecules are held rigidly in one conformation through close packing. In the melt, however, they can take random conformations. The increase in ΔS_f with chain length indicates that there is a *conformational contribution* to the entropy of fusion. The survey on *n*-paraffins, C_nH_{2n+2}, and polyethylene shows that the entropy contribution from a single, flexible C−C-bond is largely constant, being 9.5 $JK^{-1}mol^{-1}$ (here mol^{-1} means per mole of flexible bonds). Other studied small, flexible molecules are, for example, cyclic alkanes and silanes (Wunderlich *et al,* 1988). Tetra-*n*-alkylammonium cations and MBPE-*n* samples will be shown in this work to have similar size-dependent entropies of fusion. Just as the small molecules, macromolecules have only *one* positional and *one* orientational entropy of fusion contribution to give $\Delta S_{pos} + \Delta S_{orient} = 30-60$ $JK^{-1}mol^{-1}$. This contribution can be neglected relative to the much larger conformational contribution which is molecular size dependent. Melting data of 33 linear macromolecules (Wunderlich, 1980) showed that the entropy contribution from a mobile unit is again constant at 9.5 $JK^{-1}mol^{-1}$.

It should be noted that any specific type of disorderings discussed above, particularly conformational, and also orientational, may be achieved either in a single transition, or through several distinguishable transitions (stepwise). It is even possible that disordering may occur gradually without showing any transitions.

Moreover, two or all three types of disordering shown in Eq. (1) may occur concomitantly.

2.2.4 Heat Capacity

The empirical fusion rules discussed in Sect. 2.2.3 are useful to identify the state of a crystal undergoing sharp (first order) transitions. In many systems, a transition may, however, be gradual or partly gradual. In this case, if one follows the thermodynamic functions from the melt to absolute zero of temperature, the observed entropy loss during the sharp transitions would be less than predicted by the fusion rules. The 'missing' or 'excess' entropy can be identified quantitatively by knowing the temperature dependence of the heat capacities, as will be shown in Sect. 2.2.5. Other thermodynamic functions, such as enthalpy (the total amount of thermal energy and potential interaction energy), and Gibbs energy (overall stability of the chosen system), can also be obtained from the temperature dependence of the heat capacity. Therefore, to give a full description of a system, heat capacity information should be combined with data on heats or entropies of transition.

Heat capacity is the basic quantity derived from calorimetry measurement. The principles and instrumentation for the measurement of heat capacity have been well described (Wunderlich, 1990). In the following, an effort will be made to illustrate how the heat capacity information can be applied to the study of disorder and motion in crystals. It involves two steps: Calculation of the heat capacity contribution resulting from vibration alone, followed by comparison with the

measurement and, thus, evaluation of the additional contribution from the entropy of disordering $(\partial S/\partial T = -C_p/T)$.

2.2.5 Heat Capacity Calculation

The theory of heat capacity, its computations, and limitations are well documented in several publications from the laboratory of *ATHAS* (Cheban *et al.*, 1982; Lau and Wunderlich, 1983; Loufakis and Wunderlich, 1988 and Bu *et al.*, 1987). The computer programs for the necessary calculations have been described in detail (Cheban *et al.*, 1982 and Lau and Wunderlich, 1983). In short, for a crystal, the vibrational spectrum is arbitrarily divided into skeletal and group vibrations. For polyethylene and linear paraffinic crystals the heat capacity contributions from the group vibrations are computed making use of frequencies obtained from normal mode analyses based on infrared (IR) and Raman data of paraffins and polyethylene. After subtracting the group vibration contributions to the heat capacity from the experimental heat capacity at constant volume, C_v, in a temperature range where only vibrational motion is expected (below about 150–200 K). The remaining skeletal contribution to the heat capacity is fitted to the Tarasov equation with two characteristic temperatures Θ_1 and Θ_3. Reversing this procedure, Θ_1, Θ_3 and the group vibrations permit the computation of the vibrational heat capacity at constant volume over a wide temperature range. At the higher temperatures where conformational disorder is introduced one expects an increasing experimental heat capacity compared to the just computed values.

In somewhat more detail, the group vibrations from narrow frequency distributions are represented by single Einstein functions E:

$$C_v/NR = E(\Theta_E/T) = \frac{(\Theta_E/T)^2 \exp(\Theta_E/T)}{[\exp(\Theta_E/T) - 1]^2} \tag{2}$$

where Θ_E is the Einstein frequency in kelvin (K). Wider frequency ranges are averaged from an upper frequency Θ_U to a lower frequency Θ_L to compute the heat capacity contributions in a box distribution function B:

$$C_v/NR = B(\Theta_U/T, \Theta_L/T) = \frac{\Theta_U}{\Theta_U - \Theta_L}[D_1(\Theta_U/T) - (\Theta_L/\Theta_U)D_1(\Theta_L/T)] \tag{3}$$

More complicated distributions are broken into several Einstein and box terms.

The skeletal vibrations of linear macromolecules are approximated by the Tarasov model which consists of a combination of one- and three-dimensional Debye functions and is given by:

$$C_v/NR = T(\Theta_1/T, \Theta_3/T) = D_1(\Theta_1/T) - (\Theta_3/\Theta_1)[D_1(\Theta_3/T) - D_3(\Theta_3/T)] \tag{4}$$

where the one- and three-dimensional Debye functions D_1 and D_3 are represented by:

16

$$C_v/NR = D_1(\Theta_1/T) = (T/\Theta_1) \int_0^{(\Theta_1/T)} \frac{(\Theta/T)^2 \exp(\Theta/T)}{[\exp(\Theta/T) - 1]^2} \, d(\Theta/T) \qquad (5)$$

$$C_v/NR = D_3(\Theta_3/T) = 3(T/\Theta_3)^3 \int_0^{(\Theta_3/T)} \frac{(\Theta/T)^4 \exp(\Theta/T)}{[\exp(\Theta/T) - 1]^2} \, d(\Theta/T) \qquad (6)$$

T represents, as usual, the temperature in kelvin; R is the gas constant; N, the number of skeletal vibrations considered by the equation; and Θ_1 and Θ_3 are the upper frequency limits of the intra- and inter-molecular frequency distributions, expressed in kelvin (1 Hz = 8.40×10^{-11} K).

The frequencies that must be known in order to carry out a calculation of C_v for the compounds discussed in this thesis are, (1) those of the group vibrations for each functional group or segment, such as $-CH_2$, $-CH_3$, C–O, and phenylene group, etc., (2) the theta temperatures, Θ_1 and Θ_3. The approximate frequency spectra for group vibrations have been well documented for many structural segments in more than 100 polymers and a number of small molecules. For the contribution of skeletal vibrations, the estimation of Θ_1 and Θ_3 is done by fitting the low temperature heat capacity data (as low as about 10 K). When low temperature data (≤ 50 K) are not available, which is a commonly encountered situation, only Θ_1 can be obtained. Typical values for Θ_3 can then be estimated by comparison with compounds with similar chemical structure. The relative deviation at low temperature may then be

17

larger than the usual 3−5%, but the absolute value of the heat capacity at low temperatures is so small that the error in the integral functions *H, S,* and *G* at room temperature is negligible even in these cases of limited experimental data.

Heat capacity calculations of tetra-*n*-alkylammonium salts are carried out by considering additional contribution from the inter-ion vibrations. The contributions from the linear alkyl chains can be treated in a similar way shown above for polyethylene and *n*-paraffines (Jin and Wunderlich, 1991). To evaluate the contribution of the inter-ion vibrations to the overall heat capacity of tetra-*n*-alkylammonium salts, the vibrations of the cations are separated into 3 lattice vibrations, the skeletal vibrations, evaluated as in chain molecules, and the group vibrations. The ionic lattice vibrations can then be computed assuming a spherical shape and diameter and mass proportional to the number of carbon atoms in the alkyl chains. In this simplification, the ionic lattice vibrations of the salts are then treated as for a simple salts consisting of two atomic ions. It is known that heat capacities of simple salts can be reproduced quite well by three-dimensional Debye function (Debye, 1912). Examples have been documented for some crystals of elements and simple salts like LiF, NaCl, KCl, KBr, KI, RbBr, and RbI, *etc.* (Wunderlich, 1991).

The heat capacity for the three-dimensional Debye approximation is given by

$$C_v = 3RD_3(\theta_3/T) \tag{7}$$

in which $D_3(\theta_3/T)$ is the three-dimensional Debye function (Debye, 1912) given by Eq. (6). The frequency distribution $\rho_3(v)$ is quadratic in frequency v:

$$\rho_3(v) = 9Nv^2/v_3^2 \qquad (8)$$

The maximum frequency at which $3N$, the total possible number of vibrations for N atoms, is reached is v_3 or $\theta_3 = hv/k$, where k is the Boltzman's constant.

With Eqs. (6) and (7), C_v of a simple salt can be calculated, if θ_3 is known. The θ_3-temperatures for some simple salts consisting two atomic ions are (Wunderlich 1991): 680 (LiF), 280 (NaCl), 260 (KCl), 180 (KBr), 195 (KI), 130 (RbBr), 115 (RbI), 180 (AgCl), and 140 (AgBr).

It can be seen from these data that "hard solids" (with strong bonds) have higher theta temperatures, and "softer solids" (with weaker bonds) have lower theta temperatures. Somewhat less obvious from the examples is that heavy atoms have lower theta temperatures than lighter ones. These correlations are consistent with the standard calculations of frequencies of vibrators of different force constants and masses. The frequency is proportional to $(f/m)^{1/2}$, where f is the force constant and m is a appropriate mass.

The theta temperatures for tetra-n-alkylammonium salts can be obtained by extrapolating the parameters, such as, reduced masses, force constants. Because of the long distance between the nitrogen and anion (weak bond) and other factors, the tetra-n-alkylammonium salts have quite small θ-temperatures. Since vibration in

19

crystals with lower θ-temperatures are fully excited at low temperatures, and *vice versa*, the inter-ion vibrational contribution to the overall C_v is temperature dependent only at low temperatures, which is similar to the intermolecular skeletal vibrations in a linear chain.

The conversion of the heat capacity at constant volume (C_v) to that at constant pressure (C_p), and *vice versa*, is done by using a modified Nernst-Lindemann equation (Pan *et al.*, 1989):

$$C_p - C_v = 3R A_0(\text{new}) C_p T / T_m^\circ \qquad (9)$$

where $A_0(\text{new})$ is a constant fitted to experimental data on compressibility and expansivity, or approximated by a universal value of 3.9×10^{-3} (K mol)/J; T_m° represents the equilibrium melting temperature or an estimate when not available.

2.2.6 Comparison between Calculation and Measurement

It was first observed in 1962 (Wunderlich, 1962) that the measured heat capacity of crystalline polyethylene at high temperatures is systematically higher than the calculation based on the assumption that vibrations only contribute to C_v. Recently the *n*-paraffins provide another example of such deviation (Jin and Wunderlich, 1991). One assumes that at sufficiently high temperatures, large-scale motion, such as rotation about C−C-bonds, is also introduced and undoubtedly contributes to the heat capacity. Therefore, the increase in experimental heat

20

capacity beyond that caused by vibrational motion has been linked to conformational motion in the crystal at temperatures below the phase transitions (Jin and Wunderlich, 1991). For polyethylene this deviation begins somewhat below room temperature (Noid, *et al,* 1989). Similar initial deviations are estimated to appear about 110 K for pentane, 120 K for heptane, 150 K for decane, 200 K for hexadodecane, and 260 K for pentacontane. Typical deviations of all data from a smooth curve are ±20 K. The deviations in heat capacity can exceed 20% for the longer paraffins at the transition temperature. Similar comparisons will be made on the model compounds studied in this work.

The separation of the contribution of the gradually increasing conformational motion from that of vibrations is accomplished by an integration of $(C_p^{Expt.} - C_p^{Calc.})/T$, termed before as the 'missing' or 'excess' entropy. For paraffins, the excess entropy ranges from 1.4 $JK^{-1}mol^{-1}$ for decane to 8.7 $JK^{-1}mol^{-1}$ for hexacosane. Although these excess entropies are only a few percent of the total entropies of transition (118 $JK^{-1}mol^{-1}$ for decane and 279 $JK^{-1}mol^{-1}$ for hexacosane), the conformational motion is important for the understanding of chain diffusion, crystal annealing, and lamellar deformation.

Finally, a full characterization of the disorder and motion in crystal can be made by combining the excess entropy, obtained from the integration of the differential heat capacity, with the entropy changes measured at the sharp transitions. The combined value is expected to follow the empirical fusion rules given in Section 2.2.3. To test the fusion rules on a microscopic scale, *i.e.,* to know specifically where

and how the status of the motion changes in the molecule as a function of temperature or at a transition, variable-temperature NMR spectroscopy was used as the major tool of the research described in this thesis and is discussed in Sect. 2.3.

2.2.7 DSC Experimental

For the samples of tetra-*n*-alkylammonium bromides and iodides, preliminary measurements, including a check on sublimation and decomposition, were performed on the Mettler FP-800 DSC system. All samples were run from room temperature to 670 K with a check of mass loss after completion of the run. The Mettler instrument was calibrated for temperature and heat of fusion using the melting parameters of indium.

The samples were subsequently run in a Perkin-Elmer DSC-7 for a quantitative study of the transitions outside of the decomposition or sublimation range. The instrument had been calibrated for temperature with naphthalene and indium, and for heat of fusion with indium. The lowest achievable temperature was 230 K.

In addition, the temperature range from 140 K to 230 K was checked for additional transitions using the TA Instruments (previously DuPont) single-run DSC-2100 (Jin and Wunderlich, 1990a). The samples were cooled at 5 K/min to 140 K, and left there for 30 min to equilibrate. For all three instruments, the experiments were done in a dry nitrogen gas atmosphere at a heating rate of 10 K/min. In all cases, sample weights ranged from 5 to 25 mg. In order to verify whether fusion had indeed occurred at the highest-temperature transition, a digital

melting point apparatus with capillary sample containers (model MFB-595 from Gallencamp company) was also used for visual verification.

For the sample of N,N'-*bis*(4-*n*-octyloxybenzal)-1,4-phenylenediamine (OOBPD), the heats of transition and heat capacities of OOBPD were measured using the Thermal Analysis 2100 System from TA Instrument Inc. with a 912 Dual Sample DSC and a DSC Autosampler. The heating rates were 10 K/min and measurement was done under a nitrogen gas flow at 15 ml/min. A single-run heat capacity technique was used for the measurements which was discussed in detail before (Jin and Wunderlich, 1990a; 1990b; 1992). The OOBPD of 10–20 mg sample weight was enclosed in aluminum sample pans. The heat capacities were calibrated with sapphire, and the temperatures were calibrated at the transition temperatures of cyclohexane (T_d = 186.1 K, T_m = 279.7 K), cycloheptane (T_d = 134.8 K, T_m = 265.1 K), cyclooctane (T_d = 166.5 K, T_m = 288.0 K), 1-chlorobutane (T_m = 150.1 K), 2-chlorobutane (T_m = 141.9 K), *n*-octane (T_m = 216.4 K), naphthalene (T_m = 353.4 K), indium (T_m = 429.8 K), tin (T_m = 505.1 K), and KNO_3 (T_m = 607 K). Heat capacities were measured from 130 to 550 K with three sets of experiments (130–360 K, 330–520 K, and 510–550 K). Five repeated runs, each, were used to average for the reported data. All sample placement was done with the Autosampler for increased repeatability.

The DSC measurements of the polymers poly[oxy-1,4(3-methylphenylene) ethylene-1,4-phenyleneoxynonamethylene], MBPE-9, and poly[oxy-1,4(3-methyl-phenylene) ethylene-1,4-phenyleneoxypentamethylene], MBPE-5, were carried out

partially in cooperation with the *ATHAS* Laboratory at the Institute and Department of Polymer Science, College of Polymer Science and Polymer Engineering, The University of Akron, headed by Professor S. Z. D. Cheng. Thermal measurements were performed on a Perkin-Elmer DSC-2 and a Seiko 210 Thermal Analyzer. The sample weights, heating and cooling rates are similar to that for OOBPD described above.

The heat capacities were in all cases compared to and correlated with parallel or subsequent runs of Al_2O_3 (sapphire).

2.3   Solid State ^{13}C Nuclear Magnetic Resonance Spectroscopy

2.3.1   Introduction

The most recent advance in understanding of the solid state of molecular crystals is made possible by the study of disorder and large amplitude motion of the constituent ions or molecules. Solid state NMR was the first and is the most widely used technique for obtaining information on the nature of this motion. Large amplitude molecular motions (such as rotation and translation) which are possible in the liquid state are generally quenched or highly restricted in the solid state. The molecules assume relatively fixed conformations dedicated by the balance of inter- and intramolecular repulsive and attractive interactions. The remaining motion is almost exclusively vibrational, *i.e.*, a small amplitude motion. In the past, vibrational

motion was treated as the only possible motion in the solid state, *i.e.*, crystalline or glassy state. In this thesis the large amplitude motion that leads ultimately to disordering as in the mesophases or the melt will be studied for the chosen model compounds: symmetric tetra-*n*-alkylammonium bromides and iodides, N,N'-*bis*(4-*n*-octyloxybenzal)-1,4-phenylenediamine (OOBPD), and poly[oxy-1,4(3-methyl-phenylene)ethylene-1,4-phenyleneoxynonamethylene] (MBPE-9), and poly[oxy-1,4(3-methylphenylene)ethylene-1,4-phenyleneoxypentamethylene] (MBPE-5).

Conventional NMR spectra of a solid are dominated by nuclear dipolar broadening (50 kHz or larger) and anisotropic shielding effects (10 – 250 ppm), which cover a wide spectral range, comparable to, or larger than that of the whole spectrum of mobile molecules in the liquid state (5 – 200 ppm or less). In most cases such a spectrum of a solid does not give any information concerning individual atoms. It is due to this limitation that most crystals studied with wide-line solid state NMR methods are thus either small or highly symmetrical molecules and ions in which there is only one equivalent spin. This type of experiment involves measurement of the line-width and the second moment with a conventional continuous-wave (CW) spectrometer (Slichter, 1969).

The solid state ^{13}C NMR measurements described in this thesis are mainly done under the conditions of high resolution (high-resolution ^{13}C NMR). This has been made possible by the technique known as CP-MAS. It consists of the combined techniques of *Cross-P*olarization to gain sensitivity (CP) (Andrew, 1972; Pines *et al.*, 1972), *M*agic-*A*ngle *S*pinning to average the anisotropy (MAS) (Andrew *et al.*, 1959;

25

Lowe, 1959) and high-power decoupling of any coupled protons to remove the dipolar broadening. The resonances appear as relatively well-resolved signals permitting distinction among individual ^{13}C atoms in the molecule, therefore, providing valuable information on molecular motion at sites of individual atoms. From a high-resolution NMR spectrum, one can measure chemical shift values that have been found to be conformation dependent. High resolution spectra also allows one to measure spin relaxation times for individual ^{13}C atoms, which can be used to evaluate the rate of the motion. Applications of these two NMR observables (chemical shift and relaxation time) to the study of motion will be illustrated in detail in the following sections.

Besides the conventional broad-line and modern high-resolution CP-MAS techniques, one of the most frequently used ^{13}C NMR methods is the observation of the ^{13}C chemical shift anisotropy (CSA) powder pattern. A powder pattern is obtained in the same way as CP-MAS, except that the sample is kept static; therefore, only one of the two line-broadening contributions, i.e., nuclear dipolar broadening, is removed by the high-power decoupling, while the anisotropic shielding effect remains. It was shown that the appearance of the CSA powder pattern is defined by the symmetry and rate of the motion in which the observed ^{13}C atom is involved (Veeman, 1984; Mehring, 1983).

2.3.2 High Resolution NMR of Solids, CP-MAS

The major problems that prevents one from obtaining a high-resolution solid state ^{13}C NMR spectrum are: severe line-broadening due to strong nuclear dipole-dipole interactions (DD), chemical shift anisotropy interactions (CSA), and low signal intensity due to extremely long ^{13}C spin-lattice relaxation times caused by slow molecular motion.

For the dipole-dipole interactions, the Hamiltonian for an isolated $^{13}C-^{1}H$ spin pair can be expressed in the following form,

$$H_{CH}^{DD} = \frac{\gamma_C \gamma_H h^2}{16\pi^2 r^3}(1 - 3\cos^2\theta) \tag{10}$$

in which the γ's refer to the ^{13}C and ^{1}H magnetogyric ratios; r is the length of the internuclear distance; h Planck's constant, and θ the angle between the internuclear vector (of length r) and the external magnetic field. In a solid sample there may exist many such pairs of spins with different r and θ, therefore, H_{CH}^{DD} and resonance frequency is variable for different spins resulting in a broad resonance line. The linewidth due to this interaction may be as large as many kHz. Thus, a single solid state line is comparable to the width of entire liquid sample spectrum, where the local dipolar interactions are averaged to zero. For ^{13}C of natural abundance, the homonuclear dipolar interaction (*i.e.*, dipolar interactions between ^{13}C and another

27

^{13}C) are small enough (compared to ^{13}C-^{1}H heteronuclear) to be neglected because of the low concentration ($\approx$ 1.1%).

The other cause of line-broadening in a ^{13}C NMR spectrum is the chemical shift anisotropy (CSA) interaction. This arises from the fact that the nucleus under the observation is magnetically shielded to some extent from the external magnetic field because of the circulation of the electrons of the atoms or chemical bonds. The magnitude of the shielding, expressed as chemical shift value, is, however, dependent on the orientation of the electron circulation or direction of the chemical bond relative to the external field. In a powder or in a amorphous sample each molecule or molecular group may orient in all possible directions and the observed spectrum shows a spread of chemical shifts, resulting in a broad resonance band. The chemical shift anisotropy interaction was shown theoretically (Mehring, 1983 and Veeman, 1984) to be proportional to $(1 - 3\cos^2\theta)$, a factor which is also present in the Hamiltonian for dipolar interactions. The spread of the spectrum for a static powder sample ranges from 20 ppm for a methyl carbon to about 210 ppm for an non-protonated aromatic carbon (Jelinski, 1987). Although the chemical shift anisotropy contains valuable information, several overlapping chemical-shift-tensor powder patterns from chemically distinct nuclei often complicate the observed spectrum.

In addition to the problems which cause severe line broadening as discussed above, another problem in the solid state NMR of ^{13}C arises from its low intensity. This is caused by (1) long spin-lattice relaxation times, T_1, (that will be shown in Section 2.3.4 to be a result of rather sluggish molecular motion). The long relaxation

time limits the number of data acquisitions in a given period of time, thus limiting the possible gain in signal-to-noise ratio (S/N), and (2) low natural abundance and small magnetogyric ratio (γ value) of the ^{13}C nucleus, compared to that for a proton.

A typical solid state ^{13}C NMR spectrum, that of hexamethylbenzene (HMB) at room-temperature, is shown as Spectrum A of Fig. 2. The rather broad spectral line of the non-protonated aromatic carbon atoms is due to the combined effects of dipolar interaction between ^{13}C and nearby ^1H nuclei and the chemical-shift-anisotropy interactions.

A successful way of circumventing the problems described above has been found by Schaefer and Stejskal (Schaefer and Stejskal, 1976), who combined three existing techniques, namely, high power dipolar decoupling of protons, magic angle sample spinning (MAS), and cross polarization (CP). The high-power decoupling is used to remove the dipolar interaction between ^{13}C and ^1H. If the decoupling field has a radio-frequency that is the same or close to that of the proton resonance and the decoupling field is strong enough (comparable to the ^{13}C-^1H dipolar interaction), the proton spins can then be made to rotate continuously and rapidly, which results in time averaging of the dipolar moment of the proton vanishes. This is similar to the decoupling of scalar coupling interaction in liquids in high resolution NMR. A significant difference is that the field for dipolar decoupling in the solid state may be as strong as 100 kHz compared to about 200 Hz in the liquid state. (The decoupling field-strength determines the frequency with which protons precess in the rotating frame,
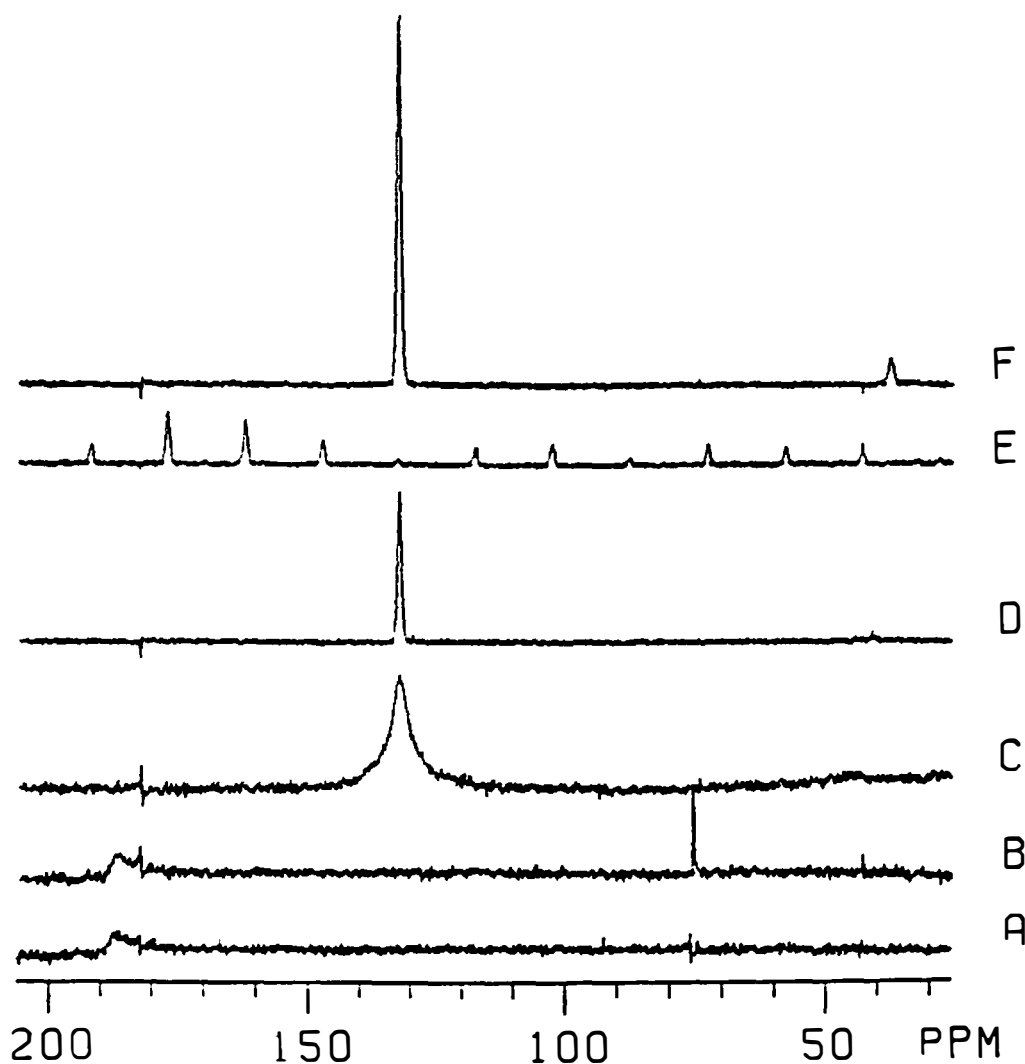
Figure 2   Solid state ^{13}C NMR spectra of aromatic carbons in hexamethyl-
benezene at 298 K. A. Without dipolar decoupling and MAS. B.
Without MAS, but with dipolar decoupling of 52 kHz. C. With MAS
only (4.5 kHz). The line-width of this highly mobile material narrows
to about 300 Hz, note the fairly low signal-to-noise ratio. D. With
both MAS (4.5 kHz) and dipolar decoupling (52 kHz). The line-width
is narrowed to 35 Hz, but signal-to-noise ratio is not yet optimal. E.
Same as in D, but with a slower spinning rate (700 Hz), note the
spinning side bands. F. three techniques are applied, i.e., CP, MAS
(4.5 kHz), and dipolar decoupling (52 kHz).

therefore, it can be expressed in Hz. In solid state NMR, the decoupling field strength, v_2, corresponds to the reciprocal of the proton 360° pulse length, $t_{2\pi}$, in seconds, *i.e.*, $v_2 = 1/t_{2\pi}$). The effect of dipolar decoupling is shown by Spectrum B of Fig.2. The line-width is still broad because of the remaining CSA contribution.

Line-broadening due to the chemical-shift-anisotropy (CSA) contribution can be eliminated by magic angle sample spinning (MAS), because it has an angular dependence, $(1 - 3\cos^2\theta)$. For a unique angle $\theta_m = 54°44'$, the term $(1 - 3\cos^2\theta)$ equals zero. The quantity θ_m is thus called the magic angle. In practice, the spin pairs of ^{13}C-^1H in a static macroscopic sample may assume all angles from 0° to 180° with respect to the external main field and yield a broad line. If the macroscopic sample is spun sufficiently fast around an axis tilted against the field axis at 54°44', all connecting vectors between ^{13}C and ^1H are brought into this 'magic direction' (54°44') on the time average. Spectrum C of Fig. 2, obtained with MAS, but without dipolar decoupling, shows the effect of MAS. The resonance becomes much more symmetric due to the removal of CSA, but the line-width is still broad due to the residual dipolar interaction. While in Spectrum D, the combined effect of dipolar decoupling and MAS (4.5 kHz) reduce the line-width to about 35 Hz.

In order to eliminate the chemical shift anisotropy completely, the spinning must be fast enough or at least comparable to the width of the powder spectrum. On a 4.7-Tesla spectrometer (50 MHz for ^{13}C), the sufficient spinning rate is, therefore, 0.5 kHz for the methyl carbon (CSA: 20 ppm) and about 5.5 kHz for the non-protonated aromatic carbons (210 ppm). If a slower spinning rate than required

is applied, a series of spinning side-bands will appear in the spectrum, which are separated from the central peak by distances of multiple of spinning rates, as shown in Spectrum E of Fig. 2.

Finally, the problems connected with low intensity of ^{13}C spins can be solved by the method of cross polarization (CP) transfer (Andrew, 1972 and Pines *et al.*, 1972). The basic idea of this method is to use the relatively strong spin polarization (large difference in the population numbers of upper and lower energy states) of the abundant spins, ^{1}H, to enhance the polarization of the rare spins ^{13}C. When the communication has been made possible between ^{13}C and ^{1}H spin systems, the effective relaxation time for ^{13}C is now determined by that of protons which is short. Thus, relatively larger number of data acquisitions can be realized within a given period of time to enhance the signal-to-noise ratio. A detailed description on CP pulse sequence is shown in Chapter 2.3.4. Spectrum F in Fig. 2 shows the effects of dipolar decoupling, and CP-MAS. The line-width is comparable to that in Spectrum D, but the signal-to-noise ratio (S/N) is enhanced due to the use of CP technique.

2.3.3   Interpretation of ^{13}C CP-MAS Spectra

In this section, brief discussions are given on the interpretation of a ^{13}C CP-MAS spectrum in terms of the signal intensity and chemical shift values of a given carbon atom. Analysis of these two fundamental parameters of a solid state ^{13}C spectrum may provide useful information on the molecular motion and conformation.

CP rate equation and related time constants: It is expected that the resonance intensity in a ^{13}C CP-MAS spectrum for a given carbon atom may vary, depending on factors such as temperature and thermal history of the sample. For the same piece of sample at the same temperature, the intensity of the CP-MAS spectrum is, however, still variable depending on the experimental parameters in the CP pulse sequence. It has been shown that the signal intensity at spin-contact time of τ, is given by the rate equation (Jelinski, 1987):

$$M_C(\tau) \sim M_H(0)\,(1 - e^{-\tau/T_{CH}})\,e^{-\tau/T_{1\rho H}} \tag{11}$$

where $M_C(\tau)$ is the ^{13}C spin magnetization, $M_H(0)$ the proton spin magnetization at $\tau = 0$, T_{CH} the time constant at which the polarization transfer occurs between the two spin systems, and $T_{1\rho H}$ is the proton spin-lattice relaxation time in the rotating frame. For rigid materials T_{CH} is on the order of 100 μs, and relation $T_{CH} < T_{1\rho H}$ holds true. According to this rate equation, the evolution of ^{13}C detectable magnetization at time τ consists of two competing processes: the polarization transfer from proton to ^{13}C with a rate constant of $(T_{CH})^{-1}$, which is $1 - \exp(-\tau/T_{CH})$; and the proton equilibration with the lattice in the spin-locked state with a rate constant of $(T_{1\rho H})^{-1}$, which is $\exp(-\tau/T_{1\rho H})$ (a decay term). The available sensitivity and faithfulness of relative intensities of individual ^{13}C nuclei are, therefore, sensitive functions of the relative rates of these two processes, which may be expressed by the ratio of $T_{CH}/T_{1\rho H}$. Figure 3 shows several plots by assuming

33
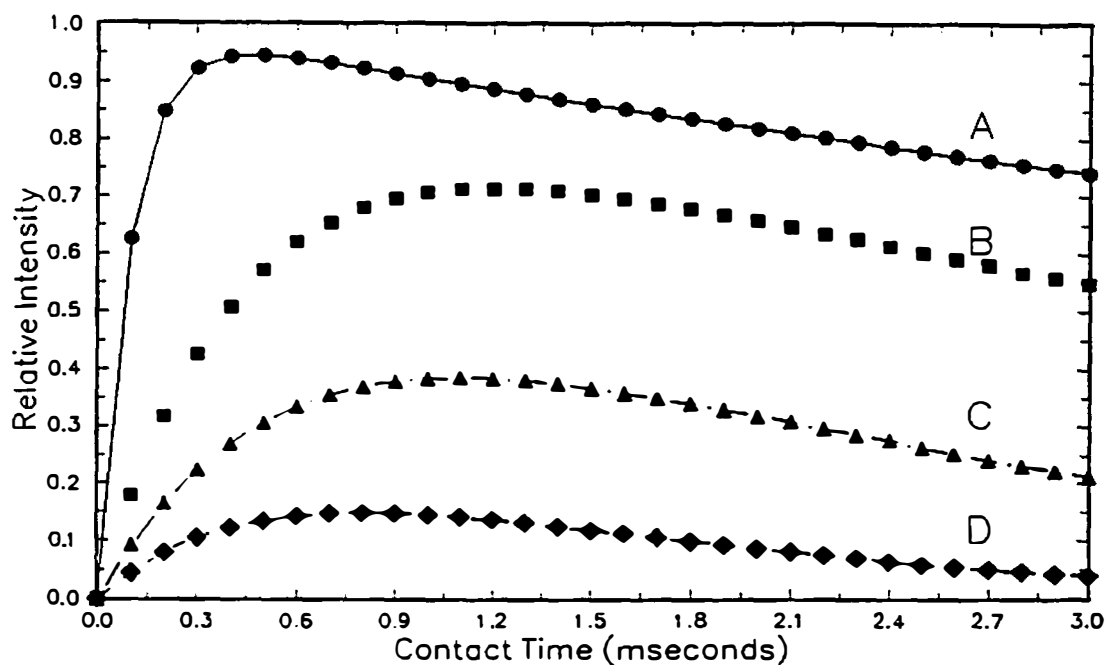
Figure 3   Cross polarization transfer rate curves. Details are given in text.

different values for $T_{1\rho H}$ and T_{CH}.

Curve A of Fig. 3 uses typical values for T_{CH} = 100 μs and $T_{1\rho H}$ = 10 ms.
Note that the maximum attainable ^{13}C magnetization is close to unity, which is the
original value for the proton and is only true when $T_{CH} \ll T_{1\rho H}$, which is, indeed, the
case for a wide variety of organic solids.

There are, however, systems in which either $T_{1\rho H}$ is uncommonly short, or
T_{CH}'s are very long, or both. Molecular motions in the kHz range are effective for

34

rotating-frame spin-lattice relaxation and in some cases may shorten $T_{1\rho H}$ to a few milliseconds or less. The presence of paramagnetic impurities may also reduce $T_{1\rho H}$. The cross polarization constant, T_{CH}, on the other hand, is approximately proportional to the inverse square of the static dipolar interaction H_{CH}^{DD} given by Eq. (10), and, therefore, may be long due to the partial averaging over the angular dependence by a fast molecular motion. The change of signal intensity as a function of spin-contact time, τ, under the influences of short $T_{1\rho H}$ and long T_{CH} is progressively illustrated in Fig. 3 with Curve B for $T_{CH}/T_{1\rho H} = 0.1$, C for $T_{CH}/T_{1\rho H} = 0.5$, D for $T_{CH}/T_{1\rho H} = 2$. As can be seen, the maximum attainable CP intensity decreases as the ratio $T_{CH}/T_{1\rho H}$ increases. For liquids, the value of T_{CH} becomes extremely long because of fast motion that diminishes the dipolar interaction, the CP pulse sequence detects no signal. For solids, measurement of cross-polarization signal intensity as a function of contact time allows to determine the time constants T_{CH} and $T_{1\rho H}$, which can be used to reveal the nature of molecular motion. It should be noted that both T_{CH} and $T_{1\rho H}$ are molecular motion rate dependent, and by changing the sample temperature, the signal intensity may be increased. Examples are shown for tetra-n-propylammonium iodide in the Chapter 4, Discussion.

Chemical shift and γ-*gauche* effect: The chemical shift of a ^{13}C has been found to be dependent of both inter- and intra-molecular interactions. The former determines the packing of molecules in the solid, and the latter influences the molecular conformation. The changes in intramolecular conformations are the most

important influence on the ^{13}C chemical shift (δ values). The intermolecular effect on the ^{13}C δ values is of secondary importance.

It was shown (Stothers, 1972, Wehrli *et al.*, 1988, and Silverstein *et al.*, 1981) that the δ value of a ^{13}C atom is influenced by substituents attached to the observed carbon in the α-, β- and γ-positions, causing so-called α-, β- and γ-substituent effects. The first two effects are constant (independent of chain conformation) as long as the chemical structure of the molecule is fixed. The γ-substituent effect, however, has a conformational contribution (Tonelli, 1981; Bovey, 1982) because the observed carbon, ^{O}C, and its γ-substituent, $^{\gamma}C$, ($^{O}CH_2 - CH_2 - CH_2 - {}^{\gamma}CH_2$) are separated such that their mutual distance and orientation depend on the conformation of the central bond (or rotational isomeric state). For a ^{13}C to be more shielded by a γ-substituent, the ^{O}C and $^{\gamma}C$ must be in a *gauche* arrangement, and the effect of γ-*gauche* shielding can be evaluated to be $\gamma_{C-C} = -5.2$ ppm and $\gamma_{C-O} = -7.2$ ppm (Tonelli, 1981). In the melt or solution between 250 and 400 K, the rotating C – C bonds are expected to have a population of approximately 40% *gauche* conformations, a value adopted by Flory for the melt of polyethylene (Flory, 1969). One would thus expect that after a transition from a fully ordered *trans* bond to 40% of *gauche*, the δ of the corresponding ^{13}C to decrease (be more shielded) by:

$$\Delta\delta = 2 \times (0.4) \times (-5.2) \text{ ppm} = -4.16 \text{ ppm}$$

The factor of two accounts for a possible γ-substituent on both sides of the observed carbon in a chain molecule. If only one of the two γ-substituents has become *gauche*

to ^{O}C, the $\Delta\delta$ would naturally be -2.08 ppm. Similarly, if neither of the γ-substituents has changed its spatial relationship with respect to ^{O}C, $\Delta\delta$ is zero. As temperature is increased, the δ of a ^{13}C in the linear paraffinic chains may thus change by values close to 0, -2, or -4 ppm due to conformational disordering only. Intermediate values for $\Delta\delta$ are also possible, since the concentration of *gauche* conformation is variable with temperature. For a ^{13}C that has an oxygen as its γ substituent, the expected change in the chemical shift is correspondingly larger.

Complications in the chemical shift arise in small molecules that have an *a priori* possibility of motion of the molecule as a whole. In this case the packing (intermolecular interaction) can change when motion begins. The influence of changes in packing on the ^{13}C chemical shifts is perhaps more important in the ionic organic crystals, such as in tetra-alkylammonium halides, since the electron shielding of the ^{13}C nucleus determines the value of ^{13}C chemical shift. Moreover, the change of packing is often coupled with changes in conformation of flexible bonds, and sometimes even with changes in valence angle, making the ^{13}C chemical shift more difficult to interpret in these cases.

Line-width: The resonance line from a solid is often too broad to reveal magnetically inequivalent atoms in a molecule due to the magnetic dipolar interaction of nuclear spins, such as that between ^{1}H and ^{13}C, as well as chemical shift anisotropy, as shown in Fig. 2. As indicated before, by using high power proton decoupling and magic angle sample spinning these line broadening mechanisms can be effectively removed. The residual line-width observed in organic solids is,

however, still broader by a factor of 10 to 100 than those in the liquid spectra. Generally, glassy solids, disordered and rigid, below their glass transition temperature, T_g, give rise to broader ^{13}C resonance lines (30 to 120 Hz at 15 MHz) than do crystalline materials (ordered and rigid) (3 to 12 Hz) (VanderHart et al., 1981). The large difference in the resonance line-widths between solid state CP-MAS and solution state NMR is due to the difference in molecular motion. In the liquid state, fast, large-scale translational, orientational, and conformational motion averages over all available intramolecular as well as the intermolecular interactions to yield sharp resonance lines. On the other hand, in a rigid, disordered glassy solid, the intramolecular energy minima and the local packing forces quench or restrict the molecular motions so that molecules may exhibit dispersions of conformations and orientations for a period of time considered to be long on the NMR time scale. Each such conformation and orientation may contribute a resonance line of unique chemical shift so that the overall lineshape appears as a chemical shift dispersion (inhomogeneous broadening). Elimination of this type of line-broadening, however, can not be done by either high-power decoupling of protons or magic angle spinning as mentioned above, but is possible only by increasing of temperature to increase the molecular mobility (motional average).

The line broadening may occur even in the crystalline state in which a slow motion in the $10^4 - 10^5$ Hz region is present. This motion is too slow to completely average the diploar interactions (the major factor of line broadening in the solid state), and the effect of dipolar broadening can neither be removed by realistically

achievable proton decoupling fields, nor with the magic angle spinning speeds (Schaefer *et al.*, 1977; VanderHart *et al.*, 1981). It was shown (Haeberlin, 1976) that under high power decoupling the average Hamiltonian of the interchain hetero-nuclear dipolar interactions increases gradually while the rate of the motion approaches the frequency-equivalent of the decoupling field strength, therefore, the line-width increases. Thus a $10-100$ kHz motion seems to be the most effective to broaden the line-width of a ^{13}C NMR obtained under the conditions of CP-MAS and dipolar decoupling.

2.3.4 Relaxation Times of ^{13}C

Relaxation times of ^{13}C are of importance for the following reasons: (1) Carbon atoms are generally the backbone of organic molecules and internal conformational motion can be linked exclusively to intramolecular interactions. (2) Due to the rather low natural abundance of ^{13}C, homonuclear dipole-dipole influence between two ^{13}C's on T_1 is negligible. Only nearby protons are effective in relaxation, and for protonated carbon atoms, the contributions from only the directly bonded protons need to be considered. (3) Solid state ^{13}C resonances are generally well resolved in chemical shift by virtue of high power dipolar decoupling of protons and MAS, thus multiple sites are often available at which to probe a molecule's motional features.

In this section, the mechanism of ^{13}C spin-lattice relaxation time, T_1, will be described. Some important equations for T_1 as a function of molecular mobility are

39

introduced. The interpretation of T_1 data for specific types of molecular systems, such as linear paraffinic chains and spherically symmetric plastic crystals, will be illustrated. Finally, the spin-spin relaxation time, T_2, will be introduced to quantitatively distinguish between a mobile and an immobile carbon atom.

Mechanisms: The relaxation time T_1 determines the return of the z-magnetization, M_z, to its equilibrium value after a perturbation and represents the time scale of energy transfer between the spin system and the lattice or environment in which some or all types of molecular motion, *i.e.*, vibrational, translational, orientational and conformational, are activated. The return of x *and* y-magnetization, M_x and M_y, respectively, to their equilibrium values (which are zero) is governed by the time constant T_2, and represents the time scale for the spin system to lose phase coherence in the $x-y$ plane after excitation by a radio frequency (rf).

The relaxations take place because the fluctuating local magnetic fields have frequency components of values appropriate for the nuclear spin transition frequency so that the energy can be transferred to the lattice. The magnetic fields are produced by some of the spins and experienced at the same time by others. The time dependence of the local fields arises from the motion of the molecular system and, therefore, there exists a relationship between molecular dynamics and the spin-lattice relaxation time (spin relaxation mechanism). Various mechanisms of spin-lattice relaxation have been proposed (Abragam, 1961; Redfield, 1965), such as, dipole-dipole (DD), spin-rotation (SR), scalar coupling (SC), nuclear electric quadrupolar coupling (NQC), and chemical shift anisotropy (CSA).

The prime source of spin relaxation in most diamagnetic solids is DD relaxation because of the short distance between spins and slow molecular motion. Especially in solids, DD arises from the local magnetic fields produced by nuclear dipole-dipole interactions. The interactions can either be intermolecular or intramolecular in nature. As indicated in Eq. (10), the dipolar interaction depends on the internuclear distance r and the angle between r and the applied magnetic field H, θ. For rigid systems of intramolecular dipoles, molecular motion imparts a time dependence to the dipolar interaction through θ. For the intermolecular case both θ and r are time dependent owing to relative translational and rotational motions. The intermolecular interaction tends to attenuate more rapidly due to the r^{-3} dependence. This has important consequences for rare spins, for example, ^{13}C, which allows one to neglect the homonuclear dipole-dipole relaxation contributions.

General formula of ^{13}C T_1: The T_1 of ^{13}C caused by dipole-dipole interaction for all types of molecular motion, has been formulated in the following general form (Lyerla Jr. and Levy, 1974; Wright et $al.$, 1986; Kitamaru, 1986):

$$\frac{1}{nT_{1C}} = \frac{\gamma_C^2 \gamma_H^2 h^2}{64\pi^2 r^6} [J_0(\omega_H - \omega_C) + 18J_1(\omega_C) + 9J_2(\omega_H + \omega_C)] \qquad (12)$$

in which n is the number of directly bonded protons, h is Planck's constant, γ_C and γ_H are the carbon and proton magnetogyric ratios (0.67266491×10^8 $s^{-1}Tesla^{-1}$, 2.67522128×10^8 $s^{-1}Tesla^{-1}$, respectively), r_{CH} is the distance between interacting ^{13}C

and ^{1}H, ω_C and ω_H are the respective resonant frequencies of the ^{13}C and ^{1}H. In a 4.7 Tesla field these frequencies are $2\pi \times 50$ MHz and $2\pi \times 200$ MHz, respectively. The functions $J_m(\omega)$, with $m = 0, 1, 2$, are the spectral densities of the motional auto-correlation functions $G_m(\tau)$ for the dipolar interactions, *i.e.*,

$$J(\omega) = \int_{-\infty}^{\infty} G(\tau) e^{i\omega t} dt \qquad (13)$$

The $G_m(\tau)$ are

$$G_m(\tau) = \sum_j \langle F_{ij,m}(t) F^*_{ij,m}(t+\tau) \rangle_t \qquad (14)$$

where

$$\begin{aligned} F_{ij,0}(t) &= r_{ij}^{-3}(1 - 3\cos^2\theta_{ij}) \\ F_{ij,1}(t) &= r_{ij}^{-3}\sin\theta_{ij}\cos\theta_{ij} e^{i\varphi_{ij}} \\ F_{ij,2}(t) &= r_{ij}^{-3}\sin^2\theta_{ij} e^{2i\varphi_{ij}} \end{aligned} \qquad (15)$$

in which r_{ij}, θ_{ij} and φ_{ij} are the spherical coordinates of the vector r_{ij} from spin i to j in a laboratory coordinate system in which the static magnetic field is along the z axis. Spin relaxation is determined by the time dependence of these coordinates. The correlation time τ_C defines the length of time that the molecule or parts of it can be considered to be in a particular state of motion. Thus the shorter the correlation times of molecules, the more rapid is their motion; the longer the

42

correlation times, the slower the motion. Before any information about molecular motion can be obtained from the relaxation time measurements, $G_m(\tau)$ must be calculated for a physically plausible model for the motion; this is by far the most difficult problem in any relaxation study. For a given model of molecular motion, a set of specific motional correlation functions can be proposed which yields a specific set of $J_m(\omega)$'s, thus T_1 assumes a different form.

Relaxation models: The most commonly assumed model is the *rigid rotor model*, which considers generally a molecular ellipsoid undergoing orientational motion. In this model, three situations may be encountered: (1) isotropic, (2) axially-symmetric, and (3) anisotropic rotations.

Isotropic molecular reorientation model considers an internuclear vector r of $^{13}C-^{1}H$ fixed in a molecular ellipsoid undergoing an isotropic, random reorientation. The auto-correlation functions $G_m(\tau)$ are simple exponential decay in form, and it can be shown that the spectral densities are:

$$J_m(\omega) = \frac{2K_m\tau_C}{(1 + \omega^2\tau_C^2)} , \qquad m = 0,1,2 \tag{16}$$

with $K_0 = (4/5)r^{-6}$, $K_1 = (2/15)r^{-6}$ and $K_2 = (8/15)r^{-6}$, and r is the distance between interacting ^{13}C and ^{1}H and normally is the $C-H$ bond distance (1.09×10^{-10} m).

Combination of Eq. (12) with Eq. (16) gives the T_1 of ^{13}C with isotropic random motion:

$$\frac{1}{nT_{1C}} = \frac{\gamma_C^2 \gamma_H^2 h^2}{40 \pi^2 r^6} \left[\frac{\tau_C}{1 + (\omega_H - \omega_C)^2 \tau_C^2} + \frac{3\tau_C}{1 + \omega_C^2 \tau_C^2} + \frac{6\tau_C}{1 + (\omega_H + \omega_C)^2 \tau_C^2} \right]$$ (17)

Based on these relations, a graph (shown in Fig. 4) in which nT_1 of carbon at a magnetic field of 4.7 Tesla changes as a function of correlation times expressed in $-\log \tau_c$ can be made. The relaxation times nT_1 clearly show minima at $-\log \tau_c = 8.6$, i.e. $\tau_C = 2.5$ ns, or $\omega_C \tau_C = 0.793$. At this point the motions are the most effective to ^{13}C nuclear relaxation, while motion with τ_C much shorter or longer than this value have much less influence on ^{13}C T_1.

The *axially-symmetric reorientation model* considers the internuclear vector, r_{CH}, which is fixed in a molecular ellipsoid undergoing axially symmetrical reorientation (Woessner, 1962 a). In this case two molecular rotational diffusion coefficients, R_1 and $R_\perp$, are involved. The molecular frame can be chosen such that one of the direction cosines of vector r equals to zero. The spectral densities are then:

$$J_m(\omega) = 2K_m \sum_{i=1}^{3} \frac{A_i \tau_i}{(1 + \omega^2 \tau_i^2)} , \qquad m = 0,1,2$$ (18)

in which K_m are the same as in Eq. (16), and

$A_1 = (3l^2 - 1)^2/4,$

$A_2 = 3l^2(1 - l^2)/4,$

44
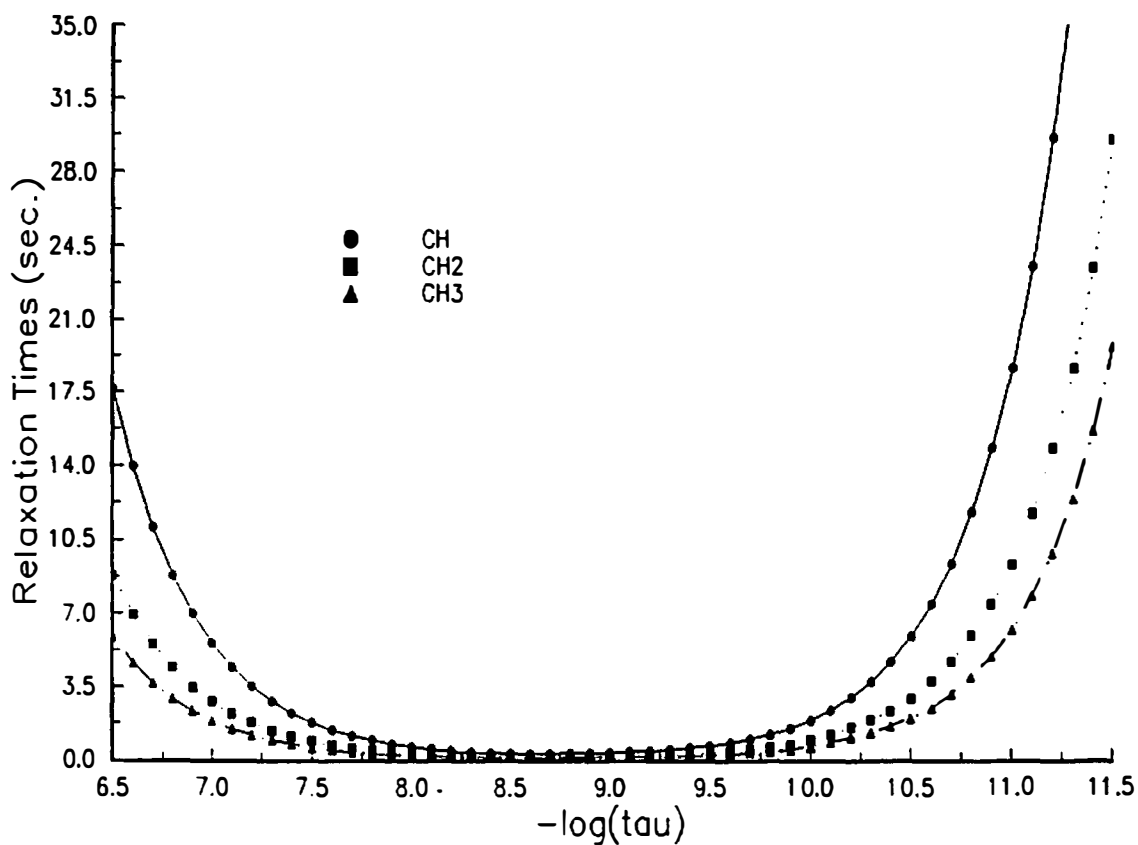
Figure 4   Spin-lattice relaxation times of a ^{13}C nucleus undergoing a random motion. The horizontal axis is the correlation time.

$$A_3 = 3(l^2 - 1)^2/4,$$

with l being one of the two non-zero direction cosines of r, and

$$\tau_1^{-1} = 6R_\perp,$$

$$\tau_2^{-1} = R_\parallel + 5R_\perp,$$

$$\tau_3^{-1} = 4R_\parallel + 2R_\perp.$$

45

The *anisotropic reorientational model*, finally, is the most general rigid-rotor-type molecular motion, it has three independent rotational diffusion coefficients around three axes of the ellipsoid. The resultant spectral densities produced by this motion are, therefore, functions of three independent correlation constants and cosines of the direction of the vector in the molecular frame.

Of particularly interests are some more realistic models in which conformational motion (or internal, segmental motion) is also considered. These are illustrated in the following.

Woessner's 2τ rotation model (Woessner, 1962 b) considers that a molecular ellipsoid undergoes isotropic diffusional reorientations with a correlation time of τ_I and the internuclear vector undergoes at the same time diffusional rotation about an axis of the ellipsoid with an angle Δ and a correlation time of τ_R. The spectral densities have the same form as given by Eq. (18), but with the following correlation times and angular dependence:

$$(\tau_1)^{-1} = (\tau_I)^{-1},$$

$$(\tau_2)^{-1} = (\tau_I)^{-1} + (\tau_R)^{-1},$$

$$(\tau_3)^{-1} = (\tau_I)^{-1} + 4(\tau_R)-1, \text{ and}$$

$$A_1 = (3\cos^2\Delta - 1)^2/4,$$

$$A_2 = 3(\sin^2 2\Delta)/4,$$

$$A_3 = 3(\sin^4\Delta)/4,$$

and the K_m's are the same as before.

Since there are two independent correlation times involved, the resultant T_1 is shown in Fig. 5 as a 3-dimensional plot and a contour plot with respect to both correlation times.
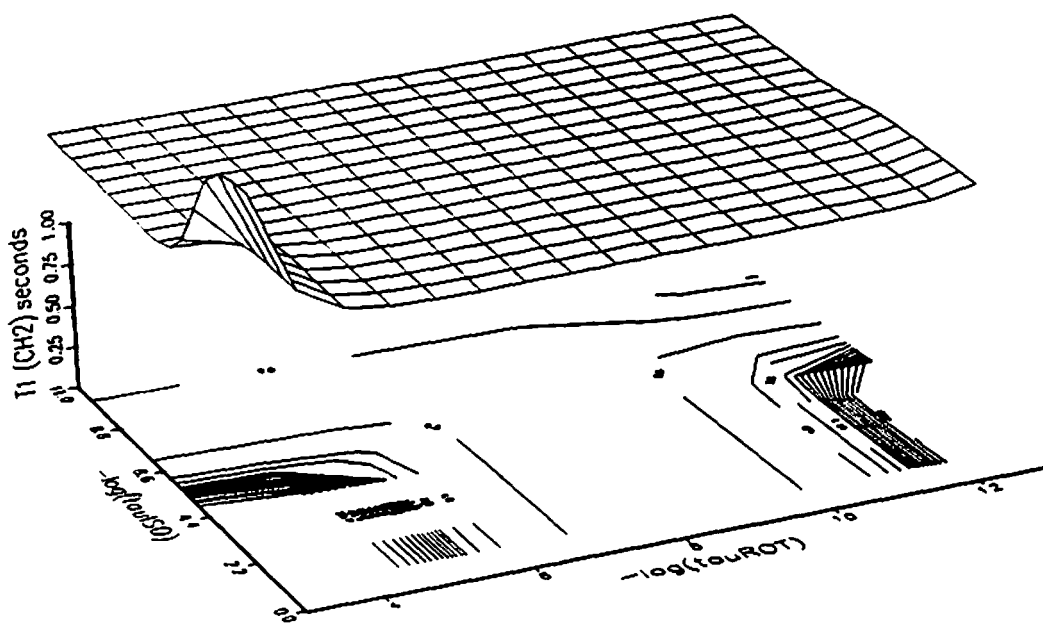
Figure 5   Three-dimensional and contour plots of ^{13}C T_1 with Woessner's 2τ rotational model.

Howarth 2τ libration model (Howarth, 1978 and 1979) is a similar model in which the molecular ellipsoid is considered to undergo isotropic diffusional reorientations with a correlation time of τ_I, and the internuclear vector further undergoes libration about an axis of the ellipsoid within a cone defined by an angle Ω and with a correlation time τ_L. Its spectral densities can also be written as Eq. (18), with the following parameters:

$$(\tau_1)^{-1} = (\tau_I)^{-1},$$

$$(\tau_2)^{-1} = (\tau_I)^{-1} + (\tau_L)^{-1}, \text{ and}$$

$$A_1 = (\cos\Omega - \cos^3\Omega)^2 / [4(1 - \cos\Omega)^2],$$

$$A_2 = 1 - A_1, \text{ and}$$

$$A_3 = 0.$$

The 3-dimensional and contour plots are shown in Fig. 6.

Finally, *Howarth's 3τ librational model* (Howarth, 1979) is the most realistic model considered in this thesis. It is illustrated in Fig. 7.

In the diagram three kinds of motions are noted for a molecular segment, such as $N-CH_2-CH_3$ in the tetraethylammonium cation: (1) the vector of r(C-H) in the methyl group rotates about C-C bond with an angle of Δ and a rotational correlation time of τ_R; (2) the vector of r(C-C) librates about N-C bond within a cone defined by an angle Ω and with a librational correlation time τ_L; and finally, (3) the vector r(N-C) is considered to be able to reorient isotropically with a correlation time τ_I at temperatures higher than the phase transitions where the dynamic orientational disorder exists. The spectral densities, $J(\omega)$'s are
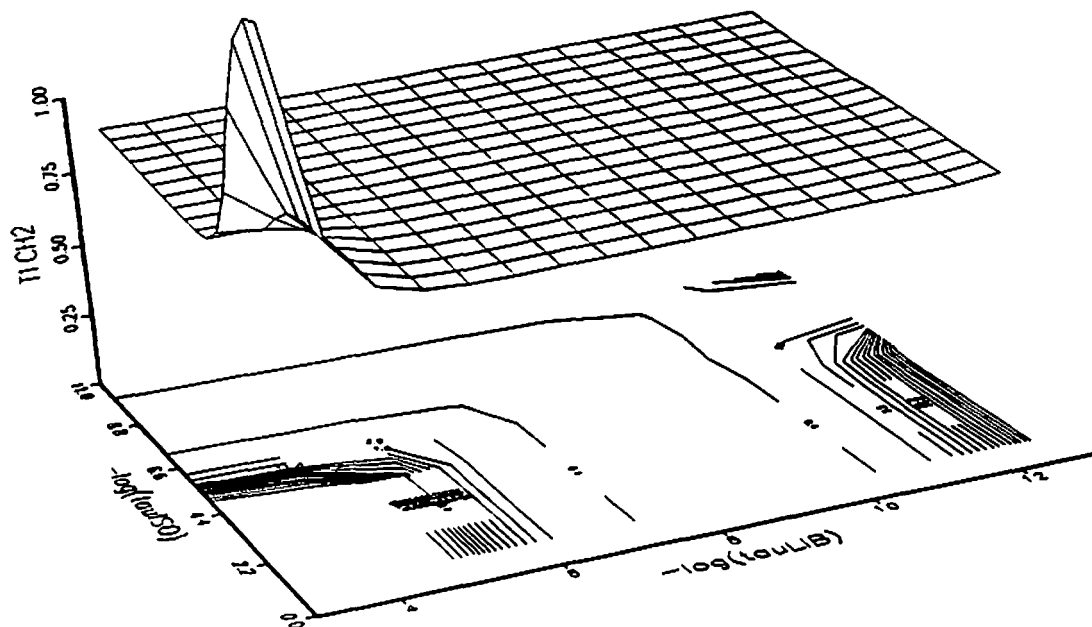
Figure 6   Three-dimensional and contour plots of ^{13}C T_1 with Howarth's 2τ librational model
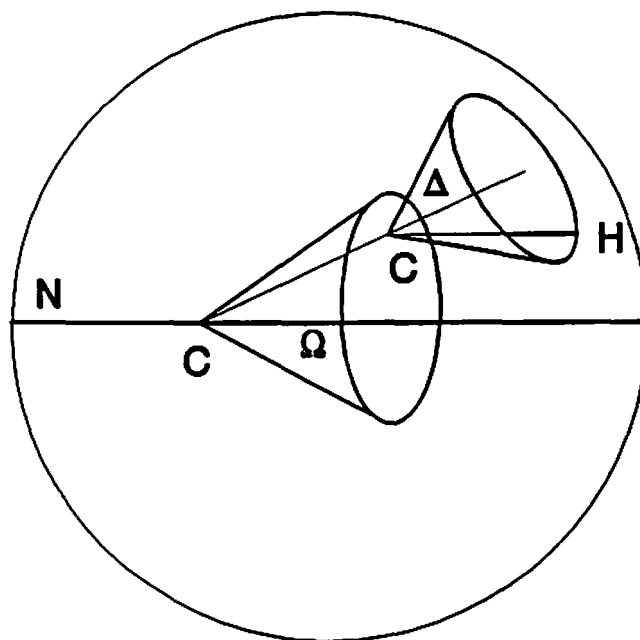
Figure 7   Schematic representation of Howarth's 3τ model

$$J_m(\omega) = 2K_m \sum_{i=1}^{6} \frac{A_i \tau_i}{(1 + \omega^2 \tau_i^2)} , \qquad m = 0,1,2 \tag{19}$$

in which,

$K_0 = 4/15,$

$K_1 = 2/15$ and

$K_2 = 8/15;$

and the constants are:

$A_1 = AD; A_2 = A(1-D); A_3 = BD; A_4 = B(1-D); A_5 = CD; A_6 = C(1-D).$

While $A = \frac{1}{4}(3\cos^2\Delta - 1)^2$

$B = \frac{3}{4}\sin^2 2\Delta$

$C = \frac{3}{4}\sin^4\Delta$

$D = \frac{1}{4}\cos^2\Omega(1 + \cos\Omega)^2$

The correlation times are

$\tau_1 = \tau_I$

$1/\tau_2 = 1/\tau_I + 1/\tau_L$

$1/\tau_3 = 1/\tau_I + 1/\tau_R$

$1/\tau_4 = 1/\tau_I + 1/\tau_L + 1/\tau_R$

$1/\tau_5 = 1/\tau_I + 4(1/\tau_R)$

$1/\tau_6 = 1/\tau_I + 1/\tau_L + 4(1/\tau_R)$

50

For the calculation some structural parameters are available, for example: bond length, $r(CH)$, bond angles, Δ and Ω defined in Fig. 7. A detailed account using this model for tetraethylammonium iodide will be given in Sect. 4.1.2.

Interpretation of ^{13}C T_1 in linear paraffinic chains: When the signals are well resolved, it is possible to measure the ^{13}C T_1 values for individual carbon atoms in the chain. It was found by Lyerla and Levy (1974), that for large molecules with a number of reorientational modes the relaxation data can be analyzed semiquantitatively to obtain effective correlation times, τ^{eff}, for each carbon *via* Eq. (17). Next, we separate the motion of the C–H vector in the alkyl chains in terms of orientational motion of the cation as a whole (the alkyl chains are considered as rigid rods) with an average rate τ_0^{-1} and an internal conformational motion about the individual C–C bonds in the alkyl chains with rate τ_i^{-1}. The expression for the rate of motions of the jth carbon in the side chain, $(\tau^j)^{-1}$, is then the sum of the two rates (Lyerla and Levy, 1974):

$$\frac{1}{\tau^j} = \frac{1}{\tau^j_o} + \frac{1}{\tau^j_i} \tag{20}$$

The differential rate between the lth and m^{th} carbons is:

$$[\tau(l,m)]^{-1} = \frac{1}{\tau^l} - \frac{1}{\tau^m} \tag{21}$$

Substituting Eq. (20) into Eq. (21), and realizing that $1/\tau'_o = 1/\tau''_o$, Eq. (21) becomes:

$$[\tau(l,m)]^{-1} = \frac{1}{\tau'_l} - \frac{1}{\tau''_l} \tag{22}$$

The quantity $1/\tau(l,m)$ should involve only internal correlation times and represents the difference in rates of the conformational motion between the lth and m^{th} carbons.

As will be shown in the discussion (Sect. 4.2), small differential rates can be found for the inner-most bonds (close to the nitrogen) in tetra-n-propylammonium halides and larger compounds, indicating slow conformational motion for steric reasons.

Effective spin-spin relaxation time, T_2^*: The effective T_2^* reflects the combined effects of dipolar interaction, magnetic field inhomogeneity of the instrument, and all other factors causing the spin system to lose phase coherence in the $x-y$ plane after excitation of a radio frequency. Since in solids the dipolar interaction is the most dominant mechanism for spin relaxation, the fluctuation of the diploar interaction between ^{13}C and ^1H determines, therefore, the T_2^* value. The ^{13}C-^1H dipolar interaction is: (1) proportional to the number of interacting protons; (2) dependent on $(r_{CH})^{-3}$, where r_{CH} is the internuclear distance; (3) inversely related to the rate of motion, i.e., a rapidly rotating group could appear as if its protons were farther away from the ^{13}C.

It is thus possible to separate the carbon atoms into three categories according to their number of attached protons and their mobility: (1) *Signals of rigid, protonated* ^{13}C will be suppressed by virtue of dephasing because of a short spin-spin relaxation time (T_2^*) arising from strong and dispersed dipolar local fields. (2) *Signals of mobile, protonated* ^{13}C will be less suppressed because of the relatively long spin-spin relaxation time arising from partially averaged, therefore, weaker dipolar local fields. The methyl carbon resonances thus still remain, because of the rapid methyl group rotations that reduce the $^{13}C - ^1H$ dipolar couplings. (3) *Signals of non-protonated* ^{13}C will be least affected because of even longer spin-spin relaxation time resulting from the fact that the carbon atoms are far away from any protons (>0.2 nm compared to 0.109 nm for a direct C–H bond).

The T_2^* value can be measured by dipolar dephasing experiment (Alla and Lippma, 1976; Opella and Frey, 1979) which is a slight modification of the standard CP-MAS experiment (for details see Section 2.3.6). The signal intensity in the dephasing experiment decreases exponentially with a dephasing delay and is assumed to follow Eq. (23):

$$I(\tau) = I(0) e^{-\tau/T_2^*} \tag{23}$$

where τ is the dephasing delay, $I(\tau)$ and $I(0)$ are the signal intensities at the dephasing delay times of τ and 0, respectively, and T_2^* is the effective spin-spin relaxation time. When $\tau = 0$, the spectrum is identical to that of a CP-MAS. This

method has been used for T_2^* measurement of ^{13}C in some plastic crystals for studying molecular motion (Alla and Lippmaa, 1976).

Correlation times of molecular orientational motion in plastic crystals: In the molecular systems studied in this thesis work, the low-homologs of tetra-*n*-alkylammonium halides, specifically, tetramethyl-, ethyl-, and propyl-ammonium bromides and iodides, have a quasi-spherical shape. If one considers the cation as a rigid body, *i.e.*, motion is only possible for the cation as a whole (for reasons given in the discussion), the low-homologs have the potential for plastic-crystal-forming motifs. In order to verify whether a plastic phase exists, one needs to characterize the orientational motion in terms of the symmetry and rate of the motion.

Orientational motion has been investigated for a number of plastic-crystal-forming molecules by proton T_1 measurements (Boden, 1979). Jumps between symmetry-equivalent orientations are generally observed below the orientational disordering transition temperature, T_d, with a correlation time, τ_C, greater than 50 ns. The most notable feature is that at T_d the orientational motion changes from jump-like to diffusional, so that disorder is introduced with an entropy gain within the range predicted ($\Delta S_{orient.} = 20 - 50 \, JK^{-1}mol^{-1}$, see Sect. 2.2.3). The correlation time, τ_C, at T_d in going to a plastic phase is about 5 ns, a decrease by roughly an order of magnitude. The average value of 5 ns for τ_C at T_d is obtained based on the following specific examples (Boden, 1979): admantane (7.1 ns), white phosphorus (2.3 ns), molybdenum hexafluoride (5.0 ns), hexamethylenetetramine (4.3 ns), hexa-methylethane (5.6 ns), hexamethyldisilane (29 ns), triethylendiamine (0.91 ns), *t*-

butylchloride (4.7 ns), and ball-shaped C_{60} (2.6 ns) (Jin *et al.*, 1992). In the plastic crystal, the correlation time of the orientational motion τ_C follows an Arrhenius law of the form:

$$\tau_C = \tau_0 e^{E_a/(RT)} \tag{24}$$

with a specific pre-exponential constant τ_0 and activation energy E_a for a given molecule. For admantane the τ_0 and E_a are 9.4×10^{-14} s and 12.9 kJ/mol, respectively. At the melting temperature, at 542 K, τ_0 is estimated to be 1.6 ps, which is approaching the correlation time for a classical free rotation $(I/kT)^{\frac{1}{2}} = 0.8$ ps. Values of τ_C have not been measured for many other organic plastic crystals, though the orientational contribution to T_1, in addition to the translational contribution, for protons is typically 10–20 s at the melting point, as compared to 16 s for admantane. A value of τ_C about 2 ps at the melting point would thus seem to be another characteristic property of plastic organic solids.

The correlation time of 5 ns at T_d and 2 ps at the isotropization temperature, T_i, would yield, according to Eq. (17), a ^{13}C T_1 of 4.7 ms and 11.6 s, respectively, for a methylene carbon atom. The just derived numerical values can be used as an additional identifier for the existence of a plastic crystal.

2.3.5 ^{13}C Chemical Shift Anisotropy Powder Pattern of Static Samples

An isotropic ^{13}C chemical shift (concerning the symmetry of the resonance frequency of a single line) is observed only in solution or in the molten state. A chemically distinct carbon in liquids generally gives a single NMR line under conditions of heteronuclear decoupling (most commonly decoupling of protons). The chemical shift is related to the electronic shielding experienced by the nucleus under observation. Because all types of rapid, large-amplitude molecular motion (tumbling) occurs in liquids, the three-dimensionality of the electronic shielding can be ignored. The single resonance line observed in the liquid state represents the isotropic average of a three-dimensional quantity, the tensor, describing the shielding of electrons.

In solids, however, molecular motion is more or less restricted, and because the shielding of the nucleus is not identical along the various directions, a broad resonance pattern results, which is refered to as *chemical-shift-anisotropy* (CSA) powder pattern. Most frequently the electronic shielding is not spherically symmetric. The CSA describes magnitude and direction of this three-dimensional shielding. The three most common cases of the line-shapes are depicted in Fig. 8 (Mehring, 1983).

In the general case (top trace of Fig. 8), three singularities are observed in the spectrum, corresponding to three principal (orthogonal) elements of the shielding tensor. The spectrum shows no symmetry, therefore, it is labeled as asymmetric. In the middle trace, the shielding will be the same in two directions giving an "axially symmetric" tensor where the elements are described as $\sigma_{\parallel}$ for the unique direction and $\sigma_{\perp}$ for the two identical elements perpendicular to it. For comparison, the iso-

σ_{11} σ_{22}

σ_{33}

Asymmetric

$\sigma_\perp$

$\sigma_{||}$

Axially Symmetric

$$\sigma_\perp = \frac{(\sigma_{11} + \sigma_{22})}{2}$$

σ_{iso}
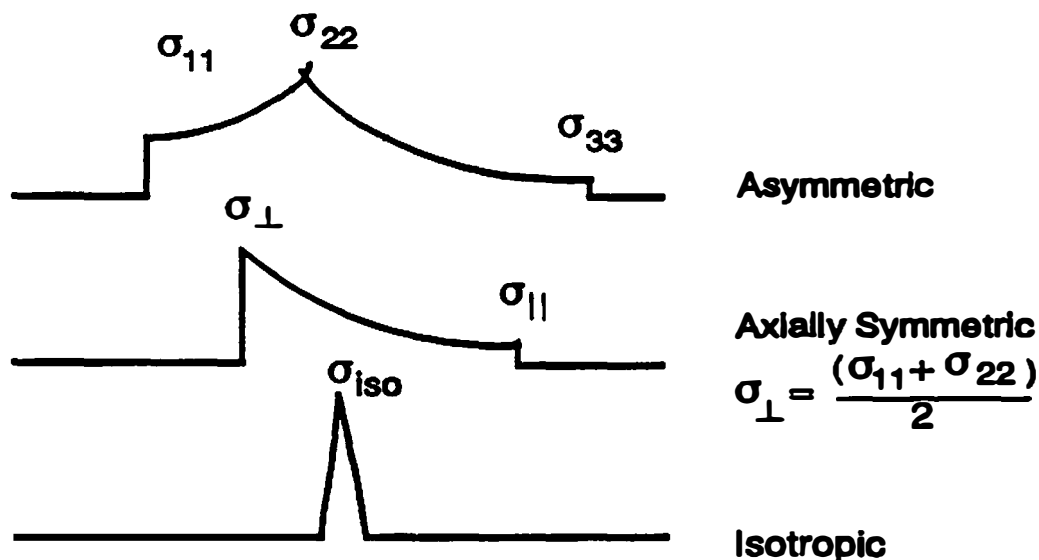
Isotropic

Figure 8   Schematic representation of ^{13}C chemical-shift-anisotropy powder patterns

tropic case is also depicted in Fig. 8. The sharp, symmetric line indicates the resonance of the isotropic average of the three-dimensional (asymmetric) or two-dimensional (axially-symmetric) shielding tensor.

Since the chemical shielding is a three-dimensional quantity, it is expected to be sensitive to the presence of molecular motion. In hexamethylbenzene (Fyfe and Veregin, 1984) and other hexa-substituted benzene derivatives (Fu *et al.*, 1992), the non-protonated aromatic carbons show a CSA powder pattern resembling the asymmetric case (top plot of Fig. 8) below the disordering transition temperature because the molecules are rigid in the crystal. As the temperature is increased, the pattern becomes axially symmetric (shown in Fig. 2, Curve B) due to the in-plane

reorientations known also from ^{1}H NMR studies. Further increase of temperature may cause orientational motion of out-of-plane or flipping of the ring which reduces the CSA powder from axially symmetric to that of isotropic. Recent studies on ball-shaped C_{60} molecules (Yannoni *et al.*, 1991; Tycko, Haddon *et al.*, 1991; Tycko, Dabbagh *et al.*, 1991) showed that at temperatures of about 77 K and below, the powder pattern is asymmetric, indicating that the motion is frozen. At about 100 K, a sharp, highly symmetric peak with isotropic chemical shift emerges from the asymmetric pattern, and further increase in temperature will cause the broad asymmetric line to disappear and the isotropic peak to dominate. In C_{60}, the asymmetric pattern collapses directly into the isotropic pattern without showing an axially symmetric pattern as in hexamethylbenzene. This fact indicates that the molecular motion must be about more than one direction. In fact, the directions of orientation are perpendicular to the planes of the pentagons and hexagons that make up the structure of C_{60}.

In both cases, *i.e.*, hexa-substituted benzenes and C_{60}, motion starts already well below the disordering transitions (hexamethylbenzene, 116 K; C_{60}, 256 K). Since the motion below T_d does not provoke any disorder (as found by entropy analysis), it must consist of jumps between symmetry-equivalent orientations. The amplitudes of the jumps are related to the symmetry of the molecule. For example, in-plane jumps in hexamethylbenzene must be in steps of 60° (six-fold), orientational jumps in C_{60} are presumably in steps of 72° (five-fold) (Jin *et al.*, 1991).

As shown above, in the presence of a molecular motion the line-shape of the CSA powder pattern changes from asymmetric to, eventually, isotropic, and consequently the width of the CSA reduces greatly. The time scale or rate of motion responsible for the reduction of the CSA line-width can be estimated from the inverse of the spectral spread of the CSA powder pattern measured at low temperatures in the absence of motion. The CSA line-widths, defined as $|\sigma_{11} - \sigma_{33}|$ (as shown in Fig. 8), have been documented for various types of carbon atoms. Typical values are listed in Table 1 (Jelinski, 1982).

Experimentally, the CSA powder pattern of a static sample can be measured by use of high-power decoupling of protons to remove the dipolar broadening, and cross-polarization technique to increase the signal-to-noise ratio of the CSA powder pattern. Details for the cross-polarization technique are given in the next section (2.3.6).

2.3.6 NMR Experimental

Spectrometer: The NMR spectrometer used in this research is a Nicolet NT200, operating at 200.07 MHz for protons and 50.30 MHz for ^{13}C. The NMR software, NMC-1280, is used for data acquisition and processing. The data system, NIC-1280, and pulse programmer, NIC-239C, permit the generation of new pulse-sequences. Some of the liquid spectra were taken on a Bruker AC250 spectrometer, operating at 250.13 and 62.68 MHz for ^1H and ^{13}C, repectively.

Table 1. Magnitude of some ^{13}C chemical-shift-anisotropy tensors[a, b]

Carbon Type	Sample	T (K)	σ_{11}	σ_{22}	σ_{33}	$\|\sigma_{11} - \sigma_{33}\|$
Non-protonated aromatic	Hexamethylbenzene	87	239	103	31	208
		294	237	71	69	168
Protonated aromatic	Durene	295	211	135	35	176
Carbonyl	Acetone	87	279	265	79	200
	Carbon monoxide	4.2	-	-	-	365
		46	-	-	-	335
Carboxyl	Oxalic acid dihydrate	298	249	132	109	140
	Glycine	298	248	180	105	143
Methylene	Polyethylene	298	50	36	12	38
	n-Eicosane (interior)	178	50	38	17	33
	Malonic acid	289	62	51	19	43
Methyl	*n*-Eicosane	178	26	22	3	23

a. Source: Jelinski, 1982. A "-" sign indicates that the values have not been determined.
b. In unit of ppm.

Solid state CP-MAS probe: The NMR probe of solid state samples was built by the Doty Scientific Inc. and is compatible with the NT200 spectrometer described above. The 90° pulses for ^{13}C and ^1H are 4.1 μs and 4.8 μs at full output of the observation transmitter and proton decoupler, respectively. With this probe a 5 mm rotor made from Vespel (Trade name for a DuPont polyimide) or sapphire and packed with sample can be spun easily at 4.5 KHz.

Temperature calibration: A temperature controller is available for the spectrometer. The probe can be used at temperatures ranging from 120 to 420 K. Temperature calibrations have been carried out by NMR spectroscopy with CH_3OH (for temperatures below room temperature) and $HO(CH_2CH_2)OH$ (for temperatures above room temperature). Both liquids are of Fisher reagent grade. The liquid samples were sealed inside the rotor by the end caps with rubber O-rings. Under MAS (spinning at 4.5 kHz) the proton spectra were measured at each displayed temperature (T_{disp}) through the decoupler coil. The separation of the two proton resonances (Δv) can be converted into temperature (T_{calc}) according to the equations given by Van Geat (Van Geat, 1969):

$$T_{calc} = 406 - 33.06(\Delta v/v_0) - 22.8(\Delta v/v_0)^2$$
200–300 K, error ±1 K (25)

$$T_{calc} = 466.4 - 102.3(\Delta v/v_0)$$
295–415 K, error ±0.4 K (26)

where Δv is the difference in chemical shifts in Hz at the Larmor frequency $v_0 = 200$ MHz, and T_{calc} is in kelvin. The calibration curves can be made to show the relationship between displayed temperatures (T_{disp}) and calculated (T_{calc}). These are:

$$T_{calc} = 1.39T_{disp} + 285 \tag{27}$$
200 – 300 K, cooling, spinning rate (4.5 ± 0.8) kHz, error ± 8 K

$$T_{calc} = 1.46T_{disp} + 277 \tag{28}$$
295 – 415 K heating, spinning rate (4.5 ± 0.1) kHz, error ± 4 K

An unexpected phenomena was that the T_{calc} or Δv is dependent on the spinning rate. At the same displayed temperature (T_{disp}), as the spinning rate increases, T_{calc} increases. The discrepancy caused by different spinning rate at the same T_{disp} is more significant at lower temperatures. It is suspected that this might be caused by: (1) the heating due to the friction because of the spinning of rotor; or (2) the density or concentration change of the sample due to the centrifugal forces of spinning. The chemical shift of OH protons depends on the concentration, while that of the CH_2 protons is not. Despite all this, the temperaure calibration curves as given by Eqs. (27) and (28) are valid, as along as the sample spinning rate is kept at 4.5 kHz.

Chemical shift calibration: The chemical shift was calibrated indirectly relative to a powder sample of hexamethylbenzene (HMB). The first ^{13}C spectrum of HMB was taken and its chemical shift value was set to 17.37 ppm, as suggested

by Earl and VanderHart (Earl and VanderHart, 1982). With the same experimental parameters, such as sweep width, offset frequency, data size *etc.* (which can be done by retrieving the first spectrum from the computer), several identical measurements were carried out at different days or months. The measured chemical shifts deviated by a maximum amount of 0.15 ppm. This value, 0.15 ppm, was considered, therefore, as the threshold below which no chemical shift change can be claimed. At the beginning of the time during which the spectrometer is available, and before any measurement was made on unknown samples, a spectrum of the HMB sample was measured and stored on disk and regarded as the standard, all the measurements on subsequent samples are then calibrated relative to it. The ^{13}C chemical shift values of various samples thus obtained are compared with the results obtained by the method of internal standards (HMB) which was mixed with the unknown samples. Good agreements (less than 0.15 ppm in discrepancy) are normally obtained.

Magic-angle setting: Correct setting of the magic-angle (54°44') is critical to obtaining a high-resolution ^{13}C NMR spectrum. The probe has a built-in rod which permits changing of the angle between the long-axis (spinning axis) of the sample rotor and the direction of the external magnetic field which is normally vertical for a superconducting solenoid. In this thesis work, the magic angle setting was done with a HMB sample under a spinning rate of about 4.5 kHz. At ambient temperature the resonance pattern of the non-protonated aromatic carbon in HMB is clearly axially asymmetric if the angle is not set to 54°44' (the magic angle). The asymmetric line can be gradually reduced to an isotropic one as the angle is adjusted

approaching the magic angle. Figure 9 shows the changes of line-shape as a function
of the angle.

35 Hz
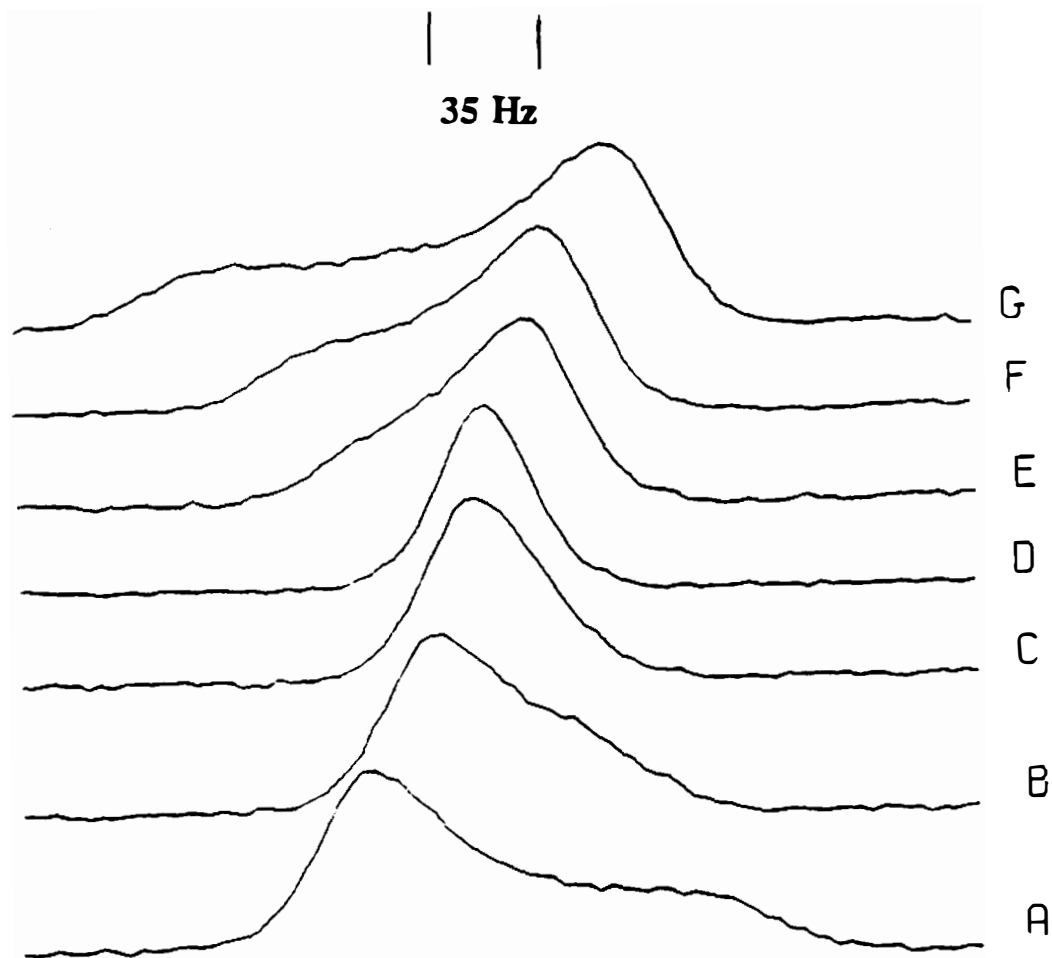
Figure 9   Effect of magic angle setting on the resonance of the aromatic ^{13}C in hexamethylbenzene. Plots A to G were obtained by turning the tuning-rod clock-wise in steps of 90°. Plot D is the optimal angle (54°44')

Experiments: Three types of experiments were conducted, they are explained in the following:

(1) *Standard CP-MAS* and high power proton decoupling during acquisition, the pulse sequences is as follows:
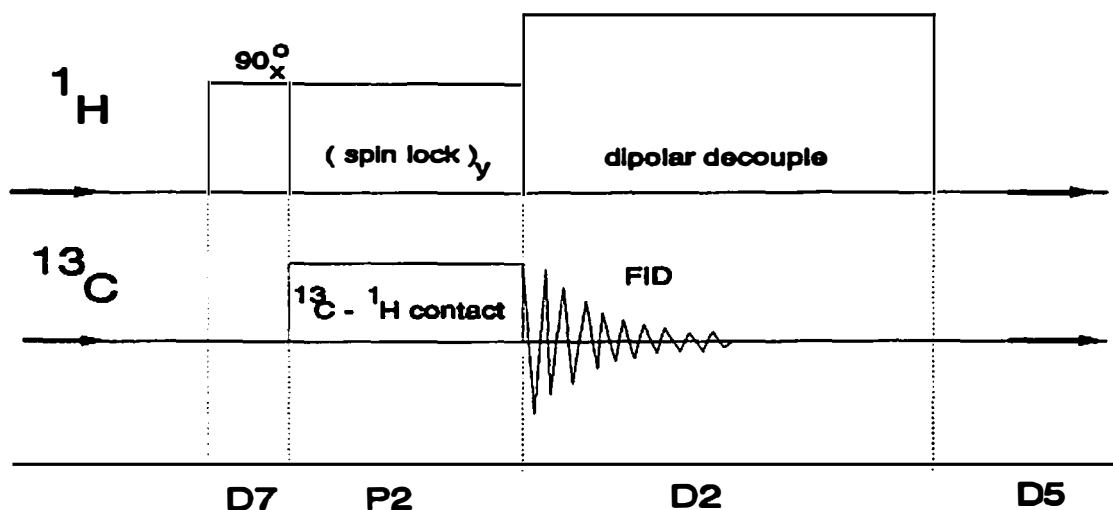
with typical parameters: D7 = 5.0 μs (90° proton pulse width), P2 = 1 to 4 ms (spin contact/lock time), D5 = 5 to 15 s (inter-sequence delay for spin relaxation), and D2 = 100 to 400 ms (signal acquisition time which is inversely proportional to the sweep width).

There are four steps to be explained in the CP-sequence: (a) First the proton nuclear magnetization is allowed to build up along the external field H_0, which is defined as the z-direction. The population difference between the upper and lower energy state is determined by the Boltzman distribution:

$$\frac{N_{upper}}{N_{lower}} = e^{-h\gamma_H H_0/(2\pi kT)} \qquad (29)$$

in which h, γ_H, H_0 and T are Plank's constant, proton gyromagnetic ratio, applied field strength, and temperature of the spin system, respectively. (b) Application of a 90° pulse, the strong magnetization of the protons is turned to the in the x'-direction, perpendicular to H_0. Immediately after this first 90° pulse, an rf-field is applied along the y'-direction to lock all proton spins along the same direction (y'). Since this is a nonequilibrium state (which corresponds to a high spin temperature), a decay will occur with a characteristic time $T_{1\rho H}$ (proton spin-lattice relaxation time in the rotating frame), typically in 1 to 100 ms. On the other hand, the ^{13}C spin system initially has no polarization in the $x'-y'$ plane. (c) In the third step, thermal contact between the two spin system is established. While the proton spins are locked during P2, a pulse in the carbon channel is switched on. If the rf field strengths H_H and H_C satisfy the necessary Hartmann-Hahn condition:

$$\gamma_H H_H = \gamma_C H_C \qquad (30)$$

then the two spin systems will have the same transition frequency in their respective rotating frames and polarization transfer is possible by the mechanism of dipolar spin-flip, ^{13}C magnetization increases rapidly according to the rate equation given by

66

Eq. (11), whereas ^{1}H magnetization decreases slightly due to its high abundance. (d) The last step of the cross polarization experiment is the observation of the proton enhanced ^{13}C free induction decay (FID), which is to be seen after switching off the ^{13}C rf field. During the ^{13}C observation time, D2, the proton rf field is still present, but now serves as the high power decoupling to eliminate the dipolar broadening, as discussed above.

Dipolar dephasing experiment (Opella and Frey, 1979) can be performed by insertion of a brief delay, τ, between spin-lock (P2) and detection of the FID (D2) in the cross-polarization experiment described above. The signal intensity decay according to Eq. (23).

Magic angle sample spinning is maintained during the whole experiment to obtain a high-resolution ^{13}C NMR spectrum. If the *chemical-shift-anisotropy powder pattern* is desired, the sample is kept static.

(2) *Bloch decay or BILEV*: when the molecular motion become fast enough, the CP method described above will fail to detect any signal, as is predicted by Eq. (11). The Bloch decay, also known as "BILEV", is a standard pulse-sequence routinely used for liquid samples.

The typical parameters are P2 = 2.0 μs (45° pulse width for ^{13}C), D1 = 0 for no Nuclear Overhauser Effect (NOE), or 1 to 3 times of ^{13}C T_1 for NOE build-up, D5 = 3 to 5 times of the longest ^{13}C T_1, S1 = 0.5 to 3 W for generation of the NOE, and S2 = 22 W for decoupling of ^{1}H during data acquisition. Since S1 and S2 are not equal, the pulse sequence is also conveniently referred as *BILEV*:

1H
decouple (S1)   dipolar decouple (S2)

13C   FID

D1   P2   D2   D5
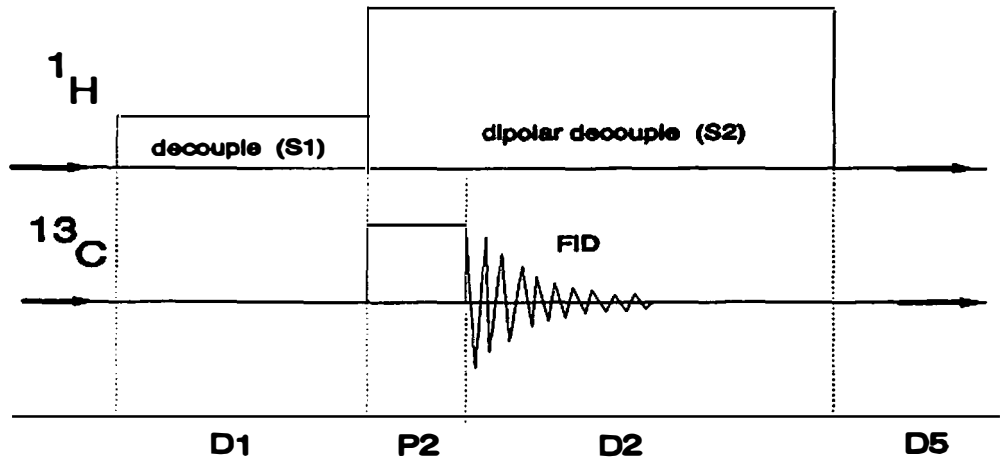
(3) ^{13}C Spin-lattice relaxation times

Inversion-Recovery: The most widely applied pulse sequence to determine T_1

is the $180° - \tau - 90°$ or inversion-recovery method, as shown in the ^{13}C channel of the

following pulse sequence diagram:

1H ∫∫
decouple (S1)   Dipolar decouple(S2)   ∫∫

13C $180°_x$ τ $90°_x$ FID

P2   P1   D2   D5

68
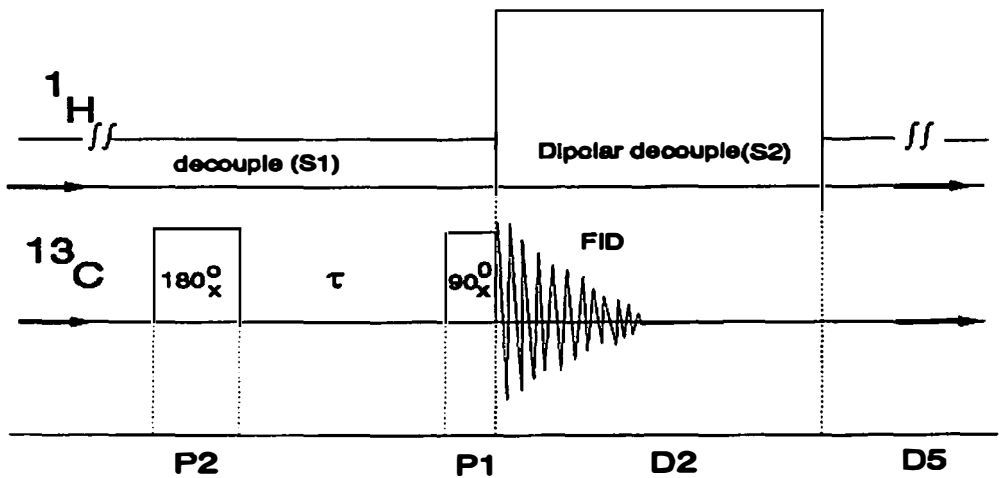
An intense rf field in the form of a square-wave rotates the magnetization M_z through 180° (inverts the spin populations), after which a time delay τ is imposed. This is followed by a 90° reading pulse that turns the recovered magnetization into the x−y plane where its free induction decay (FID) is observed. The experiment is repeated as a function of τ with a long delay, $D5$, between two repeating sequences (to allow recovery to the equilibrium situation before repetition of the sequence). The pulse sequence is represented as $(180° - \tau - 90° - D5)_n$, in which the delay time $D5$ is typically 3−5 times the longest T_1 to be determined in the experiment. The Fourier transformation of the FID gives the time-dependent intensity of each line in the spectrum. The intensity may be negative, zero, or positive, depending on the relative value of τ and the T_1 governing the resonance line. The T_1 may be calculated from Eq. (31):

$$I(\tau) = I(\infty)(1 - Ce^{-\tau/T_1}) \tag{31}$$

where $I(\tau)$ and $I(\infty)$ are signal intensity at delay time τ and ∞, respectively, and C is a constant close to 2. All three, $I(\infty)$, C, and T_1, are treated as adjustable parameters. A program for curve-fitting to Eq. (31) is available in the NMC-1280 NMR software package of the NT200 spectrometer. Less accurate T_1 values can be obtained from the null point of $I(\tau)$, where $T_1 = \tau/\ln2$.

The decoupler is gated on all the time, but with two alternating outputs, $S1$ and $S2$. The higher power $S2$ is applied only during acquisition of the FID to remove the dipolar coupling between ^{13}C and ^{1}H nuclei.

The typical parameters are: $S1$ = 0.5 to 3 W (low power decoupling to saturate protons and avoid heating of sample), $S2$ = 22 W or $ca.$ 50 kHz (high power decoupling applied during acquisition), τ ranges from 0.1 ms to $5 \times T_1$ (length of variable delay), $D5$ = 150 to 800 s (as in other relaxation pulse sequences, set to $5T_1$ of the CH_2), NA = 8, 16, or 32 (number of acquisitions per one variable delay), and number of variable delays is normally between 8 and 14.

In measuring ^{13}C T_1, the decoupling power required for saturating ^{1}H in solids, $S1$, should not be set too high, because the heat produced will change the temperature of the sample and de-tune the probe coils. High power decoupling causes more heating of the sample when determining long T_1. On the other hand, the decoupling power should not be too low, otherwise the saturation of the protons can not be accomplished, which causes an error in the ^{13}C T_1 measurement.

Progressive Saturation: This method consists two 90° pulses separated by a variable delay τ. The receiver is gated on immediately at the end of the second 90° pulse. While in the decoupling channel the high power (22 W) is, again, turned on only during data collection. The ^{13}C T_1 is calculated from Eq. (32):

$$I(\tau) = I(\infty)(K - e^{-\tau/T_1}) \tag{32}$$

where $I(\tau)$ and $I(\infty)$ are signal intensity at delay time τ and ∞, respectively, and K is a constant close to 1. As in the *inversion-recovery*, the constants $I(\infty)$, K, and T_1 are adjustable for the curve-fitting. The major advantage of this sequence is time-saving, thus, it is widely used for the measurements of long T_1. In this thesis work, relaxation times of longer than 15 s are measured with the *progressive saturation* method.

2.4   Samples

2.4.1   Tetra-*n*-alkylammonium Bromides and Iodides

Each of the tetra-*n*-alkylammonium halides has a cation, consisting of four linear, equal-length, alkyl chains and one nitrogen atom in the center, and a anion of either bromine or iodine.

Most of the samples used in this thesis work are commercially available: $(CH_3)_4NBr$, $(C_4H_9)_4NI$, $(C_6H_{13})_4NBr$, $(C_7H_{15})_4NBr$, $(C_8H_{17})_4NBr$, $(C_{10}H_{21})_4NBr$, $(C_{12}H_{25})_4NBr$, $(C_{16}H_{33})_4NBr$, and $(C_{18}H_{37})_4NBr$ were purchased from Fluka Chemical Corp. (980 South Second Street, Ronkonkoma, NY 11779); $(C_2H_5)_4NI$, $(C_3H_7)_4NI$, $(C_5H_{11})_4NBr$, $(C_5H_{11})_4NI$, $(C_6H_{13})_4NI$, and $(C_7H_{15})_4NI$ from Eastman Kodak Company (Rochester, NY 14650); $(C_{12}H_{25})_4NI$ from Lancaster Synthesis Ltd. (P.O. Box 1000, Windham, NH 03087); $(CH_3)_4NI$, $(C_2H_5)_4NBr$, $(C_3H_7)_4NBr$, and $(C_4H_9)_4NBr$ existed already in our laboratory, kindly provided by Professor G. Janz of Rensselaer Polytechnic Institute. The purities were approximately 99% in all cases. All samples were used as received, but kept in a desiccator containing $CaSO_4$. Transfer of

samples to the DSC aluminum pans for measurement and all other sample handling was done in a glove bag under an atmosphere of dry nitrogen.

We chose to still use the older samples that existed in our laboratory, as storage for a long time (in dark vials) results in perfection of crystals rather than deterioration of the samples. It was decided not to recrystallize our samples from solution, as it was shown that this does not always produce better crystals.

2.4.2   N,N'-bis(4-n-octyloxybenzal)-1,4-phenylenediamine (OOBPD)

The molecule of OOBPD is elongated, consisting of a rigid aromatic part, to be called the mesogen, and one linear, flexible oxyalkyl groups on each side of the mesogen:
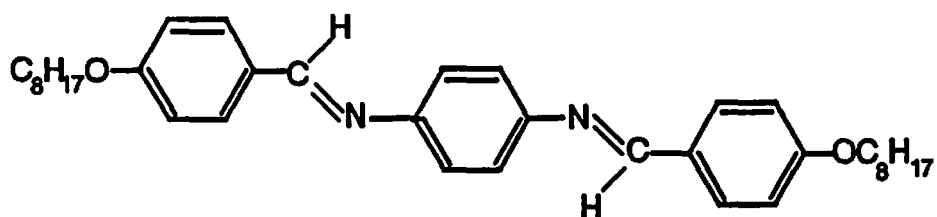
The synthesis of the OOBPD sample in our laboratory followed closely the method reported in the literature (Grey et al., 1955) and was carried out by G. Liang. Solvent recrystallization of the OOBPD sample was performed from chloroform to increase the purity, verified by both ^{1}H and ^{13}C NMR in solution. The melt-crystallized samples show little difference in the thermal parameters from samples

that were solution-crystallized, as shown in Chapter 3. The sample was continuously kept dry in a desiccator with anhydrous calcium chloride.

2.4.3 MBPE-9 and MBPE-5

MBPE-9 and MBPE-5 are two polymers that have the nomenclatures: poly-[oxy-1,4-(3-methylphenylene) ethylene-1,4-phenyleneoxynonamethylene], and poly[oxy-1,4-(3-methylphenylene) ethylene-1,4-phenyleneoxypentamethylene], respectively. The structural formulas are shown below.

$$O-\underset{CH_3}{\underset{|}{\bigcirc}}-CH_2CH_2-\bigcirc-OCH_2CH_2CH_2CH_2CH_2-$$

MBPE-5

$$O-\underset{CH_3}{\underset{|}{\bigcirc}}-CH_2CH_2-\bigcirc-OCH_2CH_2CH_2CH_2CH_2CH_2CH_2CH_2CH_2-$$
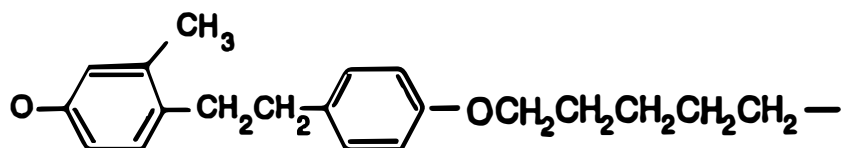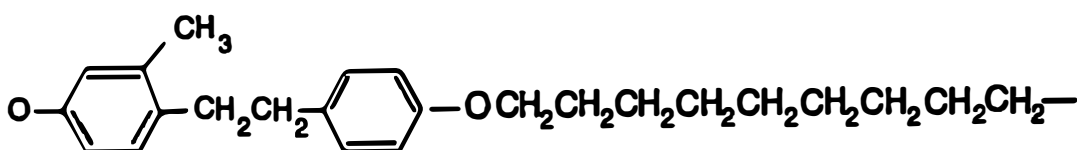
MBPE-9

The MBPE-9 and MBPE-5 samples were kindly provided by Professor S. Z. D. Cheng of Institute and Department of Polymer Science, College of Polymer Science and Polymer Engineering, The University of Akron, Akron, Ohio 44325-3909. The polymers were prepared in the laboratory of Professor V. Percec of the

Department of Macromolecular Science, Case Western Reserve University, Cleveland, Ohio 44106-2699. The preparation of the polymers involved coupling 1-(4-hydroxyphenyl)-2-(2-methyl-4-hydroxyphenyl)ethane and α,ω-dibromoalkanes (Percec and Yourd, 1989). The molecular masses were reported to be 19,000 (M_w/M_n = 1.9) and 20,600 (M_w/M_n = 1.4) for MBPE-5 and MBPE-9, respectively (Percec and Yourd, 1989). Typical crystallinities on cooling at 10 K/min, measured by comparison of the X-ray intensity in diffraction peaks and in the diffuse halo and heats of fusion were 0.44 for MBPE-5 and 0.54 for MBPE-9 (Yandrasits, 1989).

CHAPTER 3

RESULTS

This chapter contains experimental results on transition temperatures and entropies, solid state ^{13}C NMR spectra and nuclear spin relaxation times for molecules listed in sequence: Tetra-*n*-alkylammonium bromides and iodides, N,N'-*bis*(4-*n*-octyloxybenzal)-1,4-phenylenediamine (OOBPD) and polymers MBPE-9 and MBPE-5.

Tetra-*n*-alkylammonium bromides and iodides studied in this thesis, $[CH_3(CH_2)_{n-1}]_4NX$ with $n = 1$ to 8, 10, 12, 16, and 18 for the bromide (when X = Br), and $n = 1$ to 7, and 12 for the iodide (when X = I), are classified into three series: low homologs for $n = 1$, 2, and 3, intermediate homologs for $n = 4-7$, and high homologs for $n = 8$ and larger. This catogrorization is based approximately on the types of motion and disorder that are potentially present.

3.1 Thermal Properties

3.1.1 Tetra-*n*-alkylammonium Salts

All the transition temperatures and entropies were measured by Dr. Alexander Xenopoulos. The results are listed in Table 2. No transitions are observed for the methyl compounds before sublimation. The ethyl and propyl salts do not melt at the highest transition included in Table 2, as was seen in the melting

Table 2 Thermodynamic parameters of symmetrical tetra-n-alkylammonium halide first-order transitions[a]

Salt	T_{tr} (K)	ΔS_{tr} (JK^{-1}mol^{-1})	ΔS_{tr}^{tot}
Bromides			
(C_2H_5)	448.3, 462.6	44.6, 3.2	47.8
(C_3H_7)	382.2, 395.8	44.4, 0.9	45.3
(C_4H_9)	367.0, 379.2, 393.9	41.2, 1.4, 37.6	80.2
(C_5H_{11})	374.0	97.9	97.9
(C_6H_{13})	148, 167, 196, 305, 315, 374.9	8.1, 1.2, 17.5, 22, 38, 42.6	129.4
(C_7H_{15})	339.5, 366.5	13.5, 99.3	112.8
(C_8H_{17})	323.2, 374.1	11.0, 118.0	129.0
$(C_{10}H_{21})$	348.6, 363.4	160.8, 102.6	263.4
$(C_{12}H_{25})$	225.4, (346.5, 362.6)	6.4, (128.1, 206.7)	341.2
$(C_{16}H_{33})$	(370.9, 377.7)	(237.7, 251.9)	489.6
$(C_{18}H_{37})$	(375.1, 379.9)	(226.7, 328.6)	555.3
Iodides			
(C_2H_5)	471.3	44.3	44.3
(C_3H_7)	225.4, 418.9	6.4, 35.8	42.2
(C_4H_9)	394.0, 420.6	71.2, 21.3	92.5
(C_5H_{11})	(404.6, 412.1)	(41.2, 94.0)	135.2
(C_6H_{13})	(345.1, 352.3), 378.7	(83.3, 16.2), 43.9	143.4
(C_7H_{15})	355.4, (391.0, 398.7)	26.1, (6.2, 97.9)	130.2
$(C_{12}H_{25})$	284.1, (343.4, 351.2, 364.6), 388.7	12.3, (12.6, 109.1, 15.1), 122.2	271.3

a   Parentheses indicate a multiple, overlapping transition.

point apparatus. Melting occurs in these compounds along with sublimation and possibly decomposition at higher temperatures. In the low-temperature range from 140 to 230 K only minor transition peaks were found for $(C_3H_7)_4NI$, $(C_6H_{13})_4NBr$, and $(C_{12}H_{25})_4NBr$. The parameters in Table 2 were the largest ones determined.

Considerable work on the thermal properties of methylammonium salt salts has been reported before. No transitions were seen for the iodide (Coulter *et al.*, 1940) and the bromide (Chang and Westrum, Jr., 1962) from 293 K to 593 K, as also observed in the present work. Above 600 K all salts sublime and decompose.

Coker and coworkers have investigated thermodynamically 34 tetraalkyl-ammonium salts from 250 K to a few kelvins above melting (Coker *et al.*, 1969; Coker *et al.*, 1970). The studied compounds included both halides and other miscellaneous anions, as well as symmetrical and asymmetrical cations. The agreement with our data on the symmetrical ones is good.

Gorden and coworkers have also studied alkylammonium salts, focusing their research on the properties of the melt (Gorden, 1965; Andrews and Gorden, 1973). Finally, Levkov *et al.* studied iodides by DSC and infrared spectroscopy above 200 K (Levkov *et al.*, 1971). The agreement with our data is, again, very good.

3.1.2 N,N'-*bis*(4-*n*-octyloxybenzal)-1,4-phenylenediamine (OOBPD)

Transition parameters: The heats of transitions were determined by Dr. Yinmin Jin. The baseline was calculated from the vibration-only heat capacity, as shown next. The transition temperatures, heats and entropies are listed in Table 3.

Table 3   Transition parameters of OOBPD

Transition	T (K)		ΔH (kJmol^{-1})		ΔS (JK^{-1}mol^{-1})	
	S-C[a]	M-C[a]	S-C	M-C	S-C	M-C
K3–K1[b]	386.51	385.50	18.45	18.12	47.73	46.99
K1–H'	415.66	415.35	9.60	9.54	23.10	22.96
H'–G'	421.71	421.80	2.53	2.55	6.00	6.05
G'–I	427.15	427.18	0.55	0.58	1.28	1.37
I–C	436.85	436.73	3.39	3.79	9.00	8.69
C–N	476.66	476.46	5.24	5.28	10.99	11.09
N–Melt	504.85	504.76	4.12	4.49	8.17	8.90
Total			44.42	44.36	106.27	106.04

a   S-C: solution-crystallized;   M-C: melt-crystallized.
b   One letter or one letter followed by a number are the phase designations.

Heat capacities: Heat capacity measurement and calculation of OOBPD were

performed also by Dr. Yinmin Jin. The experimental heat capacity is tabulated in

Table 4. Included are also calculated heat capacity. Details on the calculation of

heat capacity will be given in Sect. 4.4.4. As can be seen that the average and RMS

errors between the experimental data and the calculated C_p are 0.13 ± 1.2 % from

140 to 250 K, the range within which the heat capacity is predominantly vibrational.

The heat capacity computed for an OOBPD crystal which shows only

vibrations and the heat capacity of the liquid are compared in Figs. 10 and 11 with

the actual measurements. One can clearly see that there are no low temperature

transitions in the K3 phase as speculated to account for the low total heats of

Table 4   Measured and calculated Heat capacities of OOBPD[a]

Temperature (K)	Measured C_p (JK^{-1}mol^{-1})	Calculated C_p (JK^{-1}mol^{-1})	Deviation (%)
130.00	390.53	373.78	−4.29
140.00	401.18	395.50	−1.41
150.00	415.67	416.67	0.24
160.00	430.88	437.34	1.50
170.00	451.11	458.03	1.53
180.00	471.07	478.81	1.64
190.00	494.44	499.57	1.04
200.00	516.15	520.68	0.88
210.00	540.16	541.79	0.30
220.00	564.95	563.37	−0.28
230.00	590.12	585.61	−0.76
240.00	615.72	607.81	−1.28
250.00	642.69	630.73	−1.86
260.00	671.82	653.41	−2.74
270.00	701.81	676.92	−3.55
273.15	713.23	684.31	−4.06
280.00	739.82	700.51	−5.31
290.00	775.93	724.67	−6.61
298.15	805.69	744.42	−7.60
300.00	812.66	748.93	−7.84
310.00	851.89	773.36	−9.22
320.00	894.07	797.80	−10.77

Table 4 (cont.)

Temperature (K)	Measured C_p $(JK^{-1}mol^{-1})$	Calculated C_p $(JK^{-1}mol^{-1})$	Deviation (%)
330.00	939.64	822.39	−12.48
340.00	989.06	846.76	−14.39
350.00	1043.52	871.64	−16.47
360.00	1108.43	896.28	−19.14
370.00	1194.15	920.97	−22.88
380.00	1310.56	945.78	−27.83
Transitions from phase K3 to K1, to H', to G', to I, to C, to N, and to Melt			
530.00	1270.12	1269.78	−0.03
540.00	1266.06	1266.69	0.05
550.00	1263.95	1263.61	−0.03

a   Befor transitions, data are caculated from approximate frequency spectra for solid. After transitions, data are calculated from a fitted liquid capacity: $C_{p,liq} = 1433.2 - 0.3084T$. Deviation (%) = $100(1 - C_{p,expt}/C_{p,cacl})$.

transition. A major increase in heat capacity beyond the vibration-only limit can be seen, however, beginning at about 200 K. In fact, at the beginning of the transition to the K2 and K1 phases the heat capacity has reached the level of the liquid. The entropy contributed by the shaded area of the graphs is 74.7 J/(K mol), more than the transitions from K3 to the liquid crystal H'.
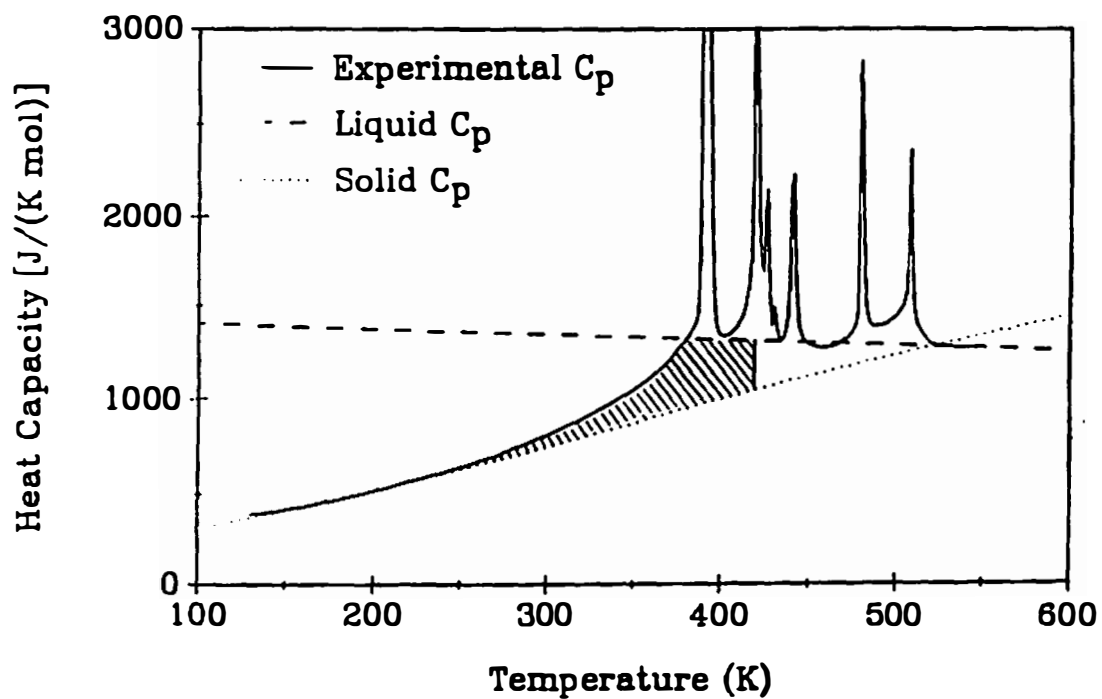
Figure 10   Comparison between the experimental C_p (solid line) and calculated C_p (dotted line) as well as liquid C_p (dashed line).
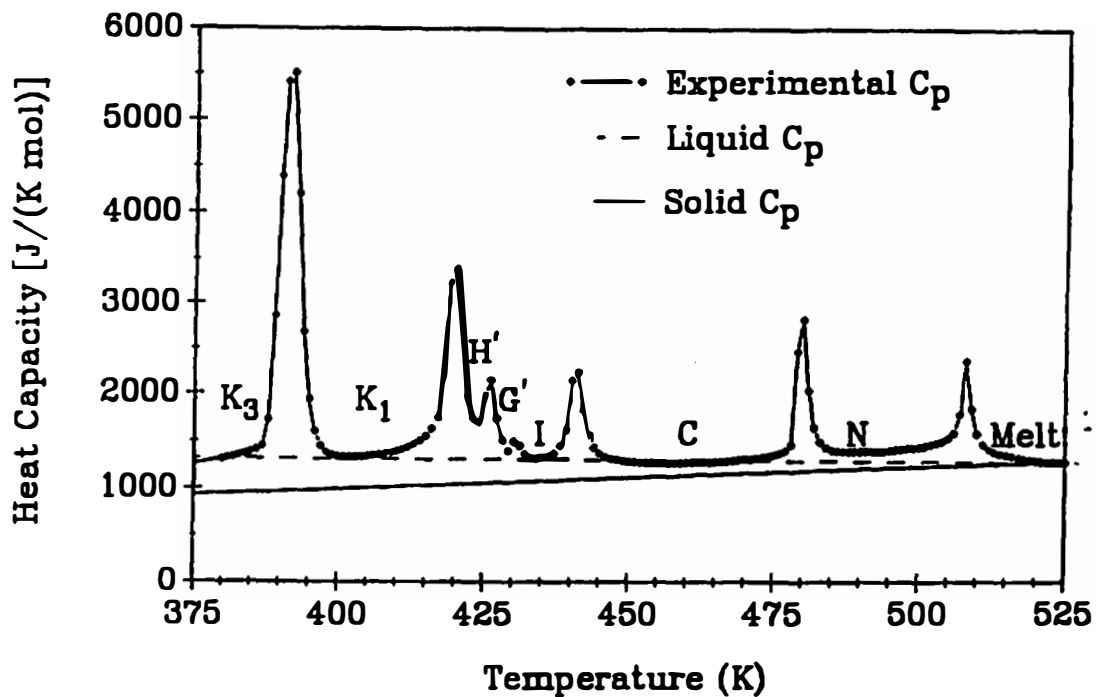
Figure 11   Section plot of Fig. 10 from 375 to 525 K showing proper baseline offered by the liquid heat capacity (dashed line).

3.1.3   MBPE-9 and MBPE-5

The transition behavior of these polymers were characterized in cooperation with Prof. S. Z. D. Cheng of University of Akron. The pertinent observations to this thesis work are that: (1) On cooling at a sufficiently fast rate from the melt, *two* exothermic transitions occur. On subsequent heating only single transitions were observed. Transition temperatures and heats are listed in Table 5. (2) The onset temperature and the heat of the transition from the melt to the metastable mesophase is independent of cooling rate, while that of the second exotherm, (*i.e.* the transition from the mesophase to the room-temperature phase) decreases in both temperatures and heats of transition with increasing cooling rate, for example of MBPE-9, the transition temperatures are 331 K at 10 K/min and 338.5 K at 2.5 K/min.

Since polymeric samples often contain certain amount of amorphous that does not contribute to the observed heats, the heats and entropies changes in going from melt to the condis state, and from condis state to well ordered crystal phase, should be calculated by taking into account of the crystallinity. The crystallinities for MBPE-5 and MBPE-9 have been determined by wide-angle X-ray diffraction (WAXD) (S. Z. D. Cheng, private communication). The results are 0.44 and 0.54 for MBPE-5 and MBPE-9, respectively.

Further understanding on the thermodynamical properties and motion in these polymers is helped by a detailed heat capacities studied by Jin *et al.* (1992). The vibration-only heat capacity of the solid polymers has been calculated based on

83

Table 5   Transition parameters of MBPE-5 and MBPE-9[a]

Polymers	T_{onset} (K)	ΔH (kJ/mol)
On Cooling from the Isotropic Melt with 10 K/min		
MBPE-5	329.3	-3.00
	318.0	-2.90
MBPE-9	345.6	-5.78
	331.0	-12.0
On Heating with 10 K/min[b]		
MBPE-5	365.0[c]	5.20
MBPE-9	355.5	18.2

a   Source: Yandrasits *et al.*

b   The samples were cooled to 220 K at 10 K/min before heating.

c   MBPE-5 shows additional transitions on heating, but the heats are small enough to be neglected.

experimental data and estimated vibrational spectra and the heat capacity of the liquid polymers has been measured. A gradual conformational disordering, starting from room temperature was confirmed and the "missing transition entropy" could be found comparing the experimental C_p heat capacity, with the calculated C_p.

3.2 Solid State ^{13}C NMR Results

3.2.1 Low Homologs of Tetra-n-alkylammonium Salts

Full ^{1}H and ^{13}C NMR characterizations of $[CH_3(CH_2)_{n-1}]_4NX$ in solution were made, where n = 1, 2, 3; and X = Br and I. The solution spectra were used to check the identities and purities of the samples used. Except for improved resolution the spectra are similar to those documented in the literature (Sadtler Research Lab.; and Asahi Research Center, Co., 1895). Of particular interest are the ^{1}H NMR spectra of the tetra-n-propylammonium halides. In Fig. 12 the resonances of the protons bonded to C-1 (C-1 is the carbon bonded to the nitrogen) are plotted for all available salts.

For tetramethylammonium iodide the solid state ^{13}C CP-MAS NMR spectral parameters, namely, chemical shift (δ), line width ($\Delta v_{1/2}$), and relative signal intensity (I), were monitored as a function of temperature. As the temperature is increased from 308 to 424 K, δ increases from 56.40 to 57.09 ppm, while $\Delta v_{1/2}$ decreases from 54.97 to 35.30 Hz and I from 100 to 40 (arbitrary units). All changes are gradual.

The ^{13}C spin–lattice relaxation times, T_1, of tetramethylammonium bromide and iodide were measured from 311 to 397 K. The results are shown in Table 6.

The variable temperature ^{13}C CP-MAS spectra of tetraethylammonium bromide are shown in Fig. 13. Up to 358 K, the methylene carbon resonance shows an asymmetric doublet. At higher temperature the resonance changes to a broad, symmetric single peak and vanishes at 395 K. For the iodide, the room-temperature
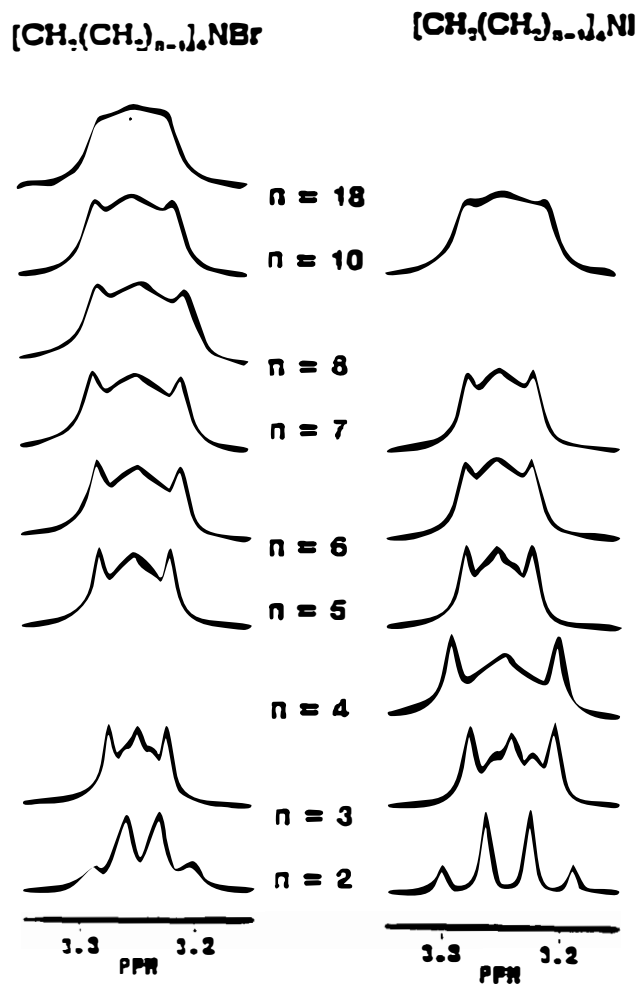
Figure 12   Section plots of the 250 MHz ^{1}H spectra for N – CH$_2$ protons in tetra-ethylammonium halides and higher homologs in either D$_2$O or CDCl$_3$ solution at room temperature.

Table 6 ^{13}C spin-lattice relaxation times, T_1, of $(CH_3)_4NBr$ and $(CH_3)_4NI$[a]

Temperature (K)	Me$_4$NBr (ms)	Me$_4$NI (ms)
311	26.53	32.82
317	26.29	34.33
324	26.34	36.09
331	26.61	38.01
337	27.05	40.19
344	27.60	42.62
350	28.26	45.31
357	28.97	48.23
364	29.75	51.47
370	30.58	55.04
377	31.47	58.81
384	32.40	62.80
390	33.42	67.20
397	34.51	71.76

a   Measured with inverse recovery method. Typical errors in T_1 are 8%.

^{13}C CP-MAS spectrum is plotted in Fig. 14, together with the CSA powder pattern of $(CH_3CH_2)_4NI$. The CSA powder pattern of $(CH_3)_4NI$ is also shown in Fig. 14 (at the top) for comparison. An asymmetric doublet pattern of the methylene carbon, as seen in $(CH_3CH_2)_4NBr$, was not observed for the iodide. The ^{13}C T_1 for both tetraethylammonium salts are listed in Table 7.

¹³CH₂ (52.0 ppm)   ¹³CH₃ (10.15 ppm)
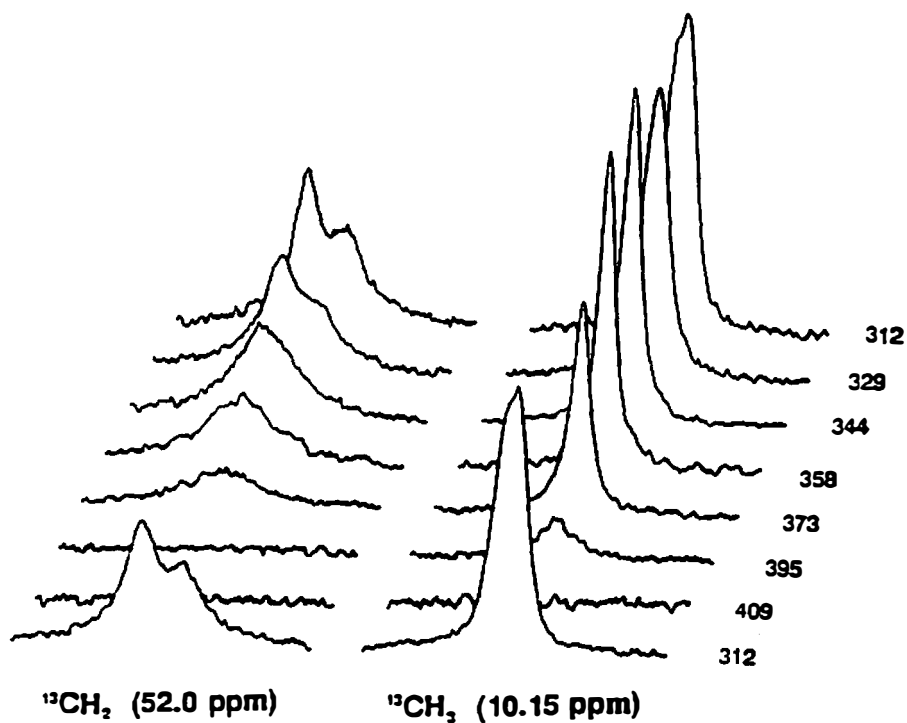
Figure 13 Variable temperature 50.3 MHz ^{13}C CP-MAS spectra of solid tetra-ethylammonium bromide below the disordering transition. Plotted regions are: 56–48 ppm and 14–6 ppm for the methylene and methyl carbons, respectively. Temperatures are (starting from top): 312, 329, 344, 358, 373, 395, 409, and again 312 K measured after cooling from 409 K.
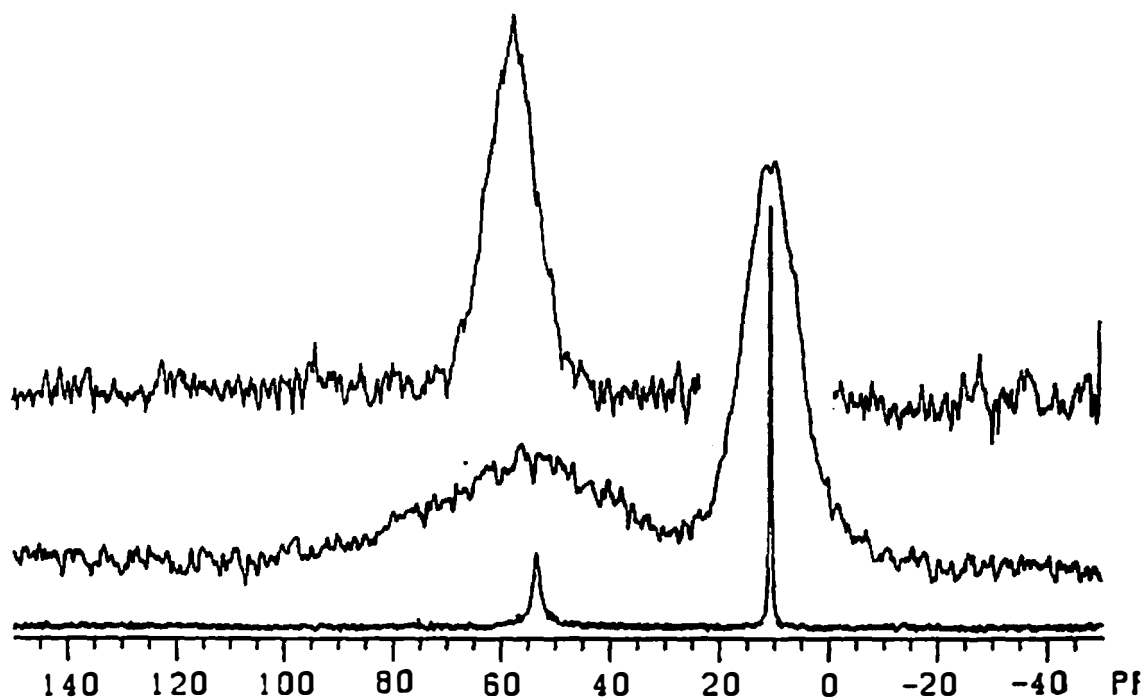
Figure 14   Room-temperature 50.3 MHz solid state ^{13}C NMR spectra of tetra-
ethylammonium iodide. Bottom spectrum: CP-MAS; middle: CSA
powder pattern measured with CP. The CSA powder pattern for tetra-
methylammonium iodide is shown on the top for comparison.

Table 7. ^{13}C spin-lattice relaxation times, T_1, of $(CH_3CH_2)_4NBr$ and $(CH_3CH_2)_4NI^a$

	$(CH_3CH_2)_4NBr$			$(CH_3CH_2)_4NI$	
T (K)	$^{13}CH_2$	$^{13}CH_3$	T (K)	$^{13}CH_2$	$^{13}CH_3$
312	14.3	1.69	308	33.6	2.8
329	14.2	1.98	336	21.9	3.5
344	17.4	2.28	358	16.3	4.3
373	17.4	3.09	380	14.4	5.9
395	20.8	3.43	402	4.5	7.3
409	7.94	3.83			

a   Measured with the progressive saturation method. The T_1 values are in s, and the errors are typically 5%.

For tetra-n-propylammonium bromide at several chosen temperatures, the static ^{13}C NMR spectra, showing CSA powder patterns, are displayed in Fig. 15. The variable-temperature high-resolution ^{13}C solid state NMR spectra obtained under conditions of MAS plus high power decoupling are reproduced in Fig. 16. The ^{13}C T_1 of tetra-n-propylammonium bromide and iodide are listed in Table 8. The correlation time, τ_c, of the motion of an individual carbon in the alkyl groups can be evaluated using Eq. (17) given in 2.3.4, which is the commonly assumed expression for spin-lattice relaxation by dipole-dipole interaction. The results of the calculations are also listed in Table 8.

For tetra-n-propylammonium iodide, a series of the variable temperature ^{13}C NMR MAS spectra from 312 to 433 K were obtained with block-decay and high-
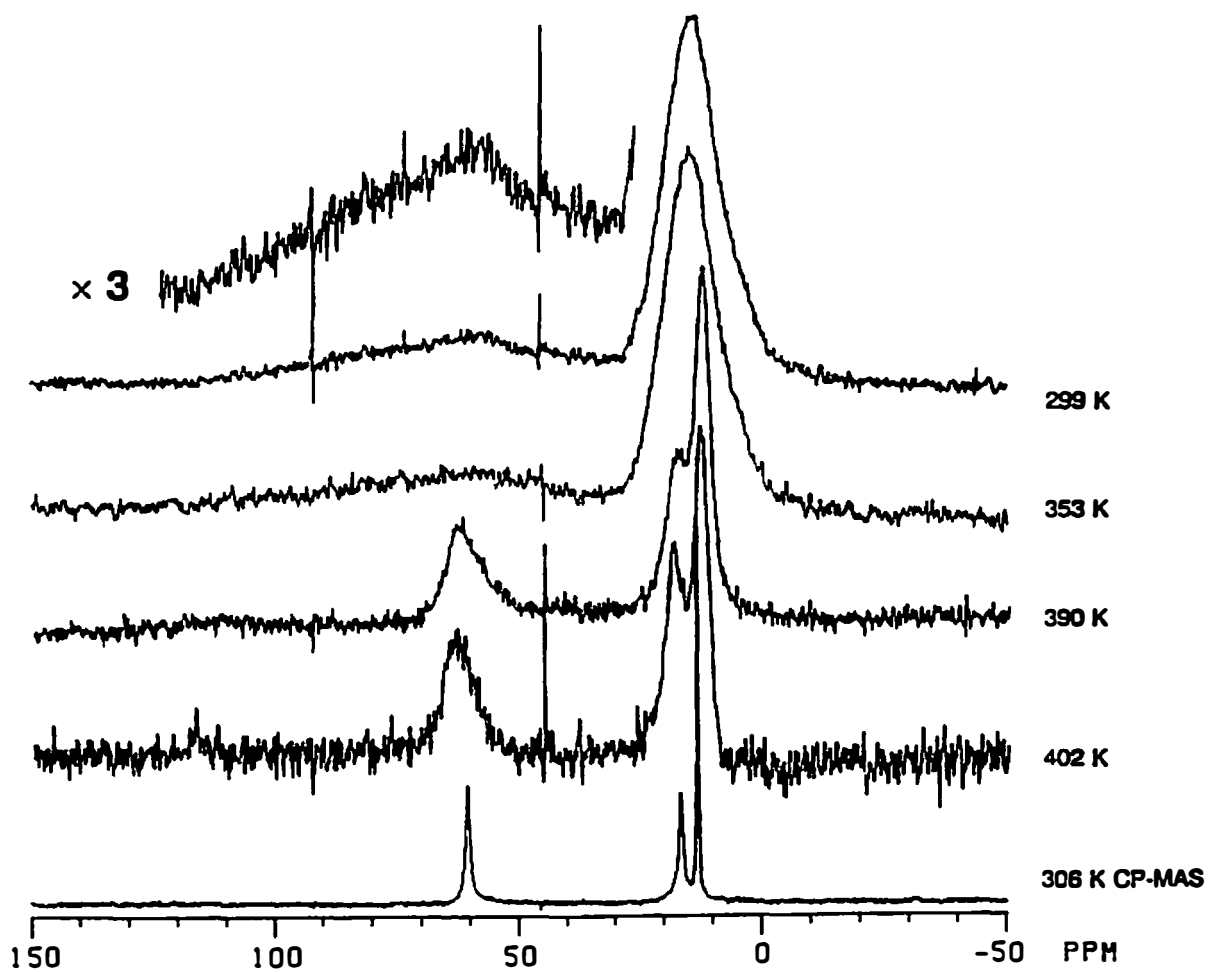
Figure 15   Variable temperature 50.3 MHz ^{13}C CSA powder patterns of tetra-*n*-propylammonium bromide. The temperatures are listed along with each spectrum. The bottom plot is the CP-MAS spectrum at 306 K to indicate the isotropic positions for all the resonances. Spectra at 299 and 353 K were obtained with CP, while above the phase transition of 382.2 K the spectra were measured with BILEV.

91
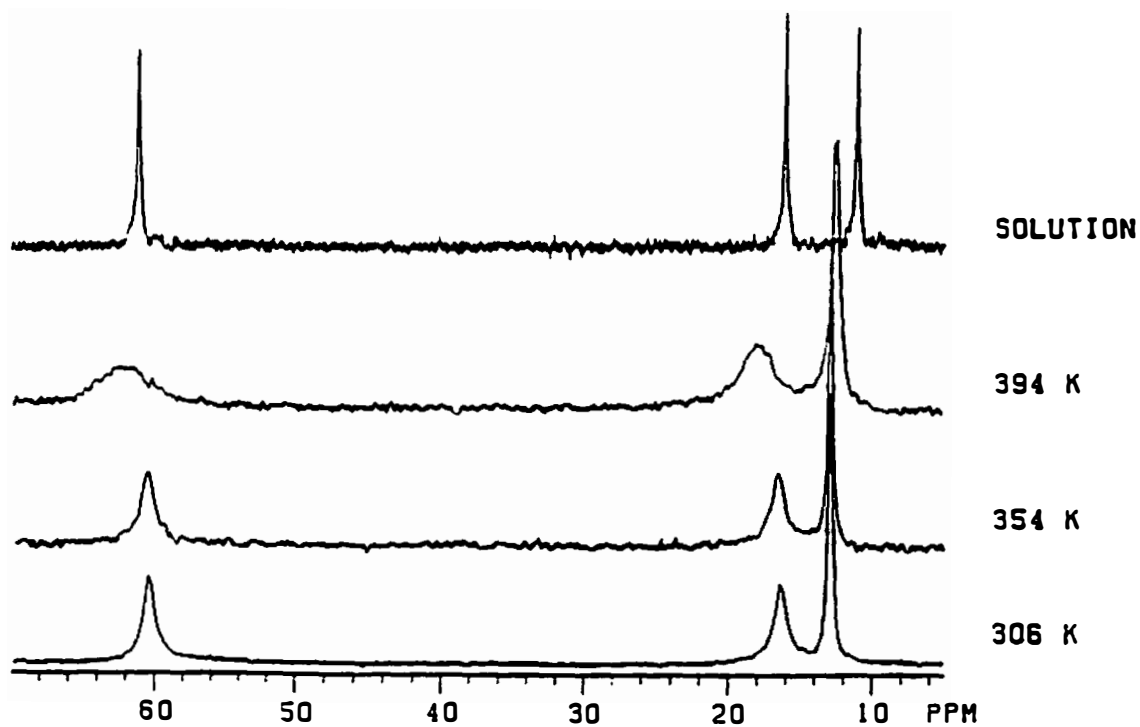
Figure 16   Variable temperature 50.3 MHz ^{13}C NMR MAS (spinning rate 4.5 kHz) spectra of tetra-*n*-propylammonium bromide with CP at 306 and 354 K, without CP at 394 K. The solution spectrum is reproduced at the top for reference.

Table 8 ^{13}C spin-lattice relaxation time, T_1, and calculated correlation time, τ_C, of $(C_3H_7)_4NBr$ and $(C_3H_7)_4I^{a,b}$

T (K)	C-1	C-2	C-3 (methyl)
	$(CH_3CH_2CH_2)_4NBr$		
306	33.2 ±2.1 (47.9 μs)	22.4 ±1.6 (32.3 μs)	1.57 ±0.11 (14.9 ps)
354	30.4 ±1.9 (43.7 μs)	20.0 ±1.5 (28.8 μs)	1.04 ±0.10 (22.1 ps)
394	0.154 ±0.002 (157 ps)	0.250 ±0.004 (94.6 ps)	1.16 ±0.03 (20.0 ps)
	$(CH_3CH_2CH_3)_4NI$		
322	3.31 ±0.35 (0.477 μs)	3.42 ±0.51 (0.493 μs)	1.20 ±0.25 (19.4 ps)
433	0.230 ±0.02 (103 ps)	0.42 ±0.04 (55.8 ps)	1.95 ±0.07 (12.0 ps)

a   Measurements at 354 K and below were done with progressive saturation method, and at 394 and 433 K with inversion recovery. Calculations were made according to Eq. (17). Correlation times were assumed to be on the long-time side of the T_1 minimum at 354 K and below; on the short-time side of the T_1 minimum at 394 and 433 K, as well as for methyl carbons at all temperatures.

b   Relaxation times are in s, and correlation times are listed in parentheses.

power decoupling of protons and are shown in Fig. 17. The MAS spectra from 177 to 312 K were obtained with CP-MAS and shown in Fig. 18. The rates of cross-polarization transfer at 308 and 408 K are shown in Figs. 19 and 20, respectively, in which a series of ^{13}C CP-MAS spectra are plotted as a function of spin-contact times. Finally, variable-temperature ^{1}H spectra of $[CH_3(CH_2)_2]_4NI$ in solution of dimethyl-sulfoxide-d_6 were measured and shown in Fig. 21.
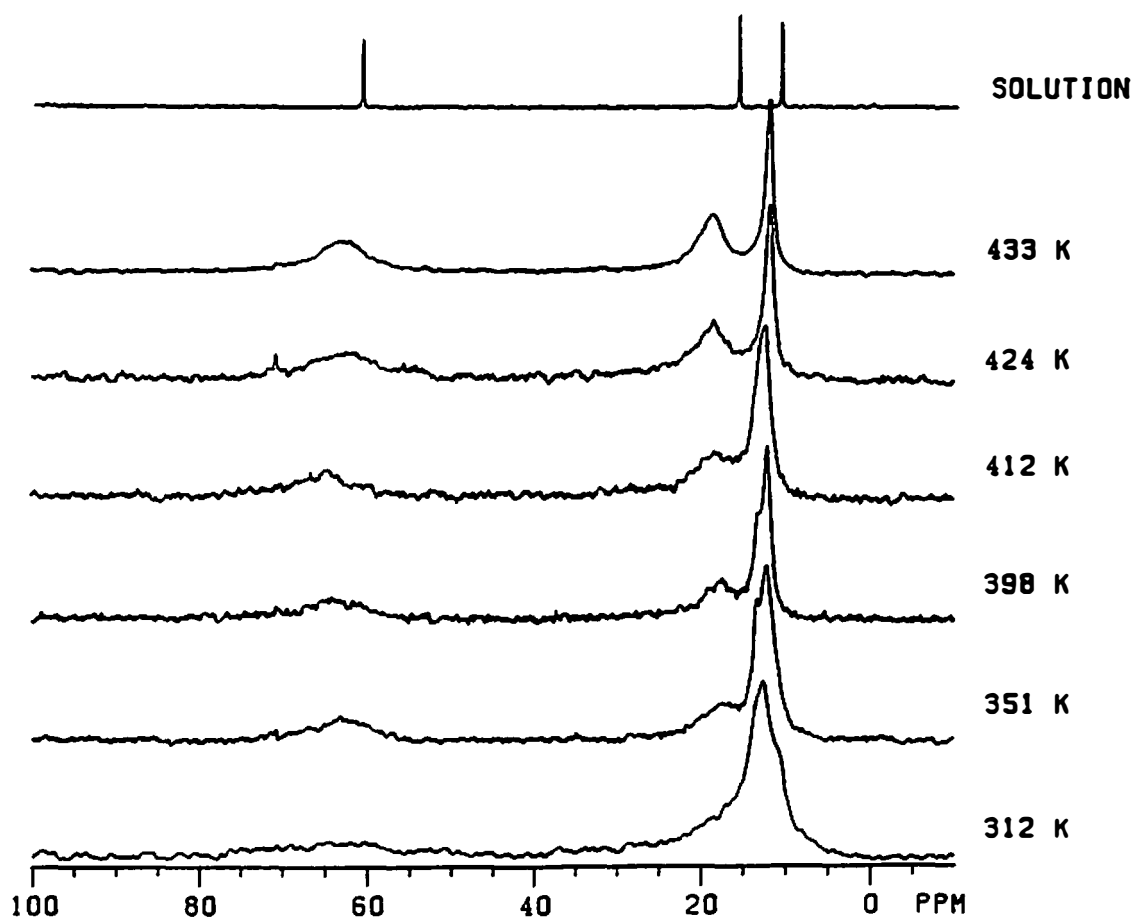
Figure 17   Variable temperature 50.3 MHz ^{13}C NMR MAS (spinning rate 4.5 KHz) spectra of tetra-n-propylammonium iodide without CP. Temperatures are listed.
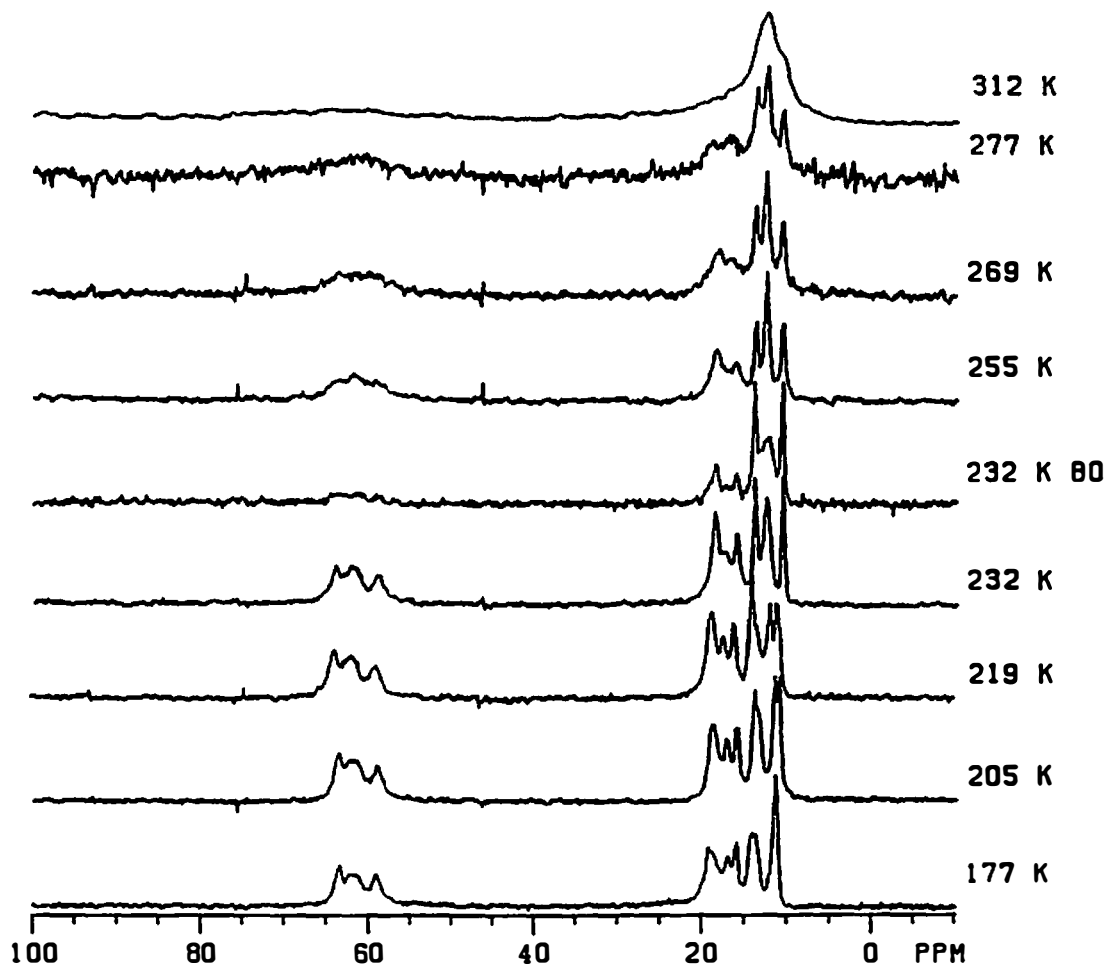
Figure 18   Low temperature ^{13}C NMR spectra of tetra-n-propylammonium iodide. Below 232 K spectra were measured with CP-MAS, while above 232 K BILEV was applied.
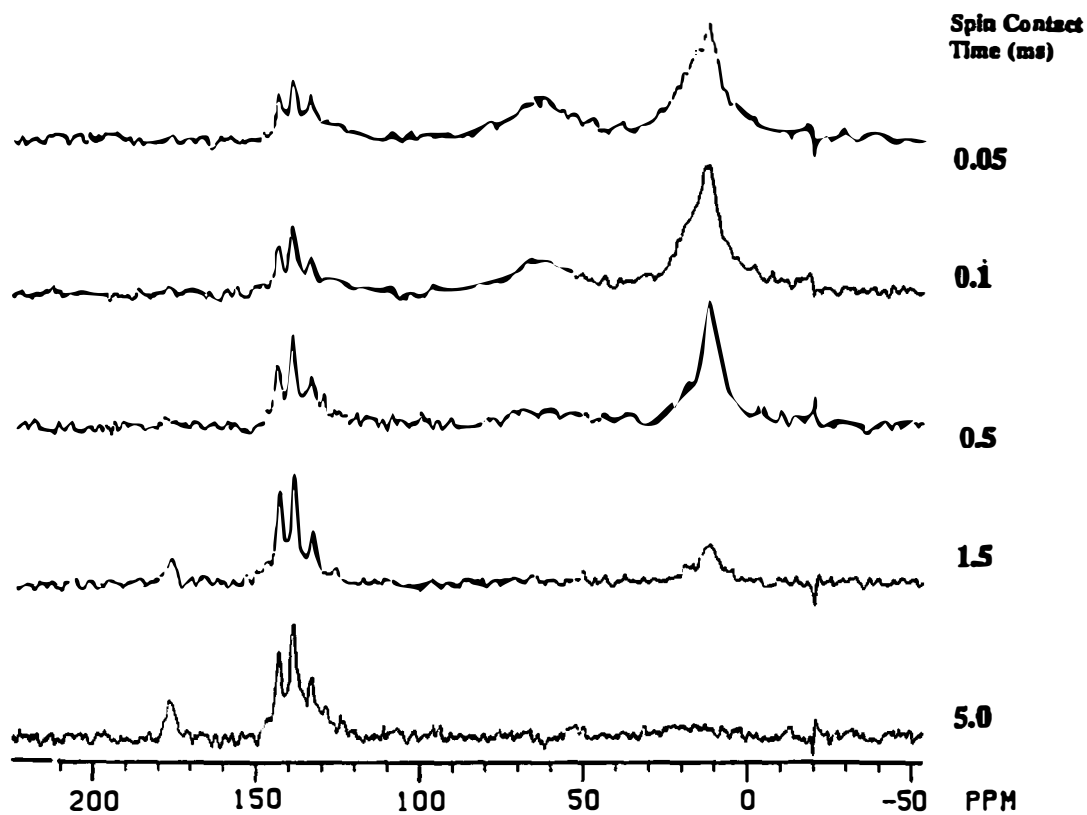
Figure 19   Variable   spin   lock/contact   time   experiment   of   tetra-*n*-propylammonium iodide at room temperature. A maximum in intensity *vs.* the contact time could not be attained. The signals between 120 and 180 ppm are from a referencing compound, tetraphenylborate sodium.

45.80	35.34	20.47
68.89	64.44	39.48
72.04	81.10	54.04
68.49	94.15	74.39
100.00	100.00	100.00
103.12	98.60	97.15
102.22	98.48	55.75
91.81	85.99	32.55
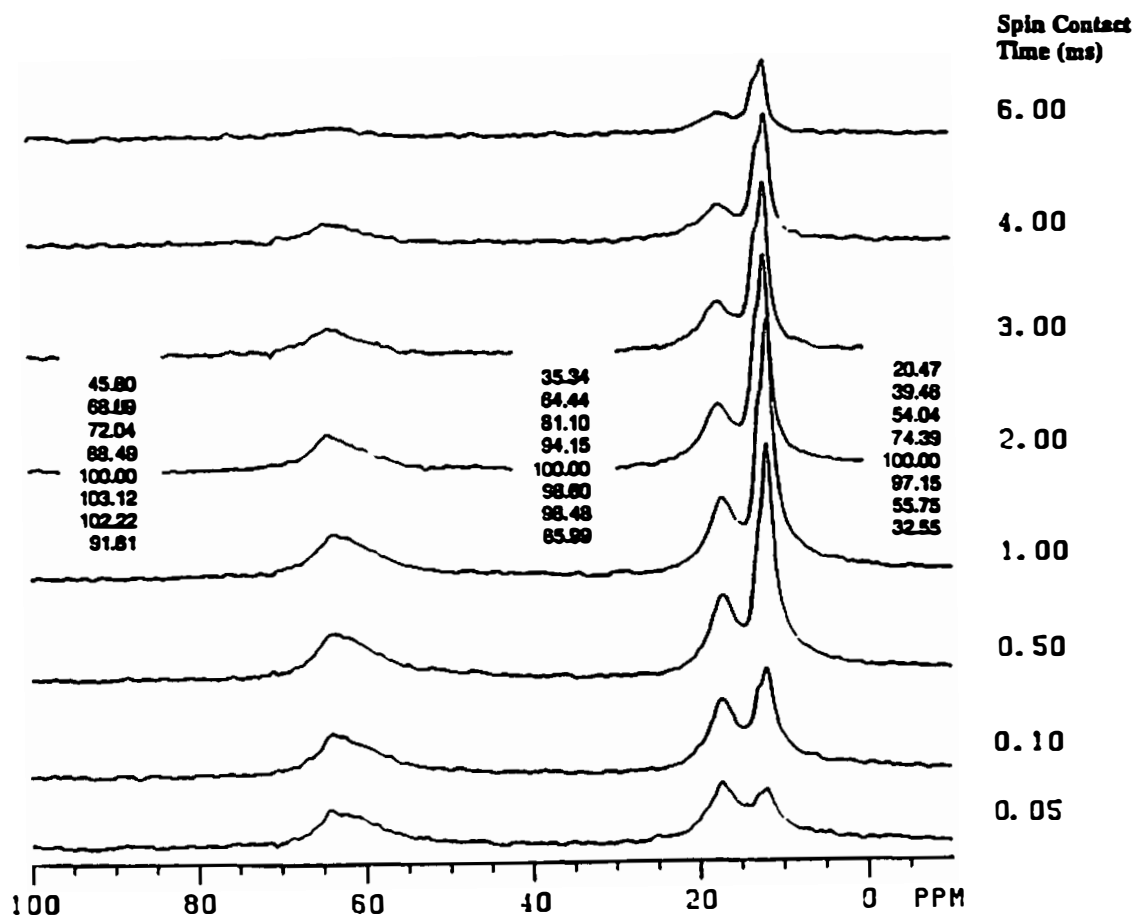
Figure 20   Same as in Fig. 19, but at 408 K. Maxima in intensity *vs.* the contact time could be attained at contact times of 0.5, 1.0, and 1.0 ms for C-1, C-2, and C-3, respectively.

97
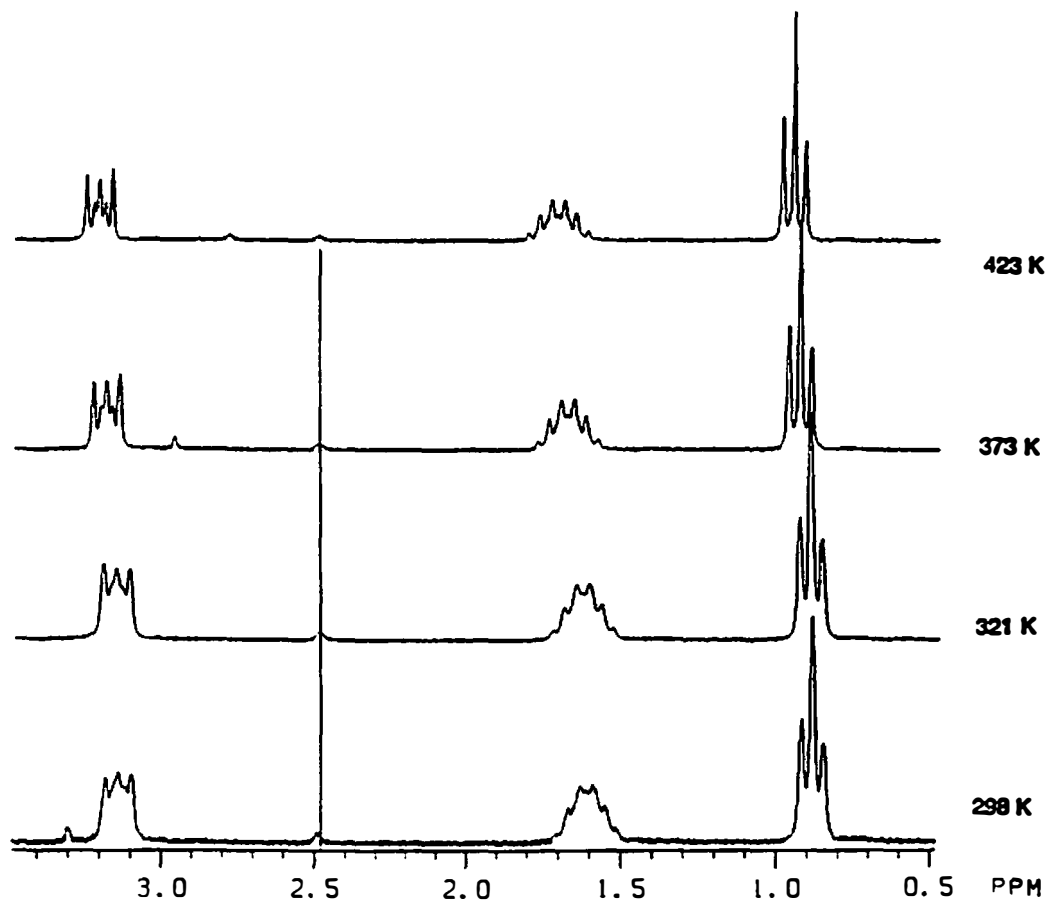
Figure 21   Variable temperature solution (in dimethylsulfoxide DMSO-d$_6$) ^{1}H
             NMR of tetra-n-propylammonium iodide. The peak at about 2.48 ppm
             is due to DMSO.

3.2.2 Intermediate Homologs of Tetra-*n*-alkylammonium Salts

Tetra-*n*-butylammonium bromide and iodide

The variable temperature ^{13}C NMR spectra of the bromide are plotted in Fig. 22 along with a solution (CDCl$_3$) spectrum. Below the lowest disordering transition (367.0 K), the large-amplitude motion is practically quenched, the ^{13}C NMR spectra are only measurable with the CP-MAS method; at temperatures close or above isotropization (393.9 K), the molecular motion is so rapid that the ^{13}C NMR spectra become no longer observable with CP-MAS, and the pulse sequence for the liquid-like samples (BILEV) had to be used; while at some intermediate temperatures (condis phase) both CP-MAS and BILEV are applicable. The same holds true for all other compounds studied in this work. Some numerical values of the chemical shifts of Fig. 22 are listed in Table 9 along with that of the solution spectrum taken at room temperature.

The variable-temperature ^{13}C NMR spectra for the iodide are shown in Fig. 23. A drastic change in the chemical shifts can be seen going to the 395 and 402 K spectra. This change corresponds to the disordering transition observed in DSC at 394.0 K with an entropy change of 71.2 JK^{-1}mol^{-1}. The spectra above 394.0 K become no longer observable with CP-MAS, but are measurable with BILEV. The numerical values of the chemical shifts are listed in Table 10. The variable-temperature ^{13}C chemical-shift-anisotropy powder patterns are graphed in Fig. 24.

The ^{13}C spin-lattice relaxation times of the bromide were measured at 384 K with the *progressive saturation* method, the results for C-2, C-3 and C-4 are 10, 1.51,
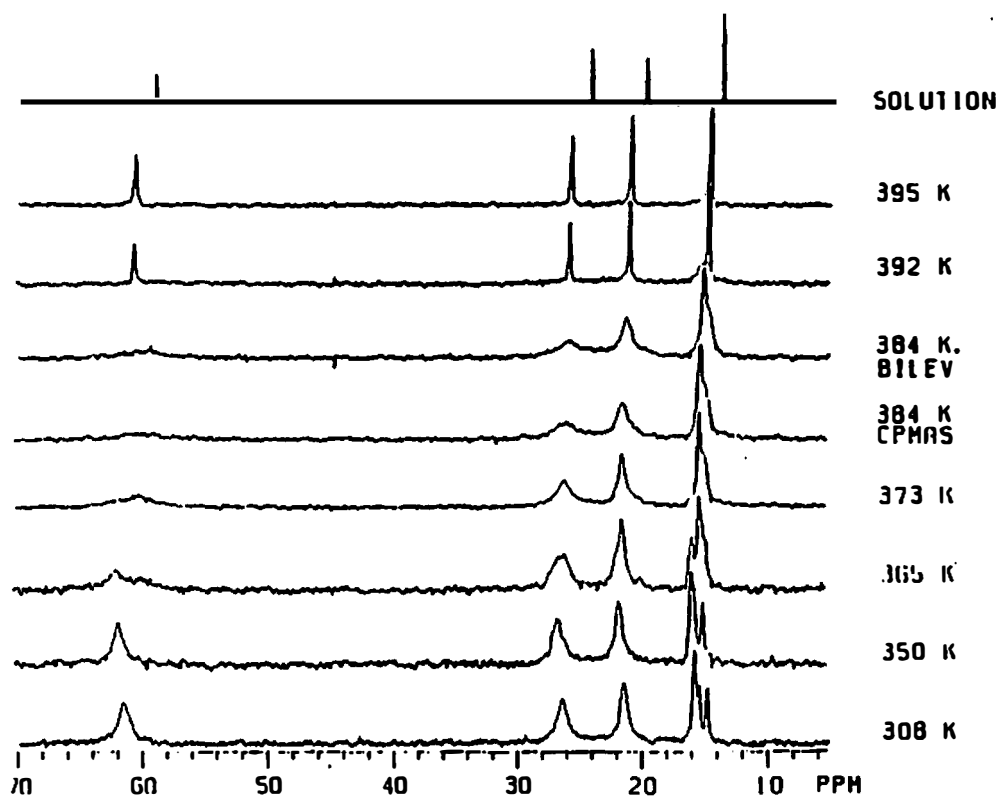
Figure 22 ^{13}C NMR spectra of tetra-*n*-butylammonium bromide. The spectra were measured at temperatures of, from bottom to top: 308, 350, 365, 373, 384 K, obtained with CP-MAS (the pulse sequence for rigid materials), and at 384, 392, and 395 K, measured with BILEV. Two spectra were obtained for the condis state at 384 K, labeled as BILEV and CPMAS. The top spectrum is measured in CDCl$_3$ solution at room temperature.

100

Table 9 ^{13}C NMR chemical shifts in $(C_4H_9)_4NBr$ at select temperatures [a]

Temperature (K)	C-1	C-2	C-3	C-4 (Methyl)
308	61.47	26.31	21.39	15.61/15.30/14.70
Disordering transition: $T_d = 367.0$ K, $\Delta S_d = 41.2$ $JK^{-1}mol^{-1}$				
373	61.37/59.84	25.63	21.09	14.96/14.47
Transition: 379.2 K, 1.4 $JK^{-1}mol^{-1}$				
384	NA[b]	25.74	21.09	14.97/14.49
Isotropization: $T_i = 393.9$ K, $\Delta S_i = 37.6$ $JK^{-1}mol^{-1}$				
395 (melt)	60.45	25.57	20.74	14.41
Solution (in $CDCl_3$)	59.09	24.23	19.79	13.74

a   Spectra of Fig. 22. Multiple values are given for carbon atoms having more than one peak. Values are given in ppm relative to TMS.

b   NA stands for data not available, because of broadness and weakness of the resonance.

and 2.58 s, respectively. The T_1 for C-1 is not available at 384 K because the resonance of C-1 is rather weak due to the line-broadening. The T_1-values for the iodide were measured at 308, 329 and 408 K and are listed in Table 11. Included in the table are also the T_1-values for $(C_4H_9)_4NClO_4$ measured in CD_3OD solutions by Coletta et al.[4]
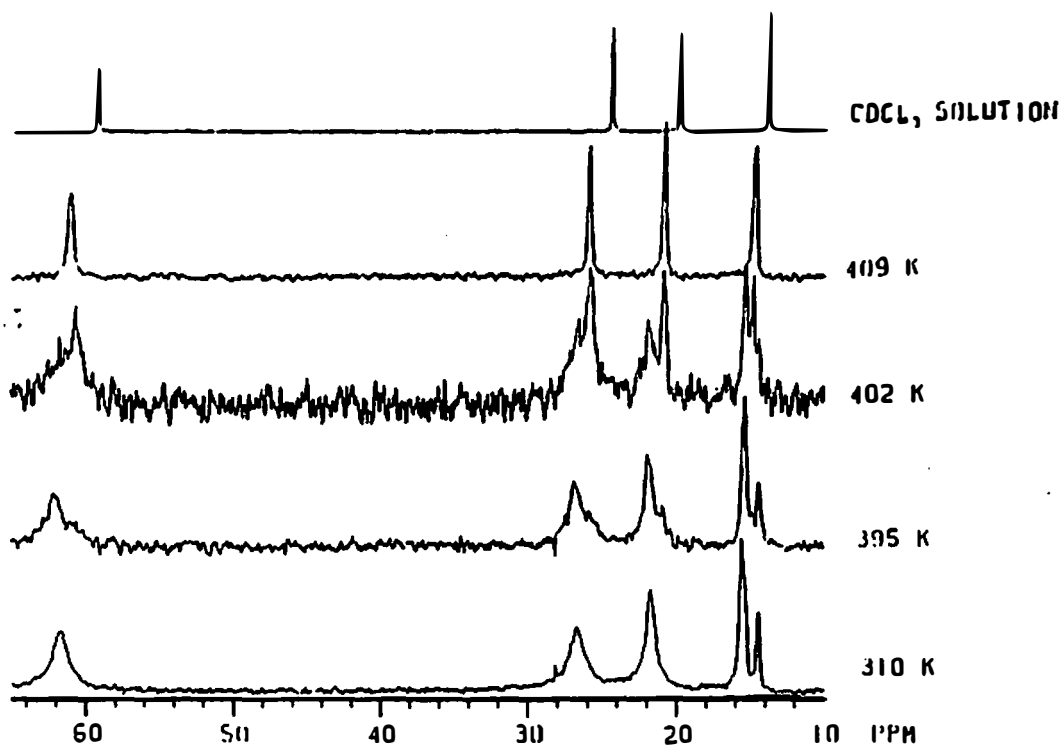
Figure 23 ^{13}C NMR spectra of tetra-n-butylammonium iodide. Spectra were obtained with CP-MAS at 310 K, and, from bottom to top: 395, 402, and 409 K, with BILEV. The top spectrum is measured in CDCl$_3$ solution at room temperature.

Table 10 ^{13}C NMR chemical shifts in $(C_4H_9)_4NI$ as a function of temperature[a]

Temperature (K)	C-1	C-2	C-3	C-4 (Methyl)
310	61.58	26.67	21.65	15.53/15.32/14.40
387	61.91	26.79	21.77	15.36/15.36/14.37
Disordering transition: T_d = 394.0 K, ΔS_d = 71.2 $JK^{-1}mol^{-1}$				
395	62.09	26.78/25.85	21.87/20.90	15.33/14.79/14.39
402	60.63	26.52/25.80	21.87/20.85	15.34/14.97/14.43
409	60.97	25.84	20.80	14.67
416	61.00	25.85	20.79	14.64
Isotropization: T_i = 420.6 K, ΔS_i = 21.3 $JK^{-1}mol^{-1}$				
Solution (in $CDCl_3$)	59.32	24.40	19.84	13.78

a   Spectra of Fig. 23 and additional spectra at 387 and 416 K. Above the disordering transition temperature (394 K), the spectra are only detectable with the pulse sequences for liquids (BILEV). Multiple values indicate double or triple peaks. Chemical shifts are given in ppm relative to TMS.
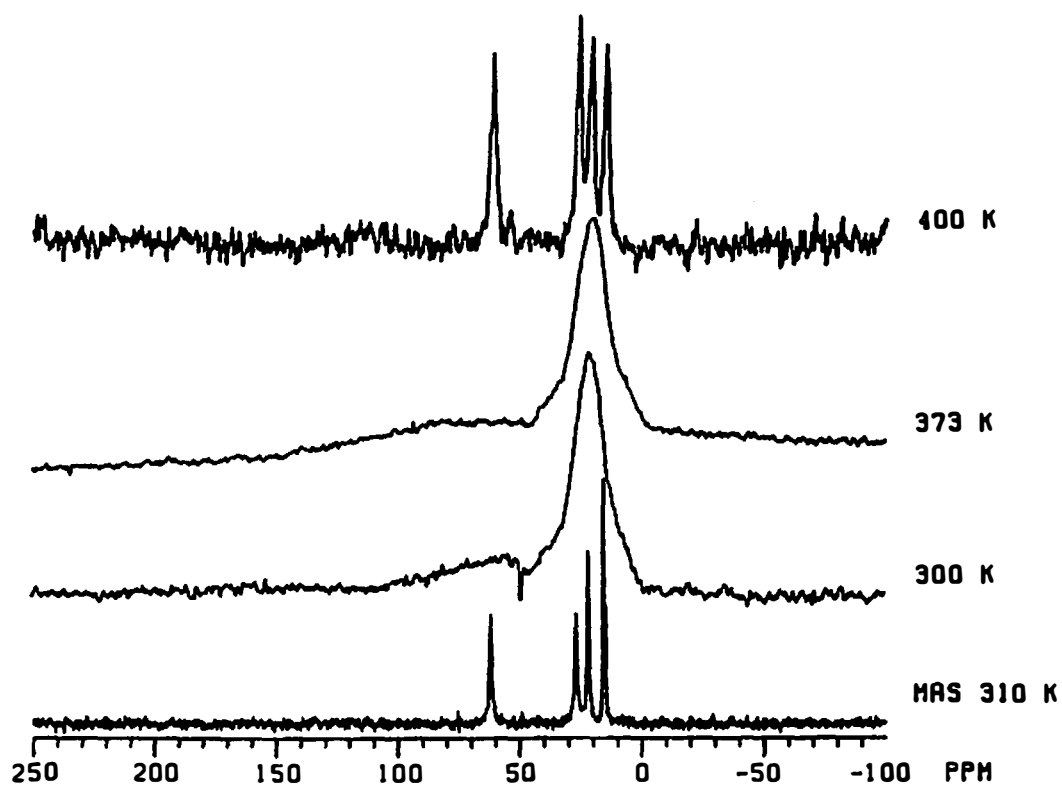
Figure 24   Variable temperature ^{13}C NMR powder patterns of tetra-n-butyl-ammonium iodide obtained at 300, 373, and 400 K. The bottom trace is the CP-MAS spectrum at 310 K to show the isotropic resonance positions.

104

Table 11 ^{13}C spin-lattice relaxation times of $(C_4H_9)_4NI$[a]

T (K)	C-1	C-2	C-3	C-4[c]
308	56.0 ± 1.7	58.5 ± 2.1	42.9 ± 1.1	1.69 ± 0.04; 1.77 ± 0.06
329	52.4 ± 1.5	60.1 ± 3.2	42.3 ± 1.0	2.34 ± 0.05; 1.89 ± 0.08
Disordering transition: $T_d = 394.0$ K, $\Delta S_d = 71.2$ JK^{-1}mol^{-1}				
408	0.120 ± 0.002	0.169 ± 0.005	0.514 ± 0.010	2.08 ± 0.02
Isotropization: $T_i = 420.6$ K, $\Delta S_i = 21.3$ JK^{-1}mol^{-1}				
Solution[b]	0.4	0.5	0.9	2.3

a   Measured with the *inversion recovery* method. Values are in s.

b   Data taken from Coletta *et al.*, (1987) for the solution of perchlorate salt of tetrabutylammonium ions in CD_3OD, measured at 305 K with a 22.6 MHz (for ^{13}C) spectrometer.

c   Data for the methyl carbon are given for the most low- and up-field resonances.

Tetra-*n*-pentylammonium bromide and iodide

Figures 25 and 26 show the variable temperature ^{13}C CP-MAS spectra for the bromide and the iodide, respectively. The chosen temperatures cover all observed solid-mesophase transitions (374 K for $(C_5H_{11})_4NBr$, 404.6 and 412.1 K for $(C_5H_{11})_4NI$). The chemical shift values at the selected temperatures are listed in Tables 12 and 13. For tetra-*n*-alkylammonium salts with chains consisting of 5 or more carbon atoms, the chemical shift value of a given carbon atom is no longer determined solely by its proximity to the nitrogen. For example, in the solution state

105
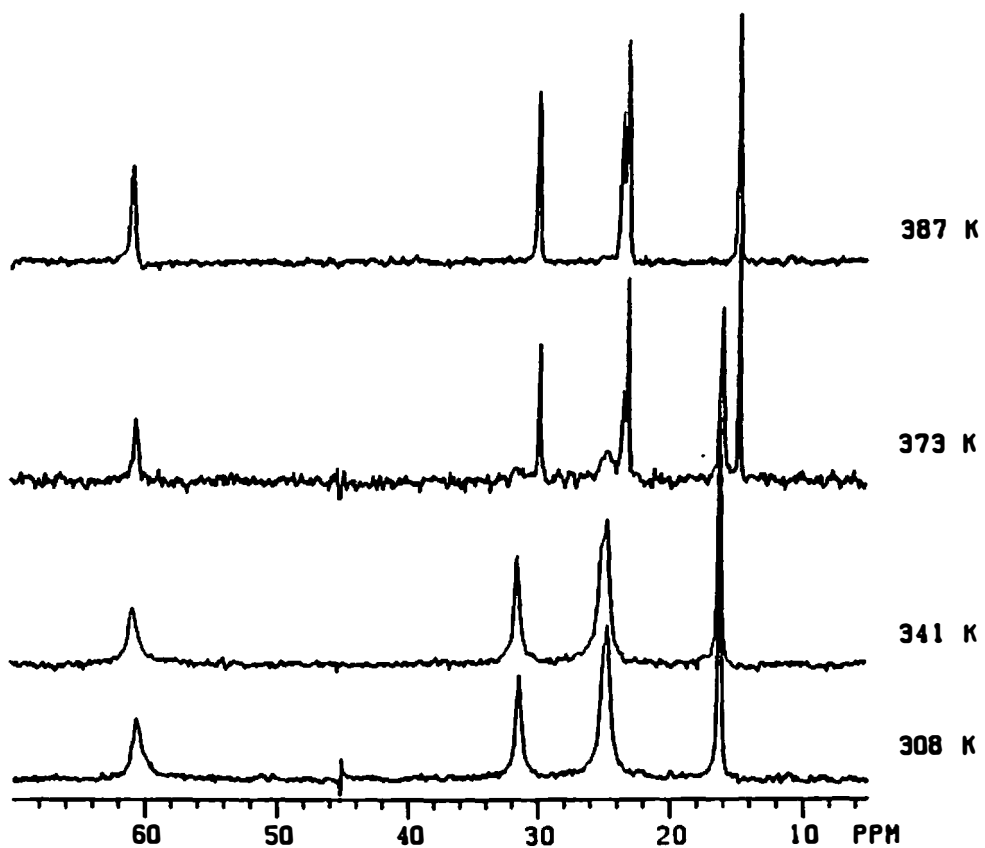
Figure 25 ^{13}C NMR spectra of tetra-n-pentylammonium bromide obtained with magic angle spinning.
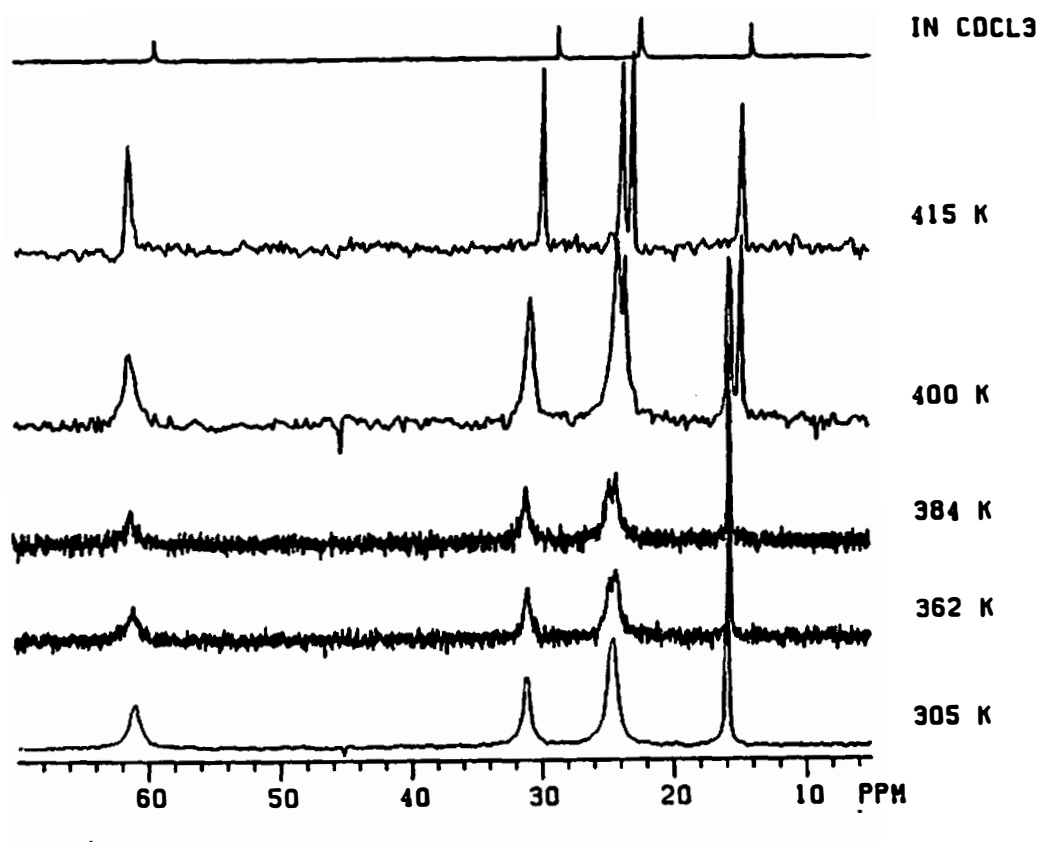
Figure 26 ^{13}C NMR spectra of tetra-n-pentylammonium iodide obtained with magic angle spinning. The top spectrum is measured in CDCl$_3$ solution at room temperature.

Table 12 ^{13}C chemical shifts in $(C_5H_{11})_4NBr$ as a function of temperature[a]

T (K)	C-1	C-2	C-3	C-4	C-5
308	60.48	24.60	31.32	24.60	16.14
341	60.57	24.85	31.27	24.42	15.95
Isotropization: T_i = 374.0 K, ΔS_i = 97.9 $JK^{-1}mol^{-1}$					
387	60.63	23.35	29.69	22.92	14.58
Solution (in $CDCl_3$)	59.27	22.06	28.45	22.25	13.83

a   Spectra of Fig. 25. Chemical shifts are in ppm relative to TMS.

Table 13 ^{13}C chemical shifts in $(C_5H_{11})_4NI$ as a function of temperature[a]

T (K)	C-1	C-2	C-3	C-4	C-5
305	60.92	24.44	31.05	24.44	15.81
362	60.85	24.15	30.86	24.60	15.54
384	60.87	23.96	30.84	24.56	15.45
400	61.11	23.91	30.52	23.40	15.52/14.71
Disordering transition: T_d = 404.6 K, ΔS_d = 41.2 $JK^{-1}mol^{-1}$					
Isotropization: T_i = 412.1 K, ΔS_i = 94.0 $JK^{-1}mol^{-1}$					
415	61.15	23.61	29.63	22.80	14.62
Solution ($CDCl_3$)	59.45	22.22	28.47	22.49	13.87

a   Spectra of Fig. 26. Two values for C-5 at 400 K show the low- and high-temperature phases. Chemical shifts are in ppm relative to TMS.

C-2 has a smaller chemical shift than all others carbon atoms, except the methyl group carbon, as can be seen in Tables 12 and 13 and the subsequent tables for longer chain salts.

The relaxation times of each individual carbon atom at different temperatures are listed in Tables 14 and 15 for the bromide and iodide, respectively.

Table 14 ^{13}C T_1 of $(C_5H_{11})_4NBr$[a]

T (K)	C-1	C-2	C-3	C-4	C-5
308	37.0±2.2	(33.8)[a]	30.6±1.1	(15.4)[a]	1.50±0.04
	Isotropization: T_i = 374.0 K, ΔS_i = 97.9 JK^{-1}mol^{-1}				
380	0.077±0.003	0.126±0.004	0.27±0.01	0.74±0.03	1.73±0.05

a   Resonances of C-2 and C-4 overlap at 308 K, their T_1 were obtained by curve fitting to a bi-exponential function defined by Eq. (34), below, for details see text. T_1 values are given in s.

Table 15 ^{13}C T_1 of $(C_5H_{11})_4NI$[a]

T (K)	C-1	C-2	C-3	C-4	C-5
310	39.1±3.8	(36.9)[a]	34.6±2.7	(21.4)[a]	1.18±0.09
	Disordering transition: T_d = 404.6 K, ΔS_d = 41.2 JK^{-1}mol^{-1}				
	Isotropization: T_i = 412.1 K, ΔS_i = 94.0 JK^{-1}mol^{-1}				
415	0.130±0.004	0.22±0.01	0.43±0.02	1.37±0.04	2.89±0.06

a   Resonances of C-2 and C-4 overlap at 310 K, their T_1's were obtained by curve fitting to a bi-exponential function defined by Eq. (34), below, for details see text. T_1 values are given in s.

Tetra-n-hexylammonium bromide and iodide

The ^{13}C MAS NMR spectra of tetra-n-hexylammonium bromide at temperatures above room-temperature are shown in Fig. 27. The low temperature spectra (from about 146 K to 310 K) are shown in Fig. 28, obtained on slow cooling (about 10 K/min). Figure 29 shows spectra obtained first on fast cooling (about 60 K/min) from 310 to 146 K, then on slow heating (10 K/min) to 310 K. The variable temperature ^{13}C NMR MAS spectra of $(C_6H_{13})_4NI$ is shown in Fig. 30, for temperatures from 308 to 375 K. The chemical shifts based on the variable-temperature spectra are listed in Table 16 for $(C_6H_{13})_4NBr$, and in Table 17 for $(C_6H_{13})_4NI$. The ^{13}C T_1 at temperatures of different phases are listed in Table 18 for $(C_6H_{13})_4NI$.

Table 16 ^{13}C chemical shifts of $(C_6H_{13})_4NBr$ as a function of temperature

T (K)	C-1	C-2	C-3	C-4	C-5	C-6
148[a]	63.56	25.07	29.82	34.31	25.94	16.43/15.79
247[a]	63.43	24.98	29.79	34.05	25.78	15.97
Disordering transitions at: 148, 167, 196, and 305 K, with entropy changes of: 8.1, 1.2, 17.5, and 22.0 $JK^{-1}mol^{-1}$, respectively						
310[a]	59.32	24.33	27.06	33.22/31.71	23.30	15.23/14.72
Disordering transition: $T_{d5} = 315$ K, $\Delta S_{d5} = 38$ $JK^{-1}mol^{-1}$ Isotropization: $T_i = 374.9$ K, $\Delta S_i = 42.6$ $JK^{-1}mol^{-1}$						
374[b]	60.46	23.59	27.13	32.07	23.14	14.57
Solut.[b]	59.33	22.41	26.10	31.25	22.41	13.93

a   Spectra of Fig. 28. Two values are given for double peaks arising form the same carbon atom. Chemical shifts are in ppm relative to TMS.
b   Spectra of Fig. 29.
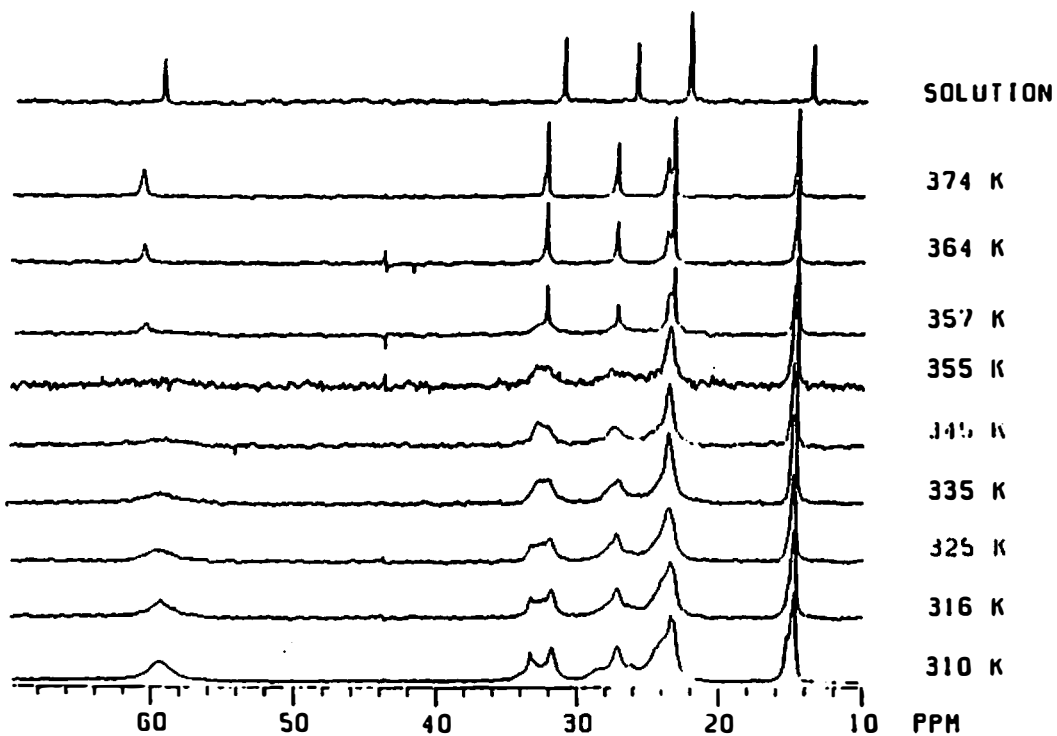
Figure 27 ^{13}C CP-MAS NMR spectra of tetra-n-hexylammonium bromide. The top spectrum is measured in CDCl$_3$ solution at room temperature.
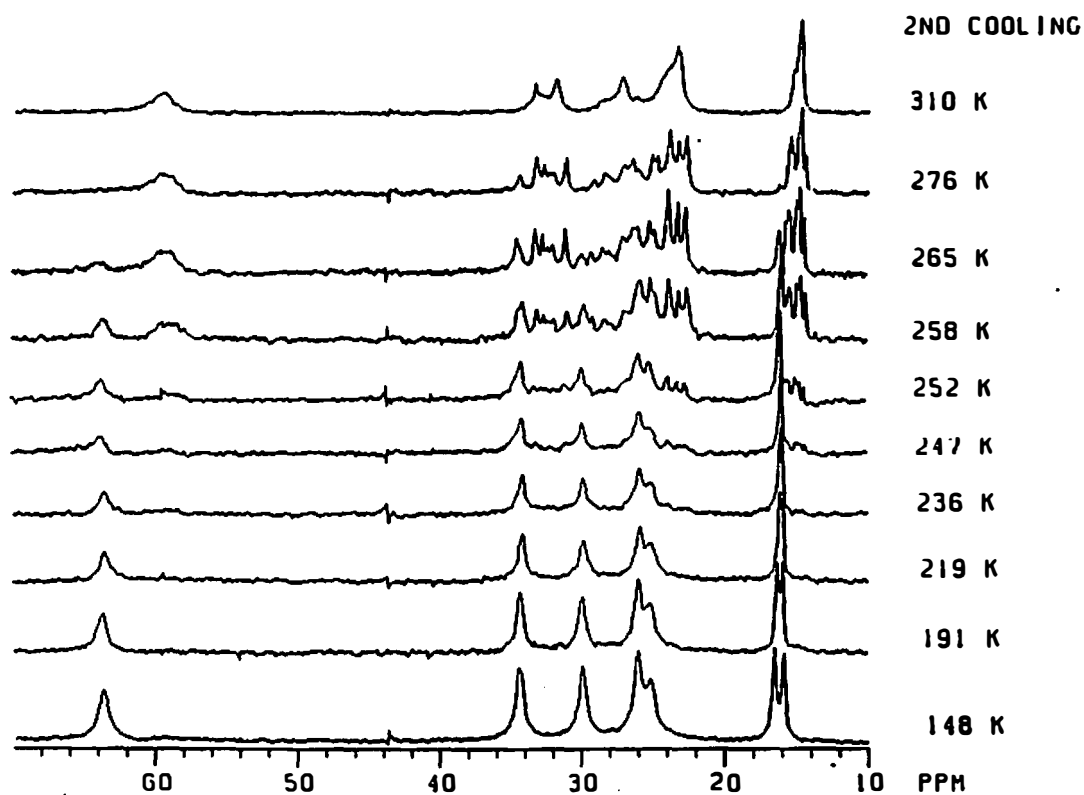
Figure 28 ^{13}C CP-MAS NMR spectra of tetra-*n*-hexylammonium bromide obtained on slow cooling (about 10 K/min) from 310 K to 148 K. The chemical shifts of the spectra at 247 and 148 K spectra are listed in Table 16.
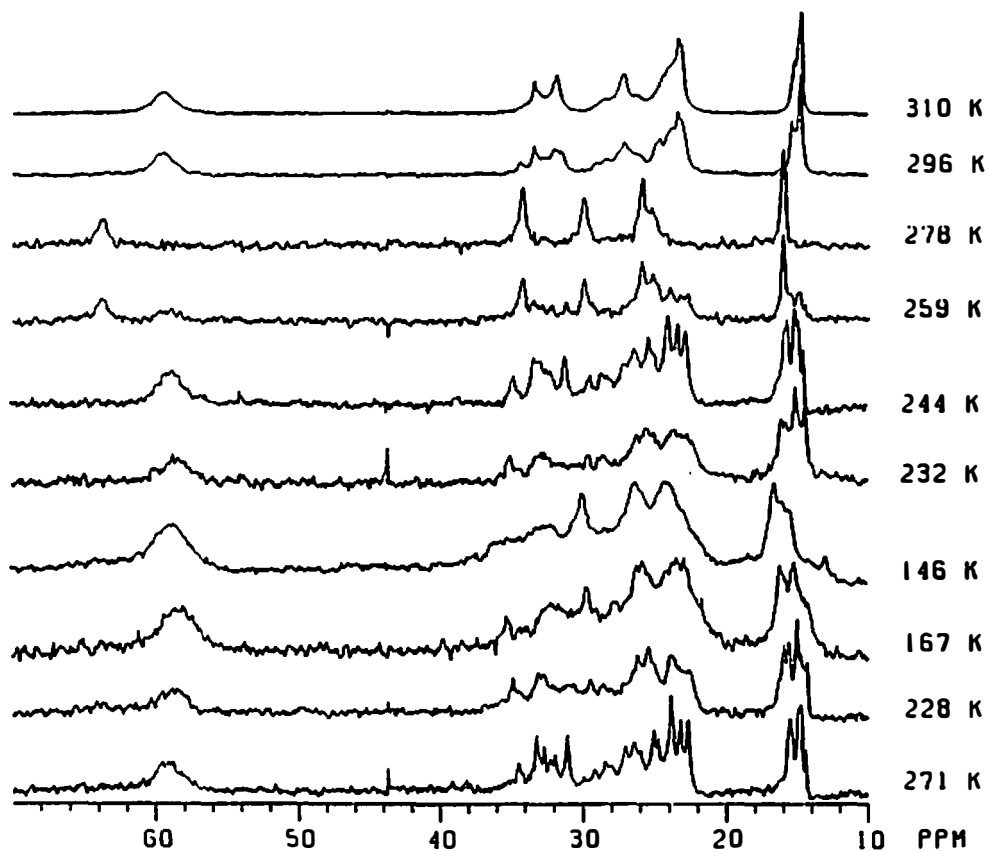
Figure 29 ^{13}C CP-MAS NMR spectra of tetra-n-hexylammonium bromide obtained on fast cooling from 271 K to 146 K (first four spectra from bottom), followed by heating of the quenched sample (about 10 K/min) from 146 K to 310 K (six spectra shown at the top).
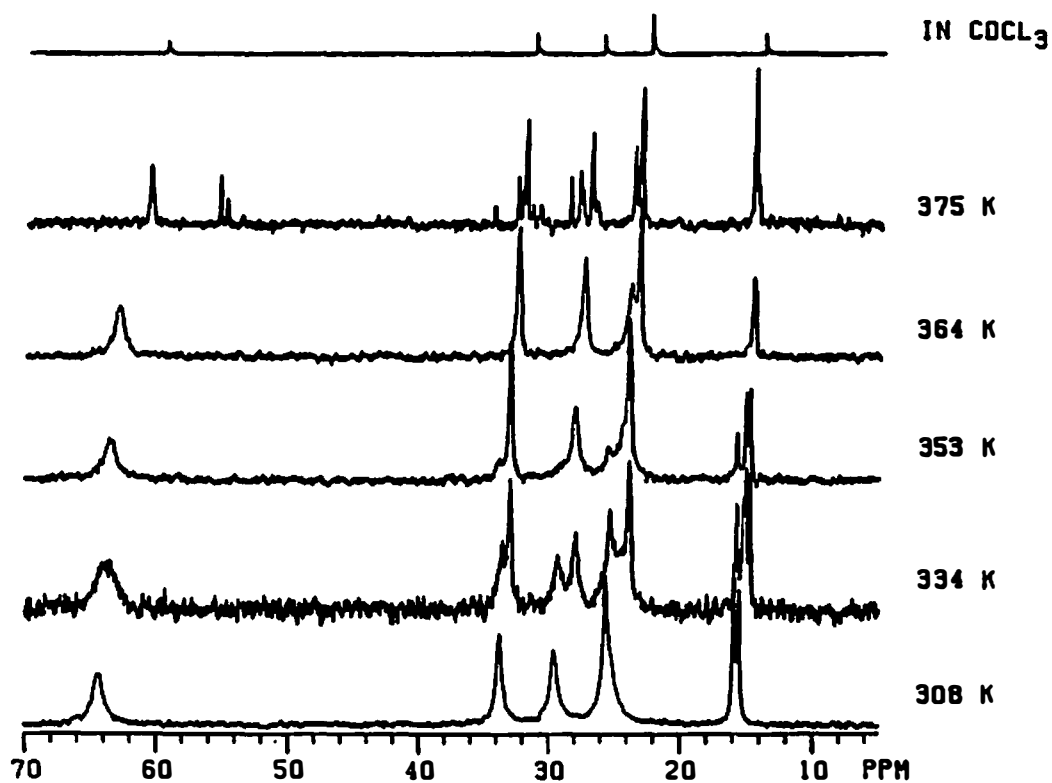
Figure 30 ^{13}C CP-MAS NMR spectra of tetra-n-hexylammonium iodide. The top spectrum is measured in CDCl$_3$ solution at room temperature.

Table 17 ^{13}C chemical shifts of $(C_6H_{13})_4NI$ as a function of temperature[a]

T (K)	C-1	C-2	C-3	C-4	C-5	C-6
308	64.41	25.00	29.47	33.66	25.52	15.83/15.45
Disordering transitions: $T_{d1} = 345.1$ K, $\Delta S_{d1} = 83.3$ JK^{-1}mol^{-1}						
$T_{d2} = 352.3$ K, $\Delta S_{d2} = 16.2$ JK^{-1}mol^{-1}						
364	62.93	23.80	27.36	32.40	23.14	14.60/14.46
Isotropization: $T_i = 378.7$ K, $\Delta S_i = 43.9$ JK^{-1}mol^{-1}						
380	60.48	23.58	26.60	31.87	23.50	14.55
Solut.	59.29	22.41	26.04	31.21	22.41	13.93

a   Spectra of Fig. 30. Two values are for the two peaks arising from the methyl carbon. Chemical shifts are in ppm relative to TMS.

Table 18 ^{13}C T_1 of $(C_6H_{13})_4NI$[a]

T (K)	C-1	C-2	C-3	C-4	C-5	C-6
308	43.0	(39.0)	36.0	29.1	(14.5)	2.5
322	36.0	(34.1)	32.5	20.2	(11.5)	2.3
Disordering transitions: $T_{d1} = 345.1$ K, $\Delta S_{d1} = 83.3$ JK^{-1}mol^{-1}						
$T_{d2} = 352.3$ K, $\Delta S_{d2} = 16.2$ JK^{-1}mol^{-1}						
358	0.29	0.43	0.87	1.78	2.44	3.46
Isotropization: $T_i = 378.7$ K, $\Delta S_i = 43.9$ JK^{-1}mol^{-1}						
380	0.094	0.108	0.32	0.98	1.95	3.61
Solut.	0.25	0.30	0.50	1.38	1.75	2.75

a.   Data in parentheses are for C-2 and C-5, since their resonances overlap, their T_1 were obtained by curve fitting to Eq. (34). The solution data are taken from Coletta et al., 1987. T_1 values are in s.

Tetra-*n*-heptylammonium bromide and iodide

Since the two heptyl salts show great similarity in their thermal behavior,[1] the detailed NMR studies were only carried out for one of them, namely, $(C_7H_{15})_4NI$. For the bromide, only a ^{13}C spectrum, shown in Fig. 31 with chemical shifts labeled on the peaks, was measured at room temperature with MAS and high-power decoupling of protons (BILEV) for comparison with the iodide. For $(C_7H_{15})_4NI$ two sets of variable temperature ^{13}C MAS spectra were obtained, one below and one above room-temperature and are shown in Figs. 32 and 33, respectively. The chemical shifts of $(C_7H_{15})_4NI$ are listed in Table 19. Solution data are also included in the table. The ^{13}C chemical-shift-anisotropy powder patterns for $(C_7H_{15})_4NI$ at some selected temperatures are shown in Fig. 34. Finally, the ^{13}C T_1 at temperatures of the different phases are listed in Table 20 for $(C_7H_{15})_4NI$.

3.2.3 High Homologs of Tetra-*n*-alkylammonium Salts

A selection of the variable-temperature ^{13}C NMR spectra recorded under magic-angle spinning with either cross-polarization (CP-MAS) or one-pulse for ^{13}C plus two-level decoupling of protons (BILEV) are shown in Figs. 35–38 for $(C_n H_{2n+1})_4NBr$, n = 8, 10, 12, and 18, and Figs. 39 and 40 for $[CH_3(CH_2)_{11}]_4NI$ at temperatures below and above 310 K, respectively.

For tetra-*n*-octylammonium bromide, all spectral lines are well resolved. The numbering of the carbon atoms starts always with C-1 for the carbon bonded to nitrogen and ends with C-8 for the methyl carbon. In Table 21 all measured chemical
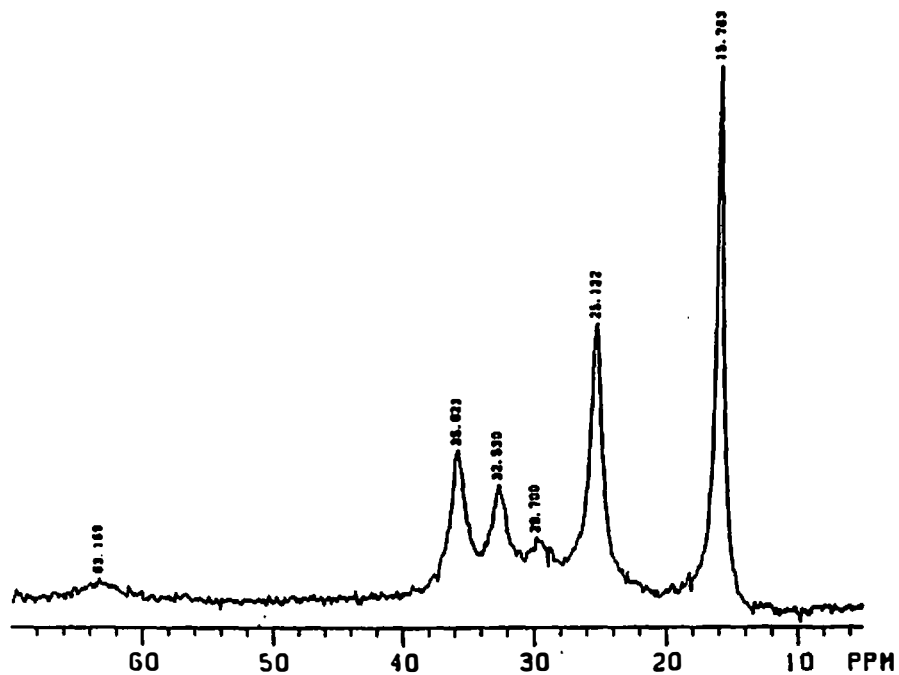
Figure 31   Room-temperature ^{13}C NMR (50.3 MHz) spectra of tetra-*n*-heptylammonium bromide obtained with magic angle spinning and BILEV decoupling. The chemical shifts are labeled on each peak.

117
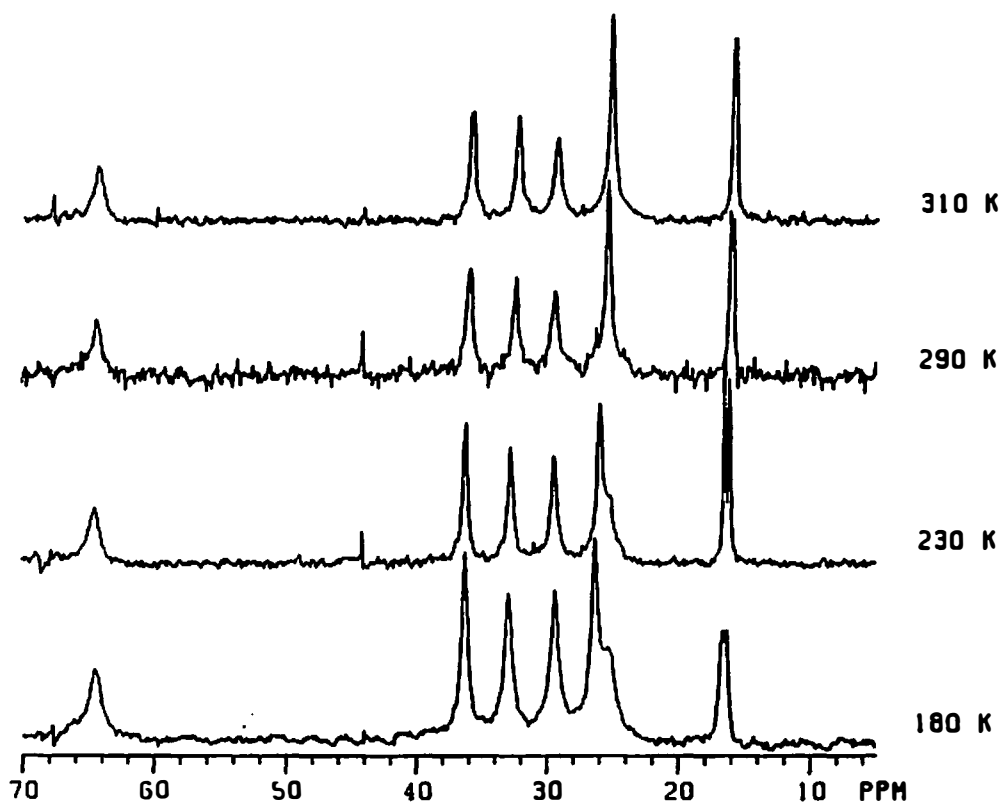
Figure 32 Low temperature ^{13}C CP-MAS NMR spectra of tetra-*n*-heptylammonium iodide.
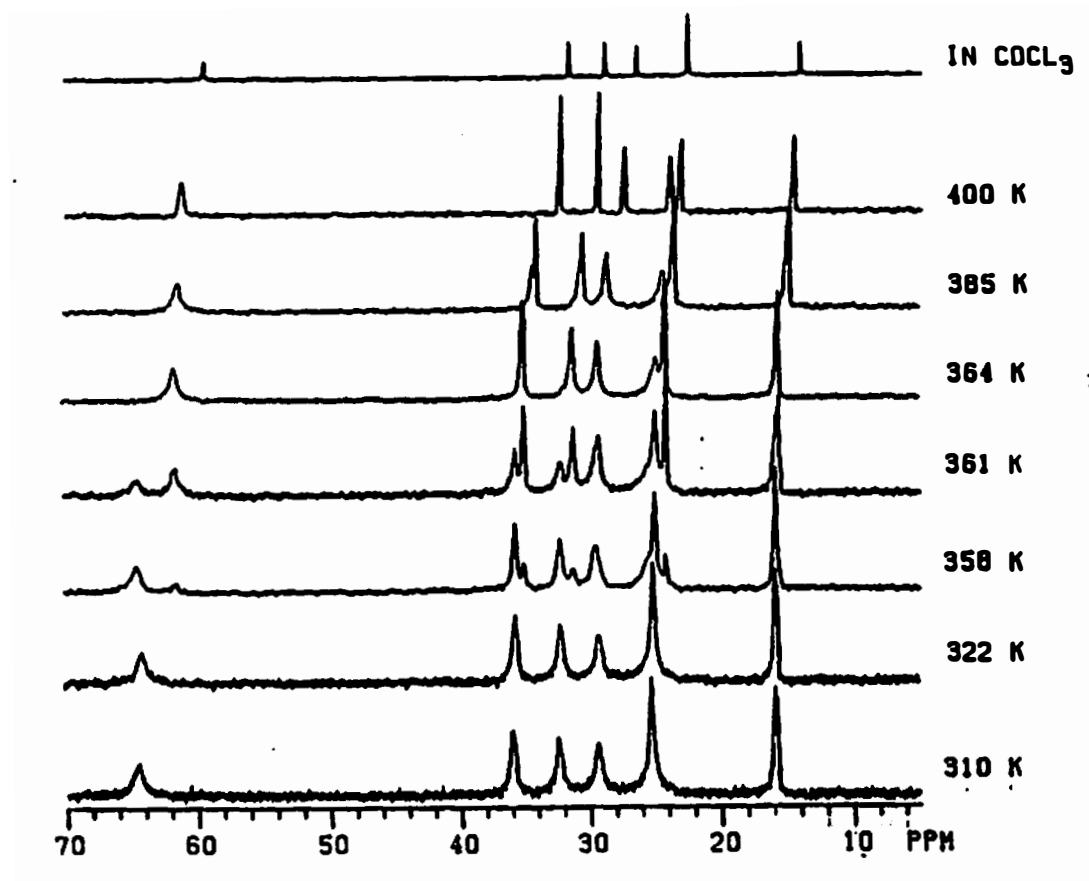
Figure 33 ^{13}C NMR spectra of tetra-n-heptylammonium iodide obtained with magic angle spinning and BILEV decoupling. The top spectrum is measured in CDCl$_3$ solution at room temperature.

119

Table 19 ^{13}C chemical shift of $(C_7H_{15})_4NI$ as a function of temperature

T (K)	C-1	C-2	C-3	C-4	C-5	C-6	C-7
180[a]	64.37	25.21	29.29	32.83	36.18	26.22	16.61/16.26[c]
230[a]	64.31	25.05	29.33	32.62	36.09	25.84	16.41/16.01[c]
290[a]	64.27	25.14	29.33	32.28	35.81	25.14	16.02/15.82[c]
310[a, b]	64.19	25.17	29.35	32.27	35.84	25.17	15.93/15.74[c]
322[b]	64.18	25.04	29.19	32.20	35.68	25.04	15.85

Disordering transition: T_{d1} = 355.4 K, ΔS_{d1} = 26.1 $JK^{-1}mol^{-1}$

T (K)	C-1	C-2	C-3	C-4	C-5	C-6	C-7
364[b]	61.51	24.78	29.20	31.15	34.96	23.44	15.58
385[b]	61.22	24.31	28.58	30.42	33.97/34.29[a]	23.44	14.77

Disordering transition: T_{d2} = 391.0 K, ΔS_{d2} = 6.2 $JK^{-1}mol^{-1}$
Isotropization: T_i = 398.7 K, ΔS_i = 97.9 $JK^{-1}mol^{-1}$

T (K)	C-1	C-2	C-3	C-4	C-5	C-6	C-7
400[b]	61.04	23.84	27.36	29.32	32.24	23.02	14.56
Solut.[b]	59.38	22.48	26.36	28.80	31.54	22.48	14.06

a   Spectra of Fig. 32. Chemical shifts are in ppm relative to TMS.
b   Spectra of Fig. 33.
c   Two values are for the two peaks arising from the same carbon atom.

shift data are summarized. For longer alkyl chains the resonances for the carbon atoms in the middle of the chains overlap, i.e., their chemical shifts can only be indicated as a range. There are, however, always six carbon atoms (three at either chain end, i.e., C-x, C-y, C-z; and C-1, C-2, C-3) that can be uniquely resolved. Tables 22–25 contain lists of the chemical shifts for $(C_nH_{2n+1})_4NBr$, with n = 10, 12, and 18, and $[CH_3(CH_2)_{11}]_4NI$, respectively. The low temperature data of chemical shifts for the salts larger than $(C_4H_9)_4NX$ are listed in Table 26.

398 K BILEV

366 K CP

366 K BILEV

310 K CP

310 K CPMAS

| 120 | 100 | 80 | 60 | 40 | 20 | 0 | -20 | PPM |
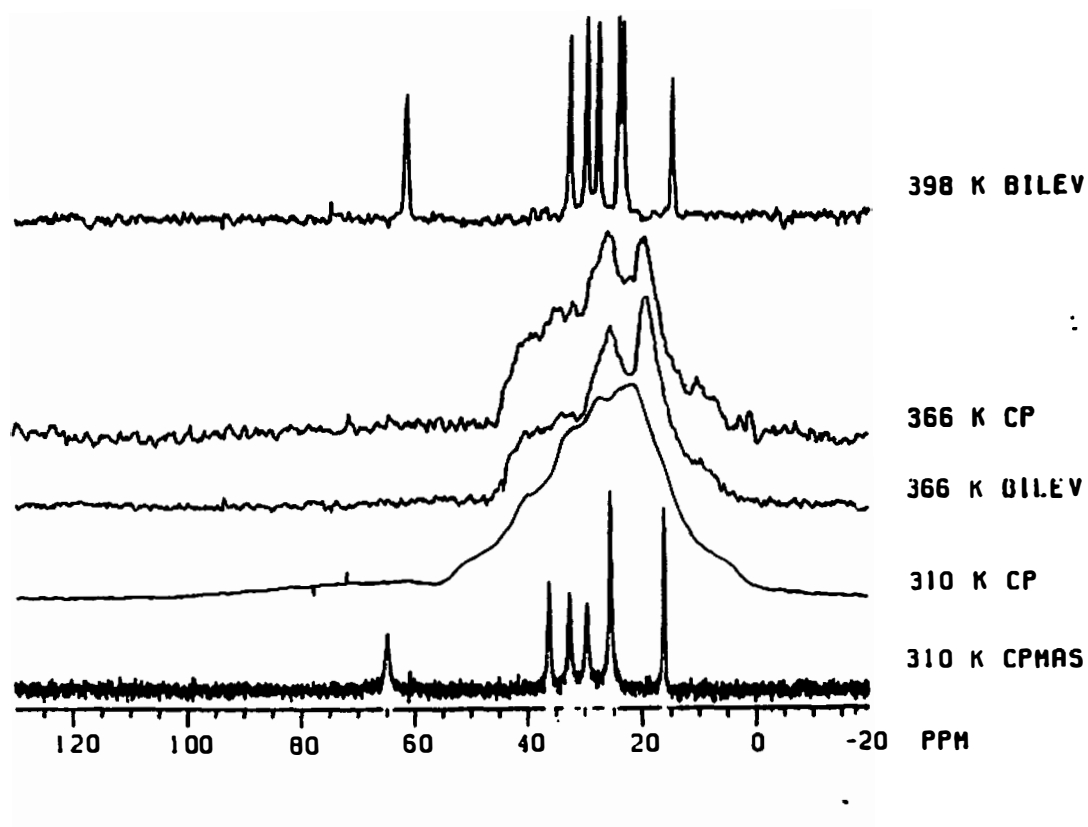
Figure 34 ^{13}C NMR powder patterns of tetra-n-heptylammonium iodide. The bottom is the CP-MAS spectrum at 310 K to show the isotropic resonance positions.

121

Table 20 ^{13}C T_1 of $(C_7H_{15})_4NI^a$

T (K)	C-1	C-2	C-3	C-4	C-5	C-6	C-7
310	33.5	(33.4)	33.3	22.3	14.4	(7.00)	2.31
322	28.0	(26.0)	24.0	15.4	10.4	(5.10)	3.10
	Disordering transition: T_{d1} = 355.4 K, ΔS_{d1} = 26.1 JK^{-1}mol^{-1}						
	Disordering transition: T_{d2} = 391.0 K, ΔS_{d2} = 6.2 JK^{-1}mol^{-1}						
395	0.25	0.35	0.37	0.79	1.06	2.15	4.29
	Isotropization: T_i = 398.7 K, ΔS_i = 97.9 JK^{-1}mol^{-1}						
405	0.09	0.16	0.39	0.73	1.44	2.14	4.55

a   Data in parentheses are for C-2 and C-6, since their resonances overlap, their T_1 were obtained by curve fitting to Eq. (34). T_1 values are in s.
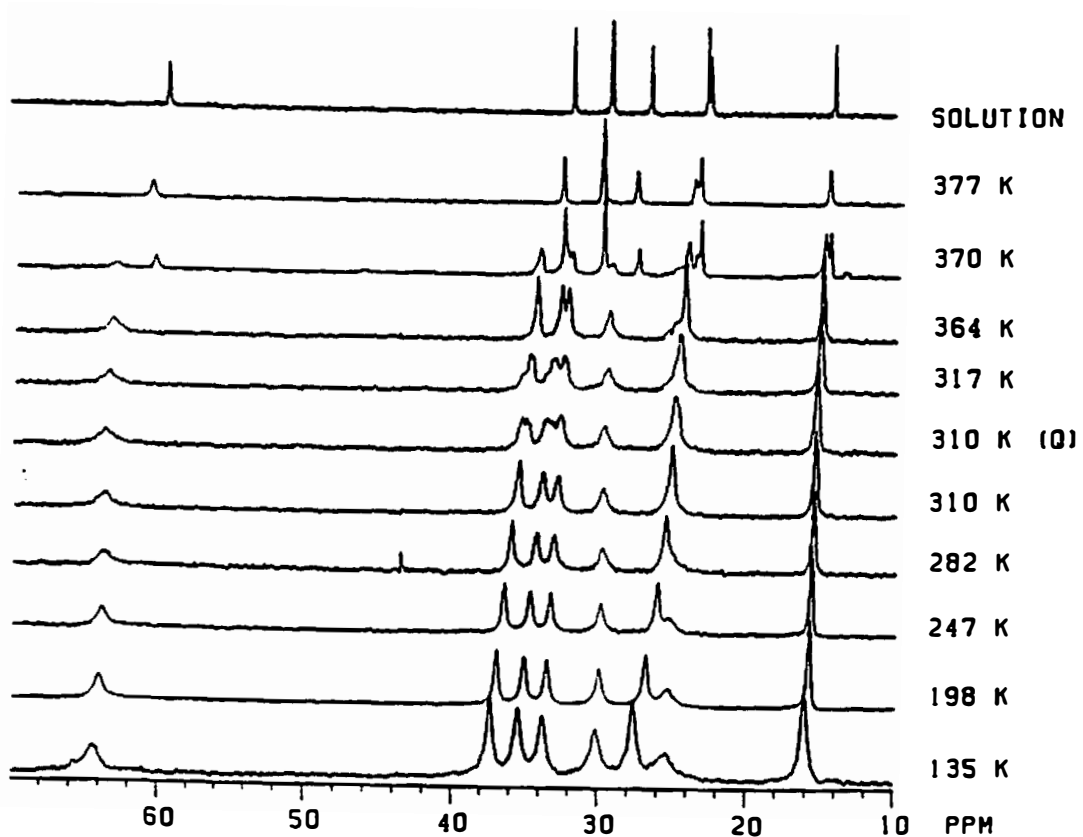
Figure 35 Variable-temperature NMR spectra of tetra-*n*-octylammonium bromide, $[CH_3(CH_2)_7]_4NBr$. The solution spectrum is shown at the top.

123
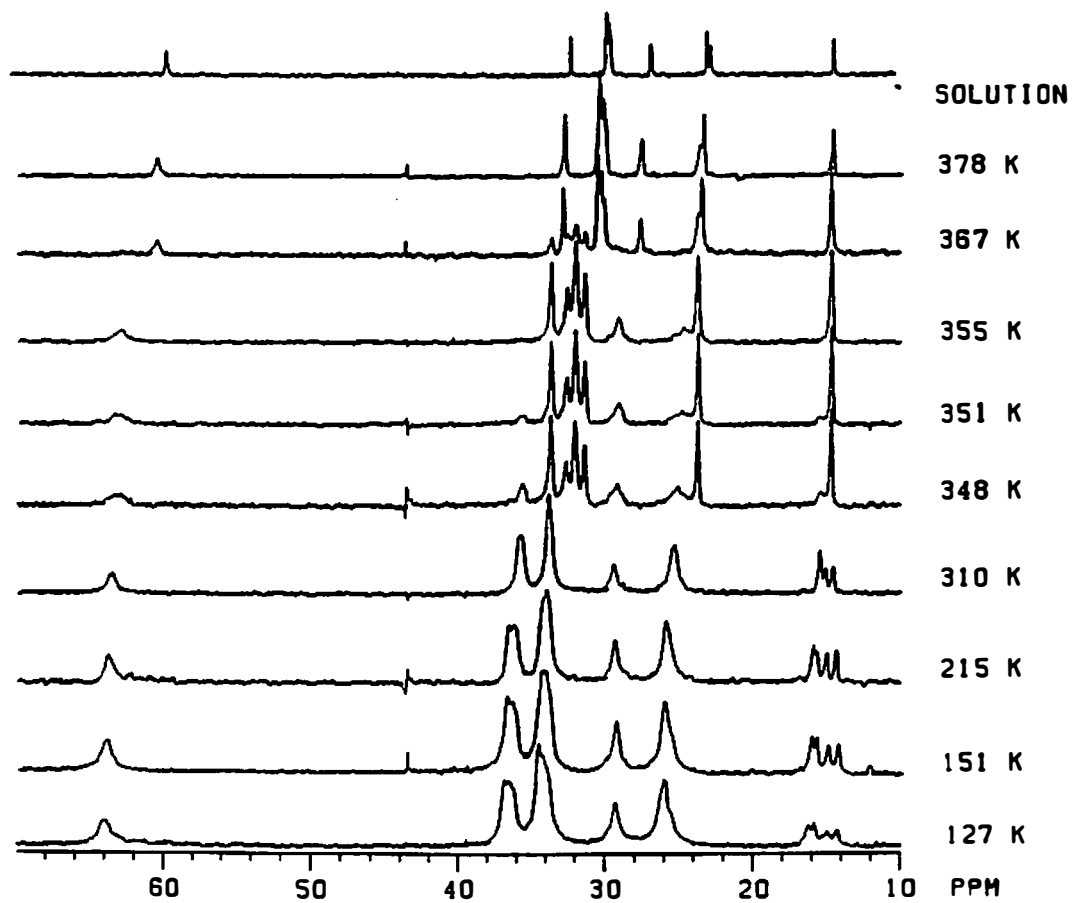
Figure 36   Variable-temperature NMR spectra of tetra-*n*-decylammonium bromide, [CH₃(CH₂)₉]₄NBr. The solution spectrum is shown at the top.

124
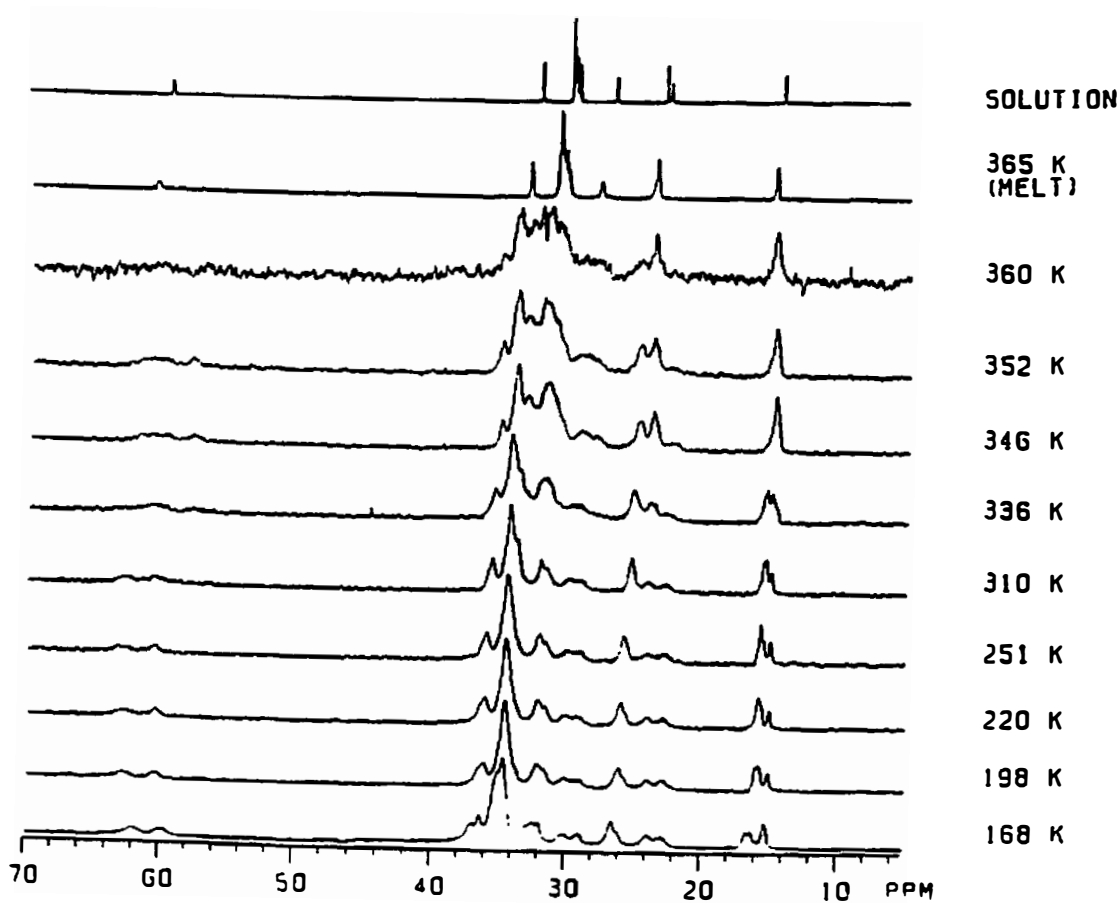
Figure 37   Variable-temperature NMR spectra of tetra-*n*-dodecylammonium bromide, [CH$_3$(CH$_2$)$_{11}$]$_4$NBr. The solution spectrum is shown at the top.
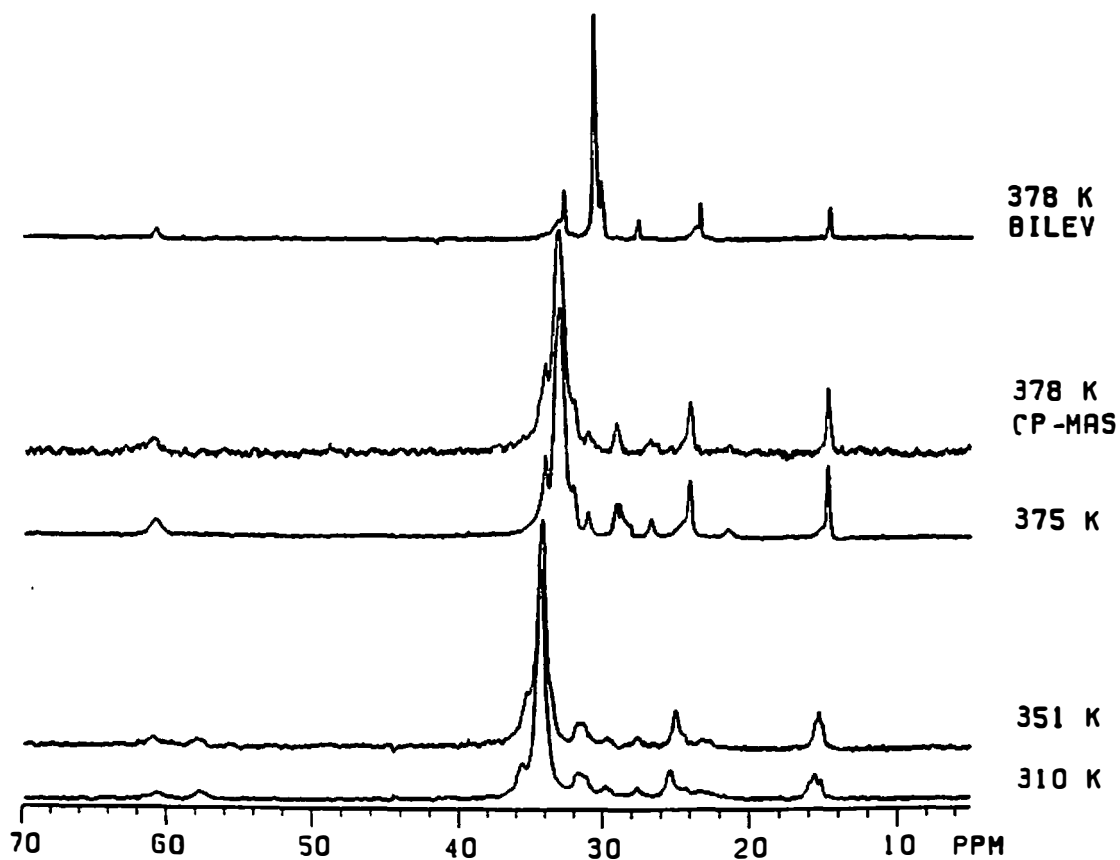
Figure 38   Variable-temperature NMR spectra of tetra-*n*-octadecylammonium bromide, [CH₃(CH₂)₁₇]₄NBr. At 378 K, two spectra were measured with BILEV and CP-MAS.
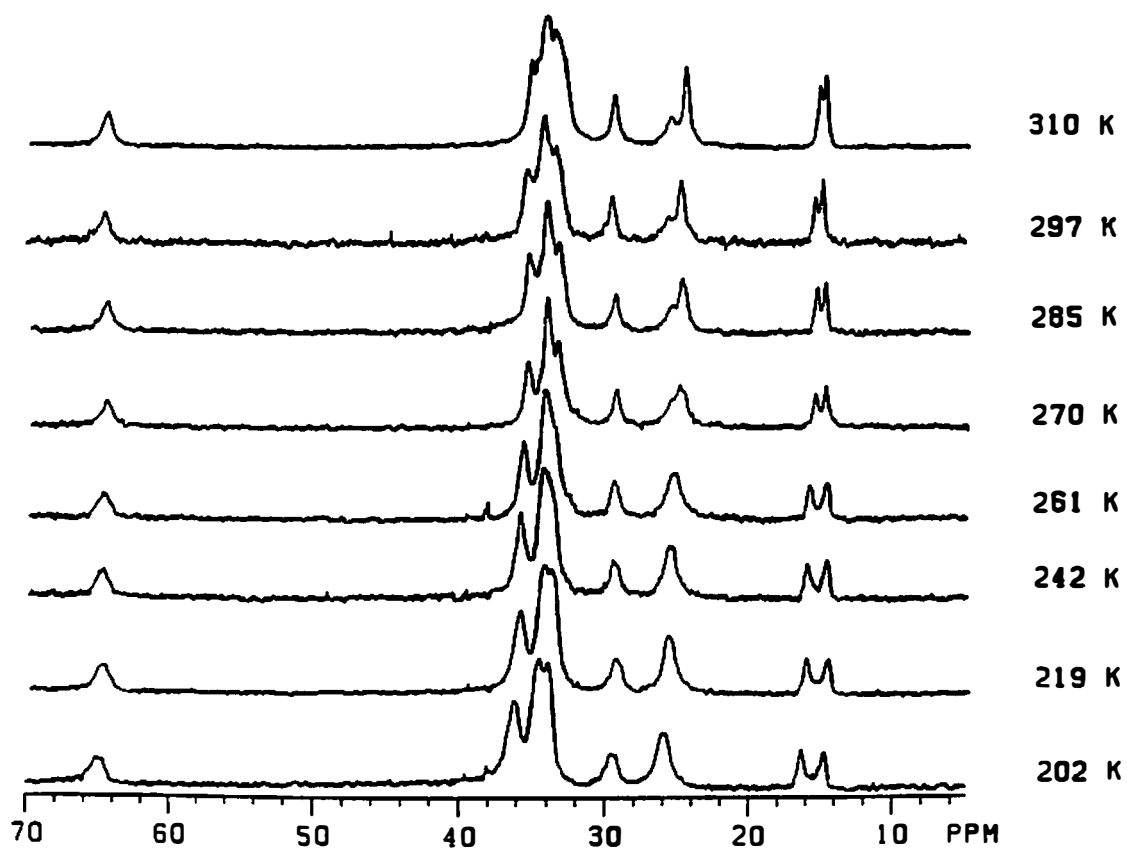
Figure 39   Variable-temperature NMR spectra of tetra-*n*-dodecylammonium iodide, [CH₃(CH₂)₁₁]₄NI.
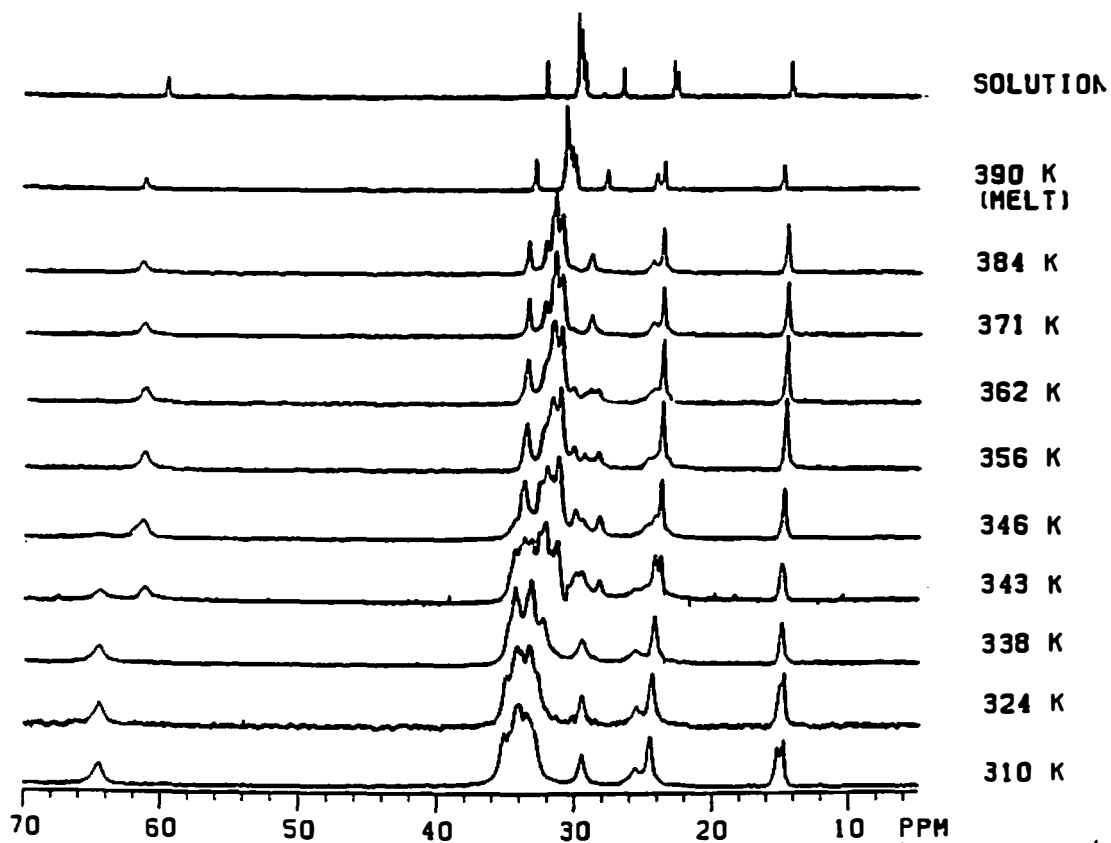
Figure 40   Same as Figure 39, but for the high-temperature range (from 310 to 390 K). The solution spectrum is shown at the top.

Table 21 ^{13}C chemical shifts (in ppm) of $(C_8H_{17})_4NBr$ as a function of temperature[a]

T (K)	C-1	C-2	C-3	C-4	C-5	C-6	C-7	C-8
135	64.4	25.3	30.0	33.7	35.3	37.3	27.6	16.0
150	64.2	25.5	30.0	33.6	35.3	37.2	27.3	15.9
185	64.0	25.3	29.9	33.5	35.1	36.9	26.9	15.8
198	64.0	25.3	29.9	33.4	35.0	36.8	26.7	15.7
218	63.9	25.3	29.8	33.3	34.9	36.7	26.4	15.7
231	63.8	25.3	29.8	33.3	34.8	36.6	26.3	15.6
247	63.8	25.3	29.8	33.2	34.6	36.4	26.0	15.6
282	63.7	25.2	29.7	33.0	34.2	35.9	25.4	15.5
298	63.7	25.2	29.7	32.8	33.9	35.6	25.2	15.4
306	63.7	25.1	29.7	32.8	33.8	35.4	25.1	15.4
310	63.6	25.0	29.6	32.7	33.8	35.4	25.0	15.4
317	63.4	24.7	29.4	32.4	33.0	34.7	24.6	15.1

Disordering Transition: T_d = 323 K, ΔS_d = 11 $JK^{-1}mol^{-1}$

T (K)	C-1	C-2	C-3	C-4	C-5	C-6	C-7	C-8
325	63.3	24.7	29.4	32.3	33.0	34.7	24.5	15.1
335	63.6	24.7	29.4	32.3	33.0	34.6	24.4	15.0
349	63.3	24.8	29.3	32.2	32.8	34.4	24.3	15.0
364	63.2	24.9	29.3	32.1	32.5	34.2	24.2	14.9
367	63.1	24.7	29.2	32.0	32.5	34.1	24.1	14.9

Isotropization: T_i = 374 K, ΔS_i = 118 $JK^{-1}mol^{-1}$

T (K)	C-1	C-2	C-3	C-4	C-5	C-6	C-7	C-8
377	60.6	23.7	27.6	29.9	29.9	32.6	23.3	14.6
Solut.	59.3	22.4	26.4	29.1	29.1	31.6	22.6	14.1

a.   Based on the spectra of Fig. 35 and additional spectra at T = 150, 185, 218, 231, 298, 306, 325, 335, 349, and 367 K. Data for the solution are taken from Cheng et al., 1992.

Table 22 ^{13}C chemical shifts (in ppm) of $(C_{10}H_{21})_4NBr$ as a function of temperature[a]

T (K)	C-1	C-2	C-3	C-4 to C-6	C-7, C-8	C-9	C-10
127	63.8	25.3	29.2	34.0 ±0.5[b]	36.6 ±0.2	25.9	14.3–16.2[c]
310	63.5	25.3	29.4	33.8 ±0.3	35.7 ±0.2	25.3	14.6–15.5

Disordering Transition: T_d = 349 K, ΔS_d = 161 $JK^{-1}mol^{-1}$

	C-1	C-2	C-3	C-4	C-5, C-6	C-7	C-8	C-9	C-10
351	63.3	24.7	29.0	32.5	31.9	31.3	33.6	23.6	14.7
355	62.8	24.6	29.0	32.4	31.9	31.2	33.5	23.6	14.6

Isotropization: T_i = 363 K, ΔS_i = 102 $JK^{-1}mol^{-1}$

	C-1	C-2	C-3	C-4 to C-7	C-8	C-9	C-10
378	60.4	23.5	27.5	30.3, 30.0, 29.9	32.7	23.3	14.6
Solut.	59.3	22.4	26.4	29.4, 29.2, 29.2	31.8	22.6	14.1

a.   Spectra of Fig. 36.
b.   Errors indicate an approximate linewidth of the broad peak.
c.   Showing the range of multiple lines.

Table 23 ^{13}C chemical shifts (in ppm) of $(C_{12}H_{25})_4NBr$ as a function of temperature[a]

T (K)	C-1	C-2	C-3	Middle	C-10	C-11	C-12
168	62.0	23.7	29.9 28.9	34.5	36.7	26.4	16.5
	59.9[b]	22.7		-31.8[c]	36.2	26.0	-15.2
220	62.5	23.8	29.9 29.3	34.4	35.9	25.8	15.7
	60.2	22.7		-31.5			-14.9

Transition: T_d = 225 K, ΔS_d = 6.4 $JK^{-1}mol^{-1}$

T (K)	C-1	C-2	C-3	Middle	C-10	C-11	C-12
310	62.5	23.9	29.7 29.1	34.2	35.4	25.1	15.4
	60.5	22.6		-31.4			-14.8
336	60.5	23.8	29.0	34.1	35.3	25.0	15.2
	57.8	22.6		-31.6			-14.9
346	60.5	23.7	29.0	33.8	35.0	24.6	14.7
	57.7			-31.4			

Overlapping Transitions: (347 K, 363 K) with ΔS (128, 207 $JK^{-1}mol^{-1}$)

T (K)	C-1	C-2	C-3	Middle	C-10	C-11	C-12
365 (melt)	60.4	23.4	27.3	30.5	32.7	23.4	14.6
				-30.0			
Solut.	59.3	22.4	26.5	29.7	31.9	22.7	14.1
				-29.2			

a.   Spectra of Fig. 37.
b.   Two values are given for the same carbon atom with two peaks.
c.   Two values separated by a "−" indicates the range, for details see Fig. 37.

131

Table 24 ^{13}C chemical shifts (in ppm) of $(C_{18}H_{37})_4NBr$ as a function of temperature[a]

T	C-1	C-2	C-3	middle	C-16	C-17	C-18
310	60.5, 57.7[b]	24.2, 23.1	27.5	34.2[c]	35.5	25.3	15.9–15.1
351	60.8, 57.9	24.2, 23.1	27.6	34.2	35.2	25.0	15.3
Overlapping Transitions: (375, 380 K), with ΔS = (227, 329 JK^{-1}mol^{-1})							
375	60.7	24.5, 21.4	26.6	32.9	33.9	24.0	14.7
378[d]	60.8	24.0	26.7	33.0	34.0	24.0	14.7
378[e]	60.6	23.6	27.5	30.5	32.7	23.3	14.6

a. Spectra of Fig. 38. b. Two values are given for the same carbon atom with two peaks. c. Indicates the strongest peak in Fig. 38. d. Measured with CP-MAS pulse sequence. e. Measured with BILEV pulse sequence.

Table 25 ^{13}C chemical shifts (in ppm) of $(C_{12}H_{25})_4NI$ as a function of temperature[a]

T (K)	C-1	C-2	C-3	Middle	C-10	C-11	C-12
202	64.9	26.0	29.5	34.4–33.8[b]	36.1	26.0	16.3, 14.7[c]
270	64.6	25.6	29.4	34.1–33.4	35.4	25.0	15.5, 14.8
Transition: T_d = 284 K, ΔS_d = 12.3 JK^{-1}mol^{-1}							
285	64.6	25.71	29.4	34.1–33.3	35.3	24.8	15.4, 14.8
310	64.4	25.6	29.4	34.1–33.5	35.1	24.5	15.2, 14.8
338	64.4	25.6	29.4	34.1–32.2	34.5	24.1	14.8
Overlapping Transitions: (343, 351, 365 K) with ΔS (12.6, 109, 15.1 JK^{-1}mol^{-1})							
346	61.2	24.6	29.2	32.0–29.9	33.6	23.6	14.7
362	61.1	24.2	28.8	31.5–30.1	33.4	23.5	14.5
384	61.2	24.2	28.7	32.0-30.8	33.2	23.4	14.4
Isotropization: T_i = 389 K, ΔS_i = 122 JK^{-1}mol^{-1}							
390	60.9	23.8	27.4	30.4–30.0	32.6	23.2	14.5
Solut.	59.4	22.5	26.4	29.7–29.2	32.0	22.7	14.1

a. Spectra of Figs. 39 and 40. b. Two values separated by a "–" indicates a range. c. Two values are given for the same carbon atom with two peaks.

Table 26 ^{13}C chemical shifts (in ppm) of some tetra-*n*-alkylammonium bromides and iodides at low temperatures and in $CDCl_3$ solutions

Salts[a]/ T (K)	C-1	C-2	C-3	C-4 to C-w[e]	C-x[e]	C-y[e]	C-z[e,f]
6Br/148[b]	63.6	25.1	29.8		34.3	25.9	16.1
6I/308[b]	64.4	25.0	29.5		33.7	25.5	15.6
7Br/308[b]	63.2	25.1	29.7	32.5	35.6	25.1	15.8
7I/180[b]	64.4	25.2	29.3	32.8	36.2	26.2	16.4
8Br/135	64.4	25.3	30.0	35.3, 33.7	37.3	27.6	16.0
10Br/127	63.8	25.3	29.2	33.5–36.5	36.8	25.9	15.2
12Br/168	62.0, 59.9	23.7, 22.7	29.9, 28.9	31.8–35.0	36.7, 36.2	26.4, 26.0	15.9
12I/202	64.9	26.0	29.5	34.4–33.8	36.1	26.0	15.5
18Br/310	60.5, 57.7	24.2, 23.1	27.5	29.6–34.2	35.5	25.3	15.5
Average	64.0 ±0.5[d]	25.3 ±0.3[d]	29.6 ±0.3[d]	29.6–36.5	35.8 ±1.2	26.0 ±0.7	15.8 ±0.4
Average[c] (Solut.)	59.3 ±0.1	22.4 ±0.1	26.3 ±0.1	28.8–29.8	31.7 ±0.3	22.6 ±0.1	14.0 ±0.1
Diff. Average[g]	4.6	2.9	3.2	0.8–6.7	4.1	3.4	1.8

a. The names of each salts are abbreviated as *m*X, in which *m* is the number of the carbon atoms in an *n*-alkyl chain, X stands for either Br or I.
b. Data for 6X and 7X are taken from Tables 16, 17, and 19.
c. Data for solution are taken from Cheng *et al.*, 1992.
d. The average values for C-1 and C-2 do not include 12Br and 18Br, for C-3 not 18Br.
e. C-*w*, C-*x*, C-*y*, and C-*z* stand for the last four carbon atoms in an alkyl chain, C-*z* is the methyl carbon.
f. The methyl carbons show multiple lines in many cases, but for convenience the values in this table were taken as the average. For details see respective tables.
g. The differential value is taken as the average (crystal) *minus* average (solution).

133

3.2.4 N,N'-bis(4-n-octyloxybenzal)-1,4-phenylenediamine (OOBPD)

The solution ^{13}C NMR spectrum and the variable temperature solid state ^{13}C CPMAS NMR spectra are shown in Fig. 41 for both the mesogenic group and the octyloxy chains. The chemical shift assignments are made based on the considerations given in the Discussion, and results are shown in Table 27 and 28 for mesogen and octyloxy carbons, respectively. The ^{13}C T_1 data at selected temperatures are presented in Table 29.

The numbering of carbon atoms in tables is shown below together with the formula of (OOBPD). The distinguishable carbon atoms in the central unit are numbered. The carbons in the paraffinic groups are numbered in sequence from C-8 (for OCH$_2$) to C-15 (for the CH$_3$).
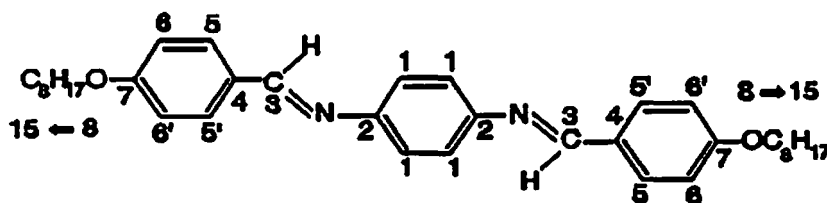
3.2.5 MBPE-9 and MBPE-5

The repeating units of the polymers MBPE-5 and MBPE-9 are shown below with the numbering of the distinguishable carbon atoms used in this paper. For MBPE-5 there are only five methylene groups in the flexible spacer, therefore, the

134
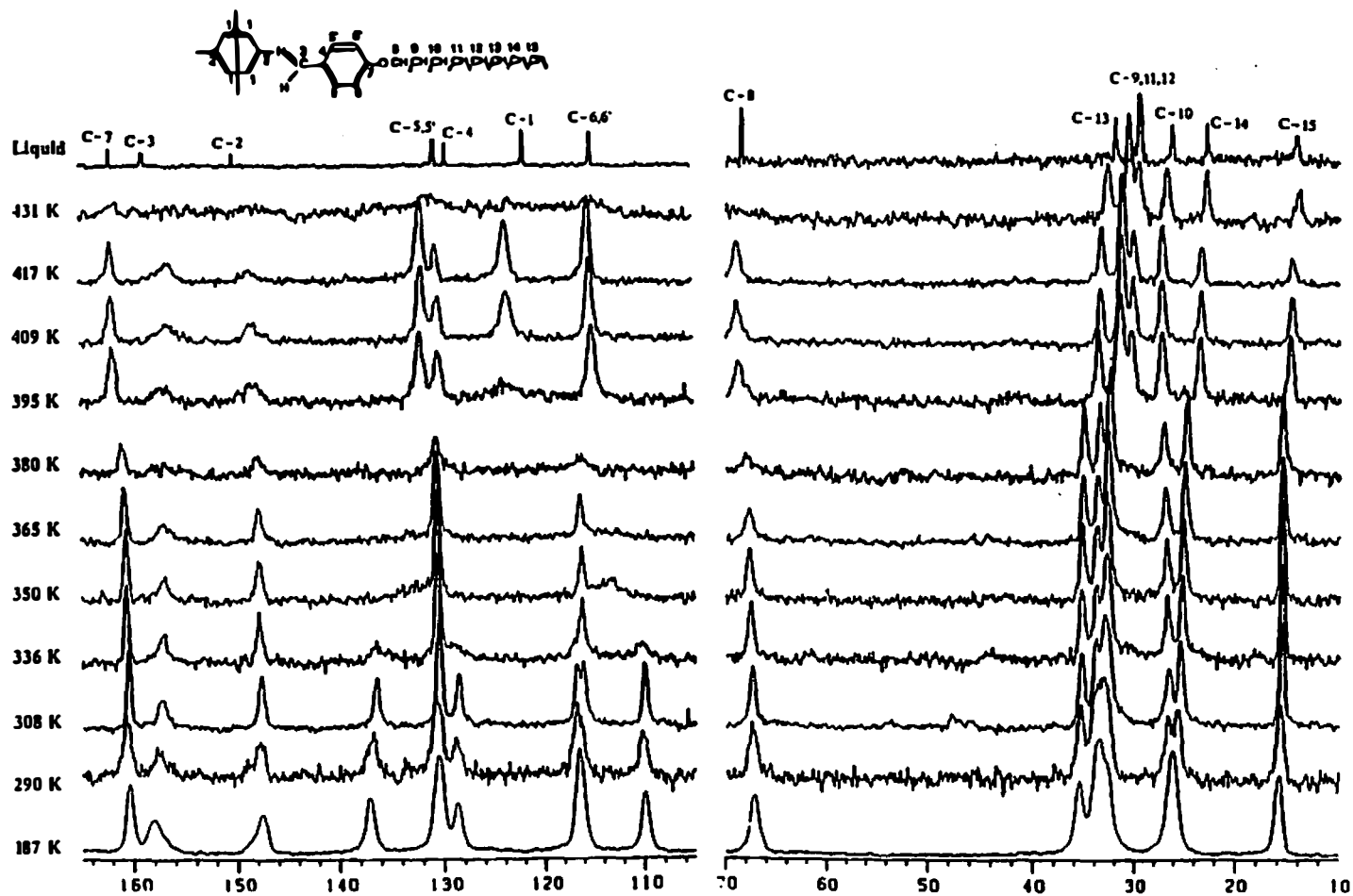
Figure 41   Variable temperature solid state ^{13}C CPMAS and solution ^{13}C NMR spectra of OOBPD. Left side: mesogenic group, Right side: octyloxy chain.

Talbe 27 ^{13}C NMR chemical shifts (ppm)[a] for the mesogenic group of OOBPD at selected temperatures and in solution[b]

	C-1[c]	C-2	C-3	C-4	C-5	C-5'	C-6	C-6'	C-7
Mesogenic Group									
187 K	116.4	147.5	158.0	130.4	128.7	137.0	109.9	116.4	160.4
290 K	116.7	147.8	157.5	130.7	128.9	136.7	110.2	116.7	160.7
308 K	116.1	147.7	157.3	130.4	128.6	136.5	110.0	116.7	160.4
336 K	116.1	147.8	156.9	130.5	129.1	136.4	110.3	116.1	160.6
350 K	116.2	147.7	156.9	130.5	NO[d]	NO	113.1	NO	160.6
365 K	116.2	147.8	156.9	130.5	NO	NO	NO	NO	160.7
380 K	116.0	147.9	156.8	130.4	NO	NO	NO	NO	160.9
↕	Transitions from phase K3 to K2 (385.2 K), to K1 (388.2 K)[e]								
395 K	124.1	148.5	156.5	130.3	131.9	131.9	114.9	114.9	161.8
409 K	123.5	148.4	156.4	130.2	131.8	131.8	115.1	115.1	161.8
↕	Transition to Phase H' (415.3 K)								
417 K	123.6	148.5	156.3	130.3	131.8	131.8	115.2	115.2	161.8
↕	Transitions to Phase G' (422.2 K), to I (426.9 K)								
431 K	NO	NO	NO	NO	NO	NO	NO	NO	NO
↕	Transitions to Phase C (436.6 K), to N (475.4 K), to Melt (505.4 K)								
Solut.	121.7	150.1	158.7	129.4	130.5	130.5	114.8	114.8	161.9

a. Spectra are shown in Fig. 41 and the chemical shift values are relative to tetramethylsilane (TMS).
b. In d-CHCl$_3$ solution at room temperature.
c. Numbering and assignment of the carbon atoms is given in the text.
d. "NO" stands for no signal is observable.
e. The transition parameters are taken from Wiedemann *et al.*, 1986.

Talbe 28[*] ^{13}C NMR chemical shifts (ppm)[a] for the alkoxy chains in OOBPD at selected temperatures and in solution[b]

	C-8	C-9	C-10	C-11	C-12	C-13	C-14	C-15
	Octyloxy Chain							
187 K	67.11	35.45	26.06	33.49	32.82	33.85	26.06	15.80
290 K	67.45	35.31	26.58	33.40	33.40	33.85	25.55	15.77
308 K	67.39	35.30	26.62	33.02	33.02	33.84	25.41	15.77
336 K	67.50	35.31	26.74	32.83	32.83	33.85	25.22	15.64
350 K	67.65	35.25	26.76	32.83	32.83	33.76	25.11	15.64
365 K	67.76	35.20	26.95	32.71	32.71	33.80	24.98	15.62
380 K	68.00	35.07	27.04	32.45	32.45	33.51	24.71	15.57
↕	Transitions from phase K3 to K2 (385.2 K), to K1 (388.2 K)							
395 K	68.86	31.44	27.29	30.34	31.44	33.72	23.46	14.87
409 K	68.94	31.25	27.21	30.16	31.25	33.45	23.35	14.70
↕	Transition to Phase H' (415.3 K)							
417 K	68.89	31.38	27.12	30.34	31.13	33.31	23.27	14.65
↕	Transitions to Phase G' (422.2 K), to I (426.9 K)							
431 K	NO	30.51	26.69	29.49	30.51	32.66	22.72	13.95
↕	Transitions to Phase C (436.6 K), to N (475.4 K), to Melt (505.4 K)							
Solut.	68.35	29.29	26.10	29.29	29.29	31.84	22.67	14.00

[*]   Footnotes a, b, c, d, and e are the same for Table 27.

137

Table 29 ^{13}C NMR spin-lattice relaxation times (s)[a] for OOBPD at selected temperatures

Mesogenic Group								
	C-1[b]	C-2	C-3	C-4	C-5	C-5'	C-6	C-6'	C-7
308 K	>100[c]	>100	>100	>100	>100	>100	>100	>100	>100
350 K	>100	>100	>100	>100	>100	>100	>100	>100	>100
380 K	>100	>100	7.81	>100	NO[d]	NO	NO	NO	40.00
↕	Transitions from phase k3 to K2 (385.2 K), to K1 (388.2 K)[e]								
395 K	5.19	15.5	1.25	8.20	0.96	0.96	0.81	0.81	11.4
↕	Transition to Phase H' (415.3 K)								
417 K	0.72	16.0	0.70	5.14	0.25	0.25	0.24	0.24	8.26
↕	Transitions to Phase G' (422.2 K), to I (426.9 K), to Phase C (436.6 K), to N (475.4 K), to Melt (505.4 K)								

Octyloxy Chain							
	C-8	C-9	C-10	C-11	C-12	C-13	C-14	C-15
308 K	>100	>100	>100	>100	>100	>100	>100	Not Ava.
350 K	>100	17.0	12.6	15.5	15.5	19.5	12.6	4.70
380 K	37.9	12.9	6.58	13.2	13.2	9.76	12.2	8.52
↕	Transitions from phase K3 to K2 (385.2 K), to K1 (388.2 K)							
395 K	2.59	1.77	1.35	2.04	1.77	3.72	4.09	7.27
↕	Transition to Phase H' (415.3 K)							
417 K	1.29	1.58	1.24	1.93	1.58	3.16	4.10	8.06
↕	Transitions to Phase G' (422.2 K), to I (426.9 K), to Phase C (436.6 K), to N (475.4 K), to Melt (505.4 K)							

a. Measured with Inversion Recovery method.
b. Numbering and assignment of the carbon atoms is given in the text.
c. T_1 is longer than 100 s.
d. "NO" stands for no signal is observable, therefore, the T_1's are not available.
e. The transition parameters are taken from Wiedemann et al., 1986.

central carbon is numbered C-15, and the numbers of C-16 through C-19 are not used.
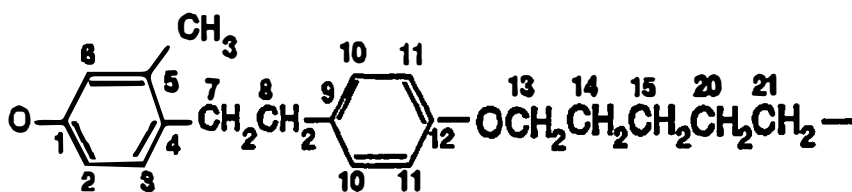
MBPE-5
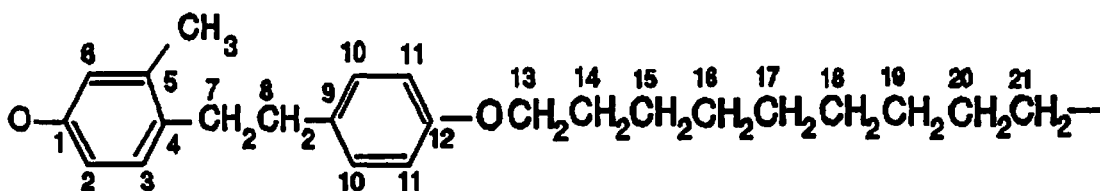
MBPE-9

The proton-decoupled ^{13}C spectra of the melts at 373 K for MBPE-9 and 410 K for MBPE-5 obtained with BILEV, are shown in Figs. 42 and 43. The chemical shifts, δ, measured on the spectra of Figs. 42 and 43 are in listed Tables 30 and 31, for MBPE-9 and MBPE-5, respectively.

For each polymer, the dipolar dephasing experiments, $(CP - \tau - FID - 5 \text{ s})_n$ as described in Sect. 2.3.4 and 2.3.6, were carried out at two temperatures: (1) between the two transitions and (2) below the second transition on cooling. The spectra are shown in Figs. 44 − 46.
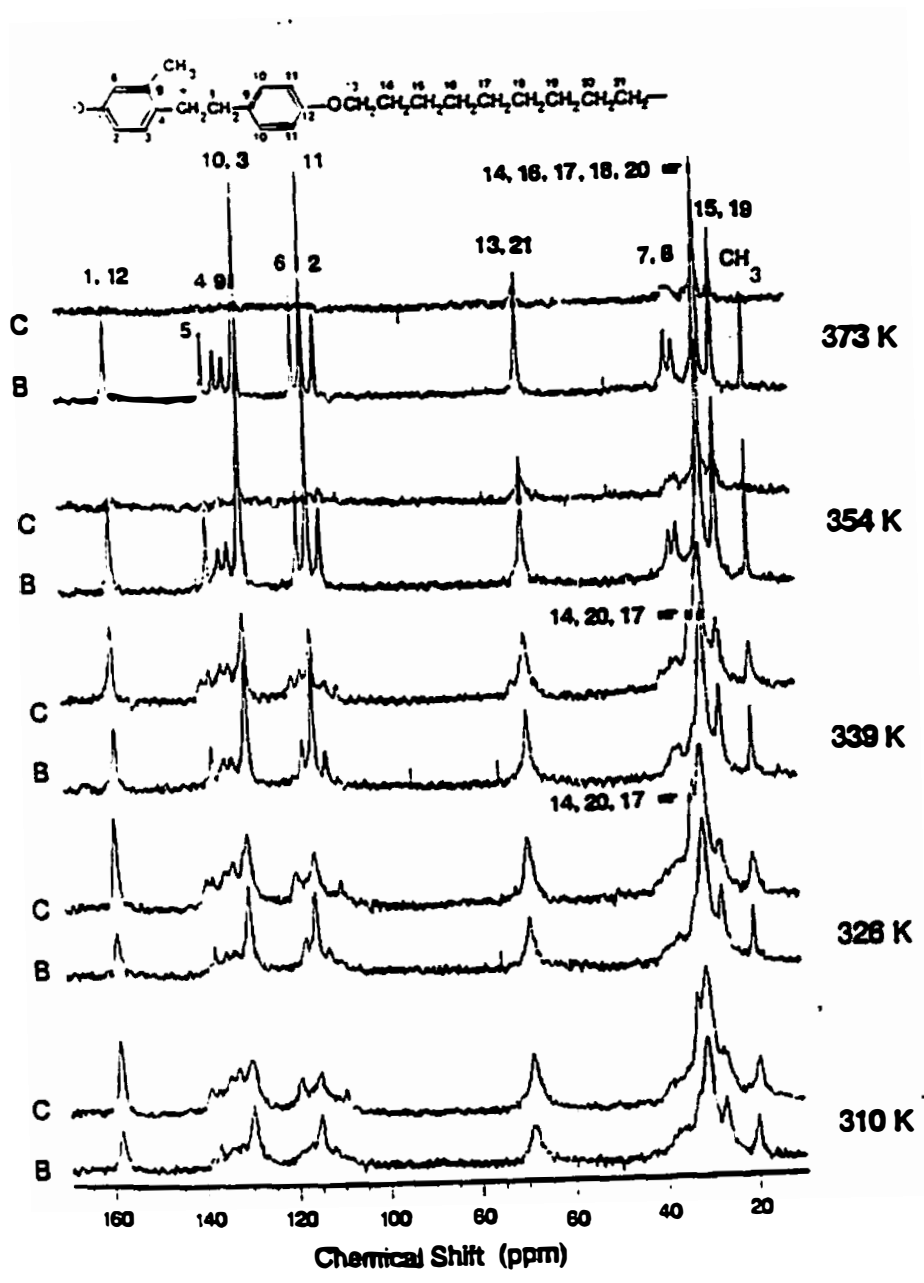
Figure 42   Variable temperature ^{13}C NMR spectra of MBPE-9. The labels B and C stand for BILEV and CP-MAS, respectively.
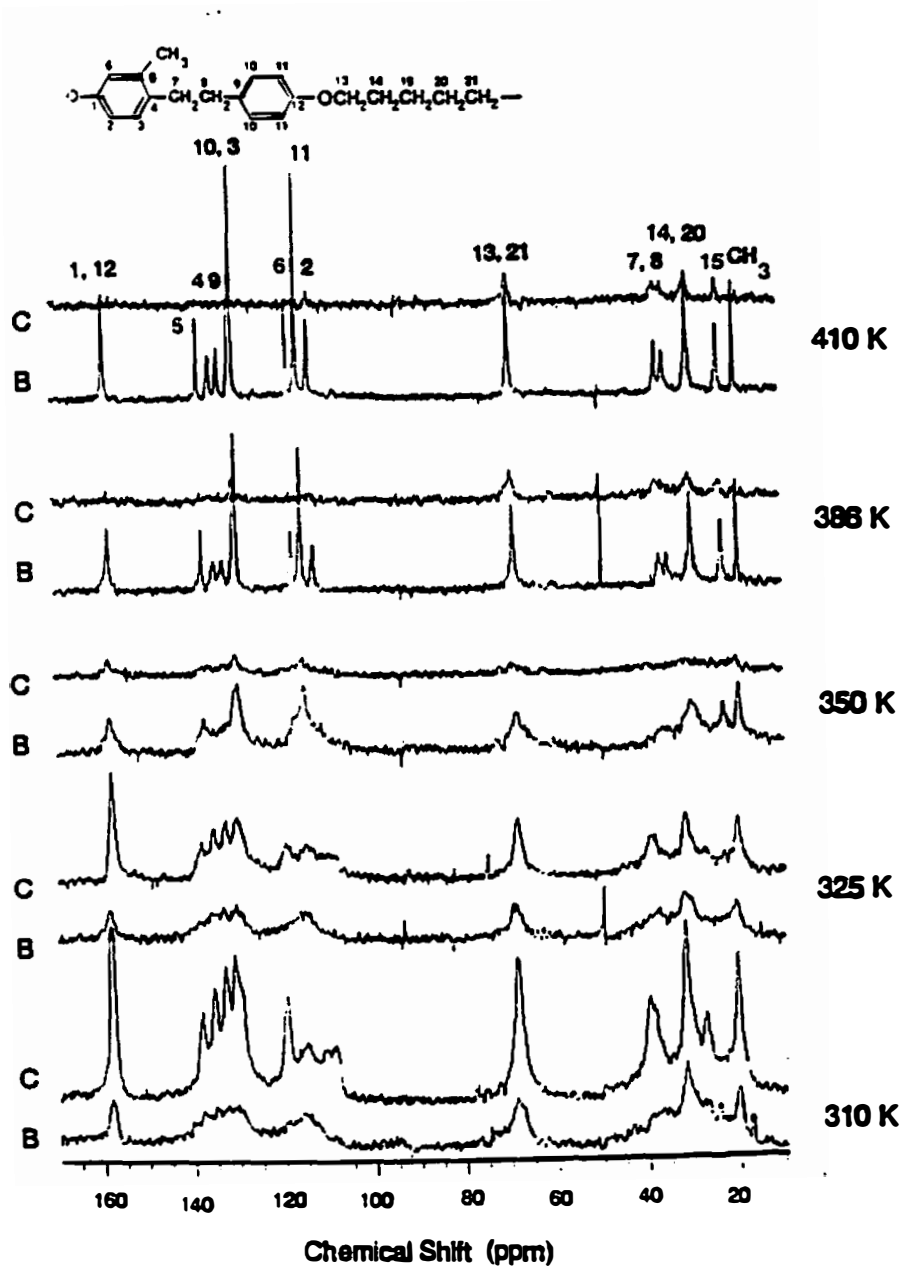
Figure 43   Variable temperature ^{13}C NMR spectra of MBPE-5. The labels B and
C stand for BILEV and CP-MAS, respectively.

141

Table 30 ^{13}C NMR chemical shifts (ppm) of MBPE-9[a]

	310 K	326 K	339 K	354 K	373 K
C1,C12	158.9/158.1	158.5/158.1	158.4/158.1	NA[b]/158.1	NA/158.2
C2	109.9/112.1	109.4/112.2	109.5/111.3	NA/112.5	NA/112.7
C3,C10	130.5/129.5	129.6/129.5	129.5/129.6	129.6/129.5	NA/129.6
C4	135.0/134.4	134.4/124.6	134.5/134.4	NA/134.4	NA/134.5
C5	139.6/137.0	138.9/137.1	138.8/137.1	NA/137.1	NA/137.1
C6	119.6/NA	119.4/117.1	119.4/117.4	NA/117.4	NA/117.5
C7	38.8–35.6[c]	39.1–35.4	39.4–35.9	NA/36.89	NA/36.82
C8	38.8–35.6	39.1–35.4	39.4–35.9	NA/35.31	NA/35.25
C9	133.2/132.4	132.8/132.8	132.9/132.7	NA/132.5	NA/132.6
C11	115.4/115.0	115.0/115.1	115.2/115.2	NA/115.2	NA/115.4
C13,C21	69.05/68.25	68.81/68.50	68.64/68.56	68.55/68.57	68.63/68.66
C14,C17,C20	33.77/32.81	33.08/30.97	33.27/30.60	30.14/30.16	30.16/30.06
C15,19	27.54/27.05	27.26/27.06	27.02/26.95	26.75/26.75	26.79/26.72
C16,C18	31.65/31.06	31.49/30.97	30.88/30.60	30.14/30.16	30.16/30.06
CH$_3$	20.00/20.03	20.08/20.14	20.00/20.05	19.95/19.92	NA/19.83

a   The first value is measured with the CP-MAS pulse sequence: (CP – FID – 5 s)$_{200}$, and the second value is from BILEV: (55° – FID –3 s)$_{200}$.

b   "NA" stands for not available, because of either no signal is detected or the signal is too broad.

c   Because of broadening, two values separated by a – sign indicates the approximate range.

Table 31[*] ^{13}C NMR chemical shifts (ppm) of MBPE-5[*]

	310 K	325 K	350 K	386 K	410 K
C1, C12	158.1/158.2	157.9/158.4	158.1/158.3	NA/158.0	NA/158.1
C2	111.0/108.7	110.2/NA	NA/NA	NA/112.6	112.7/112.8
C3, C10	130.7/130.7	130.2/130.2	129.8/129.6	129.6/129.7	129.6/129.6
C4	135.5/NA	135.4/135.8	NA/NA	NA/134.5	NA/134.6
C5	138.1/138.1	138.1/138.6	NA/137.1	NA/137.2	NA/137.2
C6	119.4/NA	119.6/NA	NA/117.2	NA/117.4	NA/117.6
C7	40.2–38.2	40.1–38.1	NA/36.4	37.0/36.74	36.7/36.63
C8	40.2–38.2	40.1–38.1	NA/36.6	37.0/35.03	35.1/34.98
C9	132.9/NA	132.7/133.1	NA/NA	NA/132.6	NA/132.7
C11	115.0/115.0	115.0/115.1	114.9/115.0	115.1/115.3	115.4/115.5
C13,C21	68.29/68.19	68.08/68.35	68.38/68.23	68.45/68.42	68.59/68.58
C14, C20	31.70/31.70	31.81/31.89	NA/30.06	29.84/29.78	29.82/29.78
C15	27.30/27.30	27.30/NA	23.20/23.13	23.38/23.27	23.40/23.31
CH$_3$	20.35/20.36	20.26/20.44	19.96/19.75	19.83/19.71	19.72/19.69

*   Table notes are the same for Table 30.

143
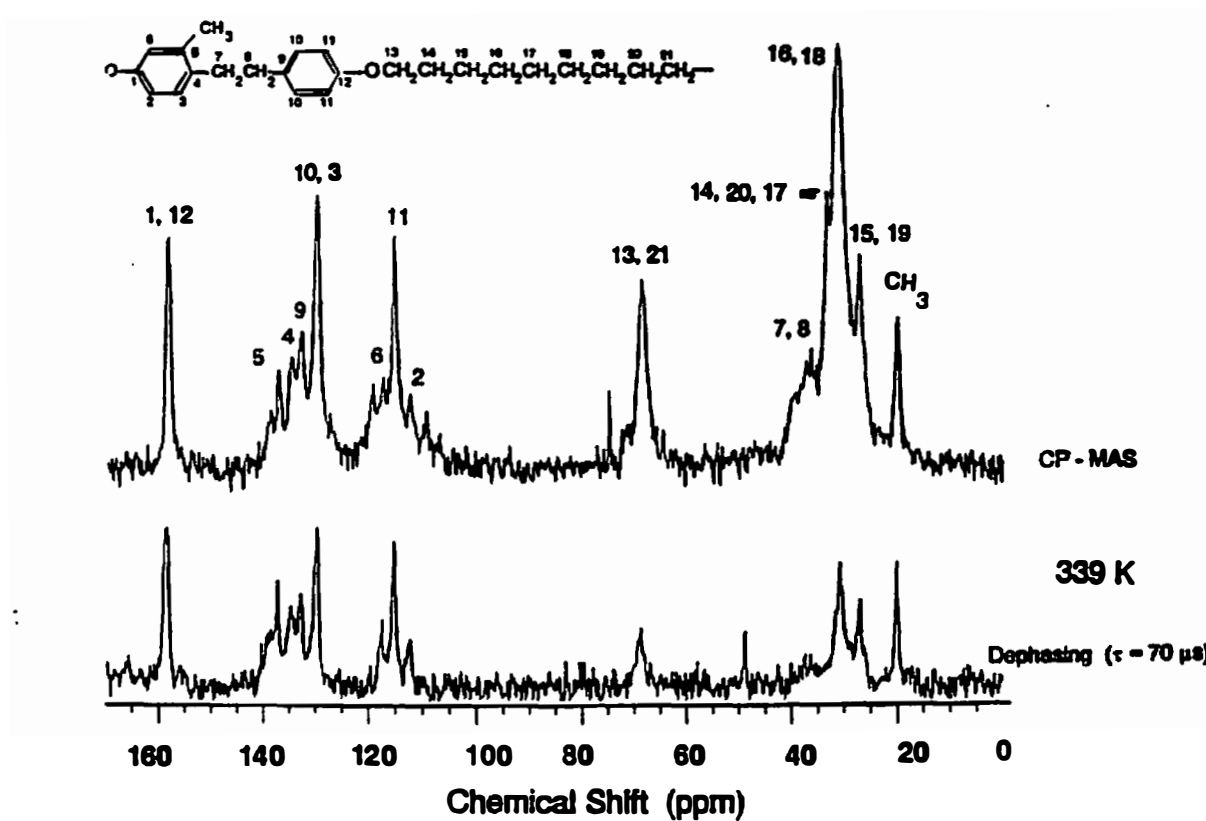
Figure 44   The ^{13}C NMR spectra of MBPE-9 at 339 K. Top: measured with CP-MAS; Bottom: measured with dipolar dephasing, with a delay of 70 μs.

144
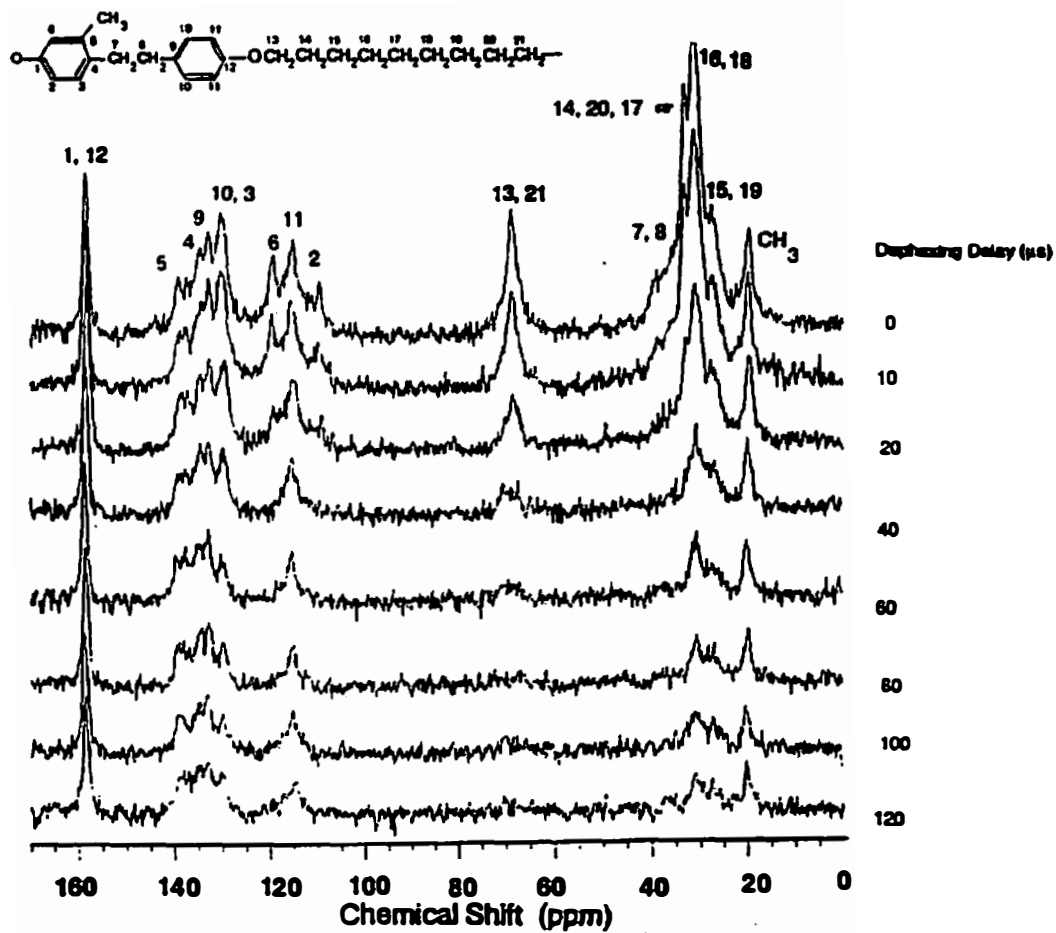
Figure 45   Variable dipolar-dephasing delay ^{13}C spectra of MBPE-9 at 310 K.
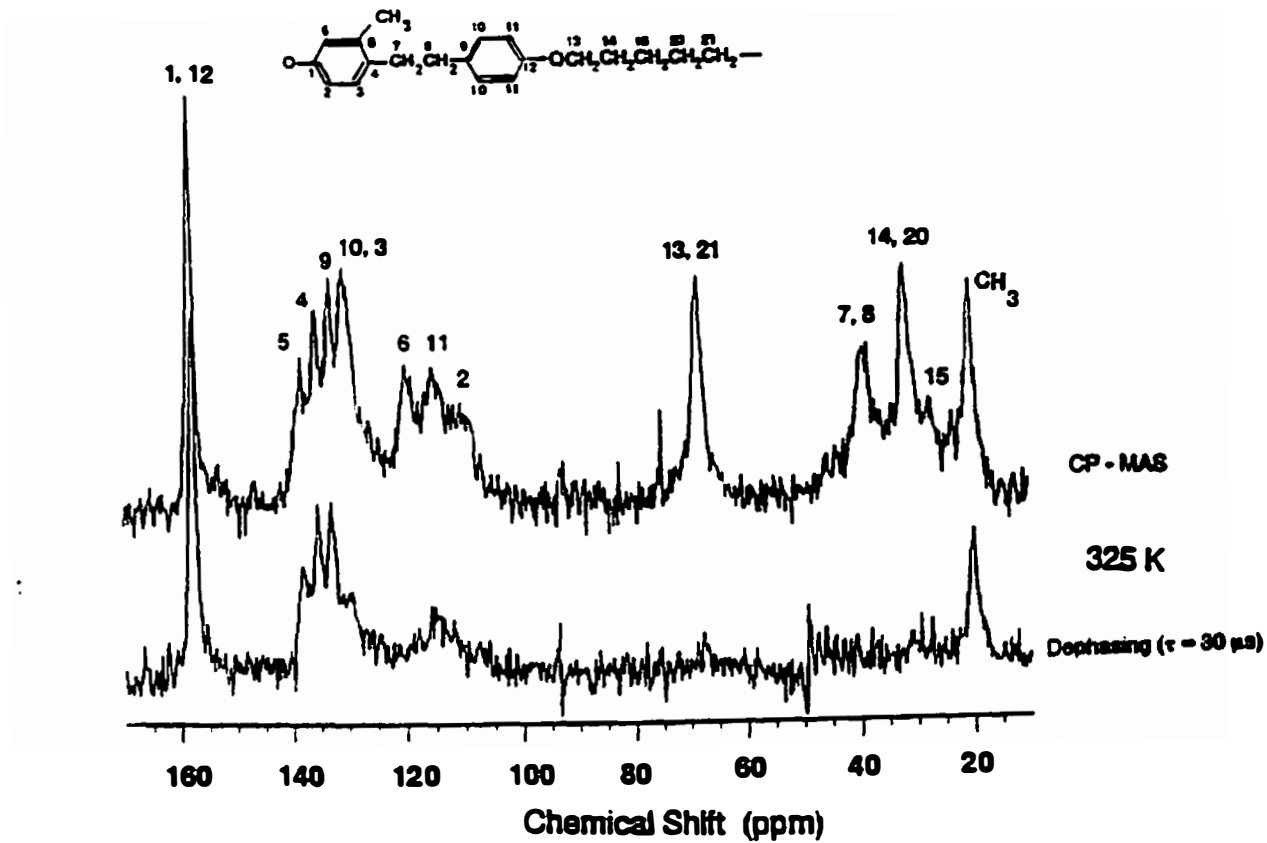
Figure 46   The ^{13}C NMR spectra of MBPE-5 at 325 K. Top: measured with CP-MAS; Bottom: measured with dipolar dephasing, with a delay of 30 μs.

146

CHAPTER 4

DISCUSSIONS

4.1   Disorder and Motion in the Low Homologs of Tetra-*n*-alkyl-ammonium Salts

4.1.1   Tetramethylammonium Bromide and Iodide

Tetramethylammonium bromide and iodide have the *a priori* possibilities of rotation of the methyl group, orientational motion of the cation as a whole about one or more axes, and diffusion through the crystal. The former two are considered to be more important in the solid state. The orientational motion of the whole cation in both salts was detected at room temperature by the proton linewidth (second moment) and proton spin-lattice relaxation (wide-line NMR) (Parsonage and Staveley, 1978). The orientational motion of the cation was considered to be random, therefore, the crystal must be classified as a plastic crystal.

The experimental evidence for the orientational motion of the cation generated in this thesis work is given by the temperature dependence of three ^{13}C CP-MAS NMR parameters for tetramethylammonium iodide, namely, the chemical shift (δ), line width ($\Delta v_{1/2}$), and relative signal intensity (I). The gradual increase of 22 Hz in chemical shift from 308 to 424 K is very small compared to the linewidth of 54.97 Hz at 308 K, indicating that the packing remains the same. The other two parameters, $\Delta v_{1/2}$ and I, decrease continuously and considerably with increasing the

temperature. These latter two parameters determine the overall NMR signal intensity, i.e. the area under the peak. The decrease of the integrated signal in a ^{13}C CP-MAS NMR spectrum was shown to be caused by the increased molecular motion as the temperature is increased (Jelinski and Melchior, 1987). The motion that influences the NMR signal intensity between 300 and 400 K is mainly the orientational motion of the cation. The methyl rotation has a much lower activation energy and its motional frequency shows little change as a function of temperature in this high temperature region, i.e., the methyl rotation does not contribute to the change of the NMR spin-relaxation related parameters.

The correlation times and activation energies of the orientational motion of the cation in tetramethylammonium bromide and iodide can be obtained from the temperature dependence of the T_1 data listed in Table 6. The correlation times τ_C of $(CH_3)_4NBr$, calculated according to Eq. (17), decreases from 3.0 ns to 0.74 ns as the temperature is increased from 311 K to 397 K. Within the same temperature range, τ_C of $(CH_3)_4NI$ decreases from 0.85 ns to 0.23 ns. The shorter τ_C's indicate a faster orientational motion in the iodide than in the bromide. The relationship between τ_C and temperature can be fitted into a simple Arrhenius equation of Eq. (24). The fitted correlation time at infinite temperature (the pre-exponential constant) τ_0, and the activation energy E_a are: 5.0 ps and 16.5 kJ/mol for the bromide, and 2.2 ps and 15.4 kJ/mol for the iodide. The experimental data given in Table 6 are evenly scattered around the fitted line for both salts. Within the experimental error (8%), the activation energies are the same for both cases. The

activation energies obtained in this work are lower than those given for the same compounds in the literature, 35 and 33.5 kJ/mol for the bromide and iodide, respectively (Parsonage and Steveley, 1978). They are, however, more in line with the activation energies for rotation of a series of tetramethyl compounds with central atoms of varying size: $(CH_3)_4C$, 4.2 kJ/mol; $(CH_3)_4Si$, 31 kJ/mol; $(CH_3)_4Ge$, 46−64 kJ/mol (Smith, 1964).

Since no phase transitions are observed for these two salts from about 5 to 500 K (Chang and Westrum, Jr., 1962; Coulter *et al.*, 1940), the orientational disorder must start gradually due to a non-coperative orientational motion, or the materials form a PC glass at sufficiently low temperatures.

4.1.2 Tetraethylammonium Bromide and Iodide

The transition entropies for both of the ethyl compounds, listed in Table 2, are well within the range for orientational disordering: $20−50$ $JK^{-1}mol^{-1}$, as shown in Sect. 2.2.3, indicating that the cations should be orientationally disordered above the phase transition temperatures.

Important information on the orientational order of the iodide salt at ambient temperature is given by the X-ray data on the crystal structure. Wait and Powell (Wait and Powell, 1958) could show that the cation in projection forms a Nordic cross (swastika) with the bond angle $N−CH_2−CH_3$ approximately $12°$ larger than the normal tetrahedral angle. This large distortion in the valence angle in the solid state results in a large decrease in chemical shifts of the methyl carbons of both

compounds on dissolution in a solvent, such as D_2O (in the solid state at 308 K the chemical shifts of the methyl carbon are 10.15 and 10.00 ppm for the bromide and iodide, respectively, while in D_2O solution they decrease to 7.10 and 7.17, respectively).

Other experimental evidence that the cation is orientationally ordered below the phase transition comes from the analysis of the NMR spectra. The asymmetric doublet pattern from the methylene carbon in $(CH_3CH_2)_4NBr$ below 348 K, shown in Fig. 13, is due to the ^{14}N quadrupole effect on the $^{13}C-^{14}N$ dipolar coupling. Such phenomena are usually observable for ^{13}C atoms bonded to such ^{14}N atoms, e.g., $-NO_2$, $-NH_2$, $>NH$, $>N-$, $-NH_3^+$, and $-CN$ (Natio et al., 1981 and 1982; Hexem et al., 1981). The asymmetric doublet pattern indicates thus that the inner part of the cation cannot have tetrahedral symmetry. By increasing the temperature, the symmetry increases and as the electric field gradient at the ^{14}N nucleus vanishes, the splitting pattern disappears. The initial absence of such asymmetric doublet pattern in Fig. 14 for the iodide indicates that the local symmetry around the nitrogen atom in the cation of iodide has the high symmetry already at room temperature.

The CSA powder pattern of the methylene carbon in $(CH_3CH_2)_4NI$, shown in the middle plot in Fig. 14, features a broad, asymmetrical pattern, indicating the methylene carbon is rigid, i.e., neither a conformational motion about the $N-C$ bonds, nor orientational motion of the cation as a whole could exist at room temperature. The methyl group, on the other hand, shows a much narrower and more symmetric peak due to the fast rotation about its C_3 axis. The CSA pattern for

the methyl compound, $(CH_3)_4NI$, (the top spectrum in Fig. 14) shows narrower linewith caused by the methyl rotation and additional orientational motion.

As discussed at the end of Sect. 2.3.4, the time scale of the orientational motion for a plastic crystal at T_d, the crystal-plastic crystal disordering transition temperature, is typically 5×10^{-9} s and decreases to about 2×10^{-12} s at the melting temperature (Boden, 1979). The correlation times for the methylene carbons in tetraethylammonium bromide and iodide, calculated from the T_1 data listed in Table 7 according to Eq. (17), indicate a motion of correlation time in the range of μs at ambient temperatures, i.e., 150–170 K below the solid–mesophase transition. At about 405 K, a temperature close to the transition, the correlation time is still much longer than is typical for plastic crystals. Therefore, the motion below T_d detected in this research is not orientational motion. A slow libration within or of the cation may be possible, but the libration must be limited to an angle that is sufficiently small so that no other orientational or conformational isomer is reached, since these would be forbidden by the X-ray and entropy data of the transition.

More details about the motion about the $N-C$ bonds can be gained from the T_1 of the methyl ^{13}C. The overall motion of the CH_3 is a composite motion of the CH_3 rotation about its C_3 axis and the motion about the $N-C$ bond. The CH_3 rotation is known to be sufficiently fast (0.1 – 10 ps) (Anderson and Slichter, 1965; Allen and Cowking, 1967; Lyerla, Jr. et al., 1974; Takeda et al., 1988), so that the influence on T_1 due to the decrease of its correlation time within the experimental temperature range is negligible. The increase in T_1 of the methyl carbon with

151

increasing temperature must thus be caused mainly by motion about the N−C bond. Therefore, the motion about the N−C bond can be studied *via* the relaxation times of the methyl carbons.

The molecular motion in the segment of N−CH$_2$−CH$_3$ is assumed to follow Howarth's 3τ librational model illustrated in Fig. 7 of Sect. 2.3.4. The isotropic orientational motion of the cation as a whole is expected to be possible only at temperatures higher than the phase transitions, since it leads to orientational disorder that must be observed by entropy changes (450 K and 470 K for the bromide and iodide, respectively). For the calculation, the required structural parameters are initially taken as: bond length, r_{CH} = 0.109 nm; bond angles: Δ = 180° − 109.5° = 70.5°; and Ω = 180° − (109.5° + 12°) = 58.5°.

For Ω, 12° is added to the tetrahedral angle based upon the results of the X-ray data on (CH$_3$CH$_2$)$_4$NI (Wait and Powell, 1958). Finally, the overall reorientation of the cation is assumed to be absent, *i.e.*, $1/\tau_I$ = 0. The motional parameters for methyl rotation have been well documented, and the correlation times τ_R fall in the order of 10^{-13}−10^{-12} s (Anderson and Slicheter, 1965; Allen and Cowking, 1967; Lyerla, Jr. *et al.*, 1974; Takeda *et al.*, 1988). Using Eqs. (12) and (19), the correlation times of the librational motion about N−C bonds, τ_L, can be calculated. Table 32 lists the results of the calculated τ_L as a function of measured T_1 and assumed correlation time of methyl rotation τ_R for (CH$_3$CH$_2$)$_4$NI.

Table 32   Calculated librational correlation times ($-log\tau_L$, τ_L in s) at the given temperatures and rotational correlation times of the methyl group (τ_R) for $(C_2H_5)_4NI^*$.

τ_R(ps)	308 K	336 K	358 K	380 K	402 K
0.10	10.23	10.33	10.42	10.56	10.65
0.20	10.23	10.33	10.42	10.56	10.66
0.50	10.24	10.34	10.44	10.59	10.69
1.00	10.26	10.37	10.47	10.63	10.74
5.00	10.42	10.58	10.74	11.01	11.21
10.0	10.67	10.87	11.07	11.37	11.57
20.0	11.02	11.23	11.43	11.75	12.02
30.0	11.23	11.45	11.68	12.18	13.61

* For the corresponding T_1's see Table 7.

The data in Table 32 are next subjected to a two-parameter curve fitting with an Arrhenius equation at each chosen τ_R:

$$\tau_L = \tau_{(L0)}e^{E_L/RT} \qquad (31)$$

where $\tau_{(L0)}$ is the correlation time at $1/T = 0$, and E_L the activation energy of the motion about $N-C$. The results of the fittings are given in Table 33 and can be examined by considering their physical meaning. It seems that the best fittings

Table 33 Linear fitting of the data of Table 32 to an Arrhenius equation[a]

τ_R (ps)	R^2	St. Deviation (%)	$-log\tau_{(L0)}$	E_L (kJ/mol)
0.10	0.9637	3.463	12.040	10.87
0.20	0.9649	3.503	12.068	11.02
0.50	0.9667	3.814	12.150	11.46
1.00	0.9634	4.285	12.304	12.27
5.00	0.9489	8.338	13.754	20.05
10.0	0.9682	7.526	14.533	23.19
20.0	0.9547	9.816	15.200	25.14
30.0	0.7472	55.32	19.868	53.08

a R^2 is the fitting correlation coefficient, other parameters in the first row are explained in the text. The measured data points are evenly scattered around the fitted lines.

(judging from the R^2 and standard deviation) can be obtained for τ_R's shorter than 1 ps. These values are, however, questionable since the methyl rotation at about 300 K has a correlation time of approximately 7×10^{-12} s in alkanes (Lyerla, Jr. et al., 1974; Anderson and Slichter, 1965), and 3×10^{-13} s in hexamethylbenzene and similar molecules (Allen and Cowking, 1967; Takeda et al., 1988). The seemingly better fit with $\tau_R < 1$ ps is thus most likely the consequence of the relaxation time becoming insensitive to the methyl rotation at such high rates (close to the vibrational frequencies). For a very long τ_R, such as 30 ps, on the other hand, the data do not

fit the Howarth 3τ model. It can, therefore, be concluded that the methyl rotation must have a correlation time shorter than 30 ps. Assuming $\tau_R = 1$ ps for the methyl rotation as a reasonable compromise, the conformational motion, *i.e.*, the libration about $N-C$, can be described by the Arrhenius equation:

$$\tau_L = 5.0 \times 10^{-13} \exp[12.3 \times 10^3/(RT)] \text{ (in s)}$$

This equation predicts that the libration about the $N-C$ bond has a correlation time of 2.4×10^{-11} s at 308 K and *ca.* 10^{-3} s at 70 K, respectively.

Similar considerations may also be applied to $(CH_3CH_2)_4NBr$, for which the libration about the $N-C$ bond follows the Arrhenius equation:

$$\tau_L = 2.2 \times 10^{-12} \exp[9.9 \times 10^3/(RT)]$$

The standard deviation is 1.2% and $R^2 = 0.9955$. At 308 K, this equation predicts that the libration about the $N-C$ bond has a correlation time of 9.8×10^{-11} s.

Examination of molecular models also reveals that the ethyl chains are sterically hindered about the bond between nitrogen and C-1. It seems possible that concerted rotations about all four $N-C$ bonds may occur, but, again the amplitude of such motion must be limited, since rotations over large angles would lead to contradictions with other experimental evidences. The impossibility for the conformational motion can be extended also to temperatures above the phase

transition, so that the solid–mesophase transition consists only of orientational disordering to the plastic crystalline state without disordering about the N–C bonds.

4.1.3 Tetra-*n*-propylammonium Bromide

Below the low-temperature disordering transition T_{d1} (382.2 K, see Table 2), the ^{13}C CSA powder pattern, shown in Fig. 15, feature broad, asymmetric resonances only. The magnified C-1 resonance at 299 K clearly shows three non-identical principle values of the chemical shift anisotropy (CSA) tensor, indicating that C-1 is rigid. The signals of C-2 and C-3 are broadened and overlapping, also due to the chemical shift anisotropy interactions. The width of the C-2 and C-3 peaks are, however, much less than for C-1 because of the methyl rotation that partially averages the CSA interaction. As the temperature is increased to 390 K, higher than T_{d1}, no signals can be detected with the CP sequence, indicating a fast motion that diminishes the cross-polarization efficiency because of weakening of dipolar interactions. The appearances of the powder spectra at 390 and 402 K, obtained with BILEV pulse sequence, are very different from that at lower temperatures. The C-1 resonance changes from asymmetric at 299 and 353 K to an axially symmetric CSA powder pattern at 390 K. The axial symmetry of a ^{13}C CSA powder pattern indicates explicitly that rotation about one preferred molecular axis has started. The CSA interactions for C-2 and C-3 are reduced so much that their resonances are clearly resolved. As the temperature is further increased to 402 K, above T_{d2} (395.8 K), the

156

spectral line widths becomes further reduced and more symmetric, indicating that the molecular orientational motion becomes more isotropic.

Figure 16 shows that below T_{d1} the spectra obtained with CP-MAS at 306 and 354 K are almost identical in terms of chemical shifts and line-width. While above T_{d1} the signals, again, become undetectable with the CP. The MAS spectrum at 394 K, measured with BILEV, shows two drastic changes compared to that at lower temperatures: (1) The line widths for all carbons have increased. For C-1, it increases from 0.9 to 4.8 ppm (1 ppm = 50.31 Hz). This heterogeneous line-width broadening is due to a distribution of the environments for the nuclei resulting from orientational disordering (detailed discussion on the mechanisms of line broadening is given at the end of Sect. 2.3.3). (2) The chemical shifts change by 1.8, 1.3, and −0.6 ppm for C-1, C-2, and C-3, respectively, on going through the transition. This global change in chemical shift clearly indicates a change in the packing connected with the orientational disordering.

As shown in Sect. 2.3.4, the mobility of conformational motion, i.e., rotation about a single bond in a linear paraffinic chain can be investigated by the difference in the ^{13}C relaxation times between the two directly bonded carbon atoms (Lyerla and Levy, 1974; Lyerla et al., 1974). The ^{13}C spin-lattice relaxation times, T_1, are shown in Table 8. Below the disordering transition, T_1 for C-1 and C-2 is long (20−35 s), indicating slow motion ($\tau_C \approx 10^{-5}$ s) in both CH$_2$-groups. The difference in the correlation time, τ_C, between C-1 and C-2 is much less than between C-2 and C-3. If one considers the fact that the shortening in T_1 of C-2 relative to C-1 is

157

largely due to the magnetic field fluctuations induced by the methyl rotation, the difference in actual motion between C-1 and C-2 is even less. As the temperature is increased above T_{d1}, T_1 of C-1 and C-2 decreases drastically to about 0.2 s. The difference in T_1 is still somewhat smaller between C-1 and C-2 than between C-2 and C-3, indicating that the bond between C-1 and C-2 is still rigid. The increase in the difference of T_1 between C-1 and C-2 at higher temperatures is caused by a librational motion about C1 – C2, similar to that in the N – C bonds of the tetraethyl-ammonium bromide and iodide. The correlation time for C-1 and C-2 at 394 K is on the order of 10^{-10} s, typical for plastic crystals (Boden, 1978). While the T_1 of the methyl carbon remain almost the same, as expected.

4.1.4 Tetra-*n*-propylammonium Iodide

The measurement of a high resolution ^{13}C MAS NMR spectrum in the vicinity of room temperature was initially attempted using the cross-polarization method. The cross-polarization efficiency using a normal spin contact time of 1 – 3 ms was, however, very poor, as shown in Fig. 19. The reasons for the insufficient cross-polarization, *i.e.*, weak signals in a CP-MAS experiment, are summarized in Sect. 2.3.3. The relationship between signal intensity and spin-contact time shown in Fig. 19 indicates that no maximum in the CP rate can be attained, suggesting that a short $T_{1\rho H}$ is the reason for the insufficient cross-polarization. If the shortening of $T_{1\rho H}$ is due to a kHz motion, then by increasing the temperature, the rate of motion can be increased, which should yield a longer $T_{1\rho H}$ and a maximum in the signal intensity

vs. spin-contact time. This is demonstrated in Fig. 20 at 408 K, just below the major disordering transition temperature of 418.9 K. The maximum signal intensities can be observed at contact times of 0.5, 1, and 1 ms for C-1, C-2, and C-3, respectively.

Another factor that may reduce $T_{1\rho H}$ is the presence of paramagnetic impurities. To verify their absence, solution ^1H and ^{13}C NMR spectra were recorded. No impurities could be found at detectable levels. This initial motivation of purity checking has, however, lead to a rather interesting finding: the proton solution spectrum of $(CH_3CH_2CH_2)_4NI$, shown in Fig. 12, shows an unexpected splitting pattern arising from the $N-CH_2$ protons. It is centered at 3.23 ppm and consists of a weak triplet inside a strong doublet. This pattern is common to all tetra-alkylammonium salts when the alkyl chain length becomes equal to or longer than three carbon atoms. The same resonance patterns are also observed for almost all tetraalkyls in solution (SadtlerResearch Lab; Ashi Research Center). In contrast, the spectrum of the C-1 protons in tripropylamine, $(CH_3CH_2CH_2)_3N$, shows the expected triplet.

The splitting of the two C-1 protons, H-1a and H-1b, is caused by the spin-spin scalar coupling or J-coupling (through chemical bonds) with the two protons attached to C-2. The coupling between H-1a and the two H-2's must thus be different from that between H-1b and the two H-2's, which is impossible if the rotation about the bond C1−C2 were free.

The splitting pattern of H-1's shows little change even on heating the solution up to 423 K, the temperature limit of our ^1H NMR probe, see Fig. 21. The down-

field drifting (about 12 Hz) of all resonance lines (but not the solvent signal at 2.48 ppm) as a function of temperature in Fig. 21 is probably due to an acceleration of tumbling of the molecule as a whole as the temperature is increased. Thus, the peculiar pattern on the C-1 protons in tetra-*n*-alkylammonium cations is additional evidence that the rotation about C1–C2 is hindered.

To understand this splitting better, a spin simulation was made by assuming a specific average conformation, shown in Fig. 47, about the bond between C-1 and C-2. The simulated spectrum for the conformation of Fig. 47 and the coupling constants, J_{HH}, listed in Table 34 is reproduced in Fig. 48.

$$\overset{1}{N}-\overset{2}{C}H_2-\overset{3}{C}H_2-CH_3$$
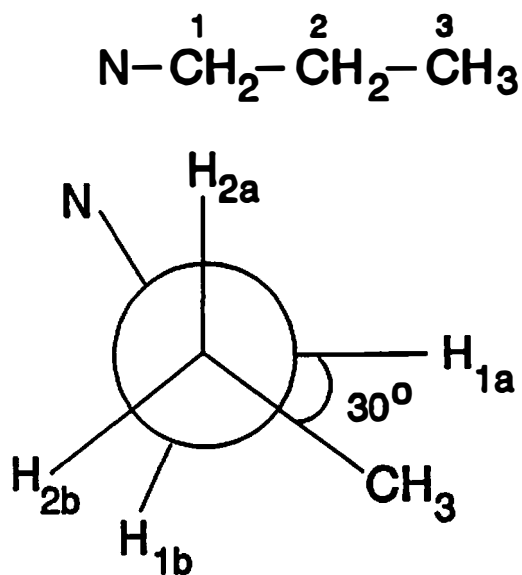
Figure 47   Assumed Newman projection of the conformation in a propyl chain in $(C_3H_7)_4NX$, X = Br and I.

160

Table 34 ^{1}H spin-spin coupling constants, J_{HH} (in Hz), of $(C_3H_7)_4NI^a$

	H-1a	H-1b	H-2a	H-2b	CH$_3$
H-2a	0.10	3.5	-	0.00	7.3
H-2b	17.2	3.5	0.00	-	7.3

a   The values were measured based on a proton spectrum in D_2O solution at room temperature.

The conformation proposed in Fig. 47 permits some small amplitude librational motion about C1–C2. The hindrance should arise from inter-alkyl chain (intramolecular) steric interactions, similar to that in the N–C bond of the tetraethylammonium ion.

The ^{13}C T_1's measured in the solid state below and above the major disordering transition (T_d = 418.9 K), listed in Table 8, show similar T_1 values for C-1 and C-2, indicating little motion about the bond between C-1 and C-2. The large difference in T_1 for both C-1 and C-2 between 322 and 433 K is due to the increase in overall motion in the cation, i.e., the presence of orientational motion at 433 K. Below the disordering transition, the iodide has a shorter T_1 than the bromide. This will be elucidated in the following through other NMR techniques. Above T_d, both iodide and bromide have similar relaxation times for the respective carbon atoms, indicative of a similar motional state in both cases. The methyl carbons show a slight increase in T_1 going through the transition for both the propyl compounds.

The MAS spectra of Fig. 17 show that the chemical shifts for all carbons change very little (<0.6 ppm) as a function of temperature, even through the phase
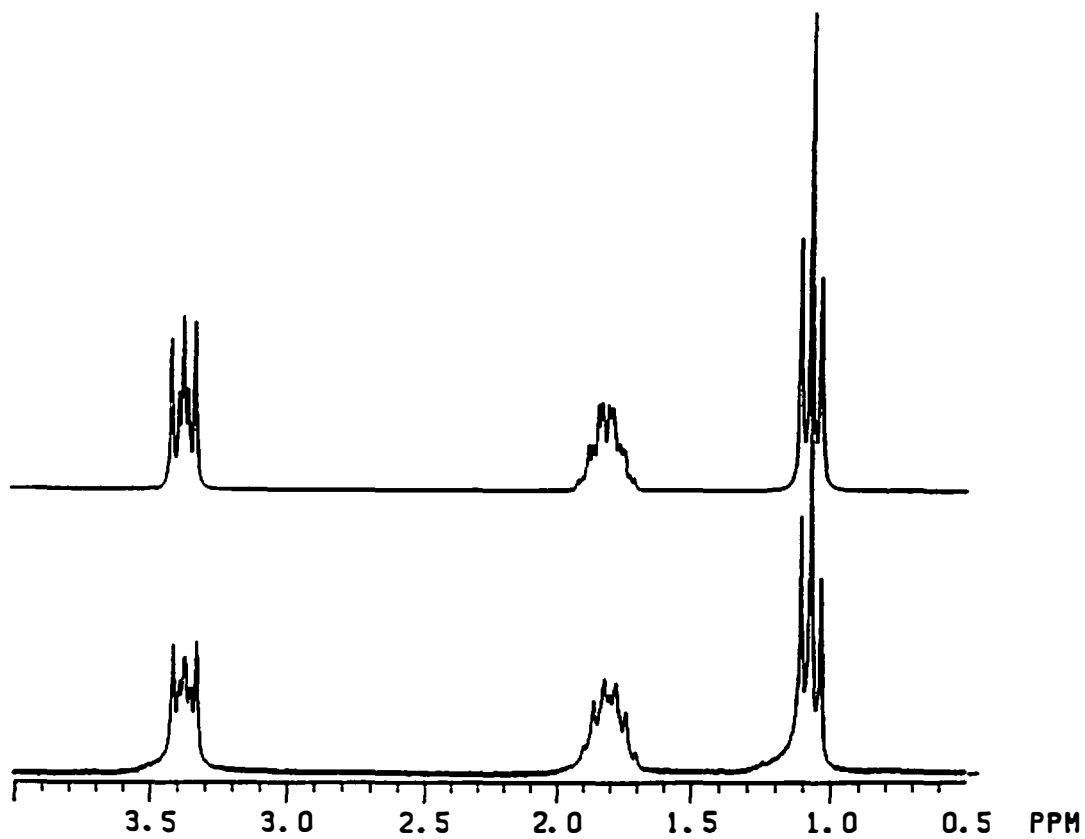
Figure 48   Simulated (top trace) and measured (bottom trace) ^1H spectra of $(C_3H_7)_4NI$ in D_2O. The 7-spin simulation was based on the data given in Table 34, and consistent with the conformation shown in Fig. 47.

transition at 418.9 K. This behavior is quite different from tetra-n-propylammonium bromide where changes are observed in the chemical shift at the transition for all carbons (Fig. 16). Only above the highest disordering transition can similarity in the ^{13}C MAS NMR spectra be found for iodide and bromide. The constancy in chemical shift of tetra-n-propylammonium iodide indicates that neither the packing of the cations nor the conformations about the bonds have changed from 312 to 433 K.

Another feature of the solid state ^{13}C MAS NMR spectra in Fig. 17 is the broadness of the peaks. The room temperature spectrum (the bottom trace in Fig. 17) shows rather broad signals for all the carbons in the propyl chain. The most up-field peak has a line-width of about 7 ppm at half-height and consists of the resonances of two carbons, C-2 and C-3 (C-3 is the methyl carbon) (compared to 0.9, 0.9 and 0.4 ppm for the line-widths of C-1, C-2, and C-3 in the bromide). As the temperature is increased, resolution of the resonances of C-2 and C-3 is possible, but the linewidths are still large (at 412 K the line-widths are 10, 6.5, and 2.8 ppm for C-1, C-2 and C-3, respectively). Since conformational disorder was shown above not to be possible, the line broadening must be caused by orientational disorder. From the discussion on the mechanism of line-broadening in a ^{13}C MAS spectrum given in Sect. 2.3.3, tetra-n-propylammonium iodide samples at room temperature fulfills the class of glass-below-T_g. This conclusion, drawn from the NMR observations, is in agreement with the somewhat smaller entropy change found at the major orientational disordering transitions for the iodide (35.8 JK^{-1}mol^{-1} at 418.9 K) than for the bromide (45.3 JK^{-1}mol^{-1} at 448.3 K). In fact, a continuous change in the ^{13}C MAS

NMR spectrum of the iodide begins at T_{d1} (225.4 K), see Fig. 18, in contrast to the bromide, in which the MAS spectra show no change below the major orientational transition (see Fig. 16 at 306 and 354 K). Only as the temperature is decreased below T_{d1}, the line-width of ^{13}C CP-MAS NMR spectrum of the iodide is narrowed to a value that is comparable to that of the crystalline phase of the bromide at room temperature.

Most interestingly, the low temperature spectra measured from 177 K to 232 K exhibit multiple lines for chemically equivalent carbons (Fig. 18). The peaks at 59.0–63.3 ppm (216 Hz of largest separation) are due to C-1, 15.9–19.1 ppm (160 Hz in largest separation) due to C-2, and 11.3–14.1 ppm (140 Hz in largest separation) are from C-3. There are four resonance lines for each of the three carbon atoms in the propyl chain within this temperature range, which must correspond to four distinguishable chains in every cation. An intermolecular inequivalence would introduce much smaller changes in chemical shift, especially for the inner-most carbons. The inequivalency agrees with the molecular structure in crystal, determined by X-ray, in which the four N–C bonds of the different propyl chains have different lengths (Yasuniwa et al., 1991). The reason for the different bond lengths is traced to the fact that the four C-1's are in different proximity to the iodide (Yasuniwa, et al., 1991).

Additional details can be seen in the C-3 resonances of Fig. 18 in the spectra from 177 to 232 K. The C-3 peaks (11.3 and 14.1 ppm at 177 K) change their splitting pattern as the temperature is increased. The inner two lines approach each

other and overlap to become a strong single line as the temperature is increased to 232 K. In this low temperature range (177–232 K) the signals for C-1 and C-2 remain unchanged, indicating that only the methyl groups of the cation are in motion.

Between 232 and 255 K, the spectrum undergoes an overall broadening, in which the C-1 and C-2 carbon resonances are most affected. The degradation in the resolution, or coalescence of the multiple lines of C-1 and C-2, indicates a motion that has generated a distribution of orientations, and corresponds to the phase transition centered at 225.4 K with an entropy change of 6.4 $JK^{-1}mol^{-1}$ and a volume increase of 2.5% in unit cell (Yasuniwa *et al.*, 1991). A further increase in temperature causes the orientational motion to have a rate comparable to that of the signal separation at low temperature (200 Hz). At this point (about 312 K) the NMR signals of C-1 and C-2 are further broadened and no longer observable. Since most of the orientational disordering is completed at 418.7 K (35.8 $JK^{-1}mol^{-1}$) and atomic coordinates can still be measured by X-ray, the motion detected at about 232 K must involve a librational jumps about a preferred orientation so that orientational order is largely maintained. The nature and rate (200 Hz) of libration of the cation as a whole permits a X-ray structure determination to give definite atomic positions within the cation, even at room temperature (Yasuniwa *et al.*, 1991).

The signals for C-1 and C-2 become detectable again at $T \geq 424$ K, (Fig. 17) and appear as single lines, indicating the presence of an isotropic orientational motion faster than 1/200 Hz $\approx 10^{-3}$ s in correlation time. This estimation of the rate

165

of motion by the peak separation agrees with the result obtained from the ^{13}C cross-polarization behavior, shown above.

In summary, in the solid state of tetra-*n*-propylammonium bromide and iodide the only possible types of large-amplitude motion are the orientational motion of the cation as a whole and the well-known methyl rotation. The former occurs in one step in the bromide, and gradually (or continuously) in the iodide. Other potential conformational motion, *i.e.*, rotation about the bonds between N and C-1, and between C-1 and C-2 are not possible for steric reasons, and proven by the ^{13}C spin-lattice relaxation times and proton spin simulation. The second conclusion made here agrees with the assumption made by Coker *et al.* (Coker et al., 1970) based solely on the examination of models. These results will be extended to the tetra-*n*-alkylammonium cations with longer chains shown next.

4.1.5 Summary

The low homologs of tetra-*n*-alkylammonium halide crystals show only orientational disordering. The disordering may be completed in one or more steps. Above the major disordering transition temperatures, the cations form plastic crystals. Except for the methyl groups, full rotations about single bonds are restricted for steric reasons, even in the liquid state. Some large-amplitude motion about the single bonds $N-CH_2$ and CH_2-CH_2 must be librations with an angle too small to reach other conformational isomers. These bonds, therefore, do not contribute to conformational entropy changes at the phase transitions. Thus, including the bonds

CH_2-CH_3, there are 3 bonds in each alkyl chain of 3 or more carbon atoms, or 12 bonds in total of four chains, that contribute little to the overall entropy change on transition to the mesophase.

4.2 Disorder and Motion in the Intermediate Homologs of Tetra-*n*-alkylammonium Salts

4.2.1 Tetra-*n*-butylammonium Bromide and Iodide

Based on the entropy data (Table 2), it could be deduced, using the empirical fusion rules, that in the iodide the orientational disordering of the cation and conformational disordering for about one bond per alkyl chain occur together at the low-temperature transition (394.0 K), while complete positional disordering takes place without major additional conformational disordering on isotropization (420.6 K). For the bromide, in contrast, the low-temperature transition (367.0 K) can only be linked to conformational disordering about *one* bond per alkyl chain. Partial orientational disordering seems then to occur gradually between the disordering and the isotropization temperature (393.9 K), helped by a minor transition at 379.2 K. This conclusion was based on the observation that the entropy change at isotropization is only about 16 $JK^{-1}mol^{-1}$ (after subtracting 21.3 $JK^{-1}mol^{-1}$ for the positional disordering of a $(C_4H_9)_4N^+$ ion obtained from $(C_4H_9)_4NI$). This is lower

than the typical $20-50$ $JK^{-1}mol^{-1}$ expected for orientational disordering, or the average value of 44.9 $JK^{-1}mol^{-1}$ for the four previously analyzed low-homolog tetraethyl and tetra-n-propyl compounds, or the value of about 33 $JK^{-1}mol^{-1}$ for $(C_4H_9)_4NI$, deduced from Table 2. Because of this complication of the bromide, the discussions of the NMR results will be given first for the "well-behaved" iodide salt.

Iodide: The state of orientational motion and disorder of the cation can be shown by several solid state ^{13}C NMR methods. The ^{13}C NMR spectra obtained under MAS conditions below T_d (see Fig. 23) show multiple lines for the methyl carbon (C-4). The resonance of C-4 can be deconvoluted into three peaks at 14.40, 15.29 and 15.53 ppm, with integral intensity ratios of 2:1:1. Since the separation between the most upfield and downfield peaks is too small (only 1.1 ppm) to account for a γ-*gauche* effect (about 2 ppm), we surmise that the multiplicity of the resonance of the C-4 carbons has an intermolecular reason, such as different distances between C-4 and the iodide ion, as was observed for the case of tetra-n-propylammonium iodide, discussed in Sect. 4.1. The area ratio of 2:1:1 implies that only two of the four C-4 atoms have the same environment in the crystal. A detailed crystal structure from single crystal X-ray data is needed to verify this interpretation. As the temperature is increased to T_d, the spectra at 395 and 402 K in Fig. 23 show clearly that another peak (14.79 ppm) at the average position of the previous peaks becomes stronger and finally dominates at 409 K. The appearance of the new peak is due to orientational motion of the cation as a whole, which renders all four methyl groups equivalent.

The orientational motion of the cation as a whole is also indicated by the changes in the other carbon signals of Fig. 23. The changes in chemical shift occur mainly during the disordering transition T_d. The differences in chemical shift between 310 and 409 K are 0.61, 0.83, 0.85 ppm for C-1, C-2, and C-3, respectively. The outer carbons are affected more, which is in line with changes in intermolecular interaction arising from orientational motion and disordering.

The most decisive information on the orientational motion of the cation as a whole is given by the variable temperature ^{13}C powder pattern shown in Fig. 24. Below 394.0 K, the resonance of C-1 yields a typically broad anisotropic pattern, indicative of the absence of motion. Above 394.0 K, the C-1 resonance is narrowed (see spectrum at 400 K). The narrowing of C-1 signal is due to orientational motion which is the only allowed freedom for C-1. Below 394.0 K, the more closely-spaced resonances of C-2, C-3, and C-4 feature also broadening to a degree that they are fused to a single peak at about 25 ppm. The orientational motion and superimposed conformational motion of the bond C2−C3 (analyzed in the following) at 400 K results in a much better resolution so that the three peaks can now be distinguished easily.

The ^{13}C spin-lattice relaxation times, listed in Table 11, can be used to evaluate the mobility of the orientational motion and disorder discussed above. Below the transition temperature, T_1 of C-1, C-2, and C-3 are of the same order of magnitude, between 40 and 60 s, corresponding to a motional correlation time τ_c between 2.9 and 4.3 μs [calculated from Eq. (17)]. This is much slower than what

is found in plastic crystals (typically, orientational motion of 5 ns at the crystal-to-plastic crystal phase transition to 2 ps at isotropization) (Boden, 1979). The relaxation time for C-4 is very short (1.7 s) because of the fast rotation of the methyl groups about their C_3-axes. As the temperature is increased to 408 K, τ_C calculated from the data in Table 11 with Eq. (17) for C-1 and C-2 is 0.54 and 0.32 ns, respectively, both typical for plastic crystals.

Of particular interest is the conformational motion and disorder initiated at T_d. In the previous section it has shown that (1) rotations about $N-C1$ and $C1-C2$ are for steric reasons practically rigid, even in solution, (2) methyl rotation starts at very low temperature and does not change the overall molecular conformation. Therefore, the conformational disordering in a tetra-n-butyl cation is expected to be introduced only through the bond between C-2 and C-3.

Using Eqs (17), and (20)−(22), the conformational motion about $C-C$ single bonds can be shown by the differential rates of motion between two directly bonded carbon atoms (Lyerla Jr. and Levy, 1974). The larger the difference in $1/\tau$, the faster is the motion about the bond. At 329 K, the correlation times, τ, calculated from the measured T_1 listed in Table 11, for C-1 to C-4 are 3.78 μs, 4.33 μs, 3.05 μs, and 19.9 ps, respectively. The small differences between the correlation times of C-1 and C-2 and between C-2 and C-3 indicate that the $C1-C2$ and $C2-C3$ bonds are rigid. As the temperature is increased to 408 K, the calculated values for τ are 0.54 ns, 0.32 ns, 92 ps and 22.4 ps for C-1 to C-4, respectively. The values of τ for C-1 and C-2 are still very close, but the difference between that C-2 and C-3 is much

larger than that between C-1 and C-2, indicating the presence of conformational motion about the bond between C-2 and C-3. The overall decrease in T_1 of all three inner carbons (C-1 to C-3) is due to the orientational motion of the cation as a whole. Similar T_1 values for C-1 and C-2 can even be found in the solution (Coletta, et al., 1987), as represented in Table 11, indicating that the bond between C-1 and C-2 is in all states prohibited from rotation.

Bromide: At room temperature the ^{13}C CP-MAS NMR spectrum, shown in Fig. 22 at 308 K, is almost the same as that for the iodide. The differences between the two butyl compounds in the chemical shifts for all the carbon atoms are very small (within 0.3 ppm, see the results in Tables 9 and 10). The methyl carbon atoms (C-4) in both salts show the same three-line pattern with the same intensity ratio of 2:1:1. These similarities suggest that the bromide salt forms as well-ordered crystals as the iodide.

The conformational motion and disorder can be inferred from the relaxation time measurements, since the chemical shifts for all carbon atoms change little in going through the disordering transitions. The spin-lattice relaxation times for C-2 and C-3 in the mesophase at 384 K are 10.0 and 1.51 s, respectively. This large difference in T_1 between C-2 and C-3 proves that the bond C2−C3 is conformationally mobile above T_d. These T_1 values correspond to correlation times of 0.72 and 0.11 μs, indicating a motion that is slower by two orders of magnitude than typically found in a plastic crystal. Thus, the mesophase formed at T_d = 367.0 K must be a condis state without orientational motion.

The condis state of $(C_4H_9)_4NBr$ (as well as all other compounds studied in this research) is spectroscopically unique, because one can use either CP-MAS (designed for rigid carbon atoms) or BILEV (routinely used for solution ^{13}C NMR) to obtain a ^{13}C spectrum with good signal-to-noise ratio. The reason is that in the condis state the mobility is intermediate between that of a rigid molecule in the crystalline state and that of tumbling molecules in the melt (or solution). Signals from the carbon atoms in conformationally mobile chains of liquid crystals, such as in OOBPD (shown next), and plastic crystals (such as in $(C_4H_9)_4NI$) can only be detected with the BILEV method, due to their having much higher mobility than the molecules in their condis state in which both orientational and positional order remain.

Information on the gradual orientational disordering can be obtained from the spectra in Fig. 22. The spectral lines for all carbon atoms show continuous broadening from 373 to 384 K. Similar line broadening was found for tetra-*n*-propyl-ammonium iodide below its crystal-to-plastic crystal transition temperature, as discussed in Sect. 4.1.4. This line broadening can be attributed to the fact that the orientational motion (of the cation as a whole) has attained a relatively large amplitude so that the intermolecular interactions are changed. This large-amplitude orientational motion is then also most probably responsible for the deficit of the orientational entropy observed on isotropization. Final confirmation is expected from a detailed analysis of the heat capacity, presently in progress. The orientational motion detected by the line broadening in ^{13}C NMR spectrum can, however, only be a restricted motion, since the C-4 (methyl) resonances consist of at least two lines

172

(Fig. 22), indicating two distinguishable methyl group placements in the crystal. If the orientational motion were the same as in the iodide, i.e., isotropic or random, the C-4 resonances should have undergone coalescence into a single, sharp peak.

At 392 K, the NMR spectrum is already largely that of the melt (395 K). The remaining differences in chemical shifts between the solution and the melt spectra, shown also in Fig. 22, are due to the differences in intermolecular interactions, if one assumes that the mobility is the same in both cases.

From this discussion, it can thus be concluded that tetra-*n*-butylammonium bromide and iodide: (1) form well ordered crystals that possess practically only vibrational motion below the mesophase transitions, (2) between the mesophase transition temperatures and the isotropization temperatures, the cations in the iodide salt form a plastic crystal with additional conformational motion and disorder about the bond C2 – C3, while the bonds N – C1 and C1 – C2 remain rigid. The cations of bromide salt are similarly conformationally disordered, but remain largely orientationally ordered with gradually increasing orientational mobility as the temperature is increased; (3) the N – C1 and C1 – C2-bonds remain in a fixed conformation in both salts even in the liquid state, therefore, the maximum degree of conformational disorder has been realized already well below isotropization.

4.2.2 Tetra-*n*-pentylammonium Bromide and Iodide

Bromide: There is only one phase transition observed for the bromide (374.0 K) with an entropy change of 97.9 $JK^{-1}mol^{-1}$. Since this transition is identified as

the melting, the entropy change consists of all three disorder contributions. If one subtracts the positional and orientational contributions from the observed entropy, one obtains $25-39$ $JK^{-1}mol^{-1}$ for conformational disordering. This conformational disorder can be attributed to 4 bonds becoming disordered. Based on the analysis of the shorter chain homologs, the tetra-n-pentylammonium cation should have, however, 8 single bonds to be disorderable, namely, C2–C3 and C3–C4. The questions are thus (1) which four bonds contribute to the entropy change? (2) what is the behavior of the other four bonds that do not contribute to the transition entropy. Are they already disordered at the lowest observation temperature or do they remain ordered even in the melt?

Figure 25 reveals the transition at 373 K through chemical shift changes (see also Table 12). In going through the phase transition, except for C-1, the chemical shift changes between 308 and 387 K are close to 1.5 ppm. The phase transition is also obvious from the drastic decreases in T_1 for all carbon atoms but C-5, as shown in Table 14. Since conformational motion about the bond between C-1 and C-2 is not possible, the sharp decrease in T_1 of C-1 and C-2 between 308 K and 380 K must be due to the orientational and translational motion. The relaxation times for C-2 and C-4 at 308 K can not be directly measured since their signals are overlapping, but since both C-1 and C-3 have large T_1 values (37.0 and 30.6 s, respectively), the T_1 of C-2 is expected to be long, too, between 37 and 30 s, permitting the assignment given in Table 14. Thus, the bond between C-2 and C-3 is considered to be conformationally rigid at 308 K. As the temperature is increased to 380 K (above

the transition), the signals of C-2 is well separated from that of C-4, as shown in Fig. 25, and it is possible to measure T_1 of C-2 and C-4 directly. The difference in T_1 between C-2 and C-3 has become larger than that between C-1 and C-2. Therefore, the bonds of C2−C3 can be assumed to contribute most to the entropy change of 25−39 $JK^{-1}mol^{-1}$ at the transition. If the bonds between C-3 and C-4 contribute little to the entropy change at the transition, one must assume them to have considerable motion and be disordered already below the transition, since they are certainly conformationally mobile above the transition (as seen from T_1 of C-3 and C-4 at 380 K).

Supporting evidence for these assumptions is as follows: The relaxation time of C-4 at 308 K could not be obtained directly from measurement due to the overlapping between signals of C-4 and C-2, it was, however, possible to carry out a reliable estimation by knowing that: (1) T_1 of C-2 is between that of C-1 and C-3, i.e. between 37.0 and 30.6 s, (2) the relationship between the measured overlapping signal intensity, $I(t)$, and the variable delay, t, could be measured using the *progressive saturation* method and fitted to the following equation:

$$I(t) = I_0[(A - e^{-t/T_1(C2)}) + (B - e^{-t/T_1(C4)})] \tag{34}$$

in which I_0 is $I(t)$ at $t = \infty$, A and B are two constants (both are close to unity), $T_1(C2)$ and $T_1(C4)$ are T_1 of C-2 and C-4, respectively. The constants, I_0, A, B, $T_1(C2)$ and $T_1(C4)$ are treated as adjustable parameters with constraints as stated

above. As shown in Table 14, the large difference in T_1 between C-3 and C-4 at 308 K agrees with the above made suggestion that C3 – C4 is in motion and disordered already at 308 K. Again, a full support of the gradual disordering about C3 – C4 is expected from a detailed heat capacity analysis, presently in progress.

Iodide: The total entropy change of the two observed phase transitions of the iodide is 135.2 $JK^{-1}mol^{-1}$,[1] which suffices to account for all disordering to occur within these closely spaced transitions. The conformational disordering applies to the 8 bonds, (C3 – C4) and (C2 – C3). The low-temperature transition at 404.6 K has an entropy change of 41.2 $JK^{-1}mol^{-1}$ and was assigned to the disordering of four equivalent bonds to a condis crystal.

It is difficult to obtain a ^{13}C spectrum for this condis phase in the slow NMR experiment. The sample undergoes a complete transition to the melt within the time of taking an NMR spectrum. The spectra of the room-temperature phase crystal (305, 362 K and 384 K) of Fig. 26 show that the signals for C-2 and C-4 become more resolved as the temperature is increased because of an up-field shifting of the C-4 resonance, while all other resonances remain practically unchanged. This change indicates that the conformational motion in the chain has already started gradually below the transition temperature. Since this excited motion does not lead to a major increase in entropy, the motion should not substantially disturb the crystal symmetry.

The biggest change in the spectra shown in Fig. 26 can be seen at the phase transition (T_d = 404.6 K). The two distinct lines arising from the methyl carbons at 400 K are representatives of the room-temperature phase (15.52 ppm peak) and the

condis phase (14.71 ppm peak). The other carbons show only single lines and their chemical shifts differ only slightly from those measured at 305 K. As the temperature is increased to 415 K (the melt), the room-temperature phase disappears, and the methyl group shows one peak only at 14.62 ppm. The C-2 and C-4 signals are clearly separated. Chemical shift changes for all carbon atoms from 400 to 415 K, listed in Table 13, are due to the combined effects of all three types of disordering during isotropization.

The ^{13}C T_1 data listed in Table 15 for tetra-n-pentylammonium iodide can be interpreted in the same way as for the bromide. In the room-temperature phase of the iodide, the bond between C-3 and C-4 is, however, more rigid than in the bromide (as can be seen from the smaller difference in the T_1's between C-3 and C-4 in the iodide). Above the melting point, the T_1 for all carbons increases from C-1 to C-5. The differences in T_1 between two directly bonded carbon atoms also increases as one approaches the chain end, indicating the increasing conformational mobility at the chain end. The small difference in T_1 between C-1 and C-2 is perhaps due to the motion in C2−C3.

4.2.3 Tetra-n-hexylammonium Bromide and Iodide

As shown in Table 2, the bromide has five disordering transitions before isotropization at 375 K. The transitions with small entropy changes (≤ 20 $JK^{-1}mol^{-1}$), are most likely crystal structure changes occurring without major increases in motion (to be verified by X-ray diffraction). These transitions of small entropies may,

177

however, cause considerable changes in the chemical shift of ^{13}C NMR and make it difficult to investigate the, for us, more interesting conformational motion and disorder. For this reason we will discuss the simpler case of the iodide first.

Iodide: Below the isotropization temperature (378.7 K) the combined entropy change for two closely spaced disordering transitions (345.1 and 352.3 K) is 99.5 $JK^{-1}mol^{-1}$, which is sufficient to account for approximately three bonds per alkyl chain (or a total of 12 bonds) to become disordered. Therefore, the sample should be a well-ordered crystalline phase at room temperature, and a condis phase with maximum amount of conformational disorder above 352 K that retains positional and orientational order. The isotropization transition (at 378.7 K) has the expected entropy change of 43.9 $JK^{-1}mol^{-1}$ for the orientational and positional disordering.

The room-temperature phase ^{13}C CP-MAS spectrum, plotted in Fig. 30, shows two lines from the methyl group, a pattern similar to that found in tetra-*n*-butylammonium iodide, suggesting that the cations are orientationally ordered. The relaxation times listed in Table 18 show that below the disordering transition all the carbon atoms have long, comparable values for T_1, suggesting that the chains are conformationally rigid. The decrease of T_1 for C-4 and C-5 is probably due to the methyl rotation.

The spectra obtained at 334, 353 and 364 K in Fig. 30 show the progressive formation of the condis phase and disappearance of the room-temperature crystalline phase. In the condis phase at 358 K, the relaxation times for all carbons atoms have decreased to values similar to that in the melt or in solution. From Table 18, the

mobility about each bond can be assessed from the differences in T_1 between directly bonded carbon atoms. At 358 K all bonds, except for C1−C2, have considerable mobility which increases when approaching the chain end.

The changes in chemical shift between room temperature and condis phase can for this chain length also be used to document conformational disorder and motion. From Table 17, the chemical shift differences between 308 and 364 K are sufficiently close to 2 ppm, to suggest that one γ-substituent of each carbon atom has substantially increased in its *gauche* content. The changes in the chemical shifts of C-1, $\Delta\delta$(C-1), is due to the conformational disorder in the bond C2−C3, and similarly, $\Delta\delta$(C-2) due to C3−C4, $\Delta\delta$(C-3) due to C4−C5, $\Delta\delta$(C-4) due to C2−C3, $\Delta\delta$(C-5) due to C3−C4, and $\Delta\delta$(C-6) due to C4−C5. This indicates that the chemical shift changes for all six carbon atoms are due to three bonds only, *i.e.*, C2−C3, C3−C4, and C4−C5, while the remaining three bonds, N−C1, C1−C2, and C5−C6 are not contributing. Both the relaxation times and chemical shift data are thus consistent with the observed total entropy change of 99.5 $JK^{-1}mol^{-1}$ resulting from the two mesophase transitions.

Bromide: The ^{13}C CP-MAS NMR spectrum at 310 K shown, in Fig. 27, is quite different from that for the iodide. The chemical shifts at room temperature for all six carbon atoms (Table 16) are smaller than those for the iodide (Table 17), but are comparable to those of the iodide in the melt, suggesting that the bromide has already achieved a high degree of disorder. Another interesting feature of the room temperature spectrum of the bromide is that C-4 shows at least two peaks (at 33.22

and 31.71 ppm). The low-field peak (33.22 ppm) is close to that of C-4 of the iodide in the condis phase (32.40 ppm at 364 K, Table 9), while the up-field peak (31.71 ppm) is almost the same as that of C-4 of the iodide in the melt (31.87 ppm at 380 K, Table 17). The spectra of Fig. 27, reveal that the two peaks of C-4 undergo a coalescence with increasing temperature, and finally merge at 32.07 ppm in the melt (374 K).

In attempting to find the cause for the change in the chemical shift of C-4 in the conformational motion about the bond C2 – C3, one must look for some change in the chemical shift for C-1 since C-1 and C-4 are both in γ-position to each other. The change in the chemical shift of C-1 by an amount of about 1 ppm is, indeed, observed within the same temperature range. The chemical shifts for the remaining carbon atoms are practically unchanged. Thus, the transition at 315 K with an entropy of 38 $JK^{-1}mol^{-1}$ can be linked to a good degree to the onset of conformational motion and disorder about the bond C2 – C3 which is, as the innermost potentially mobile bond, the last expected to become conformationally disordered. Since the coalescence of the signal for C-4 extends up to 357 K, the transition, centered at 315 K, can only be the beginning of a gradual process and its completion should also be supported by heat capacity studies, presently in progress.

Since the bond C2 – C3 becomes disordered at temperatures above 310 K, one expects that the other two disorderable bonds, namely, C3 – C4 and C4 – C5, become disordered below 310 K. The total entropy of all four transitions that occur below

180

310 K amounts to, however, only 48.8 JK^{-1}mol^{-1}, which is sufficient only for conformational disordering of about one bond per alkyl chain, rather than two.

To find out at what temperature the bonds C3 – C4 and C4 – C5 change their conformations, another variable-temperature ^{13}C CP-MAS NMR experiment was conducted by cooling from 310 to 148 K. The spectra are shown in Fig. 28. At the lowest temperature, both the appearance of the spectrum and the chemical shifts of all carbon atoms are similar to the iodide at room temperature. Therefore, one can conclude that the bromide is a well-ordered crystalline phase at this temperature. The resonances of crystalline phase become observable already at 247 K. The spectra obtained between 247 and 310 K are a series of *continuous intermediates* between the low-temperature crystal and the room-temperature condis phases, suggesting that the transition is largely gradual, interrupted occasionally by the disordering transitions listed in Table 2. The differences in the spectra between 310 K and 247 K can be interpreted by the combined effect of both conformational motion about the bonds C3 – C4 and C4 – C5, registered by the chemical shift changes of C-2/C-5 and C-3/C-6, respectively, in addition to some crystal structure changes which influence all carbon atoms. The observed transitions at 148, 167, and 196 K in the DSC experiments are, however, not clearly reflected in Fig. 28, because together they have an entropy change only large enough to account for the conformational change of little more than one bond per alkyl chain. Almost as much entropy-increase must thus occur outside of the transition regions and should be observable by heat capacity analysis.

181

The disordered state at room temperature can be preserved when quenching the sample. A quenching experiment is demonstrated in Fig. 29 by a series of ^{13}C CP-MAS NMR spectra obtained on cooling with approximately 60 K/min from 271 to 146 K (bottom four spectra). These four spectra show the effect of fast cooling, i.e., formation of a condis glass. The spectrum at 146 K in Fig. 29 shows the same chemical shifts for all carbon atoms as at 228 K. The increased line broadening at low temperatures is typical for materials in the glassy state. By heating the quenched sample from 146 K at a sufficiently slow rate, the glassy material undergoes a so-called "cold crystallization", as is illustrated by the six spectra at the top of Fig. 29. The spectrum at 232 K is still a typical amorphous glass, but the spectrum at 244 K has sharper resonances (especially for the outer carbon atoms, presumably because of motional averaging). As the temperature is increased further to 259 K, and eventually to 278 K, the spectra for the ordered crystalline phase can be observed (compared to Fig. 28 at 247 K and lower). Such discrepancy in the "crystallization" temperature between heating and cooling is often noted for polymers. As the temperature is further increased to 310 K, the crystalline phase disappears again. The spectrum of 310 K in Fig. 29 is the same as that of a fresh sample (Fig. 27). The glass transition temperature of the 271 K condis crystal can thus be estimated to occur at about 230 K and the cold crystallization at 260 K.

182

4.2.4 Tetra-*n*-heptylammonium Bromide and Iodide

Bromide: At room temperature, the bromide shows almost no cross-polarization efficiency, indicative of the presence of a motion in the kHz range that reduces the value of $T_{1\rho H}$ to very short values ($T_{1\rho H}$ is the proton spin-lattice relaxation time in the rotating frame). The spectrum measured with BILEV, shown in Fig. 31, indicates broad peaks for all carbon atoms (because of the kHz motion). The chemical shift values listed in the figure are, however, close to those of the iodide at the same temperature (see Table 19). The thermal transitions are also similar for both bromide and iodide (Table 2). The conformational motion and disorder is, therefore, expected to be similar for both cases. For these reasons, a detailed analysis will be carried out only for the iodide.

Iodide: In the tetra-*n*-heptylammonium cation, four bonds per alkyl chain are expected to disorder in going from a well ordered crystalline state to the isotropic melt. These bonds are, C2–C3, C3–C4, C4–C5, and C5–C6. In the DSC experiment one observes two transition regions. A first disordering at T_{d1} = 355.4 K with an entropy change of only 26.1 $JK^{-1}mol^{-1}$, and a second of two overlapping transitions at T_{d2} = 391.0 K and T_i = 398.7 K with entropy changes of 6.2 and 97.9 $JK^{-1}mol^{-1}$, respectively. After subtracting the entropy for positional disordering (*ca.* 21 $JK^{-1}mol^{-1}$) and orientational disordering (20–50 $JK^{-1}mol^{-1}$) from the combined entropy change of the latter two transitions of 104.1 $JK^{-1}mol^{-1}$, one obtains entropy changes for conformational disordering only of 33.1–63.1 $JK^{-1}mol^{-1}$, which is sufficient for only about one bond per alkyl chain becoming disordered in these

transitions. This bond is C2−C3, as can be seen from the T_1 values for C-2 and C-3 in going from 395 K to 405 K (see Table 20). At 395 K, C-2 and C-3 have similar T_1 values, while at 405 K (above the isotropization), the difference is obvious.

The three outer bonds, C3−C4, C4−C5, and C5−C6, must thus have been disordered at temperatures lower than T_{d2} (391.0 K). There is, indeed, the low-temperature transition at T_{d1} of 355.4 K, it shows, however, a rather small entropy change, 26.2 $JK^{-1}mol^{-1}$, and is insufficient to account for even one full bond per alkyl chain becoming disordered. The situation of "entropy deficit" was encountered above in $(C_5H_{11})_4NBr$ and $(C_6H_{13})_4NBr$, and similarly in another small, liquid crystal forming molecule, N,N'-bis(4-n-octyloxybenzal)-1,4-phenylenediamine (OOBPD), that shows additional condis crystal polymorphs at low temperature (shown in Sect. 4.4). A macromolecule with phenylene, ether, and methylene sequences, MBPE-9, forming condis crystals below the melting transition could also be proven to have such entropy deficit (also shown in Sect. 4.5). In all examples it could be shown by variable-temperature solid-state ^{13}C NMR and comparison between the experimental and calculated heat capacities that the disordering between some single C−C bonds occur gradually, i.e., over a wide range of temperatures without transition. For the tetra-n-heptylammonium cation under consideration, the same analyses is attempted next.

The variable-temperature NMR spectra measured from 180 to 310 K (considerably below T_{d1}), shown in Fig. 32, show little changes in chemical shift. The numerical values of chemical shift of each carbon atoms are listed in Table 19. Only

184

C-6 and C-7 show noticeable changes. At 180 K, C-6 resonates at 26.22 ppm and is separated from C-2 (at 25.21 ppm). As temperature increases to 290 K, the signal of C-6 becomes gradually superimposed on C-2 (at 25.74 ppm). The two signals of C-7 (the methyl carbon) experience also a gradual up-field shifting. The difference for both C-6 and C-7 between 290 and 180 K is too small (< 0.5 ppm) to account for conformational disordering, thus below T_{d1} the iodide forms an ordered phase in which motion is allowed only in the end groups.

The first phase transition on heating (355.4 K) is reflected by changes in the variable temperature ^{13}C NMR spectra from 322 to 364 K (Fig. 33). The changes in chemical shift from 322 to 364 K for the carbon atoms are: C-1, -2.67 ppm; C-2, -0.17 ppm; C-3, $+0.01$ ppm; C-4, -1.05 ppm; C-5, -0.72 ppm; C-6, -0.97 ppm; and C-7, -0.27 ppm. These changes can not be interpreted exclusively by the γ-gauche effect, therefore, the cause for this low-temperature transition must be a combined effect of conformational and packing changes. In fact, one finds the following: the largest change for C-1, small changes for C-2, C-3 and C-7, and moderate changes for C-4, C-5 and C-6. The chemical shift of C-1 is largely influenced by its partial positive charge, not by the change in the rotational state of the bond $C2-C3$, since this bond is known not to be flexible below the high-temperature transition. Thus, a re-distribution of the charge on C-1 is plausible. The charge redistribution on C-1 arises if the anion, I^-, changes its position in the crystal relative to the C-1. The approximately 1 ppm changes in chemical shifts in the outer carbon atoms, C-4, C-5, and C-6, are not likely to be due to the anion positional change, since they are

practically neutral carbons. Because C-2 and C-3 are less charged atoms and, at the same time, are also remote from the mobile chain end, their chemical shifts are influenced less by the inter-ion distance change and little by the conformational motion. The same is true even when considering the wider range of temperatures from 180 to 385 K. The methyl carbon, C-7, shows a pattern changes from a doublet at and below 310 K to a single line at 364 K and higher, and the average chemical shift decreases by 1.67 ppm between 180 and 385 K, indicative of its large mobility due to rotations about its C_3-axis as well as motion about C5 – C6. Results of X-ray structure analysis are needed for a more detailed explanation for the changes of chemical shift that could not be interpreted by the conformation-dependent γ-*gauche* effect.

Of particular interest is the behavior of the high-temperature condis phase formed between T_{d1} = 355.4 K and T_{d2} = 391.0 K. Except for C-1, the chemical shifts of all other carbon atoms in the heptyl chain undergo further up-field drifting as temperature is increased from 364 to 385 K (Fig. 33 and Table 19). The chemical shift changes are comparable to or larger than that observed at T_{d1} (355.4 K). These sizeable gradual changes are indicative of a development of conformational disordering. This conclusion is supported by the mobility seen from the ^{13}C NMR powder spectra measured on a static sample shown in Fig. 34. The conformational motion in the heptyl chain at 366 K averages the chemical-shift-anisotropy interactions to such a degree that the spectral lines are much more resolved than at 310 K. Since the chemical shift anisotropy of a rigid methylene carbon is expected

to extend over *ca.* 40 ppm (2 kHz at 4.7 Tesla) (Jelinski and Melchior, 1987), the time scale of the motion of the carbon atoms that show well resolved signals at 366 K must be about 1/(2 kHz) or 500 μs. Condis crystals with motion of such an intermediate mobility show both CP and BILEV signals, as is demonstrated in the spectra of Fig. 34 (see also the spectra for $(C_4H_9)_4NBr$ in Fig. 22 at 384 K).

Finally, the large chemical shift changes are found at the overlapping transitions ranging from T_{d2} (391.0 K) to T_i (398.7 K). The loss of positional, orientational, and the remaining conformational order between the bonds C2–C3 must be responsible for the observed changes in entropy and the chemical shifts shown in Table 19.

In summary, tetra-*n*-heptylammonium iodide is a condis crystal below its isotropization, and never a plastic crystal. The conformational motion and disorder is developed to a large extent gradually between the two disordering transitions. This observation explains the entropy deficit observed at the phase transitions by DSC. Further support for this surprising discovery will be shown by X-ray diffraction (Habenschuss *et al.*, 1992) and heat capacity analyses (Xenopoulos *et al.*, 1992), presently in progress. Based on the similar entropy data and ^{13}C chemical shift values measured at room-temperature, the tetra-*n*-heptylammonium bromide is expected to also have a gradual conformational disordering process occurring either below the low-temperature transition (339.5 K) or between the disordering transition and isotropization (366.5 K).

4.2.5. Summary

In the intermediate chain length tetra-n-alkylammonium bromides and iodides, two types of mesophases are possible below the isotropization temperature: plastic crystals with orientational and conformational disorder and motion, and condis crystals with conformational disorder only. Furthermore, the condis crystals may be quenched to glasses.

In tetra-n-butylammonium iodide, the molecules become orientationally and conformationally disordered in a single crystal-to-plastic-crystal transition. The plastic crystal in $(C_4H_9)_4NI$ has a maximum degree of conformational disorder (one bond per butyl chain). In tetra-n-butylammonium bromide, although the mesophase is a condis crystal, it shows considerable orientational motion (libration) introduced gradually as a function of temperature.

As the alkyl chain-length becomes longer, complete orientational and positional disordering takes place only on isotropization. Below T_i, the molecules may still be disordered conformationally (condis crystal). The conformational disordering occurs differently for different crystals.

In the tetra-n-pentylammonium salts, one of the two disorderable bonds per alkyl chain ($i.e.$, C_3-C_4) gains conformational disorder on isotropization at T_i, while the other one ($i.e.$, C_2-C_3) becomes gradually disordered for the bromide (without transition), and for the iodide disordered in one step during a low-temperature transition with the expected entropy.

188

In tetra-*n*-hexylammonium iodide, all three disorderable bonds of the hexyl chain become conformationally disordered below T_i through two overlapping transitions. In tetra-*n*-hexylammonium bromide the conformational disordering is more complicated. Two of the three disorderable bonds of the hexyl chain become disordered more or less gradually at lower temperatures, and the other one is also disordered largely gradually, however, at higher temperatures. The condis phase of the bromide can be quenched to a glass.

In tetra-*n*-heptylammonium iodide, the conformational disordering of the outer bonds occurs to a large extend gradually between the two disordering transitions. Of the two relatively small disordering transitions T_{d1} and T_{d2}, the first is likely to be caused mainly by anion rearrangement, and initiates the conformational disordering of the outer bonds. The other (together with isotropization) causes the disordering of the innermost potentially mobile bond C2 – C3. The bromide is expected to behave similarly.

In the cases of gradually gaining conformational disorder, *e.g.*, in tetra-*n*-pentylammonium bromide, tetra-*n*-hexylammonium bromide, and tetra-*n*-heptyl-ammonium iodide, heat capacity studies are in progress in this laboratory to support the NMR conclusions with quantitative entropy information.

4.3 Disorder and Motion in the High Homologs of Tetra-*n*-alkyl-ammonium Salts

4.3.1 ^{13}C Chemical Shift Value of the Crystalline Phase

So far, the ^{13}C NMR spectra have been obtained for all the available tetra-*n*-alkylammonium salts. It is interesting to examine the low temperature ^{13}C chemical shifts. The ^{13}C CP-MAS NMR spectrum of the crystalline phase is characterized by the well separated resonances of the different carbon atoms (fingerprint). There are at least six resolvable signals arising from a sufficiently long alkyl chain, as is shown in the low temperature spectra of Figs. 35–39. These six resolvable peaks can be assigned by comparison with solution ^{13}C spectra, studied using two-dimensional NMR techniques (Cheng *et al.*, 1992), to six carbon atoms, three being close to the nitrogen as C-1, C-2, and C-3, and the other three at the chain end as C-*x*, C-*y*, and C-*z*; C-*z* being the methyl carbon atom).

The chemical shift assignments for the crystals of all available compounds at sufficiently low temperatures are given in Table 26. The prior reported data for tetra-*n*-hexyl- and heptyl compounds (see Sect. 4.2) are also included in this table. Except for some of the inner carbons in $[CH_3(CH_2)_{11}]_4NBr$ and $[CH_3(CH_2)_{17}]_4NBr$, the chemical shift values for a given carbon atom in different compounds are close enough to obtain average values. Table 26 contains also the average chemical shifts measured in $CDCl_3$ solution, which were determined using two-dimensional NMR

techniques [namely proton homo-nuclear shift correlated (COSY) and ^{13}C-^{1}H shift correlated (XHCORR)] (Cheng, *et al.*, 1992).

From Table 26, one observes the following: (1) The three carbon atoms on either end often have comparable values. The exceptions listed in Footnote d of Table 26 may point to special crystal structures of these compounds. Such a special crystal structure would also explain the double peaks of C-1 in 18Br and of all carbons in 12Br. (2) Comparisons of the average chemical shift values for the crystals in Table 26 and those of solutions show that upon dissolution, the shielding of C-1 changes the most (−4.6 ppm), while for the rest of the carbon atoms the difference in chemical shift exhibits a maximum towards the middle of the chain. The large change of chemical shift for C-1 (which carries the largest positive charge) is due to the obvious change in distance between nitrogen and the anion on dissolution. The changes of chemical shift for the more neutral carbon atoms, C-2 through methyl carbon, should be caused mainly by conformational disorder which is present in solution, but largely absent in the crystalline phase due to crystallization to a mainly *trans* conformation. The trend that the carbon atoms at the middle of the chain have a maximum differential chemical shift is brought about because only they may have two γ-substituents that become partially *gauche* on dissolution. Since each of the *γ-gauche* substituents contributes a shielding effect of −5.2 ppm (Tonelli, 1989) for one *gauche*-bond γ to the carbon atom in question, the observed contribution of the *γ-gauche* effect in going from all-*trans* in the crystalline phase to the typically 40% *gauche* concentration in solution is about −5.2 × 0.4 × 2 = −4.16

ppm for two *gauche*-bonds γ to the analyzed carbon. The observed differences for C-4 through C-*w* between crystal and solution are, thus, expected to be about −4.16 ppm. For C-1, C-2, C-3, C-*x*, C-*y*, and C-*z* which have only one possible γ-*gauche* effect, the observed differences are expected to be closer to half of this value. Although this rule is not perfectly obeyed it can in many cases give a satisfactory explanation of the observed chemical-shift differences between two phases.

4.3.2 Tetra-*n*-octylammonium Bromide

From calorimetry, the total entropy of fusion is 129.0 $JK^{-1}mol^{-1}$ (Table 2). According to the empirical fusion rules (Wunderlich and Grebowicz, 1984; Wunderlich *et al.*, 1988), this value is less than expected by about: $[(\Delta S_{conf.} \times 4 \times 5) + \Delta S_{orient.} + (\Delta S_{pos.} \times 2)] - 129.0 = [(9.5 \pm 2.5) \times 4 \times 5 + (35 \pm 15) + (10.5 \pm 3.5) \times 2] - 129.0 = 116.6 \pm 24.5$ (in $JK^{-1}mol^{-1}$). The multiplier 4 accounts for the four alkyl chains per cation, the multiplier 5 for the five single C−C bonds that can be disordered, and the multiplier 2 accounts for the positional disorder of both cation and anion. The entropy deficit of 116 $JK^{-1}mol^{-1}$ may well be made up by conformational disordering of *three* bonds per alkyl chain ($9.5 \times 4 \times 3 = 114$ $JK^{-1}mol^{-1}$) that occurs outside of the transitions.

A detailed look at the changes of the chemical shifts is given by Fig. 49. The atoms C-3 to C-8 show a continuous decrease in chemical shift below T_d (323 K). All atoms show a break at T_d and only C-1 and C-2 show irregular, almost constant chemical shifts between T_d and T_i (374 K). In the melt, C-1 to C-4 and C-8 show the
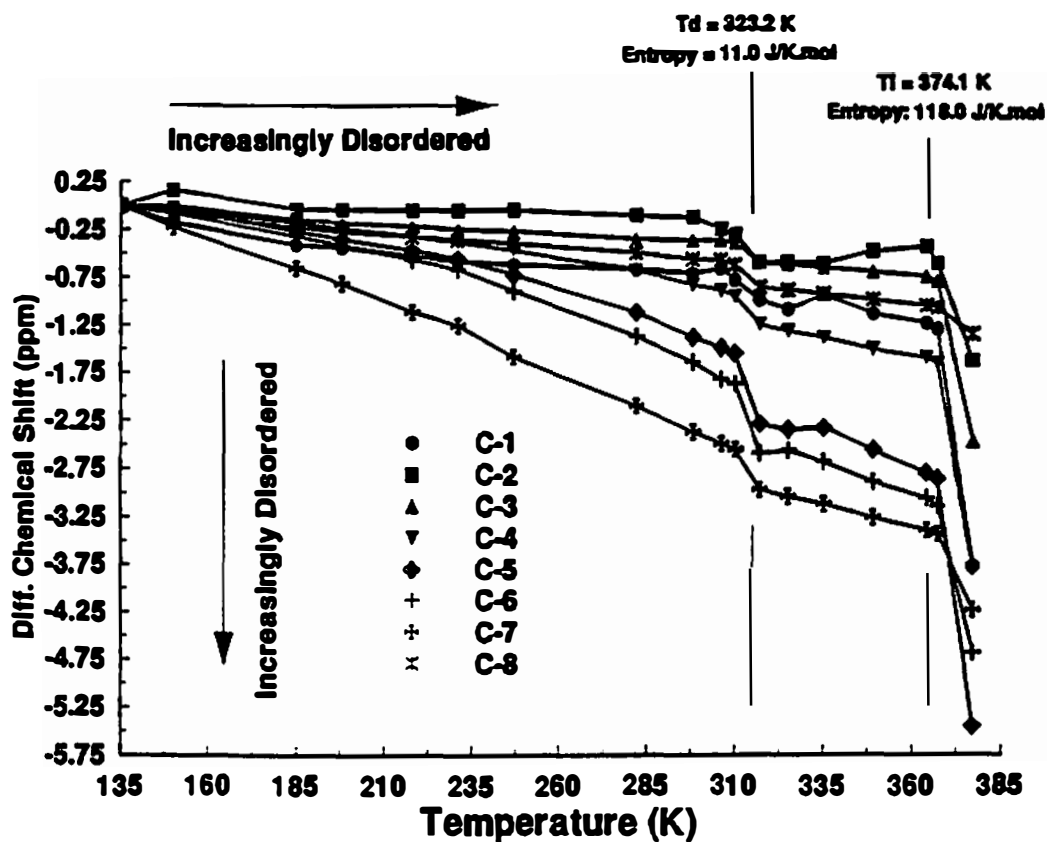
Figure 49   Plots of differential chemical shifts for all carbon atoms in tetra-*n*-octylammonium bromide (chemical shift at *T minus* the chemical shift at 135 K). The transition temperatures observed by DSC are marked by the two vertical lines, and are also listed in the figure along with the entropy changes.

expected decreases in chemical shift (see Table 21), while C-5 to C-7 show 2–4 ppm larger chemical shifts than expected from the discussion of Table 26, above. If one assumes that the extra chemical-shift changes originate from intermolecular sources and are changing largely parallel with the increase in motion in the vicinity of the carbon atom in question, one can speculate that motion is introduced as follows: At about 150 K bonds C6–C7, C5–C6, and C4–C5 become mobile with a decreasing degree of *gauche* concentrations in the sequence listed. Almost all of the change in chemical shift in C-5 to C-7 is, however, caused by intermolecular effects, as judged from the smaller decreases for C-3, C-4, and C-8. For equal *gauche* concentrations in these three bonds, equal γ-*gauche* effects are expected for C-3 to C-8. The transition at T_d brings (because of its small entropy) mainly a packing adjustment with further increase in the disorder about bonds C6–C7, C5–C6, and C4–C5 occurring above T_d. Only on isotropization are bonds C2–C3 and C3–C4 randomized, as seen from the larger changes in chemical shift of C-5 and C-4 (affected by two bonds) as well as C-1 and C-2, and as is expected from the entropy of isotropization of 118.0 $JK^{-1}mol^{-1}$ [conformational: $(7-12) \times 4 \times 2 = 56-96$, orientational: $20-50$, positional: $(7-14) \times 2 = 14-28$, all in $JK^{-1}mol^{-1}$].

The important aspects of motion and disorder in tetra-*n*-octylammonium bromide are thus: (1) It forms a well-ordered crystal at low temperatures (below 150 K) as indicated by the typical values of ^{13}C chemical shifts, (2) Most (90%) of the entropy of fusion is observed at the isotropization. (3) The difference between the experimental entropy of fusion and that of predicted (deficit of entropy of fusion) is

194

comparable to the entropy change of 3 bonds per alkyl chain that become conformationally disordered below T_i. (4) If one realizes the fact that the long alkyl-chain tetra-n-alkylammonium salts loose their orientational and positional order at isotropization only, these observations then suggest that this salt exists as a condis mesophase below isotropization with 3 bonds disordered. It is probable that the already-disordered bonds are those at the chain end, namely, C4−C5, C5−C6, and C6−C7. The conformational disordering is seen to be a rather gradual process over a temperature range from as low as 150 K. (5) The phase transition at 323 K does not introduce additional major disorder and can be looked upon as a change in crystal structure between two condis crystals.

It is hoped that detailed heat capacity and X-ray diffraction studies in progress can resolve the remaining questions concerning this interesting salt.

4.3.3 Tetra-n-decylammonium Bromide

The ^{13}C NMR spectra, plotted in Fig. 36, show only small changes below the disordering transition (T_d = 348.6 K, with ΔS_d = 160.8 JK^{-1}mol^{-1}), suggesting that major disordering occurs only at and above T_d. The entropy change corresponds to 4 bonds per alkyl chain becoming disordered. These four bonds can be proven by the γ-$gauche$ effect to be those at the chain end, namely, C5−C6, C6−C7, C7−C8, and C8−C9. Comparison between the spectra at 310 and 351 K shows that the chemical shifts for C-1, C-2, and C-3 remain constant, while the others change by different amounts (see Table 22). The chemical shift change for C-4 (−1.3 ppm) is

195

due to the disordering about the bond C5−C6, the changes of C-5 and C-6 (−1.8 ppm) are due to the bonds C6−C7 and C7−C8, respectively; the C-7 (−4.4 ppm) shows uniquely effects due to two *gauche*-bonds C5−C6 and C8−C9; the change of C-8 (−2.1 ppm) is due to C6−C7; C-9 (−1.7 ppm) due to C7−C8; and finally C-10 (−0.71 ppm) is due to C8−C9. Although the change for the methyl carbon (C-10) is small, its resonance pattern changes from four lines to one, a clear indication of averaging over different crystal positions. The smaller change for C-4 permits further up-field shifting at higher temperatures discussed in the next paragraph. In contrast to the octyl compound the changes in the decyl cation are abrupt at the transition instead of gradual before the transition.

On isotropization, the spectra in Fig. 36 show large changes in the resonance positions for C-1, C-2, and C-3, indicating conformational disordering about the bonds C2−C3, C3−C4, and C4−C5, respectively. Other carbon atoms, for example, C-4 to C-8, undergo further up-field changes in the chemical shift (but with relatively smaller amplitudes), indicating perhaps further increase in the *gauche* content in the corresponding bonds. A comparison between the spectra of melt and solution in Fig. 36 reveals that there is still an about 1 ppm difference in the chemical shift values for the inner carbon atoms, such as C-1, C-2, C-3, and perhaps C-4, but there is almost no difference for the chain-end atoms, such as C-9 and C-10. The reason may be that the inner-bonds have less *gauche* concentrations or mobility and different charge distributions in the molecules of the melt.

From this analysis, it is concluded that tetra-n-decylammonium bromide forms a well-ordered crystal phase below T_d = 348 K, a condis phase between T_d = 348 K and T_i = 363 K with only four bonds disordered per alkyl chain, and finally a melt above T_i with all bonds except N-C1, C1-C2, and C9-C10 contributing to conformational disorder. Disordering seems to occur stepwise only.

4.3.4 Tetra-n-dodecylammonium Bromide and Iodide

Bromide: The observed total entropy of fusion for tetra-n-dodecylammonium bromide (341 $JK^{-1}mol^{-1}$) is within the expected range of 286–510 $JK^{-1}mol^{-1}$. The large uncertainty of the empirical rules for such long alkyl chains, however, leaves the possibility of disordering of 2–3 bonds per alkyl chain outside of the transitions.

Below the lowest transition temperature (225 K), the ^{13}C NMR spectra show double peaks for each distinguishable carbon from C-1 to C-11, while for the methyl carbon, C-12, four lines are clearly evident (Fig. 37). This complicated spectrum proves non-equivalency among the four alkyl chains, i.e., a low symmetry of the cation. The spectra below and above the 225 K transition do not indicate any significant change. The transition must thus be a solid-solid transition without major change in mobility and relative packing of the motifs of the crystal. The rather low entropy of transition is in accord with such interpretation.

Examining the wider range of temperature, from 168 K to 346 K (just below the second transition temperature on heating), reveals that: (1) the methyl carbon (C-12) resonance undergoes a coalescence from four-lines to a single line, (2) the

chemical shift values for C-11 decreases gradually from 26.4/26.0 ppm (doublet) to 24.6 ppm (single peak). (3) similar to C-11, C-10 also experiences such gradual change (from a double peak of 36.7/36.2 ppm to single line of 35.0 ppm), (4) changes for the carbons in the middle of the alkyl chain, and even more for the innermost carbon atoms, are less. These observations suggest that the chain ends undergo, indeed, a gradual disordering below the major transition temperature.

The onset of the overlapping transitions from 347 to 363 K is reflected by the obvious up-field shifting of the carbon atoms in the middle of the chain, as shown from the spectra from 336 to 352 K. These carbons resonate at about 34 ppm at 336 K, while at 352 K an enhancement in the intensity of the peak at about 31.5 ppm is apparent. The change of about −2.5 ppm can again be explained by the γ-*gauche* effect. Unfortunately, due to the serious overlapping between the resonances of carbon atoms in the middle of the dodecyl chain, it is difficult to make an quantitative evaluation of the bonds that have become *gauche*.

Upon isotropization (363 K), the peaks of the carbon atoms in the middle (at about 34 and 31.5 ppm) move further down-field to 30.5−30.0 ppm, as indicated in Fig. 37 and Table 23. The inner-most carbon atoms also show changes. The double-peak of C-1 becomes a singlet in the melt, the C-2 signal decreases by 1.4 ppm, and C-3 changes from a rather broad peak centered at about 29 ppm to a sharp one at 27.3 ppm.

Another interesting feature in this salt is the change of the C-1 resonance. The double-peak undergoes a up-field shifting between 310 and 336 K, a temperature

range where no transition is observable in the DSC experiment. This change is probably associated with a crystal structure change in which the distance between the nitrogen and bromide is altered. Similar up-field shifting of the C-1 resonance in the octyl- and decyl-compounds were only observed on isotropization, as shown in Figs. 35 and 36.

Iodide: A series of transitions was reported for this salt as shown in Table 5. The data in parentheses indicate overlapping transitions. Unlike the bromide discussed above, the total entropy of fusion for the iodide (271 $JK^{-1}mol^{-1}$) is clearly below the expected range of $286-510$ $JK^{-1}mol^{-1}$.

The resonances of carbon atoms at the chain end undergo a clearly noticeable continuous change from 202 to 310 K (see Fig. 39). The separation of the doublet of C-12 (methyl carbon) decreases from 1.57 ppm at 202 K to 0.41 ppm at 310 K; C-11 initially superimposes with C-2 at 26.0 ppm at 202 K, but shifts to 24.5 ppm at 310 K (while C-2 remains at the same position); C-10 also undergoes a gradual, up-field change from 36.1 to 35.1 ppm. Because of the chemical shift changes in C-12, C-11, and C-10, the resonances of their γ-substituents C-9, C-8, and C-7, respectively, undergo similar changes (γ-*gauche* effect) as evidenced by the noticeable change in the overlapping signal at about 32 ppm. The gradual changes in the three chain end atoms and their γ-substituents, thus, explain the entropy deficit. The peaks for the inner-most carbon atoms remain unchanged.

The transition at 284.1 K shows an entropy change of only 12.3 $JK^{-1}mol^{-1}$, which is much less than that for the conformational disordering of even one bond per

alkyl chain (about 38 $JK^{-1}mol^{-1}$). This transition is, nevertheless, reflected by the change in resonances of carbon atoms in the middle of the chain, as can be seen from the up-field shifting of the peaks at about 34.5 ppm in going through the transition. A transition involving mainly changes in cation packing is the likely explanation.

From 310 K to 343 K, although no transition is observable in DSC experiment, the line shape of the peak arising from the carbons in the middle of the chain at about 34 ppm undergoes further gradual change (see Fig. 40). Above 343 K, the overlapping endotherms observed in the DSC corresponds to a gradual change in the peaks of around 31.5 ppm (middle of the chain) shown in the spectra from 346 to 371 K (Fig. 40). The 343 K transition may also involve a crystal-structure change, as indicated by a rather large up-field shifting in the peak for C-1 (changes from 64.4 ppm at 338 K to 61.2 ppm at 346 K).

Finally, the comparison between the spectra at 384 and 390 K shows that on isotropization (389 K) another stepwise up-field shifting of the peaks for the middle of the chain is introduced. It is interesting to see that the signals for C-1 and C-2 change by −0.3, −0.4 ppm only, but C-3 by −1.3 ppm. This behavior may indicate that the bonds C2−C3 and C3−C4 are still rigid even in the melt of 390 K, and may also be used to explain the entropy deficit. With increasing of the temperature, the signals of C-1 and C-2 are expected to become more shielded (smaller chemical shifts).

In summary, the dodecyl compounds of bromide and iodide start to show gradual conformational disordering at the chain ends at temperatures below the reported transitions. The disordering and isotropization transitions observed in the DSC experiments can be linked with the stepwise conformational disordering about the bonds in the middle of the chain (C-4 through C-9). Below the isotropization, both salts may have a crystal structure change involving the rearrangement of the distances between nitrogen and the anion, as indicated by the large abrupt change in the C-1 resonance.

4.3.5 Tetra-*n*-octadecylammonium Bromide

Below the transition of 375 K, the low temperature ^{13}C NMR spectrum, similar to tetra-*n*-dodecylammonium bromide, shows double peaks for the inner-most carbons, C-1 and C-2 (see Fig. 38 at 310 K), indicating the low symmetry of the cation. The carbon atoms at the chain end, on the other hand, behave as expected for a well-ordered crystal in terms of multiplicity and chemical shift values. The spectra obtained at 310 and 351 K show no obvious difference except for rather small changes of resonance pattern for the methyl carbon (C-18) and a slight up-field shifting of C-17 and C-16 by about −0.4 ppm (see Table 24). The strongest peak containing approximately 8−10 carbons (out of the total of 18) moves very little. Thus, the conformational disordering below the phase transition is small.

At the phase transition (375 K), major change is found for the strongest peak between 351 and 375 K. A decrease from 34.2 to 33.0 ppm can be linked to the

observed entropy change of 227 $JK^{-1}mol^{-1}$. The signals of C-1 change from two lines at 351 K to a single sharp peak at 375 K is, again, indicative of the rearrangement of ions (caused by a crystal structure change). Isotropization is indicated by yet another obvious change (-2.5 ppm) for the strongest peak between the two spectra measured with different pulse sequence (BILEV and CP-MAS), both at 378 K. The top spectrum in Fig. 38 was obtained using BILEV method which shows mainly the liquid signals, while the CP-MAS spectrum shows only the solid signals.

Thus, in tetra-n-octadecylammonium bromide, only stepwise conformational disordering is observed. The phase transitions are mainly caused by the conformational changes in the middle of the alkyl chains. The entropy contribution from the gradual conformational disordering about the bonds at chain end is small.

4.3.6   Summary

The high homologs of symmetric tetra-n-alkylammonium bromides and iodides form well-ordered crystal phase at sufficiently low temperature, indicated by their typical ^{13}C NMR spectra (fingerprint) and unique chemical shift values.

Conformational motion and disordering starts from the chain ends either gradually or stepwise. Gradual conformational changes at the chain end are found for tetra-n-octylammonium bromide, tetra-n-dodecylammonium bromide, and tetra-n-dodecylammonium iodide, while a stepwise change is seen for the bromides of tetra-n-decylammonium and tetra-n-octadecylammonium. As the temperature is increased

further, the bonds in the middle of the chain become disordered in steps within the mesophase-transition detected in the DSC experiments. Finally, isotropization occurs with all remaining types of disordering, *i.e.*, positional, orientational, and conformational.

Crystal structure changes, indicated by a large up-field shifting of the C-1 resonance, occurs below isotropization in the cases of tetra-*n*-butylammonium bromide, tetra-*n*-hexylammonium bromide, and tetra-*n*-heptylammonium iodide, as shown in Sect. 4.2 and the bromide and iodide of tetra-*n*-dodecylammonium and bromide of tetra-*n*-octadecylammonium, shown in this section.

4.4   N,N'-*bis*(4-*n*-octyloxybenzal)-1,4-phenylenediamine   (OOBPD)

4.4.1   Introduction

It was suggested using calorimetry and structure analyses of the transitions (Wunderlich *et al*, 1986;   Wiedemann *et al*, 1986) that the assignment of the mesophase structure K3/385.2/K2/388.2/K1/415.3/H'/422.2/G'/426.9/I/436.6/C/ 475.4/N/505.4/Melt (temperatures in K) could be refined by stating that K1 to K3 are still mesophases that are conformationally disordered (condis crystals). It will be shown that it is not only possible to have a stepwise freezing of motion and disorder of the melt to nematic (N) and the various smectic phases (C, I, G' and H'), but also to continue this stepwise freezing through several condis states (K1, K2, and K3).

203

In addition a large amount of conformational entropy is gained outside of the transition regions. In the condis state the crystals have lost the translational disorder and mobility of the liquid crystals, but maintain still various degrees of conformational disorder and mobility (Wunderlich and Grebowicz, 1984).

In order to fully characterize the proposed condis phases K1 – K3 and their relationships to the liquid crystalline phases G' and H', direct observations of the mobility of both the octyloxy chains and the mesogen are made using variable-temperature solid state ^{13}C CP-MAS NMR. In addition, the heat capacity has been measured between 130 K and 550 K by DSC and fitted at low temperature to an approximate frequency spectrum. The calculated vibration-only heat capacity starts to show deviations from the measured one at about 200 K, reflecting beginning contributions of conformational disorder and motion in the octyloxy chains which is initially similar to paraffins such as octane (Jin and Wunderlich, 1991), then reaches, however, the much higher level of the liquid, so that a major entropy gain beyond that of a hypothetical rigid, vibration-only crystal occurs outside and before the sharp endothermic transition peaks from K3 to K2 and K1.

4.4.2 Chemical Shift Assignments of the Solution NMR Spectrum

A correct assignment of chemical shifts (δ values) to the individual carbon atoms is important because the δ value is sensitive to the molecular motion *and* conformation.

The measurement of an NMR spectrum in the melt was not possible because the melting temperature for OOBPD (505.4 K) is higher than the highest allowable temperature of the NMR probe (430 K). The melt spectrum is, nevertheless, expected to be the same as a solution spectrum because the molecular motion should be similar in both liquids. Therefore, the solution spectrum has been compared with the spectra of the solid state at lower temperatures. With the solution spectrum shown in Fig. 41, one can make the δ assignments for all the carbons as shown in Tables 27 and 28 for the mesogenic and alkoxy groups, respectively.

The assignment of the methylene ^{13}C's in the octyloxy chain (see Table 28) was made by comparing with the spectrum of n-octane whose ^{13}C δ values are known to be, from the end (methyl) to the center, 14.2, 23.2, 32.6, and 29.9 ppm (Silverstein *et al.*, 1981). In OOBPD the chemical shifts of methylene carbons of the octyloxy chain are, however, subject to the influence of *substituent effects* from the oxygen. The available data (Sadtler Research Lab) on the alkyl carbons of aralkyl ethers (with the group of phenylene − oxygen − alkyl) show that when the alkyl chain consists of more than 5 carbons, the oxygen has a positive substituent effects (deshielding) of +55 and +5.8 ppm on the α- and β-carbons, *i.e.*, C-8 and C-9, respectively. Thus, the measured values of 68.35 and 29.29 ppm are assigned to C-8 and C-9, respectively. The oxygen, however, has an negative substituent effect (shielding) of about −6.5 ppm on the γ-carbon, which causes C-10 to resonate at 26.10 ppm. The rest of the carbons are not influenced by the oxygen. Their δ values agree well with the respective carbons in n-octane. The signals of C-11 and C-12 are one single, intense

peak at 29.29 ppm, overlapping with C-9, while C-13, C-14 and C-15 appear at 31.84, 22.67 and 14.00 ppm, respectively.

For the aromatic carbons, the assignments can also be made based on the consideration of substituent effects. Detailed values of the substituent effects on aromatic ^{13}C's can be found in the literature (Silverstein *et al.*, 1981; Stothers, 1972). The predicted values are in good agreement with the measured ones. Table 27 summarizes the results for all carbon atoms in the mesogenic group.

4.4.3 Conformational Isomers

Mesogen: Fig. 41 shows that, except at 431 K (where the carbons in the mesogenic group show hardly any resonances), all solid state ^{13}C spectra at and above 395 K are similar to the solution spectrum, therefore, the δ values of Tables 27 and 28 are close to that of the solution.

In the spectrum at 380 K, below the transition to the K3-phase, the chemical shifts of all non-protonated carbons, C-2, C-4, and C-7 as well as the methine carbon C-3 remain approximately the same and continue at these values down to the lowest temperature measured (187 K), while the δ for the protonated aromatic carbons, namely, C-1, C-5, C-5', C-6, and C-6' change significantly. The δ value for C-1 changes from 124.1 ppm at 395 K to 116.2 ppm at 365 K. The signals for C-5, C-5' become not observable at 380 and 365 K, and split into a pair as the temperature decreases further from 350 to 308 K. The same is also observed for C-6 and C-6'. At 321 K (the spectrum is not shown, but is very similar to that of 308 K) and below,

signals of C-5 and C-5' can be observed at about 136.5 and 128.6 ppm, respectively. While C-6 and C-6' resonate at about 116.7 (distinguishable from C-1 at 116.1 ppm), and 110.0 ppm, respectively.

These features of the mesogen indicate the process of an increasing mobility of 180° phenylene ring flipping with increasing temperature. At temperatures below 321 K, the absence of the ring flip induces magnetic inequivalence in two pairs of carbon atoms on the ring, namely C-5/C-5' and C-6/C-6'. The C-5 is more shielded (smaller δ value) than C-5' because of the stronger steric interaction arising from the shorter distance between C-5 and H-3 (the proton attached to C-3). The inequivalence of C-6 and C-6' is due to a locked orientation of the alkoxy group with respect to the benzene ring, which can always be found in a series of thermotropic phenyl benzoates. As temperature is increased to about 336 K, the phenylene rings become mobile. If the motion is that of a rotation about its 1,4 axis (flipping), C-5 will exchange position with C-5', and C-6 with C-6'. When the rate of the flipping is comparable to the frequency separation of the signals at lower temperatures (about 400 Hz for C-5/C-5', and 325 Hz for C-6/C-6'), coalescence of the signals is to be observed. The spectra at 336 and 350 K show the onset of this coalescence, where the spectral lines are too broad to be observed. At temperatures higher than the transition to the K1 state (385 K), the sufficiently fast phenylene ring flipping averages between C-5 and C-5' as well as C-6 and C-6', resulting in average positions of 131.9 and 114.9 ppm for C-5/C-5' and C-6/C-6', respectively.

The coalescence of the signals of a pair of carbon atoms that are inequivalent in the solid state has been observed for a residue of bisphenol A by Garroway and co-workers (Lyerla *et al.*, 1982). The signals of two *meta*-carbons (meta to the oxygen) were observed to be distinct over the temperature range 150–350 K, and then undergo coalescence at higher temperatures as motional averaging occurs. The same situation was also found for the two *ortho*-carbons in the bisphnol A residue. The inequivalency of the ^{13}C's in the identical symmetry positions in the phenylene rings of poly(*p*-hydroxybenzoic acid) and poly(2,6-dimethoxy *p*-hydroxybenzoic acid) was also observed in the solid state (Fyfe, *et al.*, 1979).

The phenylene ring flipping starting gradually at about 336 K in OOBPD occurs considerably lower than the first sharp transition. This temperature and the observed entropy change of 47 J/(K mol) will be shown below to be largely the consequence of disordering in the paraffin chains. The total combined entropy of all transitions at higher temperatures, *i.e.*, to H', G', I, C, N, and melting, is about 59 J/(K mol) from the present measurement, somewhat larger than the earlier value of 41.6 J/(K mol) of Wiedemann *et al.*, (Wiedemann *et al.*, 1986), because of a better baseline adjustment. This value is within the range of 20 to 59 J/(K mol) for the positional and orientational disordering of a single, rigid, nonspherical motif (average value 36 ± 10 J/(K mol), anthracene = 58.9 J/(K mol)) (Wunderlich, 1980).

In OOBPD, the motionally averaged δ value of 131.9 ppm for C-5/C-5' at higher temperatures is approximately the middle of the two resonances at lower temperature, 132.6 ppm, while the δ value for C-6/C-6' at higher temperatures, 114.9

ppm, differs somewhat from the middle of the two at lower temperature, 113.4 ppm. All C-1 carbons appear to be equivalent at all temperatures by having a single peak. This is probably due to the rather long distance between the central phenylene ring and H-3 that renders C-5 and C-6 to be inequivalent from C-5' and C-6', respectively, at low temperatures. The temperature at which the δ of C-1 changes is well within the ranges of the transitions between the K phases (385 – 388 K), the signal jumps from 116 ppm at 380 K to about 124.1 ppm at 395 K.

The rate constant, k, of the ring flip at coalescence temperatures, 336 – 380 K, can be evaluated from exchange-broadened NMR spectra, using the expression shown by Sandström (1982):

$$k = \pi(\delta v)/\sqrt{2} \qquad\qquad (35)$$

where δv is the frequency separation of the signals below the temperatures of coalescence. As shown above, δv is about 400 Hz at 308 K, thus at the coalescence temperatures centered at 365 K, the rate of the ring flipping is about 900 s^{-1}.

The T_1 data can be used to evaluate the mobility and to support the δ assignments made above. In the solid state the motional correlation time is usually on the long-time side of the T_1 minimum (except for the methyl carbon). Therefore, as the mobility increases because of the temperature increase, the values of T_1 decreases, as shown in Table 29.

At 350 K and below, the T_1's of the ^{13}C's in the mesogenic group are estimated to be much longer than 100 s, indicating the fact that the motion in this part of the molecule is frozen. As the temperature is increased from 380 to 395 K, to pass the transitions to K2 and K1, T_1 for the observable carbons, C-1, C-2, C-3, C-4, and C-7, decreases drastically by a factor of 10 or more. At the temperature just above the K transitions, 395 K, the C-1 of the central ring shows a much longer T_1 (5.19 s) than either C-5/C-5' (T_1 0.96 s) or C-6/C-6' (T_1 0.81 s) in the side rings. This is also true at the even higher temperature of 417 K, although the difference is less profound. This indicates clearly that the motion in the central ring is slower than the side rings at a given temperature.

It is interesting to examine the relaxation behavior of C-4. Its T_1 is much shorter than that of C-2 and C-7 at 380 K. This is most likely due to the proximity between C-4 and H-3, which provides an effective relaxation mechanism through the dipolar interaction between them. Thus H-3 serves to: (1) provide a relaxation pathway for C-4, (2) render the inequivalence between C-5 and C-5' as well as between C-6 and C-6' at low temperatures, (3) impose an energy barrier to the rotation of the side rings via the steric interaction with H-5 or H-5'.

n-Octyloxy groups: The ^{13}C NMR spectrum in this part of the molecule has a rather different temperature dependence from that of the mesogen. For convenience of analysis, the carbons are grouped into two types according to the variation in their δ values. As shown in Fig. 41 and Table 28, type I carbons are those carbons that have almost constant δ values over the entire range of experi-

mental temperature. This type of ^{13}C can be easily recognized as C-8, C-10 and C-15, whose resonances at 308 K are at 67.39, 26.62 and 15.77 ppm, respectively. The C-13 resonates at 33.84 ppm at 308 K may also be attributed to the type I for reasons that will be given below. The rest of the carbons whose δ values decrease with temperature (up-field shifting) belong to type II.

For type I carbons C-8, C-10, and C-15 (and also C-13 as will be shown next), the chemical shifts in Fig. 41 and Table 28 remain constant over temperature range 187–431 K, and are also very close to that of the liquid. This comparison immediately implies that C-8, C-10, and C-15 already posses *gauche* character comparable to the value in the solution. The corresponding bonds are marked with the sign ¤ in Fig. 50:
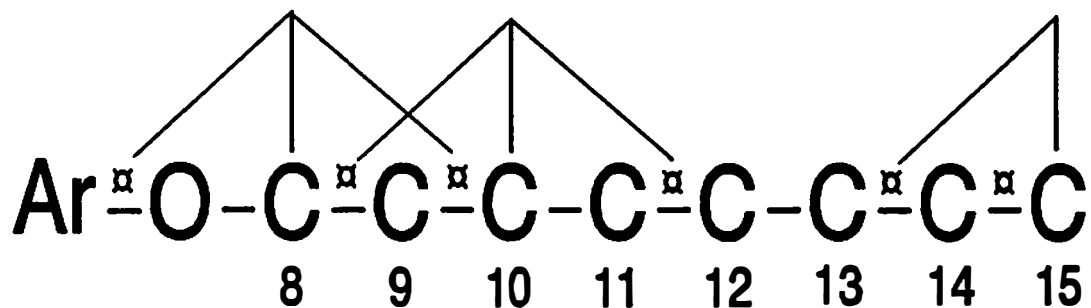
Figure 50   Bond conformations of the octyloxy chain below the K transitions. The bonds marked with the sign ¤ are of the *gauche* character.

The methyl rotation is also marked in Fig. 50, because its motion is known to start at the lowest temperature of any other conformational motion (Woodward *et al.*, 1961). Based on Fig. 50 as developed to this point, one can easily predict δ for C-13. The δ of C-13 is expected not to change with temperature because the only bond that may cause the C-13 signal to move up-field is already known to be of some *gauche* content at very low temperature from the behavior of C-10 (between C-11 and C-12). Thus, the signal of 33.84 at 308 K must, with certainty, be assigned to C-13, permitting the full correlation of liquid and solid spectra.

It should be noted that about the bonds marked ¤ in Fig. 50 shown above, the *trans* conformation is still possible with a chance of perhaps 60%, and because of rotational motion the conformations must change with time. The actual conformation of a given bond depends on the conformation of the nearest-neighbors, as well as the mode of intermolecular packing. Nearest neighbors may not have simultaneously *gauche* conformations (pentane effect) and in order to maintain largely parallel packing, only kinks or jogs as detailed by Pechhold (Wunderlich, 1980; Pechhold, 1968) can be placed along the octyloxy chain. With three of the bonds fixed in the *trans* conformation it is possible to have 2g1, 2g2, 2g3, or 3g2 kinks. The nomenclature 2g or 3g indicates the number of *gauche* bonds in the kink or jog. The final number (1, 2, or 3) indicates the shortening of the chain in multiples of half the unit cell length of the crystallographic orthorhombic chain. Due to the equilibrium concentration of *gauche* in the liquid being about 40% and the specific geometry of

the kinks larger than 2g2, one expects at an average only one of these defects at any one time in each of the octyloxy chains.

From the analysis of γ-*gauche* effect on group I carbons, one derives thus that the octyloxy chains have already developed considerable conformational freedom at temperatures below *any* transitions observed in this and the earlier calorimetric work (Wiedemann *et al,* 1986). These bonds, therefore, can not have contributed to the earlier observed total entropy change over the various stages of fusion of 87.2 J/(K mol). Similar conformationally disordered crystals were also demonstrated by the thermal properties of some segmentally fluorinated paraffins chains (Wunderlich, 1988). Easily recognizable phases with mobile alkanes (condis crystal phases) could be identified in these cases.

One consequence of the decrease in the mobility at low temperatures should be an increase of the linewidth. The linewidth of the spectrum at 187 K shown in Fig. 41 is 50 Hz, while that of 310 K is only 20 Hz. As shown in Sect. 2.3.3, line broadening may be due to two possible causes: (1) A motion in the $10^4 - 10^5$ Hz region has become dominant. (2) The conformational motion may have been frozen, which forms a distribution of conformations.

At this point, it is not known whether in OOBPD shift-dispersion or incomplete motional narrowing, or both account for the increased line width at 187 K. It would be, however, of interest to follow the spectrum to even lower temperature at which all the motion is quenched. One expects to see additional changes in the δ values particularly for the type I carbons.

To find out at what temperature the motion in the bonds marked ¤ in Fig. 50 starts, the heat capacity for the vibration-only case has been calculated to compare with the measured one. The results, discussed below, show that the motion starts at about 200 K, just at the lowest experimental temperature of our NMR probe (approximately 190 K).

For the type II carbons C-9, C-11, C-12 and C-14, abrupt changes in their δ values can be seen at the transition to the K1 state. The δ of C-14 decreases by $\Delta\delta$ = -1.25 ppm, C-11 by -2.11 ppm, C-12 by -1.01 ppm, and C-9 by -3.63 ppm. The large change in δ of C-9 is due to two γ-gauche effects (the bonds O$-$C8 and C10$-$C11). The overall change is that of "fusion" of about two to three *trans* bonds (marked with ¤ in Fig. 50), or four to six for the total molecule. From these 4$-$6 bonds one expects an entropy change of $(4-6) \times 9.5$ J/(K mol) = $38-57$ J/(K mol) for the transitions, which matches the newly observed value of 47 J/(K mol).

At temperatures above the K transitions, small decreases in the δ values can still be observed for all the carbons, especially for C-9 and C-12 that overlap at 31.44 ppm at 395 K. These decreases in δ values are much less than that observed at the transitions to the K1 phase, and can be easily attributed to the expected gradual increase in the *gauche* conformation with temperature.

Spin-lattice Relaxation Times: While the γ-*gauche* effect has been used to predict the overall changes in bond conformations, the nuclear spin relaxation times, shown in Table 29, are useful to reveal their mobilities. Except for the methyl carbon (C-15), the T_1 of all other ^{13}C at temperatures below 350 K is estimated to

be much longer than 100 s, indicating slow motion and causing the convensional one-pulse with two-level decoupling (BILEV) pulse sequence fail to detect any signal. As the temperature is increased to 350 and 380 K (phase K3), the T_1's of C-9 through C-14 decrease to about 15 s, indicating that substantial motion has already started. The shorter T_1's of the octyloxy chain carbons when compared to the carbons of the mesogen indicate that the alkyl chain is more mobile than the mesogen, although ring flipping has also started. Between 350 and 380 K, a larger decrease in T_1 can be found for the type I methylene carbons C-8, C-13, and C-10 than for the group II methylene carbons. As the temperature is further increased to 395 K, just above the transition to phase K1, the T_1's of all carbons undergo a decrease. The condis phase K1 is thus much more mobile than condis phase K3. Upon going to the liquid crystalline phase H' at 417 K, the T_1's do not change much except for C-1, C-5, and C-6. The latter indicates that the mesogen has now lost its positional and some of its orientational order, as expected for a condis-crystal to liquid-crystal transition.

The correlation time, τ_C, of the motion in the octyloxy chain can be evaluated using the commonly assumed expression for spin-lattice relaxation by dipole-dipole interaction, as has been given by Eq. (17). Using the T_1 data in Table 29, the correlation times, τ_C, on the long-time side of the T_1 minimum, defined by Eq. (17) are thus: longer than 10 μs below 350 K, decrease to 1 μs at 350 and 380 K (in the K3 phase), while in the K1 phase the correlation times decrease further to about 0.1 μs and then remain approximately the same up to the highest NMR experimental temperature in this work (417 K).

Unlike the methylene carbons, the T_1 of the methyl carbon increases within the K3 phase with temperature. Since its motion (the combined rotations about various bonds along the chain) is fast, its correlation time is at the short-time side of the T_1 minimum. This conclusion is also in agreement with the conformational motion about the C−C bonds between C-13 and C-14 below any observed transition.

4.4.4 Heat Capacities and Heats of Transition

Following the standard treatment, the total number of skeletal vibrational modes of OOBPD is taken to be 55, and the remaining number of group vibrational modes is 209. The detailed assignment is summarized in Table 35. The group

Table 35   Number of groups and vibrations in OOBPD

Group	Number of Groups in Molecule	Number of Group Vibrations	Number of Skeletal Vibrations
$-CH_3$	2	$2 \times 9 = 18$	$2 \times 3 = 6$
$-CH_2-$	14	$2 \times (7 \times 7 - 1)^* = 96$	$2 \times 7 \times 2 = 28$
$-C_6H_6-$	3	$3 \times 27 = 81$	$3 \times 3 = 9$
$-O-$	2	$2 \times 2^* = 4$	$2 \times 2 = 4$
$-CH=N-$	2	$2 \times 5 = 10$	$2 \times (2+2) = 8$
Total		209	55

*   Note that in a C−O−C sequence there are two O−C stretching frequencies, decreasing the −CH₂− sequence by one C−C stretching frequencies and adding it to the −O−. The skeletal vibrations would have to be separated furthermore into inter and intramolecular vibrations. The Tarasov model accomplishes this separation by assigning a proper θ_3/θ_1 ratio.

216

vibration frequencies as derived from our Advanced THermal Analysis System (ATHAS) data bank are listed in Table 36. A universal constant A_0 (3.9×10^{-3} K mol/J) was used to convert the experimental C_p to C_v [$C_v = C_p(1 - 3RA_0T/T_m)$]. Because heat capacity measurements started at 130 K, only θ_1 could be determined, to be 593 ± 1 K. A typical value for θ_3 was guessed at to be 80 K. It will not influence the calculated C_p above about 100 K, but should improve the extrapolated low-temperature data. The calculated heat capacity has been shown in Table 4 of Sect. 3.1.2, together with that of the measured for comparison. As can be seen that the average and RMS errors between the experimental data and the calculated C_p are 0.13 ± 1.2 % from 140 to 250 K, the temperature range for which the heat capacity is predominantly vibrational. The computation from 0 to 600 K are shown in Fig. 51. The heat capacity computed for an OOBPD crystal which shows only vibrations and the heat capacity of the liquid are compared in Figs. 10 and 11 with the actual measurements. One can clearly see that there are no low temperature transitions in the K3 phase as speculated about earlier to account for the low total heats of transition. A major increase in heat capacity beyond the vibration-only limit can be seen, however, beginning at about 200 K. In fact, at the beginning of the transition to the K2 and K1 phases the heat capacity has reached the level of the liquid. The entropy contributed by the shaded area of the graphs is 74.7 J/(K mol), more than the transitions from K3 to the liquid crystal H'. A more detailed discussion will be made now treating, as before, mesogen and octyloxy groups separately.

Table 36   Group vibrational frequencies of OOBDP

Vibrational Mode	Frequencies (K)		N	OOB -PD	OOB -PD
−CH₃ (from PP etc.)					
CH₃ asym. stretch	4262		1.00	2N	2.00
CH₃ asym. stretch	4259		1.00	2N	2.00
CH₃ sym. stretch	4174		1.00	2N	2.00
CH₃ asym. bend	2107		1.00	2N	2.00
CH₃ asym. bend	2101		1.00	2N	2.00
CH₃ sym. bend	1987		0.25	2N	0.50
	1973	1987	0.38	2N	0.76
	1973		0.37	2N	0.74
C−CH₃ stretch	1568	1614	0.44	2N	0.88
	1534	1614	0.56	2N	1.12
CH₃ rock (+ CH₂ wag)	1453	1521	0.55	2N	1010
	1453		0.45	2N	0.90
CH₃ rock (+ C−C chain stretch)	1361	1393	0.65	2N	1.30
	1333	1361	0.21	2N	0.42
	1336		0.14	2N	0.28
Total			9.00		18.00
−CH₂− (from PE etc.)					
CH₂ asym. stretch	4148		1.00	14N	14.00
CH₂ sym. stretch	4098		1.00	14N	14.00
CH₂ bend	2075		1.00	14N	14.00
CH₂ wag	1698	1977	0.65	14N	9.10
	1977		0.35	14N	4.90
CH₂ twist and rock	1690	1874	0.48	14N	6.72
	1874	1874	0.52	14N	7.28
C−C stretch	1378	1638	0.34	12N	4.08
	1378	1525	0.35	12N	4.20
	1525		0.31	12N	3.72
CH₂ rock and twist	1494		0.04	14N	0.56
	1038	1494	0.59	14N	8.26
	1079		0.37	14N	5.18
Total			7.00		96.00

218

Table 36 (cont.)

Vibrational Mode	Frequencies (K)		N		OOBPD
$-C_6H_6-$					
CH stretch	4400		4.00	3N	12.00
C−C stretch	2352	2389	1.00	3N	3.00
C−C stretch	2369	2379	0.30	3N	0.90
	2284	2369	0.70	3N	2.10
C−C stretch C−C−H bend	2172		0.26	3N	0.78
	2172	2251	0.55	3N	1.65
	2251		0.19	3N	0.57
C−C stretch C−C−H bend	2071		0.44	3N	1.32
	2071	2136	0.56	3N	1.68
C−C−H bend	1910		0.29	3N	0.87
	1910	1966	0.50	3N	1.50
	1966		0.21	3N	0.63
C−C stretch	1838	1854	1.00	3N	3.00
C−C stretch	1824	1858	1.00	3N	3.00
C−C stretch, C−C−H bend	1621		1.00	3N	3.00
C−C stretch, C−C−H bend	1546		1.00	3N	3.00
C−C str., CCC bend, CCH bend	1480	1512	1.00	3N	3.00
C−C str., CCC bend, CCH bend	1392		0.22	3N	0.66
	1392	1464	0.55	3N	1.65
	1464		0.23	3N	0.69
C−C stretch, C−C−C bend	1162	1217	0.33	3N	0.99
	932	1162	0.56	3N	1.68
	926	932	0.11	3N	0.33
C−C−C bend, C−C−H bend	866	892	1.00	3N	3.00
C−C stretch, C−C−C bend	636		0.30	3N	0.90
	439	636	0.59	3N	1.77
	433	439	0.11	3N	0.33
CH wag	1382		1.00	3N	3.00
CH wag	1359		1.00	3N	3.00
CH wag	1200		1.00	3N	3.00
CH wag	1136	1207	1.00	3N	3.00
C−C deform, C−C torsion	1016	1093	1.00	3N	3.00
C−C deform, C−C torsion	659	770	0.56	3N	1.68
	770	806	0.44	3N	1.32
C−C torsion	577		1.00	3N	3.00
Additional	60	90	2.00	3N	6.00
Total			27.00		81.00

219

Table 36   (continued)

Vibrational Mode	Frequencies (K)		N	OOBPD	
−O− (from POP, PO, etc.)					
C−O stretch	1385		0.11	2N	0.22
	1632		0.06	2N	0.11
	1385	1632	0.34	2N	0.67
O−C stretch	1305		0.50	2N	1.00
O−Ar stretch	1800		1.00	2N	2.00
Total			2.00		4.00
−CH=N−					
CH stretch	4347		1.00	2N	2.00
CH bend	1016	1914	2.00	2N	4.00
C−N stretch	1502		1.00	2N	2.00
C=N stretch	2302		1.00	2N	2.00
Total			5.00		10.00

Mesogen: An increasing mobility of $180°$ phenylene ring flipping with temperature starting at 336 K, as shown by NMR, will not contribute much to the entropy. Since after a flip has occurred, the molecule is indistinguishable from the starting conformation. Consequently one expects also no major increase in the heat capacity due to the mesogen motion in the phase K3 (and K2 and K1). It is a well-known fact that a vibrator changing to a rotator or undergoing jump-like motion shows a gradual decrease in heat capacity over a large temperature range rather than
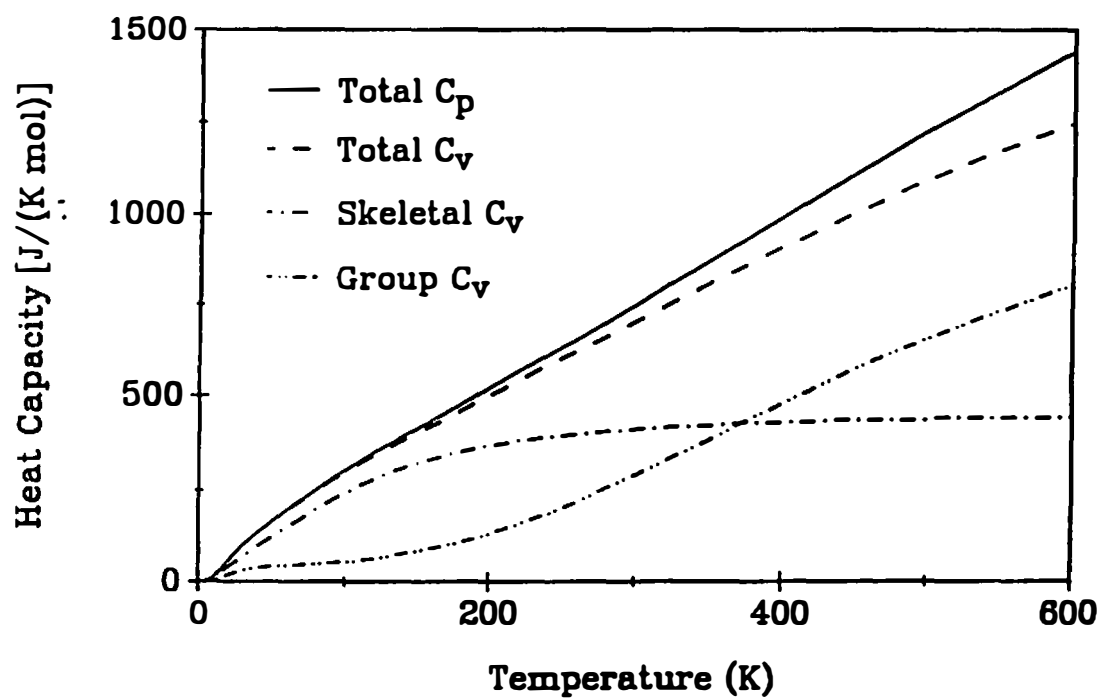
Figure 51   Calculated C_p of OOBPD

increase, since the limiting heat capacities of vibrators and rotators are R and $R/2$, respectively (Wunderlich and Bauer, 1970).

As the condis crystal K1 changes to the smectic liquid crystal, and ultimately to the melt, the jump-like motion changes to rotation and the whole mesogen undergoes orientational and positional diffusion. Indeed, all transitions from phase K1 to the melt show a combined ΔS of 59 J/(K mol), an amount close to what is expected for such motion and the resulting disorder, as was outlined above.

n-Octyloxy Groups: From previous work on *n*-paraffins it was shown that molecules such as octane start to show conformational disorder in the crystal from about 200 K (Jin and Wunderlich, 1991). At the melting temperature of octane (216 K), the heat capacity of the crystal is about 10% higher than expected from the vibration-only computation. Taking into account that the K3 to (K2 and K1) transition occurs in OOBPD more than 150 K higher in temperature and that the paraffinic chain is not as well ordered as in a paraffin crystal it is not surprising that the heat capacity is more than 40% higher and reaches the value of the liquid. One expects thus that the liquid heat capacity is linked to the large motion in the octyloxy groups.

As was pointed out in the discussion of the NMR data, the K3 to K1 transition changes approximately 5 *trans* bonds to the equilibrium *gauche* fraction in the liquid, so that K1 contains practically fully disordered flexible chains, but positionally and orientationally fixed mesogens.

The remaining high-temperature transitions between the various liquid crystalline phases were already described in the prior work (Wiedemann *et al.*, 1986). Figures 10 and 11 show that the baseline for all transitions is, however, practically the heat capacity of the liquid state and not a connection from the beginning to the end of each of the various endotherms. As a result, all transitions are somewhat larger than reported before. The total combined entropy is 106 J/(K mol) instead of 87.2 J/(K mol). Thus, it is neccessary to replace the older transition enthalpy and entropy data (Wiedemann *et al.*, 1986) with a new one determined by the heat capacities, as shown in Table 3 in Sect. 3.1.2. It can also be seen from Table 3 that crystal grown out of solution or melt showed only insignificant differences in thermal behaviors.

The transition temperatures listed in Table 3 agree within one kelvin with the prior results. Either set is within typical DSC precision for transitions of such nature.

Finally, a speculation can be made about the ultimate low-temperature structure of OOBPD. There is no sharp glass transition, as one finds for the cooperative freezing of liquids to an amorphous glass, as well as no further first order transition. One expects thus that the attached paraffinic chains gain order continuously on cooling, without changing the *gauche*-to-*trans* ratio significantly (as shown by the NMR evidence). This type of ordering must, since it occurs over such a broad temperature range, also be a rather local ordering to avoid cooperative freezing in form of a crystallization or glass formation. Comparing with the earlier estimate (Wiedemann *et al.*, 1986) that a molecule like OOBPD should have an

overall entropy of fusion of about 210 J/(K mol) (152 J/(K mol) for the flexible chain, rest for the mesogen), one can see that at about 250 K the experimental data are within 30 J/(K mol) of this value (106 J/(K mol) from the transitions and 74.7 J/(K mol) for the increased heat capacity). The entropy of an amorphous CH_2-group at absolute zero (see *ATHAS* data bank) derived from polyethylene heat capacity and heats of fusion is 3 J/(K mol), just the right amount for the 10 bonds marked with a ¤ in Fig. 50 between Ar and C-14 to be in a state similar to glassy polyethylene.

4.4.5 Summary

A detailed account has been given for the order and motion in OOBPD. As suggested before, all liquid crystalline phases have full conformational disorder and motion. The K1 phase is still fully conformationally disordered (condis crystal), only the mesogen has gained orientational and positional order. Ring flipping by 180° is still possible in K1, but freezes at about 336 K in the K3 phase. The transition from K1 to K3 involves the fixing of 5−6 specific bonds in the two octyloxy chains predominately in the *trans* conformation. The remaining 10 bonds show a very high heat capacity in the K3 phase that ultimately drops at 200−250 K to the heat capacities of a vibrator with a residual entropy close to that expected for glassy polyethylene. Specific geometries and correlation times could be suggested and a link to the thermally induced defect motion in paraffins could be made.

4.5   Macromolecules, MBPE-9 and MBPE-5

4.5.1   Introduction

As shown in Sect. 3.2.5, these macromolecules show monotropic mesophases, *i.e.*, two transitions are observed on cooling from the isotropic melt, but only one transition (isotropization) is observed on subsequent heating (see Table 5), in another words, the mesophase exists only on cooling.

In order to classify the mesophase formed on cooling, a thermodynamic analysis was carried out for the transition from the isotropic melt to the mesophase (Cheng, Yandransits, and Percec, 1991; Yandrasits Ph.D thesis). The result showed a close-to-zero entropy contribution of the pre-assumed mesogenic group $(C_6H_3CH_3-CH_2-CH_2-C_6H_4-)$ to ΔS_i, the entropy of isotropization (*i.e.*, the transition to the isotropic melt). This is at variance to observations made for typical liquid crystal forming systems (Blumstein and Thomas, 1982; Lenz and Jin, 1981; Lenz, 1985; Ober *et al.*, 1982; Wunderlich and Grebowicz, 1984). On the other hand, the total equilibrium transition entropy changes from the room temperature phase to the melt (81.4 and 106.3 $JK^{-1}mol^{-1}$ for MBPE-5 and MBPE-9, respectively (Cheng, Yandrasits, and Percec, 1991), both computed for 100% presence of the ordered phase) do not suffice to account for the expected entropies of fusion from the empirical rules, valid for large numbers of large and small molecules (Wunderlich and Grebowicz, 1984) (about 100 and 140 $JK^{-1}mol^{-1}$ for MBPE-5 and MBPE-9, respectively). A similar deficiency in heats of fusion was shown above for the liquid-

crystal forming small molecule (OOBPD) and could be linked to remaining conformational disorder that ultimately and gradually freezes to a glassy condis phase.

The questions that need to be clearfied in the MBPE-n series are concerned with the changes in order and motion in the mesophase and in the room temperature phase. Direct observation of the mobility of the individual carbons is possible through high resolution solid state ^{13}C NMR.

4.5.2 ^{13}C Chemical Shifts Assignments of the Melts

The assignments can be made in a similar way to that for OOBPD, *i.e.*, using the substituent shielding effects documented for aromatic, alkoxy group containing molecules (Silverstein *et al*, 1981; Stothers, 1976). The assignment of the methylene ^{13}C's in the alkoxy chain of MBPE-9 was made by starting with the spectrum of *n*-nonane whose ^{13}C δ values are known to be, from the end (methyl) to the center, 14.2, 23.3, 32.6, 30.0 and 30.3 ppm (Silverstein *et al*, 1981). The available substituent-effect data on the alkyl carbons of aralkyl ethers (with the group of phenylene−oxygen-alkyl) show that when the alkyl chain consists of more than 5 carbons, the oxygen has positive substituent effects (deshielding) of +55 and +5.8 ppm on the α- and β-carbons, *i.e*, C-13/C-21 and C-14/C-20, respectively (Sadtler Research Lab., 1986). Thus the measured values of 68.66 and 30.06 ppm, listed in Table 30, are assigned for C-13/C-21 and C-14/C-20, respectively. The oxygen, however, has an negative substituent effect (shielding) of about −6.4 ppm on the γ-

carbon, *i.e.,* C-15 and C-19, which causes them to resonate at 26.72 ppm. The rest of the carbons are not influenced by the oxygen, therefore, their δ values agree well with the respective carbons in *n*-nonane. The signals of C-16 through C-18 show one single, intense peak at 30.06 ppm, overlapping with C-14/C-20.

The ^{13}C's in the ethylene linkage between the two phenylene rings (C-7 and C-8) show a pair of less intense signals at 36.82 and 35.25 ppm, respectively. The weaker signals for these two ^{13}C's are caused by less mobility than for the other methylene ^{13}C's.

For the aromatic carbons, the assignments can also be made based on the consideration of substituent effects. Detailed values of the substituent effects on the aromatic ^{13}C's can be found in the literature (Silverstein *et al.,* 1981; Stothers, 1976). The predicted values are in good agreement with the measured ones. The δ values for all the aromatic carbons are also listed in Table 30.

Similar considerations as for MBPE-9 apply for MBPE-5 with the exception of C-15. The C-15 carbon in MBPE-5 is special because it has two oxygens as γ-substituents from the ends of the aliphatic spacer. In this case two γ-substituent effects, $2\times(-6.4$ ppm), should be added to the base value of 34.7 ppm of *n*-pentane, to give 21.9 ppm, being closest to the observed signal at 23.31 ppm. The chemical shifts for MBPE-5 are listed in Table 31.

Differences between the predicted and measured δ values are due to the fact that the predictions are based on *solution* spectra of *small molecules*, therefore, they may not be fully applicable to the molten state of polymers. Nevertheless, the

predictions are still sufficiently close to the measurements to permit an unambiguous assignment.

4.5.3   Mesophase Behavior of MBPE-9

In Fig. 42, the ^{13}C CP-MAS spectrum of the melt (373 K) still shows some signals from the CH_2-sequence, although they are much weaker than that of the BILEV spectrum. This indicates that even in the melt there are some alkoxy chains that are still rigid enough to cross-polarize. The $(C_6H_3CH_3-CH_2-CH_2-C_6H_4-)$ group, in contrast, shows no signal with CP-MAS, indicating that rotational motion of the phenylene groups is rather fast.

As temperature is decreased to 354 K, the intensities of the ^{13}C CP-MAS signals increase as a result of decreased mobility. For the first time the phenylene carbons show also weak signals. The intensity of the BILEV spectrum is, however, still much higher, indicating that the molecules are still mobile.

On cooling to 339 K, calorimetry shows an exothermic transition with an entropy loss of 16.7 $JK^{-1}mol^{-1}$ (see Table 5). This transition was interpreted as a change from liquid to liquid crystal in the literature (Cheng, Yandrasits, Percec, 1991; Unger et al., 1990), but it was also shown at the same time that practically all of the entropy of transition originates in the "flexible" CH_2- sequence (Yandrasits et al., 1992).

The observation that CH_2-groups contribute to ΔS_i are supported by a comparison of the NMR spectra between 354 and 339 K. In the methylene

sequence, the CP-MAS signals of C-14 and C-20 are shifted downfield by 3.1 ppm, while all others remain largely unchanged (see Fig. 42 and Table 30). Using the γ-gauche effect, one expects the four bonds involved in this large change to be O−C13, C15−C16 (for C-14), C18−C19, and C21−O (for C-20). The change of conformations in these four bonds on transition to trans could cause an entropy change of up to 4×9.5 JK^{-1}mol^{-1} = 38 JK^{-1}mol^{-1}. This value is then multiplied by the fraction of crystallinity of 0.54, to give a value of 20.5 JK^{-1}mol^{-1}, which is close to the observed value of 16.7 JK^{-1}mol^{-1}. The crystallinity was determined before by wide-angle X-ray diffraction and calorimetry (Cheng, Yandransits, and Percec, 1991; Yandrasits Ph.D thesis), and is in agreement with an estimate of the mole fraction of cross-polarizable ^{13}C's (seen by the peak area of the C-14/C-20 resonances in CP-MAS at 339 K) versus the total number of carbons (seen by the area of peaks in CP-MAS plus that in BILEV at 339 K).

The chemical shifts of C-15 and C-19 remain approximately the same before and after the transition, indicating that the bonds C13−C14, C16−C17 (for C-15), C17−C18, and C20−C21 (for C-19) remain at the same trans-to-gauche ratio as in the melt and thus do not contribute to the entropy change. Similarly, the unchanged chemical shifts of C-13 and C-21 indicate that the bonds C14−C15 and C19−C20 also remain at a comparable gauche content. Based upon these results, one can predict that the signals of the remaining carbon atoms C-16, and C-18 should be relatively constant (only 0.7 ppm shifting is observed), while that of C-17 should again show two γ-gauche effects and move to low field by $2 \times 0.4 \times 5.3$ ppm = 4.2 ppm,

placing it within the peak at 33.27 ppm which also contains the contributions from C-14 and C-20.

In the dephasing spectrum in Fig. 44, the greatest signal suppressions can be achieved for C-14, C-20, and C-17. This is to be interpreted that the motion of these carbons is reduced most after going through the transition, being consistent with the observation of the BILEV experiment in Fig. 42 at 339 K. The signals of these rigid carbons C-14, C-20 and C-17 can not be seen in the BILEV spectrum, also shown in Fig. 42, while the fairly good signal-to-noise ratio of the other carbons suggests that they are more mobile.

The above observation concerning the alkoxy chain carbons leads to the conclusion that the entropy change of 16.7 $JK^{-1}mol^{-1}$ at the first transition on cooling is due to a partial ordering of the alkoxy chain and not of the group ($C_6H_3CH_3-CH_2-CH_2-C_6H_4-$), which is in agreement with a close-to-zero entropy contributions from the aromatic part which was inferred before by Yandrasits *et al.* by extrapolating the transition entropy to zero number of methylenes in the "flexible" chain (Yandrasits *et al.*, 1992).

To further support this surprising result of rigidity in the flexible chain, one needs also examine the mobility of the aromatic group ($C_6H_3CH_3-CH_2-CH_2--$ C_6H_4-) itself. At 339 K, a comparison between the CP-MAS and the dephasing spectra of MBPE-9, shown in Fig. 44, indicates that: (1) the signal intensities of non-protonated carbons C-1, C-4, C-5, C-9, and C-12 are, as expected, the least affected when compared to those of protonated carbons. This observation can also be used

as further confirmation that the chemical shift assignments for the nonprotonated carbons were correct; (2) the signals from the protonated aromatic carbons C-2, C-3, C-6, C-10, and C-11 have been somewhat suppressed. The suppression of the signals from these carbons is, however, only slight, even with a long dephasing delay of 70 μs. This indicates that considerable motion is left in the rings. The motion must, in addition, be similar to that found in the melt, otherwise, if there were a change of motion from the random diffusional rotation (as in the melt) to 180° flips (jumps between two identical symmetry sites), there would have been a noticeable entropy change. Thus, there must not be any ordering of the $(C_6H_3CH_3-CH_2-CH_2-C_6H_4-)$ groups.

The spectrum of $(C_6H_3CH_3-CH_2-CH_2-C_6H_4-)$ obtained with CP-MAS at 339 K in Figs. 42 and 44 can be decomposed into two sets of resonance lines. One resembles the higher temperature (354 or 373 K) BILEV spectrum, and the other is that found at lower temperature (326 or 310 K) in the CP-MAS spectrum.

The discussion of the motion and entropy gives a better understanding of the nature of the mesophase of MBPE-9 formed after the first transitions on cooling. The about equal intensities of the BILEV and CP-MAS spectra indicates an approximately 50% rigid part of the molecules. Since this fraction does not change significantly on going beyond the second transition (see Fig. 42), and the calorimetric crystallinity of similarly cooled samples at room temperature is 54%, one can identify this rigid fraction with the part that will ultimately end up as the room-temperature crystallinity. An important conclusion of this observation is that the high-temperature

231

mesophase only involvs about 50% of the sample. Assuming from the calorimetric extrapolation with CH_2-spacer chain length and the present discussion of motion that little or no entropy change occurs in the ($C_6H_3CH_3-CH_2-CH_2-C_6H_4-$) sequence on going through the high-temperature exotherm, one can calculate that the measured entropy of transition of 16.7 $JK^{-1}mol^{-1}$ matches the estimated entropy of transition of 50% of the 9 CH_2-groups to an atmospheric pressure condis phase which was shown by Wunderlich *et al.* (Wunderlich *et al.*, 1988) to have an entropy of transition of about 3.5 J/(K mol CH_2). The γ-*gauche* effect lets one furthermore derive that bonds $O-C13$, $C15-C16$, $C18-C19$, and $C21-O$ are practically always in the *trans* conformation after cooling through the high-temperature exotherm. The loss of conformational disorder of these four bonds of the 50% of the sample that become ordered, accounts also for about $0.5 \times 4 \times 9 = 18$ $JK^{-1}mol^{-1}$, close to the measured amount. Furthermore, the specific conformational restrictions derived from the NMR data allows one to suggest the predominant existence of 2g1, 2g2, 2g3, and 3g3 kinks and jogs out of the class of conformations which leave the bundles of CH_2-sequences in a largely extended, parallel, low-energy conformation (Wunderlich 1973), as was proposed by Pechhold (Pechhold, 1968). The nomenclature 2g or 3g indicates the number of *gauche* bonds in the kink or jog. The final number (1, 2, or 3) indicates the shortening of the chain in multiples of half the unit cell length of the crystallographic orthorhombic chain. In addition to the shortening in the chain direction, there are displacements in the a- and b-directions. The 2g defects introduce 33% of *gauche* conformations, the 3g defects, 50%. It is thus easy to make

232

up the above assigned equilibrium concentration of *gauche* conformations in the sequence restricted by the experimentally determined *trans* bonds. The mechanisms of alternating between the various possible defects were shown in the recent molecular dynamics simulations of Sumpter, *et al.* to be frequent and based on the thermal, random generation of *gauche* defects at times in the picosecond range (Sumpter *et al.*, 1990).

The $(C_6H_3CH_3 - CH_2 - CH_2 - C_6H_4 -)$-sequence shows in this high-temperature mesophase only a beginning restriction of motion, insufficient to increase the entropy significantly. It is interesting to note that the analogous polyparaxylylene [PPX, $(C_6H_4 - CH_2 - CH_2 -)_x]$ shows also high temperature condis phases. These have been studied by thermal analysis (Kirkpatrick and Wunderlich, 1985; 1986), and by molecular mechanics computation (Miller *et al.*, 1990). In the high-temperature mesophase of MBPE-9 the aromatic sequence must be much more disordered than in the β_2-phase of PPX, which shows an entropy of 14.3 $JK^{-1}mol^{-1}$ on crystallization.

On further cooling of MBPE-9 from the high-temperature mesophase at 339 K to 326 and 310 K, the chemical shift values of the alkoxy chain carbons do not change significantly (≤ 0.7 ppm), as can be seen in Table 30 and Fig. 42. The dephasing experiment at 310 K, Fig. 45, shows that even with the a dephasing delay of 120 μs, the signals of C-15 and C-19 (at 33.77 ppm) as well as C-16 and C-18 (31.65 ppm) can still be observed, indicting a residual mobility which keeps the chain conformationally disordered. The observed entropy at the second transition (36.3

$JK^{-1}mol^{-1}$, with a cooling rate of 10 K/min) (see Table 5) is thus not likely to be due to major amounts of ordering in the alkoxy chain.

On the other hand, a large change can be observed in the $(C_6H_3CH_3-CH_2--CH_2-C_6H_4-)$ sequence after the second transition to the room temperature phase. The coexistence of the different conformations seen at 339 K in the CP-MAS spectrum becomes no longer observable, as indicated by the resonances of C-2, and C-6 in Fig. 42. Each distinguishable carbon atoms in the rings produces only a single "rigid" line. In the dipolar dephasing experiment, shown in Fig. 45, the CP-MAS signals from C-2 (109.9 ppm), C-6 (119.6 ppm), and C-3 (130.5 ppm) can be suppressed with a shorter dephasing delay (40 μs), indicating that the methyl-substituted phenylene ring has become much less mobile. The slow-down of motion in this ring may introduce sufficient order to be linked to the observed entropy change of 36.3 $JK^{-1}mol^{-1}$. The signals of the phenylene (unsubstituted), on the other hand, can not be suppressed, even with a τ of 120 μs, as can be seen from the signals of C-11 (115.4 ppm) and C-10 (130.5 ppm) in Fig. 45. Thus, this ring remains quite mobile at 310 K. Judging from the mesophase transitions in polyparaxylylene (PPX) [$\Delta S_i = 14.3$, $\Delta S_{d2} = 2.7$, $\Delta S_{d1} = 9.9$ $JK^{-1}mol^{-1}$], one could expect an entropy change of about 54 $JK^{-1}mol^{-1}$ for complete, or 29.2 $JK^{-1}mol^{-1}$ for 54%, crystallization of the $(O-C_6H_3CH_3-CH_2-CH_2-C_6H_4-O-)$ group. Additional perfection in the packing of the $(CH_2-)_9$-sequence, which is indicated by the gradual increases of their δ values with decreasing the temperature from 339 to 310 K, can easily make up the remaining entropy loss of (36.3 − 29.2) = 7.1 $JK^{-1}mol^{-1}$.

The reason for the methyl-substituted phenylene ring to become immobile at 310 K may be looked for in the inter- and intra-molecular interactions. The latter causes a strong steric interaction between the CH_3 and the methylene group of C-7. This type of interaction has been discussed for the two adjacent methyl groups in hexamethylbenzene (Takeda *et al.*, 1989). The unsubstituted phenylene ring is, in contrast, relatively free to rotate about its 1,4-axis. The former can be deduced from the thermal behavior of PPX.

The low temperature phase of MBPE-9 (310 K) is still conformationally disordered to some degree as is indicated by the observations that: (1) the unsubstituted phenylene ring is still mobile, (2) there are still 6 bonds in the CH_2-spacer which possess a high *gauche* character. From these 6 disordered bonds one expects a further entropy of disordering of about 57 $JK^{-1}mol^{-1}$ (or 31 $JK^{-1}mol^{-1}$ for the 54% crystalline sample). On further cooling this excess entropy can be reduced by continued ordering as in a normal liquid, ending in a glass transition which could be proven by an analysis of the heat capacity.

Quantitative thermal analysis of the heat capacity for a sereies of MBPE-*n* (*n* = 4 – 12) has been carried out by Jin *et al.* (Jin *et al.*, 1992). As demonstrated for OOBPD in Sect. 4.4, the calculated heat capacities at sufficiently low temeparture (the vibration-only) and that of the melt provide the most accurate baseline for the determination of the transition parameters, *i.e.*, heats and entropies. In Fig. 52 a comparison between the experimental and calculated heat capacities is made. One can find an entropy of 45.2 $JK^{-1}mol^{-1}$ using the liquid basline for this 43% crystal-
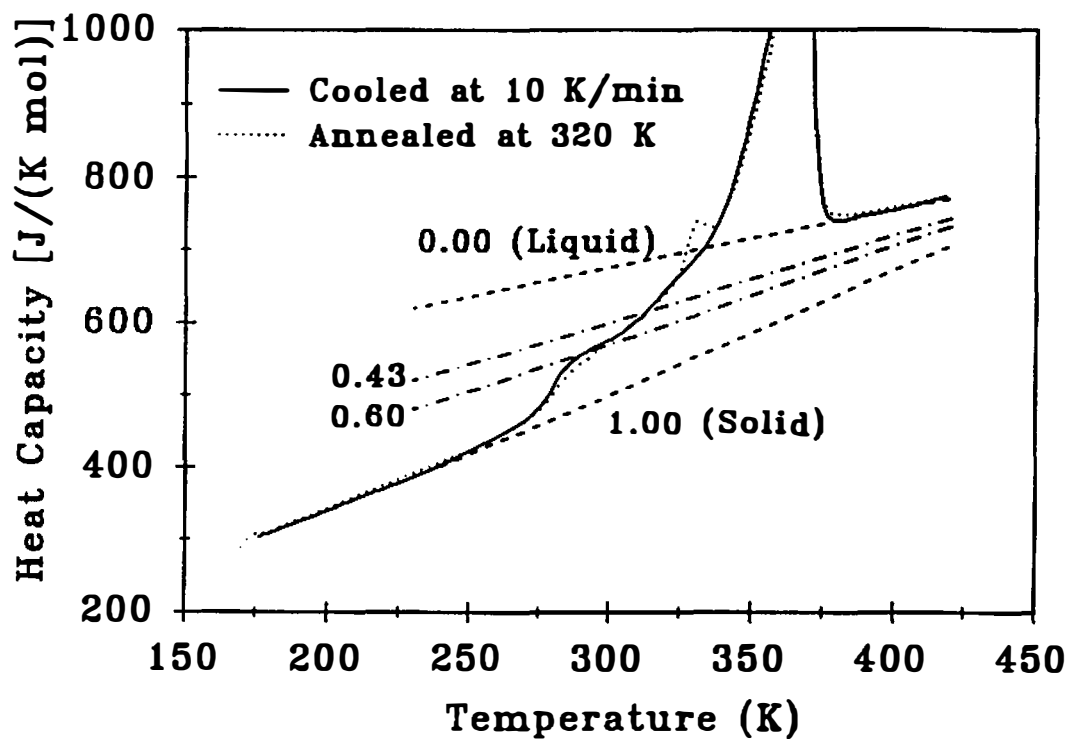
Figure 52   Heat capacity comparison for semicrystalline MBPE-9. Solid line: experimental C_p; dashed lines: solid and liquid C_p; dot-dahsed lines: semicrystalline C_p calculated as indicated.

line sample, or 106 $JK^{-1}mol^{-1}$ for 100% crystalline MBPE-9. On the other hand, judging from the polymers that make up the MBPE-9 repeating unit when added, namely poly(p-xylylene) (Kirkpatrick and Wunderlich, 1985) [ΔS_n = 14.3, ΔS_{d2} = 2.7, ΔS_{d1} = 9.9 J/(K mol)], poly(oxy-2,6-dimethyl-1,4-phenylene) (Varma-Nair and Wunderlich, 1991) [ΔS = 10.3 J/(K mol)] and the poly(oxide nonamethylene) $-O-(CH_2)_9$ [ΔS = 93.9 J/(K mol)] (Gaur and Wunderlich, 1981), one expects an entropy change of about 131.1 J/(K mol) for 100%, or 54.6 J/(K mol) for 43%, crystallization of MBPE-9. The 20% "missing entropy" of 11.2 J/(K mol) could easily be found from the gradually increase in heat capacity shown in Fig. 52, which is about 10.2 J/(K mol) (Jin *et al.*, 1992). A similar treatment was also applied to MBPE-5. The "missing" entropy of 16.3 J/(K mol) between experimental (81.4) and expected (97.7) was also found in a rise in heat capacity at lower temperature. The additional entropy due to an increase in heat capacity between glass transition and beginning of fusion was 12.5 J/(K mol).

4.5.4 Mesophase Behavior of MBPE-5

The same analysis can be made on the sample of MBPE-5. The variable-temperature NMR spectra are shown in Fig. 43. At 410 K, in the isotropic melt, the CP-MAS spectrum shows residual resonances of the CH_2-sequence, but not of the aromatic part, indicating again rigidity of the flexible spacer even in the melt, similar to that of MBPE-9.

As the sample is cooled to 401 K (spectra not shown) and 386 K, still above the reported first transition temperature, the spectra are essentially the same as that of the isotropic melt, as can be seen in Fig. 43 and also the chemical shift values in Table 31. This indicates that on cooling the sample remains liquid at 386 K or even lower.

At 350 K, the CP-MAS spectrum shows increased intensities in the $(C_6H_3CH_3-CH_2-CH_2-C_6H_4-)$ group as a result of reduced mobility. On the other hand, the spectrum shows a decreased signal intensities of the $-CH_2$-sequence. This is probably due to a motion having correlation time of $10^{-5}-10^{-6}$ s^{-1} which is most effective to reduce the proton spin-lattice relaxation time in the rotating frame to such a small value that the cross polarization can no longer occur. In the BILEV spectrum, although the chemical shift values are still that of the melt, the linewidths are broadened significantly as compared to those at higher temperatures (e.g., 386, 401 and 410 K). As shown in Sect. 2.3.3, the broadening arises when the motion of the groups under consideration give rise to strongly fluctuating dipolar fields. The broadening caused by the motion of $10^{-5}-10^{-6}$ s^{-1}. Thus, both the CP-MAS and BILEV spectra indicate that the CH$_2$-sequence undergoes a large-amplitude motion of $10^{-5}-10^{-6}$ s^{-1}. This motion is considered to be a slow motion on the NMR time scale and is most probably the chain diffusions. The diffusion also exists at higher temperatures, but with somewhat higher rate such that the dipole-dipole interaction can be averaged and results in line-narrowing. These observations can be interpreted with the beginning of a crystallization process, in which the $(C_6H_3CH_3-CH_2-CH_2--$

C_6H_4-) groups are gaining order, which is made possible (or helped) by the decreased motion of the alkyl chains. The spectra of 350 K are thus an intermediate between the melt and the room-temperature phases. The appearance of the spectra are expected to be dependent on the length of isothermal time.

At 325 K, a single phase transition was observed in DSC (onset temperature is 329.3 K) when the sample is cooled at a rate of slower than 2.5 K/min, which is the average cooling rate used in the NMR measurements. The NMR spectra of both BILEV and CP-MAS in Fig. 43 are almost identical to that of 310 K, except that the intensity of CP-MAS spectrum is slightly lower than that of 310 K. In the dephasing experiment, Fig. 46, except for the $-CH_3$ carbon, signals from all other protonated carbons were suppressed even with a shorter delay (30 μs compared to 70 μs for MBPE-9). The chemical shift values also indicate stiffening of the molecule. For C-15, the δ changes from 23.2 ppm at 350 K to 27.30 ppm at 325 or 310 K. This large difference must be attributed to two γ-gauche effects and corresponds to the change of the conformation in the bonds of C13−C14 and C20−C21 from a high gauche concentration in the liquid phase (386 K and above), to an all trans on stiffening. While for the indistinguishable carbons C-14 and C-20, the δ changes by about 2 ppm, due to one γ-gauche effect in the bonds of C13−O and C21−O, respectively. On the other hand, δ of C-13 and C-21 remain constant when temperature is decreased, indicating that the conformation in the bonds C14−C15 and C15−C20 at 310 K have comparable gauche character as in the melt.

From the analysis of γ-*gauche* effect above, one can easily derive the entropy loss for the transition. Except two bonds, namely, C14−C15 and C15−C20, all other bonds in the CH_2-sequence have changed their conformation and should each contribute 9.5 $JK^{-1}mol^{-1}$, amounts to 4 × 9.5 $JK^{-1}mol^{-1}$ = 38 $JK^{-1}mol^{-1}$. The ($C_6H_3CH_3-CH_2-CH_2-C_6H_4-$) group contributes additional 54 $JK^{-1}mol^{-1}$ (see analysis on MBPE-9 above). Therefore, for a sample of 100% crystallinity at 310 K, one expects to observe an entropy of fusion of 38 + 54 = 92 $JK^{-1}mol^{-1}$. This value is in good agreement with the value of 81.4 $JK^{-1}mol^{-1}$ observed by DSC (Jin *et al.*, 1992). On the other hand, the "missing entropy" contributed from the two bonds [which is 16.3 J/(K mol) between experimental (81.4) and expected (97.7)], namely, C14−C15 and C15−C20, could easily be found from the gradually increase in heat capacity at lower temperature.

The similarity between the spectra at 310 and at 325 K can be attributed to the fact that rather slow cooling rate (≤3 K/min) had to be used for decreasing the sample temperature in the NMR experiment. It was shown before by DSC that the existence of the mesophase is largely dependent on the cooling rate. The mesophase of MBPE-5 is not observable if cooling rate is slower than 2.5 K/min.

4.5.5   Summary

(1) The mobility of the ($C_6H_3CH_3-CH_2-CH_2-C_6H_4-$) and the alkoxy chain have been described for MBPE-9 and MBPE-5. The results suggest that conformational disorder exists in all phases of both polymers.

(2)   The order of the higher-temperature phase of MBPE-9, observed on cooling between two exotherms, is realized by partial ordering of CH_2-sequences (with 4 C–C bonds being largely fixed in the *trans* conformation), while in the room-temperature phase, the methyl-substituted phenylene ring also participates in creating increased order without much further increase in the order of the CH_2-sequence.   The observed transition entropies could be linked to the transition of polyethylene from the melt to its condis phase and of polyparaxylylene from the melt to its crystal phase.

(3)   For MBPE-5, the high-temperature mesophase, observed by DSC on cooling, cannot be traced by NMR, because it undergoes fast transformation to the room-temperature phase.   Since the low temperature CP-MAS spectrum shows a larger down-field movement in the chemical shifts compared to that of the melt, and a very short effective T_2^*, MBPE-5 seems to be able to form more perfect crystals than MBPE-9. Still, the room-temperature phase has two disordered bonds, making the crystals conformationally disordered.

CHAPTER 5

CONCLUSIONS

It has demonstrated through the chosen molecular systems, *i.e.*, tetra-*n*-alkylammonium bromides and iodides (with n = 1 to 18), liquid-crystal-forming molecule N,N'-*bis*(4-*n*-octyloxybenzal)-1,4-phenylenediamine (OOBPD), and polymers poly[oxy-1,4-(3-methylphenylene)ethylene-1,4-phenyleneoxynonamethylene](MBPE-9), and poly[oxy-1,4-(3-methylphenylene) ethylene-1,4-phenyleneoxypentamethylene] (MBPE-5) that:

1. *Con*formationally *Dis*ordered crystals (condis crystals) can be found almost always in those molecules that containing flexible chains. The molecules of a condis crystal are disordered among some major conformational isomers formed by rotations about carbon-carbon bonds. The condis molecules are positionally and orientationally ordered.

2. Condis crystal is a unique mesophase which exists in addition to the traditionally recognized mesophases, namely, liquid crystal and plastic crystal. In liquid crystal, molecules are conformationally and positionally disordered, and maintain only orientational order; In plastic crystal, the molecules are conformationally and orientationally disordered, and maintain only positional order.

3. The processes leading to the formation of a condis crystal may be: (1) a first-order transition (stepwise change in entropy and ^{13}C chemical shifts), (2) a gradual change (transitionless transition), and (3) a combination of the above. These

processes can be explained by the temperature dependence of the free energy (G) curve. The sharp transition indicates a discontinuity in the relationship between G and T; while the gradual change makes a smooth connection in the G vs T curve between the condis crystal and the phase involved in the transition.

4. Conformational motion and disorder can be studied independently by solid state ^{13}C NMR and thermal analysis. The experimental results show different aspects of the problem, and the results are consistent and complementary to each other.

LIST OF REFERENCES

LIST OF REFERENCES

A. Abraham, *"The Principles of Nuclear Magnetism"*, Chapters 2 and 8, Oxford University Press, London, 1961.

M. Alla and E. Lippmaa, *Chem. Phys. Lett.,* **37**, 260 (1976). High Resolution Broad Line ^{13}C NMR and Relaxation in Solid Norbornadiene.

P. S. Allen and A. Cowking, *J. Chem. Phys.* **47**, 4286 (1967). Nuclear Magnetic Resonance Study of Molecular Motions in Hexamethylbenzene.

J. E. Anderson and W. P. Slichter, *J. Phys. Chem.,* **69**, 3099 (1965). Nuclear Spin Relaxation in Solid *n*-Alkanes.

E. R. Andrew, *Progr. NMR Spectrosc.*, **8**, 1 (1972). The narrowing of NMR Spectra of Solids by High-speed Speciman Rotation and the Resolution of Chemical Shift and Spin Multiplet Structures of Solids.

E. R. Andrew, A. Bradbury and R. G. Eades, *Nature (London)*, **183**, 1802 (1959). Removal of Dipolar Broadenning of Nuclear Magnetic Resonance Spectra of Solids by Specimen Rotation.

J. T. S. Andrews and J. E. Gorden, *J. Chem. Soc., Faraday Trans. 1*, **69**, 546 (1973). Adiabatic Calorimetry of Organic Salts: Tetra-*n*-hexylammonium Perchlorate.

Asahi Research Center, Co., Ltd., Tokyo, Japan, ed., *Handbook of Proton-NMR Spectra and Data*, Vol. 1 – 10, Academic Press, Tokyo, New York, 1985 – 1986.

R. T. Bailey, "Infra-Red and Raman Studies of Molecular Motion in Plastic Crystals", in *The Plastically Crystalline State (Orientationally-Disordered Crystals)*, Ed. J. N. Sherwood, John Wiley and Sons, Chichester, (1979).

A. Blumstein, O. Thomas, *Macromolecules*, **15**, 1264 (1982). Odd-Even Effect in Thermotropic Liquid Crystalline 4, 4'-Dihydroxy-2,2'-dimethylazoxybenzene-Alkanedioic Acid Polymers.

N. Boden, "NMR Studies of Plastic Crystal", in *The Plastically Crystalline State (Orientationally-Disordered Crystals)*, Ed. J. N. Sherwood, John Wiley and Sons, Chichester, (1979).

F. A. Bovey, *Chain Structure and Conformation of Macromolecules;* Academic Press, New York, 1982.

G. H. Brown, (ed.), "*Advances in Liquid Crystals*," Academic Press, 1975-present.

H. S. Bu, S. Z. D. Cheng, and B. Wunderlich, *J. Phys. Chem.*, **91**, 4179 (1987). Study of the Skeletal Vibrations Used to Compute Heat Capacities of Solid Macromolecules.

A. Cabana, Chapt. 2 in "*Vibrational Spectra and Structure*", ed. by J. R. Durig, Vol. 4, Elsevier, Amsterdam, 1975.

S. -S. Chang and E. E. Westrum, Jr., *J. Chem. Phys.*, **36**, 2420 (1962). Heat Capacities and Thermodynamic properties of Two Tetramethylammonium Halides.

Yu. V. Cheban, S.-F. Lau, and B. Wunderlich, *Colloid Polymer Sci.*, **260**, 9 (1982). Analysis of the Contribution of Skeletal Vibrations to the Heat Capacity of Linear Macromolecules.

J. Cheng, A. Xenopoulos, and B. Wunderlich, *Magn. Res. in Chem.*, in press, 1992. Two-dimensional NMR Studies on the Additivity Rules of Carbon-13 Chemical Shifts in Tetra-*n*-alkylammonium Halides.

S. Z. D. Cheng, *Maromolecules*, **21**, 2475 (1988). Kinetics of Mesophase Transition in Thermotropic Copolyesters. 1. Calorimetric Study.

S. Z. D. Cheng, M. A. Yandrasits, and V. Percec, *Polymer*, **32**, 1284 (1991). Phase Behavior in a Thermotropic Polyether Involving Rod-like Mesogenic Groups Based on Conformational Isomerism.

T. G. Coker, J. Ambrose, and G. J. Janz, *J. Am. Chem. Soc.*, **92**, 5293 (1970). Fusion Properties of Some Ionic Quaternary Ammonium Compounds.

T. G. Coker, B. Wunderlich, and G. J. Janz, *Trans. Faraday Soc.*, **73**, 3361 (1969). Melting Mechanisms of Ionic Salts: Tetra-n-Amyl Ammonium Thiocyanate.

F. Coletta, G. Moro and P. L. Nordio, *Mol. Phys.*, **61**, 1259 (1987). Mobility of Alkyl Chains in Quaternary Ammonium Salts.

L. V. Coulter, K. S. Pitzer, and W. M. Latimer, *J. Am. Chem. Soc.*, **62**, 2845 (1940). The Entropies of Large Ions. The Heat Capacity, Entropy and Heat of Solution of Potassium Chloroplatinate, Tetramethylammonium Iodide and Uraryl Nitrate Hexahydrate.

P. Debye, *Ann. Physik*, **39**, 789 (1912).

F. D. Doty, and P. D. Ellis, *Review of Scientific Instruments*, December (1981). Design of High Speed Cylindrical NMR Sample spinners.

D. A. Dows, Chapt. 11 in *"Physics and Chemistry of the Organic Solid State"*, Ed. by D. Fox, M. Labes, and A. Weissberger, Vol. I., Interscience, New York, 1963.

W. L. Earl and D. L. VanderHart, *J. Magn. Res.* **48**, 35 (1982). Measurement of ^{13}C Chemical Shifts in Solids.

J. Economy, W. Volksen, C. Viney, R. Geiss, and T. Karis, *Macromolecules*, **21**, 2777 (1988). The Nature of the Thermal Transitions in Poly(p-oxybenzoate).

P. A. Egelstaff, *"Thermal Neutron Scattering"*, Academic Press, New York, 1965.

P. Ehrenfest, *"Phase changes classified according to the singularities of the thermodynamic potential"*, Acade. Sci., Amsterdam, 1933

P. J. Flory, *"Statistical Mechanics of Chain Molecules"*, Wiley-Interscience, New York, 1969.

M. H. Frey and S. J. Opella, *Chem. Commun.* 474 (1980). High-Resolution Features of the ^{13}C NMR Spectra of Solid Amino Acids and Peptides.

Y. Fu, Y. Jin, J. Cheng, and B. Wunderlich, research in progress, 1992. Disorder and Motion in Some Hexa-substituted Benzene Derivcatives studied by X-ray, DSC, and Solid State NMR.

C. A. Fyfe and R. P. Veregin, *Trans. Am. Crystallogr. Assoc.*, **20**, 43 (1984). NMR Investigations of Molecular Motions and Chemical Exchange Processes in the Solid State.

U. Gaur and B. Wunderlich, *J. Phys. Chem., Ref. Data*, **10**, 1001 (1981). Heat Capacity and Other Thermodynamic Properties of Linear Macromolecules III. Polyoxides.

J. E. Gorden, *J. Am. Chem. Soc.*, **87**, 4347 (1965). Fused Organic Salts. IV. Characterization of Low-melting Quaternary Ammonium Salts. Phase Equilibria for Salt-salt and Salt-nonelectrolyte Systems. Properties of the Liquid Salt Medium.

A. Habenschuss, A. Xenopoulos, and B. Wunderlich, *Mol. Cryst. Liq. Cryst.*, to be published, 1992. Mesophases of Alkylammonium Salts VI. X-ray Diffraction Evidences.

U. Haeberlin, *Adv. Magn. Reson.*, Supplement 1, 1976. High Resolution NMR in Solids.

J. G. Hexem, M. H. Frey and S. J. Opella, *J. Am. Chem. Soc.* 103, 224 (1981). Influence of ^{14}N on ^{13}C NMR Spectra of Solids.

O. W. Howarth, *J. Chem. Soc. Farady Trans. II* 74, 1031 (1978). Effect of Internal Librational Motions on the ^{13}C Nuclear Magnetic Resonance Relaxation Times of Proteins and Peptides.

O. W. Howarth, *J. Chem. Soc. Farady Trans. II* 75, 863 (1979). Effect of Internal Librational Motions on the ^{13}C Nuclear Magnetic Resonance Relaxation Times of Polymers and Peptides.

L. W. Jelinski, in *"Chain Structure and Conformation of Macromolecules"*, ed. F. A. Bovey, Academic Press, New York, 1982.

L. W. Jelinski and M. T. Melchior, "High-Resolution NMR of Solids", Chapter 6 in *NMR Spectroscopy Techniques*, (C. Dybowski and R. L. Lichter, eds.), Marcel Dekker, Inc., New York and Basel, 1987.

Y. Jin, J. Cheng, M. Varma-Nair, G. Liang, Y. Fu, B. Wunderlich, X. Xiang, R. Mostovoy, A. K. Zettl, and M. L. Cohen, *J. Phys. Chem.*, submitted, 1991. Thermodynamic Characterization of C_{60} by Differential Scanning Calorimetry.

Y. Jin and B. Wunderlich, *J. Thermal Analysis*, 36, 765 (1990)a. Single Run Heat Capacity Measurements.

Y. Jin and B. Wunderlich, *J. Thermal Analysis*, 36, 1519 (1990)b. Single Run Heat Capacity Measurements. II. Experiments at Subambient Temperatures.

Y. Jin and B. Wunderlich, *J. Phys. Chem.*, 95, 9000 (1991). Heat Capacities of Paraffins and Polyethylene.

Y. Jin and B. Wunderlich, *J. Thermal Analysis*, to be published, (1992). Single Run Heat Capacity Measurements. III. Data Treatment.

Y. Jin, J. Cheng, S. Z. D. Cheng, and B. Wunderlich, *Polymers for Advanced Technology*, submitted, 1992. Heat Capacity and Entropy of Thermotropic Polyethers based on the Semiflexible Mesogen 1-(4-Hydroxyphenyl)-2-(2-methyl-4-hydroxyphenyl)ethane.

T. Kato and F. Uryu, *Mol. Cryst. Liq. Cryst.*, **195**, 1 (1991). Conformational and Crystallographic Effects on Solid-State CP-MAS ^{13}C NMR Spectra of Thermotropic Phenyl Benzoates.

D. E. Kirkpatrick and B. Wunderlich, *Makromolekulare Chemie*, **186**, 2595 (1985). Thermal Analysis of the Phase Transitions of Poly(p-xylylene).

D. E. Kirkpatrick and B. Wunderlich, *J. Polymer Sci., Part B, Polymer Phys.* **24**, 931 (1986). On the Reversibility of the Crystalline Phase Transitions of Poly(p-xylylene).

R. Kitamaru, "C-13 Nuclear Spin Relaxation Study as an Aid to Analysis of Chain Dynamics and Conformation of Macromolecules", Chap. 3 in "Applications of NMR Spectroscopy to Problems in Stereochemistry and Conformational Analysis", ed. by Y. Takeuchi and A. P. Marchand, Vol. 6 of *Methods in Stereochemical Analysis*, ed. A. P. Marchand, VCH Publishers, Inc., Deerfield Beach, Florida, 1986.

S.-F. Lau and B. Wunderlich, *J. Thermal Anal.*, **28**, 59 (1983). Calculation of the Heat Capacity of Linear Macromolecules from θ-Temperatures and Group Vibrations.

J. Levkov, W. Kohr, and R. A. Mackay, *J. Phys. Chem.* **75**, 2066 (1971). Phase Transitions in Tetraalkylammonium Iodide Salts.

K. Loufakis and B. Wunderlich, *J. Phys. Chem.*, **92**, 4205 (1988). Computation of Heat Capacity of Liquid Macromolecules Based on a Statistical Mechanical Approximation.

I. J. Lowe, *Phys. Rev. Lett.*, **2**, 285 (1959). Free Induction Decay of Rotating Solids.

J. R. Lyerla, Jr., G. C. Levy, "Carbon-13 Nuclear Spin Relaxation", Chapter 3 in *"Topics in Carbon-13 NMR Spectroscopy"*, vol. 1, ed. by G. C. Levy, John Wiley & Sons, New York, 1974.

J. R. Lyerla, Jr., H. M. McIntyre, and D. A. Torchia, *Macromolecules*, **7**, 11 (1974). A ^{13}C Nuclear Magnetic Resonance Study of Alkane Motion.

M. Mehring, *"High Resolution NMR in Solids"*, 2nd ed., Springer-Verlag, Berlin, 1983.

K. J. Miller, H. B. Hollinger, J. Grebowicz, and B. Wunderlich, *Macromolecules*, **23**, 3855 (1990). On the Conformations of Poly(p-xylylene) and its Mesophase Transitions.

A. Naito, S. Ganapathy and C. A. McDowell, *J. Chem. Phys.* **74**, 5393 (1981). High Resolution Solid Sate ^{13}C NMR Spectra of Carbons Bonded to Nitrogen in a Sample Spinning at the Magic Angle.

A. Naito, S. Ganapathy and C. A. McDowell, *J. Magn. Res.* **48**, 367 (1982). ^{14}N Quadrupole Effects in CP-MAS ^{13}C NMR Spectra of Organic Compounds in the Solid State.

D. W. Noid, B. G. Sumpter, M. Varma-Nair, and B. Wunderlich, *Makromolekulare Chemie, Rapid Commun.*, **10**, 377 (1989). Molecular Dynamics Results for a Polyethylene-like Crystal.

S. J. Opella, M. H. Frey and T. A. Cross, *J. Am. Chem. Soc.* **101**, 5856 (1979). Detection of Individual Carbon Resonances in Solid Proteins.

R. Pan, M. Varma, and B. Wunderlich, *J. Thermal Anal.*, **35**, 955 (1989). On the C_p - C_v Conversion for Solid Linear Macromolecules. II.

N. G. Parsonage and L. A. K. Staveley, *"Disorder in Crystals"*, Chapters 7, 9 and 10, Clarendon Press, Oxford, 1978.

W. Pechhold, *Kolloid Z. Z. Polymer*, **228**, 1 (1968). Molekülbewegung in Polymeren I. Teil: Konzept einer Festkörperphysik mackromolekularer Stoffe.

V. Percec, and R. Yourd, *Macromolecules*, **22**, 524 (1989). Liquid Crystalline Polyethers Based on Conformational Isomerism. 2. Thermaotropic Polyethers and Copolyethers Based on 1-(4-Hydroxyphenyl)-2-(2-methyl-4-hydroxyphenyl)ethane and Flexible Spacers Containing an Odd Number of Methylene Units.

R. A. Pethrick, Chapt. 4, "Dielectric and Acoustic Studies", in *The Plastically Crystalline State (Orientationally-Disordered Crystals)*, Ed. J. N. Sherwood, John Wiley and Sons, Chichester, (1979).

J. G. Powles and H. S. Gutowsky, *J. Chem. Phys.*, **21**, 1695 (1953). Proton Magnetic Resonance of the CH_3 Group. I. Investigation of six tetrasubstitute Methane.

J. W. Richards, *Chem. News*, **75**, 278 (1897). Relations between the Melting-Points and the Latent Heats of Fusion of the Metals.

J. A. Ripmeester, *Chem. Phys. Lett.*, **74**, 536 (1980). Application of Solid-state ^{13}C NMR to the Study of Polymorphs, Clathrates and Complexes.

G. Ronca and D. Y. Yoon, *J. Chem. Phys.*, **76**, 3295 (1982). Theory of Nematic Systems of Semiflexible Polymers. 1. High Molecular Weight Limit.

Sadtler Research Lab., ^{1}H and ^{13}C NMR Spectra Collection.

H. Saitô, *Mag. Res. in Chem.* **24**, 835 (1986). Conformation-dependent ^{13}C Chemical Shifts: A New Means of Conformational Characterization as Obtained by High-resolution Solid-state ^{13}C NMR.

J. Schaefer and E. O. Stejskal, *J. Am. Chem. Soc.*, **98**, 1031 (1976). Carbon–13 Nuclear Magnetic Resonance of Polymers Spinning at the Magic Angle.

J. Schaefer, E. O. Stejskal, and R. Buchdahl, *Macromolecules*, **10**, 384 (1977). Magic-angle ^{13}C NMR Analysis of Motion in Solid Glassy Polymers.

N. S. Schneider, C. R. Desper, and J. J. Beres, in *"Liquid Crystalline Order in Polymers."*, Blumstein, A. ed. Academic Press, New York, 1978.

J. N. Sherwood, (ed.) *"The Plastically Crystalline State,"* (Orientationally-Disordered Crystals), John Wiley and Sons, Chichester, 1979.

R. M. Silverstein, G. C. Basler, and T. C. Morrill, *"Spectrometric Identification of Organic Compounds"*, John Wiley & Sons, New York, 1981.

K. Sköld, *J. Chem. Phys.*, **49**, 2443 (1968). Effects of Molecular Reorientation in Solid Methane on the Quasielastic Scattering of Thermal Neutrons.

C. P. Slichter, *"Principles of Magnetic Resonance"*, third Ed., Springer-Verlag, New York, 1969.

D. Smith, *Chem. Phys. Lett.*, **25**, 268 (1974). Hindered Rotational Energy Levels of Solid CD_4 (III).

G. W. Smith, *Bull. Am. Phys. Soc.* **9**, II, 25 (1964). Proton-Magnetic-Resonance Studies of Solid Tetra-methyl-Silicon, Germanium, Tin, and Lead.

C. P. Smyth, *"Dielectric Behavior and Structure"*, McGraw-Hill, New York, 1955.

E. O. Stejskal, D. E. Woessner, T. C. Farrar and H. S. Gutowsky, *J. Chem. Phys.*, **31**, 55 (1959). Proton Magnetic Resonance of the CH_3 group. V. Temperature Dependence of T_1 in Several Molecular Crystals.

J. B. Stothers, *"Carbon-13 NMR Spectroscopy"*, Academic Press, New York, 1972.

B. G. Sumpter, D. W. Noid, and B. Wunderlich, *J. Chem. Phys.*, **93**, 6875 (1990). Computer Experiments on the Internal Dynamics of Crystalline Polyethylene: Mechanistic Details of Conformational Disorder.

S. Takeda, T. Fujiwara and H. Chihara, *J. Phys. Soc. Japan*, **58**, 1793 (1988). Methyl Rotation in 1, 3, 5-Trichloro-2, 4, 6-trimethylbenzene as Studied by Nuclear Magnetic Resonance: A Comparison with Methyl Rotation in Hexamethylbenzene.

A. E. Tonelli, *"NMR Spectroscopy and Polymer Microstructure: The Conformational Connection"*, VCH Publishers, New York, 1989.

R. Tycko, G. Dabbagh, R. M. Fleming, R. C. Haddon, A. V. Makhija, and S. M. Zahurak, *Phys. Rev. Lett.*, **67**, 1886 (1991). Molecular Dynamics and the Phase Transition in Solid C_{60}.

R. Tycko, R. C. Haddon, G. Dabbagh, S. H. Glarum, D. C. Douglass, and A. M. Mujsce, *J. Phys. Chem.*, **95**, 518 (1991). Solid-State Magnetic Resonance Spectroscopy of Fullerenes.

G. Ungar, J. L. Feijoo, A. Keller, R. Rourd, and V. Percec, *Macromolecules*, **23**, 3411 (1990). Simultaneous X-ray/DSC Study of Mesomorphism in Polymers with a Semiflexible Mesogen.

G. Ungar, J. L. Feijoo, V. Percec, and R. Yourd, *Macromolecules*, **24**, 953 (1991). Liquid-crystalline Polyethers Based on Conformational Isomerism. 16. Hexagonal Columnar Phase (Φ_n) in a Nondiscotic Copolyether Based on 1,2-Bis(4-hydroxyphenyl)ethane, 1,8-Dibromooctane, and 1, 12-Dibromododecane and the Novel 2-Dimensional - 3-Dimensional Φ_n-S_B Transition.

D. L. VanderHart, *J. Magn. Res.*, **44**, 117 (1981). Influence of Molecular Packing on Solid-State ^{13}C Chemical Shifts: The n-Alkanes.

D. L. VanderHart, W. L. Earl, and A. N. Garroway, *J. Magn. Res.*, **44**, 361 (1981). Resolution in ^{13}C NMR of Organic Solids Using High-Power Proton Decoupling and Magic-Angle Sample Spinning.

A. L. Van Geat, *Abstracts of the 10th Experimental NMR Conferences*, Mellon Institute, Pittsburgh, PA, March, 1969.

A. L. Van Geat, *Anal. Chem.*, **42**, 679 (1970). Calibration of Methanol Nuclear Magnetic Resonance Thermometer at Low Temperature.

M. Varma-Nair and B. Wunderlich, *J. Phys. Chem., Ref. Data,* **20**, 349 (1991). Heat Capacity and Other Thermodynamic Properties of Linear Macromolecules. X. Update of the *ATHAS* 1980 Data Bank.

W. S. Veeman, *Progress in Nuclear Magnetic Resonance Spectroscopy,* Vol. 16, Pergamon Press, Oxford, 1984.

E. Wait and H. M. Powell, *J. Chem. Soc.* 1872 (1958). The Crystal and Molecular Structure of Tetraethylammonium Iodide".

P. Walden, *Z. Elektrochem,* **14**, 713 (1908). über die Schmelzwärme, spezifische Kohäsion und Molekulargrösse bei der Schmeltemperatur.

F. W. Wehrli, A. P. Marchand, and S. Wehrli, *"Interpretation of Carbon-13 NMR Spectra",* second ed., John Wiley & Sons, New York, 1988.

D. E. Woessner, *J. Chem. Phys.* **36**, 1 (1962) a. Spin Relaxation Processes in a Two-Proton System Undergoing Anisotropic Reorientation.

D. E. Woessner, *J. Chem. Phys.,* **37**, 647 (1962) b. Nuclear Spin Relaxation in Ellipoids Undergoing Rotational Brownian Motion.

D. A. Wright, D. E. Axelson, and G. C. Levy, *"Topics in Carbon-13 Nuclear Magnetic Resonance Spectroscopy",* ed., G. C. Levy, Vol. 3, Chap. 2, Wiley-Interscience, New York, 1980.

B. Wunderlich, *J. Chem. Phys.,* **37**, 1207 (1962). Motion in Polyethylene. II. Vibrations in Crystalline Polyethylene.

B. Wunderlich, *"Macromolecular Physics, Volume 1, Crystal Structure, Morphology, Defects",* Academic Press, New York, 1973.

B. Wunderlich, *"Macromolecular Physics, Volume 3, Crystal Melting",* Academic Press, New York, 1980.

B. Wunderlich, *"Thermal Analysis",* Academic Press, New York, NY, 1990.

B. Wunderlich and J. Grebowicz, "Thermotropic Mesophases and Mesophase Transitions of Linear, Flexible Macromolecules", in *Adv. Polymer Sci,* **60/61**, 1 (1984).

B. Wunderlich, M. Möller, J. Grebowicz, and H. Baur, "Conformational Motion and Disorder in Low and High Molecular Mass Crystals." *(Adv. Polymer Sci.,* Volume 87), Springer Verlag, Berlin, 1988.

M. A. Yandrasits, Ph.D Dissertation, Department of Polymer Science, The University of Akron, Akron, Ohio 44325-3909.

M. A. Yandrasits, S. Z. D. Cheng, A. Zhang, J. Cheng, B. Wunderlich, and V. Percec, *Macromolecules*, accepted.

C. S. Yannoni, R. D. Johnson, G. Meijer, D. S. Bethune, and J. R. Salem, *J. Phys. Chem.*, **95**, 9 (1991). ^{13}C NMR Study of the C_{60} Cluster in the Solid State: Molecular Motion and Carbon Chemical Shift Anisotropy.

M. Yasuniwa, Private Communication on the X-ray Crystal Structures of Tetra-*n*-propylammonium Iodide, 1991.

A. Xenopoulos and B. Wunderlich, *Mol. Cryst. Liq. Cryst.*, in preparation. Mesophases of Alkylammonium Salts V. Heat capacities of tetraalkyl-ammonium halides.

VITA

Jinlong Cheng was born in Kuitun, Xinjiang, the People's Republic of China on January 4, 1961. He attended elementary and high schools in the County 130 (Kuitun) Area School District and graduated in June, 1978. The following september he entered Beijing (Peking) University and in July, 1982 received the degree of Bachelor of Science in Physics. He worked as a major operator of analytical instruments at the Analytical and Testing Center, Lanzhou University from September, 1982 to August, 1988. In September, 1988, he entered University of Tennessee, Knoxville as a graduate student for a Doctor of Philosophy degree in Chemistry.